Control of the invadopodia/MT1-MMP axis by mTORC1/TFEB signaling pathway in breast cancer cells

David Remy

PSL UNIVERSITÉ PARIS

THÈSE DE DOCTORAT
DE L'UNIVERSITÉ PSL

Préparée à l'Institut Curie
Equipe Dynamique de la Membrane
et du Cytosquelette

Control of the invadopodia/MT1-MMP axis by mTORC1/TFEB signaling pathway in breast cancer cells.

Caractérisation du contrôle de l'axe invadopode/MT1-MMP par la voie de signalisation mTORC1/TFEB dans les cellules de cancer du sein.

Soutenue par
David REMY
Le 12 décembre 2022

Ecole doctorale n° 515
Complexité du Vivant

Spécialité
Biologie Cellulaire

Composition du jury :

Ana-Maria, LENNON DR, Institut Curie	*Présidente*
Constantinos, DEMETRIADES Group Leader, Max Planck Institute	*Rapporteur*
Sophie, VASSEUR DR, CRCM	*Rapporteur*
Mario, PENDE DR, Institut Necker	*Examinateur*
Philippe, CHAVRIER DR, Institut Curie	*Directeur de thèse*

institut Curie

ACKNOWLEDGMENTS

Lengthy by nature, a Ph.D. represents a significant portion of one's life. As such, the thesis involves a great many people that will stand between the student and its doctorate, through luck or misfortune, for better or for worse. I would like to highlight the contribution of some of these people in this acknowledgments section.

I would like to start by extending my deepest thanks to **Sophie Vasseur**, **Constantinos Demetriades**, **Mario Pende,** and **Ana-Maria Lennon-Duménil** who agreed to be part of my thesis jury, and I look forward to the discussion and comments around my work. More specifically, I would like to thank **Sophie Vasseur** and **Constantinos Demetriades** for their role in revising my thesis manuscript, I know how much work it represents, and I am genuinely grateful for their comments and feedback. Thank you to **Ana-Maria Lennon-Duménil** who accepted to preside the jury and to **Mario Pende** who has followed my work for the past three years as a member of my thesis committee and who always had great feedback on my work.

Je continuerais dans ma langue maternelle pour adresser quelques mots de remerciements à tous ceux qui m'ont accompagné et soutenu pendant cette aventure.

A **Philippe Chavrier**, mon directeur de thèse, j'aimerais lui adresser toute ma gratitude pour m'avoir accueilli dans son laboratoire. Si tu as réussi à m'insuffler ne serait-ce qu'un iota de ta rigueur expérimentale et de ta passion pour la science, la bonne, la vraie, alors je pourrais terminer cette thèse confiant dans mes capacités de scientifique. Je te remercie sincèrement de m'avoir accompagné tout au long de ce projet tout en me laissant la liberté d'amorcer des sous-projets annexes ~~plus ou moins fructueux~~. Tu n'as jamais perdu patience devant mes lacunes théoriques et pratiques et ton encadrement quotidien a été déterminant dans le succès de cette thèse.

Je remercie chaleureusement les membres du laboratoire, actuels et passés pour leurs conseils et apports scientifiques considérables. A **Pedro Monteiro**, merci pour ta bonne humeur constante (le réel soleil du laboratoire), tes blagues fines et mûries et ton altruisme exemplaire. J'imagine la tête de nos collègues en lisant cette phrase, ils doivent se dire « de qui il parle là ?». « Nan mais sérieusement », merci pour les discussions, les encouragements, les conseils et d'avoir été mon fidèle compagnon de route pour descendre prendre un café au Green. La perspective de passer encore quelques mois dans le même bureau que toi à parler science et philosophie (mais surtout ragots) est une pensée des plus réjouissante. Si tu pouvais juste y aller mollo sur les analogies sans queue ni tête, ce serait parfait.

To **Amulya Priya**, I wish to express my most genuine gratitude for your guidance, your advice, and your contagious laugh. The complicated mTOR field became so much clearer through your extensive knowledge. Without your words of encouragement and your kindness, I would have not made it through the first year so bahut dhanyavaad, from the bottom of my heart. Although you moved across the ocean, I hope to see you soon, share Indian food, and laugh about anything and everything as we used to do.

Adèle Berlioz, ma stagiaire qui n'a finalement jamais été ma stagiaire, merci pour tous ces moments de franche rigolade, pour ton soutien et tes encouragements, et pour avoir écouté mes plaintes, 19 fois par jour s'il le fallait. Je suis très content que tu aies rejoint le labo, tant sur le plan scientifique que personnel car j'ai trouvé en toi une camarade de galère : j'ai été longtemps le seul thésard du labo, mais la relève est bien assurée avec toi et Cécile.

Merci à **Cécile Gamblin** pour m'avoir encouragé à modifier les pratiques d'hygiène et sécurité du laboratoire, tu nous as tous sauvés d'un cancer induit par la PFA. Merci pour tes conseils extensifs sur la couleur des graphs, le meilleur thé vert et quelles fragrances se marient le mieux pour un parfum d'intérieur.

Au dinosaure du laboratoire, **Carine Rossé**, « basically » merci pour tes conseils et tes réassurances, pour le partage de ton expertise et de tes vastes connaissances sur divers sujets de biologie cellulaire. Tes commentaires et tes idées ont toujours été pertinents et bienveillants.

Parmi les anciens membres du laboratoire, j'aimerais remercier **Sophie Grouard de Toqueville**, une étudiante motivée, appliquée, rigoureuse et toujours de bonne humeur. Travailler avec toi et t'encadrer fût un plaisir et je suis persuadé à 1012% que Patrick de l'Institut Imagine s'est déniché une thésarde en or. N'oublie pas de m'inviter à ta soutenance ! Merci à **Alessia Robiolo** (ou Alessa Robilo, je ne sais plus), qui a partagé mon bureau lorsque j'étais tout seul et avec qui j'ai pu énormément rigoler, discuter de collagen stretching et de tubes Falcons, je te souhaite le meilleur pour la suite et permets-moi de te dire bravo pour avoir finalement terminé ton rapport de stage de M2. Merci aux trois mousquetaires, **Clémentine Villeneuve**, **Robin Ferrari**, et **Émilie Lagoutte**, l'ancienne génération qui m'a chaleureusement accueilli dans le laboratoire et m'auront passé le flambeau. **Marie-Ange Deugnier**, **Anna Zagryazhskaya-Masson** et **Fiona Routet** ce fut bref, mais j'ai beaucoup apprécié vos conseils et nos discussions. Je souhaite à **Marie-Ange** un épanouissement pour la retraite bien méritée auprès de tes enfants et petits-enfants, et à **Anna** et **Fiona** plein de réussite dans leurs carrières respectives. J'aimerais remercier quelques membres du 1er étage du bâtiment Burg, nouveaux et anciens : merci à **Michèle Colineau** pour ton aide précieuse,

ta disponibilité et ton savoir-faire pour naviguer les méandres administratifs de Curie. Je te souhaite une retraite heureuse et paisible. J'ai passé autant de temps à régler des problèmes scientifiques que des problèmes administratifs et je remercie du fond du cœur **Charlotte Lozach** qui ne m'a pas lâché et m'a épaulé sur le plan administratif. Merci à **Sabine Bardin** et **Séverine Divoux** qui ont su rendre l'étage plus accueillant et divertissant mais qui m'ont surtout bien formé aux bonnes pratiques de laboratoire, hygiène et sécurité. Je suis toujours ravi de m'arrêter dans un couloir pour discuter avec vous. A ma co-thésarde galérienne de l'autre côté du couloir, **Khadija Oukacha**, échanger avec toi sur les problématiques administratives qui accompagnent une soutenance m'a sauvé la vie (et ma thèse). Je te souhaite beaucoup de courage pour la fin de ce marathon, je suis certain que tu vas être brillante le jour de ta thèse (je serais parmi les premiers dans l'amphithéâtre à applaudir).

La biologie cellulaire n'est pas le seul domaine scientifique dans lequel j'ai été formé. Grâce à **Anne-Sophie Macé**, je me suis pris de passion pour la programmation informatique au service de l'analyse d'images de microscope. Merci pour ta patience infinie et ton entrain contagieux, pour ta sagesse et pour m'accompagner lors de nos randonnées matinales d'Arcueil jusqu'à Curie. Je me réjouis d'avance des nombreuses heures que nous passerons devant un code à se creuser les méninges… !

La coutume veut que la famille soit remerciée à la fin. C'est donc à la transition entre collègues de labo et membres de la famille que viennent naturellement mes remerciements pour **Sandra Antoine**. **Sandra**, ingénieure d'étude au laboratoire, a été la marraine de ce bébé-projet, celle qui a co-piloté ce projet avec moi et qui a aidé à façonner la direction qu'il prenait grâce à son travail remarquable. Merci pour m'avoir épaulé, encouragé et (surtout) supporté. Tu es devenue une amie précieuse et cette thèse n'aurait pas eu la même saveur sans toi et je n'oublierais pas ta présence indéfectible dans les moments joyeux au laboratoire et en dehors, mais également dans les moments les plus difficiles. Ton optimisme et ta bonne humeur constante, ta présence continue et ton aptitude à relativiser ont été des piliers sur lesquels je me suis reposé tout le long de la thèse, et je t'en suis très reconnaissant. Personne (pas même toi) ne comprend vraiment où tu seras dans quelques mois mais je te souhaite de t'y épanouir, et d'y être heureuse. J'espère qu'un jour, dans un futur proche, je pourrais enfin profiter d'un barbecue dans ta nouvelle maison perdue au fin fond de l'Île de France (si jamais elle finit par être construite…).

J'aimerais terminer par remercier du fond du cœur les personnes qui n'ont pas été directement impliquées dans la thèse, mais qui me sont le plus chères et qui ont été un appui fantastique et inébranlable au cours de ces années. Mes amis de l'ENS et de la prépa agreg

qui ont été tout simplement là, à m'encourager. Un merci tout particulier à la Manounette, je ne sais pas où je serais sans toi, sans tes encouragements intarissables et ton oreille attentive (soyons honnêtes, je serais probablement dans un asile). Mes cousines, qui ne sont pas vraiment mes cousines, qui pour certaines sont là depuis ma naissance, qui m'ont toujours remonté le moral et m'ont redonné confiance en moi lorsque ça n'allait pas. Vous êtes les seules à entendre mon rire d'hyène hystérique car je ne rigole jamais autant qu'avec vous. J'ai hâte de vous retrouver au parc de l'hippodrome de la Tour de Salvagny autour d'un tchoy sabz un dimanche après-midi, dans 5 mois tout comme dans 50 ans.

Ma mère et mon père, mon frère et ma sœur, ma très chère grand-mère, pour leurs prières, leur amour et leur soutien inconditionnel, à la fois moral et économique, qui m'a permis de réaliser les études que je voulais. Ma gratitude et ma reconnaissance est infinie et se passe donc de mots. Vous avez cru dur comme fer en moi et mes capacités et c'est ce qui m'a permis de continuer. J'espère aujourd'hui vous avoir rendu fier. Maman, Papa, je vous jure les études c'est fini.

TABLE OF CONTENTS

INTRODUCTION

1. Physiology of the adult normal breast

1.1. Normal breast histology

Mammary glands are the defining organs of mammals that produce milk to nourish offspring. The breast is a peculiar organ that reaches full development after birth, and although the gland is present both in males and females, it is only functional in the post-partum female.

1.1.1. Histology of the breast

The breast is made of three tissues: the epithelium forming the gland, the adipose tissue, and the extracellular matrix tissues. The major component of the breast is the adipose tissue, which is primarily composed of fat-storing adipocytes, and which surrounds the gland (Hovey & Aimo, 2010a). Mammary glands are composed of fifteen to twenty lobes, each lobe containing multiple lobules. The lobules are subdivided into alveoli (or acini) that drain into a series of intralobular ducts. These ducts merge into a single lactiferous channel that opens onto the surface of the nipple where milk is ejected (**Figure 1**) The mammary lobes are connected by dense connective tissue composed of a stromal extracellular matrix (ECM), vascular and lymphatic vessels as well as immune cells, and fibroblasts (Johnson, 2010).

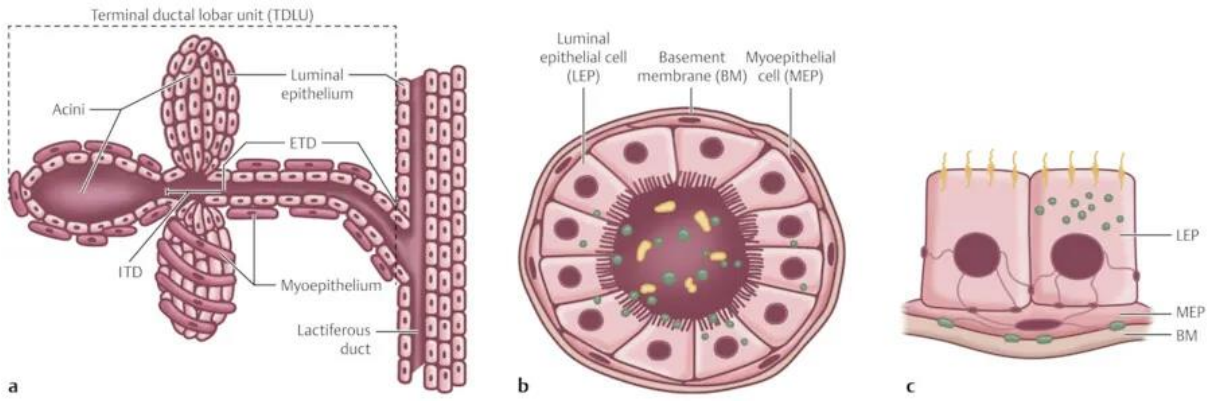

Figure 1: Schematic drawing of a sagittal cross-section of a female breast, the terminal ductal lobular unit (TDLU), and the acinus. *(a, b) The mammary gland consists of 15 to 20 lobes subdivided into lobules, then TDLU and acini. Muscle and fatty tissue are interspersed among the lobes of the gland. Each acinus consists of epithelial cells producing milk and ejecting it into a duct system converging on the opening of the nipple. (c) Two cell types comprise the epithelium that lines the ducts and lobules: the milk-secreting luminal cells and the contractile myoepithelial cells which contact the supporting basement membrane.*

1.1.2. Mammary epithelium organization

Mammary ducts are epithelial tissues composed of luminal epithelial cells facing the lumen of the ducts, and myoepithelial cells resting on a basement membrane (BM) (**Figure 1**).

Luminal cells are specialized in milk production and secretion. Like most epithelial exocrine cells, mammary luminal cells are cuboidal and present a complete lateral belt of tight junctions (*zonula occludens*) at their apex to prevent leakage from secreted molecules. E-cadherin-positive adherent junctions (*zonula adherens*) and desmosomes (*macula adherens*) on the lateral surfaces bridge the plasma membrane of neighboring cells and assure the integrity and stability of the epithelium (Johnson, 2010). They typically express luminal cytokeratins (CK-7/8/18/19) and most luminal cells express estrogen and/or progesterone receptors (Deugnier et al., 2002).

The myoepithelial cells are located between the luminal cell layer and the BM, which they secrete (**Figure 1**). They have many features common to smooth muscle cells such as the expression of smooth muscle actin (SMA), calponin, smooth muscle myosin heavy chain (MHC), and exhibit parallel arrays of myofilaments, and dense bodies, thus allowing them to contract for milk ejection during feeding. They also show epithelial cell characteristics, express cytokeratins 5 and 14 and adhere to each other and the BM through desmosomes and hemidesmosomes. They interact directly with the luminal cells and aid them in acquiring polarity by synthesizing the BM, composed of fibronectin (a large glycoprotein that mediates adhesion), laminin, collagen IV and nidogen (a glycoprotein that links laminin to collagen IV) (Johnson, 2010).

1.1.3. The basement membrane

The extracellular matrix (ECM) is a three-dimensional network of supramolecular assemblies of proteins, proteoglycans, and glycosaminoglycans that is present in all tissues and is essential for life. The ECM is a physical support for cells that maintains tissue integrity, and provides elasticity and resistance to compression, but is also a dynamic structure controlling cell behavior and fate (Hynes, 2009). Two main types of ECM differ in location and composition: the interstitial connective tissue matrix and the basement membrane (BM). The BM is a dense and thick sheet-like network of extracellular proteins, glycoproteins, and proteoglycans separating epithelial cells from the stroma. More than 50 distinct macromolecules are comprised in the BM with a tight meshwork of laminin and type IV collagen acting as a scaffold for the deposition of other glycoproteins (nidogens, fibronectin, entactin, HSPGs, etc.) (Paulsson, 1992; Rowe & Weiss, 2008b).

In Vertebrates, laminins form a family of 16 heterotrimeric glycoproteins composed of a 400-kD α chain, a 200-kD β chain, and a 200-kD γ chain. The self-assembly of the three different chains is mediated by the N-termini of each arm and leads to the formation of a cruciform trimer

stabilized by disulfide bonds. Supramolecular organization at the plasma membrane is triggered *via the* binding of the C-termini domain of the α chain (the long arm) to cellular receptors (integrins, sulfated glycolipids, or dystroglycan depending on the tissue). In turn, the C-termini of the β and ɣ chains (the short arms) form stable interactions resulting in the organization of a sheet of oriented laminin heterotrimers (**Figure 2**) (Rowe & Weiss, 2008b).

Type IV collagen is a family of six α chains produced by distinct genes. The N-termini of three of these α chains come together to form a heterotrimeric molecule, which theorizes the existence of 56 different combinations of triple-helix of type IV collagen. However, the collagen IV composition in human BM remains largely unknown as most of the current understanding of the structure and self-aggregating properties of type IV collagen is derived from mice sarcoma studies where only α1 and α2 chains are expressed. The protomer (triple helix) is divided into an N-terminal 7S domain, a middle triple-helical domain, and a C-terminal NC1 globular domain (Kalluri & Cosgrove, 2000; Rowe & Weiss, 2008b). Upon exocytosis, protomers face an increase in chloride concentration which induces the assembly of a dimer by the interaction of two NC1 domains (Pedchenko et al., 2019; Tsilibary & Charonis, 1986). Chloride also induces the connection of four protomers in a spider-shaped structure connected by the association of the 7S domains (**Figure 2**) (Kühn, 1995; Pedchenko et al., 2019).

Once secreted and self-assembled in the extracellular space, laminins and collagen are connected by various glycoproteins, such as nidogens, perlecan, or other types of collagens (types VI, XV, or even XVIII) (**Figure 2**). Epithelial cells adhere to the BM on their basal pole, which provides them with structural support and dictates cell polarity, survival, and proliferation. In the mammary gland, the composition and density of the BM greatly influence ductal morphogenesis, as BM is accumulated at the terminal end buds, constricting and elongating the buds (Jayadev & Sherwood, 2017). The BM is a semi-permeable barrier with pores the size of 50 nm allowing only small molecules to passively diffuse through (Rowe & Weiss, 2008b). It is a highly dynamic structure and is constantly modified: multiple cell types develop different cellular processes to reorganize the BM components and traverse the membrane barriers in the course of developmental, inflammatory, fibrotic, and neoplastic processes.

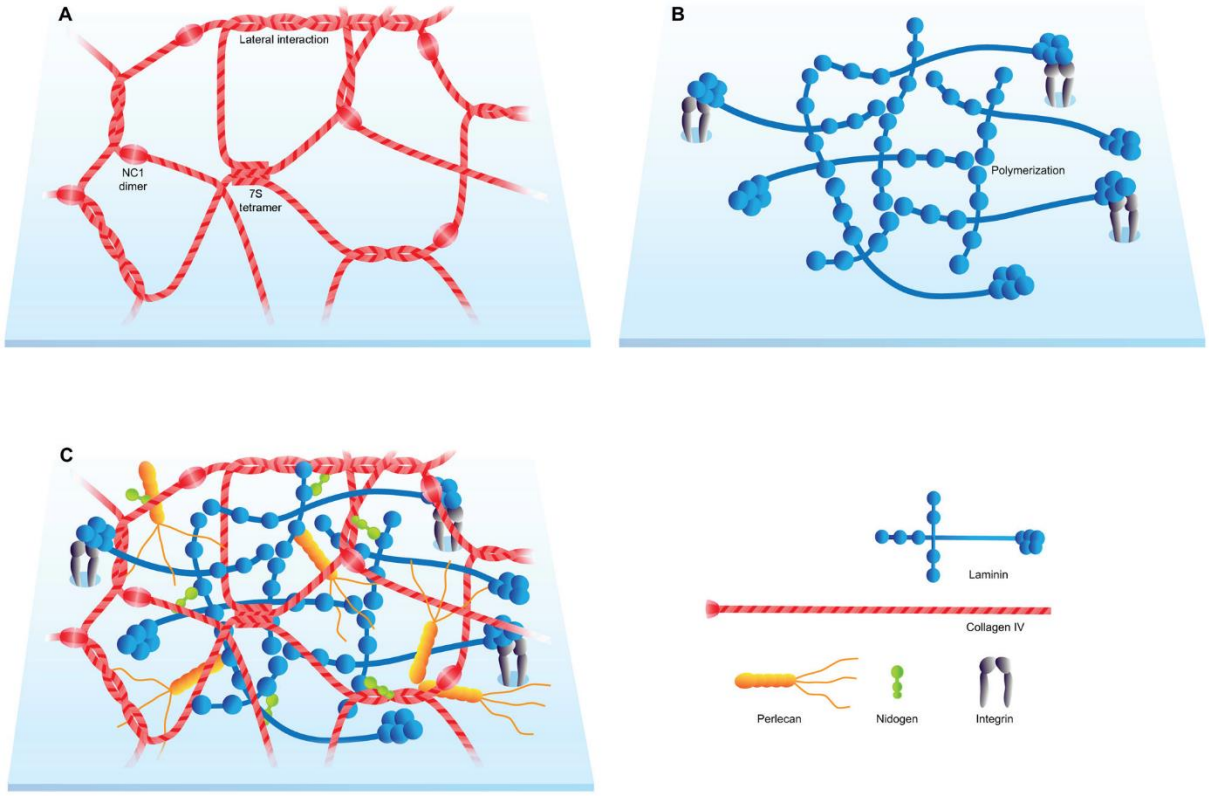

Figure 2: Schematic representation of the basic structure of the basement membrane. *(A) Type IV collagen promoters can dimerize through their NC1 regions and self-assembly by the association of the 7S domains. (B) Laminin is a homotrimer protein that self-organizes as a supramolecular structure. (C) Schematic representation of the collagen-laminin scaffold bridged together by additional matrix proteins (perlecan, nidogen) resulting in the formation of the basement membrane* (Sekiguchi & Yamada, 2018).

1.1.4. The mammary gland stroma

The stroma is a meshwork of cellular and acellular material that surrounds and interacts with the mammary ducts and alveoli. The acellular material is composed of loose intralobular connective tissue, dense irregular interlobular connective tissue, and interlobular adipose tissue. Type I collagen makes up the major component of the aqueous matrix in the interlobular connective tissue matrix. As in all collagen molecules, type I collagen comprises three polypeptide alpha-chains [(α1)2(α2)1], each formed from a repetition of a residue of glycine, frequently combined with imino acids, proline (Pro), and hydroxyproline (OH-Pro) (Mienaltowski et al., 2021; Shoulders & Raines, 2009a). The self-assembly of type I collagen is a complex multi-step process that starts in the rough endoplasmic reticulum of the stromal fibroblasts: alpha chains form a triple helical molecule, the procollagen. Once transported to the Golgi apparatus, the procollagen undergoes several post-translational modifications, such as the hydroxylation of Pro residues by the prolyl-4-hydroxylase (P4H). It was demonstrated that OH-Pro stabilizes collagen at a temperature of 43°C while non-hydroxylated collagen was

denatured at such a temperature. Furthermore, the removal of P4H activity is lethal in animal models (Bella, 2016).

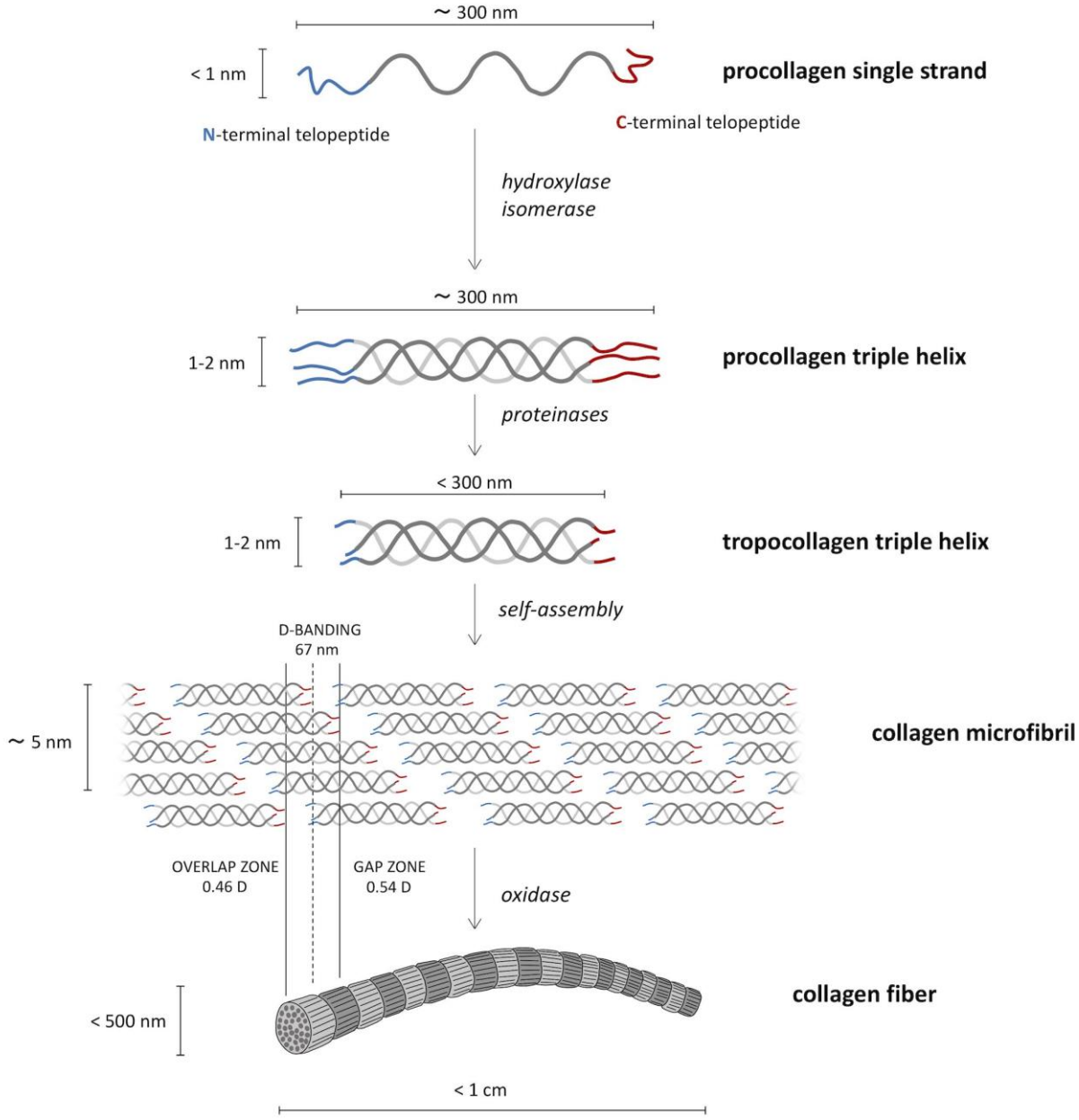

Figure 3: Biosynthetic route from the molecular procollagen to collagen fibrils. *Three helical procollagen single strands are mature and hydroxylated in the cell organelles and form a procollagen triple helix. The tropocollagen molecules, resulting from proteinases cut of N- and C-termini, go toward the supramolecular assembly that forms collagen type I fibrils.* (Salvatore et al., 2021)

Procollagen is packed in vesicles and secreted in the extracellular space where it becomes a tropocollagen molecule through the cleavage of its C- and N-termini by various proteases. The

newly exposed C- and N-termini telopeptides from various tropocollagen molecules can interact and form a collagen microfibril. The telopeptides are cross-linked subsequently by lysyl oxidase enzymes which endow mature collagen fibrils with strength and stability (**Figure 3**) (Shoulders & Raines, 2009b). Other stromal ECM components include fibrous bridging proteins such as fibronectin or elastin, as well as glycoproteins, such as hyaluronic acid, aggrecans, and perlecans, all of which form a compliant, hydrated meshwork capable of resisting to tensile and compressive stresses (Frantz et al., 2010). Proteoglycans are also a reservoir of growth factors (FGF, EGF, HGF) which can be released and influence mammary cell behavior (Johnson, 2010). Direct cell-matrix interactions through adhesion of integrins with the ECM molecules can also control cell survival, proliferation, differentiation, and migration (Schatzmann et al., 2003).

The adipose tissue is a complex, essential, and highly active metabolic and endocrine organ. A large part of the stromal adipose tissue is made of adipocytes filled with lipid, a reservoir of fat that is critical for the metabolically demanding process of milk production (Gregor et al., 2013). Adipocytes are also thought to synthesize many diverse molecules, such as estrogens and growth factors (IGF-I, HGF, VEGF, and TGF-β) that were all shown to have a role in the pre-, and post-natal development and function of mammary epithelial and stromal cells alike (Hovey & Aimo, 2010b).

1.2. Mammary gland development

1.2.1. Embryonic and post-natal development

Studies of prenatal human breast development have, by necessity, been observational postmortem and not experimental. Therefore, most of our understanding of mammary gland development is derived from studies in mice. In the early stages of embryogenesis (4-6th fetal week), epithelial cells in the epidermis of the thoracic region proliferate and give rise to primary mammary buds penetrating the lower mesenchyme. After a while, the primary buds sprout and branch out and form mammary glands, later all connected by the lactiferous ducts. Late in the fetal period, the original invagination site of the primary bud evaginates to form the nipple (**Figure 4**) (Javed & Lteif, 2013). Many studies have shown that extensive crosstalk between the epithelial and the mesenchymal tissue was required for normal breast development (Parmar & Cunha, 2004).

Most of the branching in the mammary gland is triggered by the hormones released by the hypothalamus-pituitary axis and the ovaries at the beginning of puberty. High levels of estrogen promote thickening of the epithelium as well as the elongation, invasion, and branching out of ducts' terminal ends. Estrogens also stimulate the expansion and differentiation of the stromal tissue.

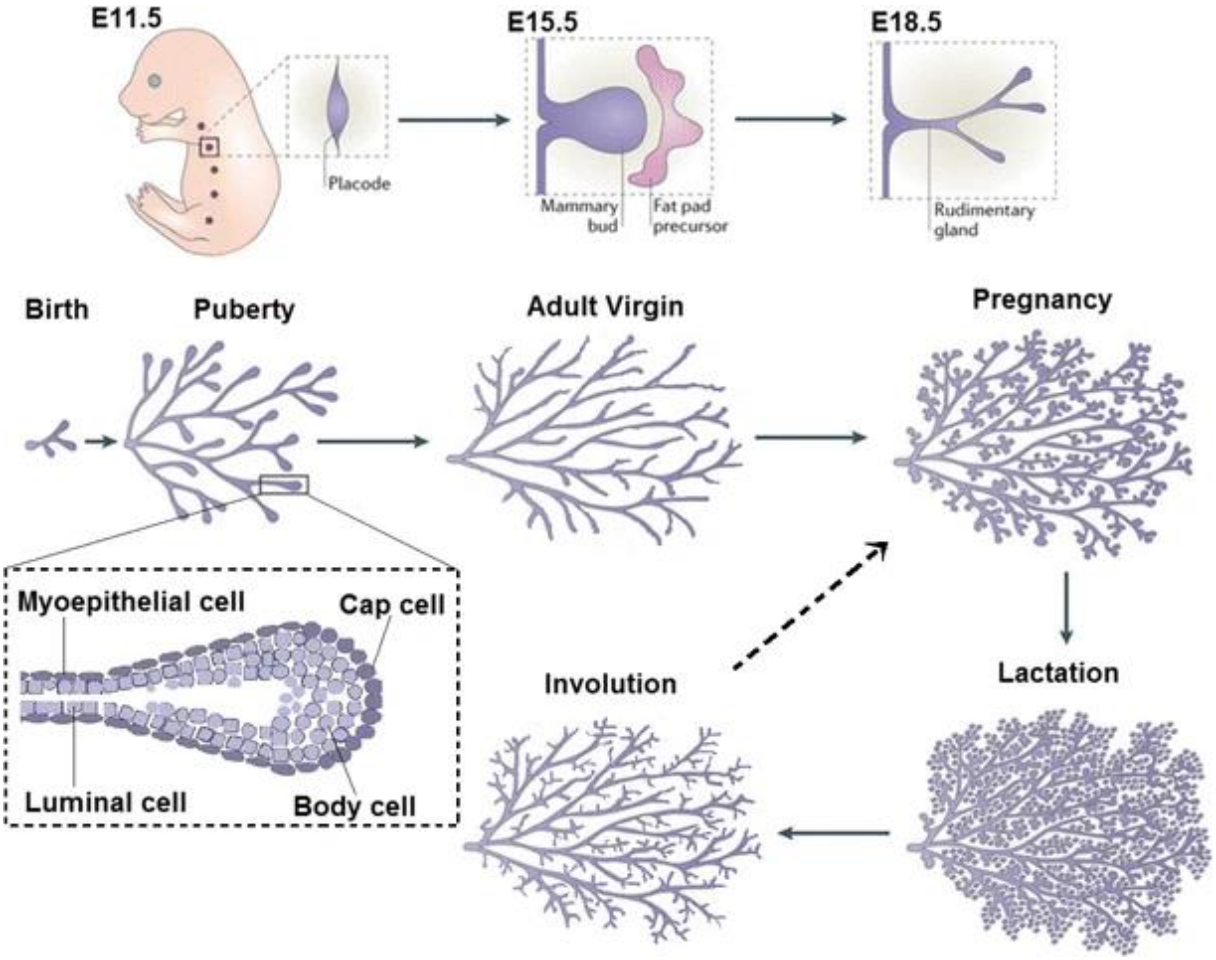

Figure 4: Overview of mammary development. *After 15 weeks, the mammary bud sinks into the fat bad precursor and expands in a rudimentary duct. On the onset of puberty and release of hormones (namely estrogen), terminal ends buds are formed and elongate. During pregnancy, the mammary tree expands, and the ducts' terminal ends bud and differentiate into milk-producing cells. Once the child is weaned, massive epithelial cell apoptosis occurs during the involution process to go back to a pre-pregnancy state.* (Paine & Lewis, 2017)

In the premenopausal adult breast, menstrual cycles profoundly change the architecture of the mammary gland to fulfill the milk-secreting primary function. During the luteal phase (after ovulation), the stroma becomes more vascular while the epithelial cells grow and proliferate. In the event of a pregnancy, placental estrogens promote distal ducts branching and the creation of more lobules and more alveoli within each lobule. Progesterone and prolactin (respectively produced by the placenta and the pituitary gland) induce luminal epithelial cells differentiation into milk-secretory cells. After birth, oxytocin and prolactin are synthesized by the pituitary gland and released by the suckling reflex. Prolactin continues to promote the synthesis and secretion of milk during normal lactation while oxytocin stimulates the contraction of myoepithelial cells to eject milk from alveoli into lactiferous ducts. Post-

lactational involution involves alveolar cell apoptosis and phagocytosis as well as regrowth of stromal adipose tissue (**Figure 4**) (Javed & Lteif, 2013; Johnson, 2010).

1.2.2. Role of stem cells

Mammary stem cells (MaSC) give rise to a daughter stem cell and one luminal or myoepithelial progenitor cell. The concept of MaSC emerged in the 1950s to try to explain the profound changes during the female hormonal cycle. The purification of MaSCs has proved elusive but the use of flow cytometry to identify mammary epithelial cell subpopulations provided evidence that the transplantation of a single cell from a distinct population into a cleared mammary fat pad could reconstitute the entire mammary epithelium (Shackleton et al., 2006). Based on this procedure, concentration of stem cells was highest in ducts, and they tend to be found between the luminal and basal compartments of the mammary epithelium (Villadsen et al., 2007). By interacting with surrounding cells and the ECM, stem cells are maintained in their niche in an undifferentiated state which grants them self-renewal and proliferation properties. Defects in the tight regulation of stem cell properties and uncontrolled cell proliferation can lead to neoplasia and further down the line to cancer (S. Liu et al., 2005).

1.2.3. Regulation of breast structure and function by hormones and other regulators

The mammary gland undergoes dramatic and complex changes during puberty and pregnancy, changes that must be tightly controlled to avoid dramatic potential consequences. Cyclic changes in hormone levels are known to be major regulators of the modifications occurring in the breast, such as estrogens and progesterone. These hormones are released cyclically by the ovaries under the direct influence of the hypothalamic-pituitary axis which releases gonadoliberins (GnRH), luteinizing hormone (LH), and follicle-stimulating hormone (FSH) into the bloodstream. As described above, estrogens promote the development of the stromal tissue in the breast as well as the growth of the breast ductwork. Progesterone prepares the breast for lactation by inducing the differentiation of the breast lobules.

The intracellular estrogen receptors exist in two isoforms (α and β), coded by two different genes. ERα is expressed in 30% of luminal epithelial cells and induces transcriptional changes related to cell proliferation. Interestingly, in mice, the binding of estrogen to ERα in ERα-positive cells stimulates the proliferation of neighboring ERα-negative cells but not of the ERα -positive cell. This dissociation between ERα -positive cells and proliferating cells implies that paracrine factors mediate the mitogenic activity of estrogen: amphiregulin, HGF, EGF, TGF, IFG, and FGF3 have all been proposed as paracrine mediators of estrogen effects. For instance, EGF is a potent mitogen that is essential in mammary ductal growth and branching. EGF works with HGF and TGF-β to promote lobuloalveolar development (**Figure 5**) (Garner et al., 2011; Sternlicht, 2006). On the other hand, ERβ is found in myoepithelial cells and is

important for the expression of adhesion molecules and the development of the *zonula occludens* in myoepithelial cells, required for lactation (Johnson, 2010).

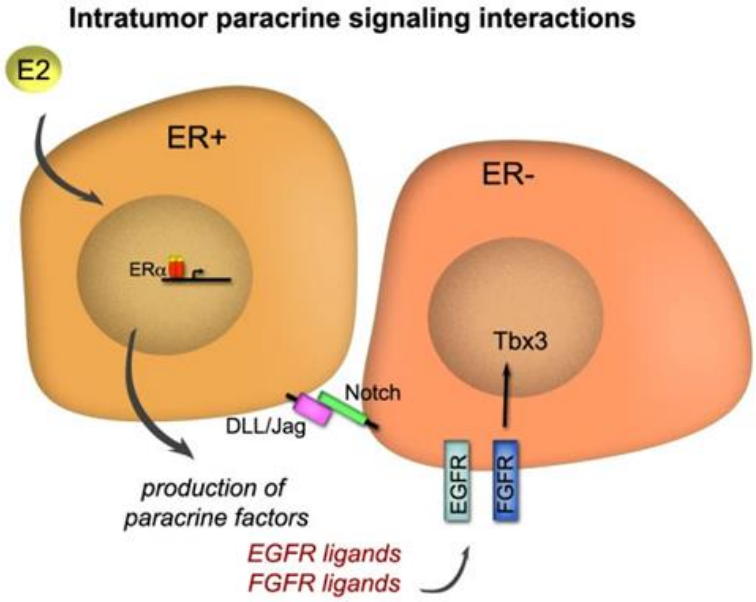

Figure 5: The dissociation in ER+ cells and proliferating cells in mammary development and cancer lead. *ER+ cells produce growth factors upon estrogen signaling that have a paracrine action on neighboring ER- cells and induce their proliferation.*

The two isoforms of PR (α and β) are encoded by a single gene. PR knockout mice have demonstrated the critical role of progesterone in ductal branching and lobuloalveolar development during pregnancy. The PR-progesterone complex also translocates to the nucleus and binds to DNA and promotes the expression of paracrine factors stimulating cell proliferation, inducing lateral branching and alveogenesis (Johnson, 2010).

One of the consequences of the large number of divisions occurring during the development of the mammary gland is the acquisition of somatic mutations and the creation of genetic mosaicism which are risk factors for breast cancer development.

2. Breast cancer progression

Breast cancer (BC) is the leading cause of death by cancer in women in France with an incidence of near 60 000 cases in 2020 and a mortality rate of 7.6% with 14 000 deaths in 2020 (source: Global Cancer Observatory by the International Agency for Research on Cancer). 95% of BC are derived from the epithelial cells (carcinoma) of the mammary gland (adenoma, adenocarcinoma) (Vinay et al., 2005). Epithelial cells proliferate uncontrollably and abnormally but remain confined within the duct by the myoepithelium (myoepithelial cells and basement membrane), forming a ductal carcinoma *in situ* (DCIS). In one-third of cases, the initial DCIS lesion progresses to invasive ductal carcinoma (IDC) (Rebbeck et al., 2022; Risom et al., 2022a).

The physiopathology of BC is multidimensional and still poorly understood, but certain risk factors are known, such as advancing age and female sex. A family history of BC is also a risk factor with high-penetrance germline mutations accounting for about 10% of all BC cases. In particular, the “breast cancer genes 1 and 2” (BRCA1 and 2) which are highly expressed in proliferating mammary cells and protect genomic stability, have so far been identified as tumor suppressor genes inactivated in BCs (Venkitaraman, 2019).

2.1. Intertumoral heterogeneity

The majority of BC cases (90%) are sporadic, caused by the accumulation of acquired somatic mutations. The diversity and intertumoral heterogeneity of breast tumors is a therapeutic challenge and thus it became a pressing necessity to classify the diverse mammary tumor entities. For several decades, mammary tumors were classified based on the histological type, the tumor grade, and their stage of progression. According to their localization, breast tumors are defined as lobular or ductal carcinoma (in the mammary lobule or the duct, respectively). If tumor cells are confined within the lobule or the duct, the carcinoma is characterized as *in situ*. However, if the cancer cells have breached the myoepithelium and the basement membrane and started to invade the surrounding stroma (in clinics IDC diagnosis is based on p63 and SMA staining), then the carcinoma is defined as invasive. About 50% to 80% of newly diagnosed BC cases are invasive ductal carcinoma (IDC). The rest are invasive lobular carcinoma (ILC) (Nascimento & Otoni, 2020). Studies show that in 75% of cases, DCIS will not progress to IDC, but because of the lack of markers and absence of a predictive signature of DCIS-to-IDC transition, the current guidelines often recommend surgical removal of the DCIS (Barrio & van Zee, 2017; Solin, 2019). The tumor grade is a descriptive indicator of how quickly a tumor is likely to grow and spread based on the morphological aspect of the cancer cells. The TNM scoring system considers the size (T), the status of the regional nodes (N), and the invasion into distant sites to form metastasis (M) to attribute a grade to the tumor (Cserni et al., 2018).

With the introduction of transcriptomic analysis in the 2000s, large-scale profiling studies allowed for the characterization of the genomic landscape of BC and revealed new layers of complexity and heterogeneity within BCs (Perou et al., 2000). Four distinct transcriptional programs emerged from these molecular stratification studies (**Figure 6**). Luminal tumors are characterized by the expression of ER and luminal cytokeratins CK8 and CK18. The luminal A subtype expresses high levels of estrogen receptors and a low rate of proliferation as measured by the staining of the proliferative marker Ki67. The luminal B subtype expresses low levels of estrogen receptors and has a high proliferation rate through overexpression of cyclin B1. Therefore, luminal A tumors are responsive to hormonal aromatase inhibitors (AI) and selective estrogen receptor modulators treatments and patients with this subtype of cancer present a relatively low relapse rate. Luminal B tumors, however, do not respond well to AI treatment and are of worse prognosis than luminal A. Numerous clinical trials are testing inhibitory molecules of the PI3K/AKT/mTOR pathway to establish neoadjuvant chemotherapy achieving a complete pathological response. Luminal tumors represent 50 to 70% of BCs (Taurin & Alkhalifa, 2020). HER2+ tumors (15% of accounted breast tumors) are defined by the overexpression of the human epidermal growth factor receptor (HER2) following the amplification and/or repetition of the ERBB2 gene on the large amplicon 17q12-21. These tumors are highly proliferative and have a weak prognosis. However, the dependency of these tumors on ERBB2 makes the HER2 gene product an actionable therapeutic target: patients with a HER2 BC can a gain 10-year disease-free advantage by the combinatory treatment of chemotherapy and immunotherapy using the humanized anti-HER2 monoclonal antibody Herceptin (trastuzumab) (Taurin & Alkhalifa, 2020; Yersal, 2014). Basal-like tumors (or triple-negative BC, TNBC) are characterized by the expression of myoepithelial/basal cytokeratins CK5/6 and CK17, no expression of PR and ER, and a normal expression of HER2. They represent 10% of all BCs but have a worse prognosis than luminal tumors with a high relapse rate. Extensive transcriptomic analysis of basal-like tumors allowed further stratification into 6 different subtypes (basal-like 1, basal-like 2, immunomodulatory, mesenchymal-like, claudin-low, and luminal androgen receptor) (Yersal, 2014). Finally, “normal-like” tumors present a genomic expression profile similar to normal breast tissue.

Rigorous molecular stratification of breast tumors help oncologists orient BC patients toward the best course of treatment and have set the stage for the emergence of personalized molecular medicine. However, the systematic classification of a tumor in a clinical subtype has yet to be established for diverse reasons such as the lack of reproducibility and quality control in current molecular tools as well as the cost of systematic screens (Eliyatkın et al., 2015). Furthermore, these types of characterization largely ignore the heterogeneous and structurally

complex nature of the organ, namely the importance of the stroma in the tumor progression (Mueller & Fusenig, 2004).

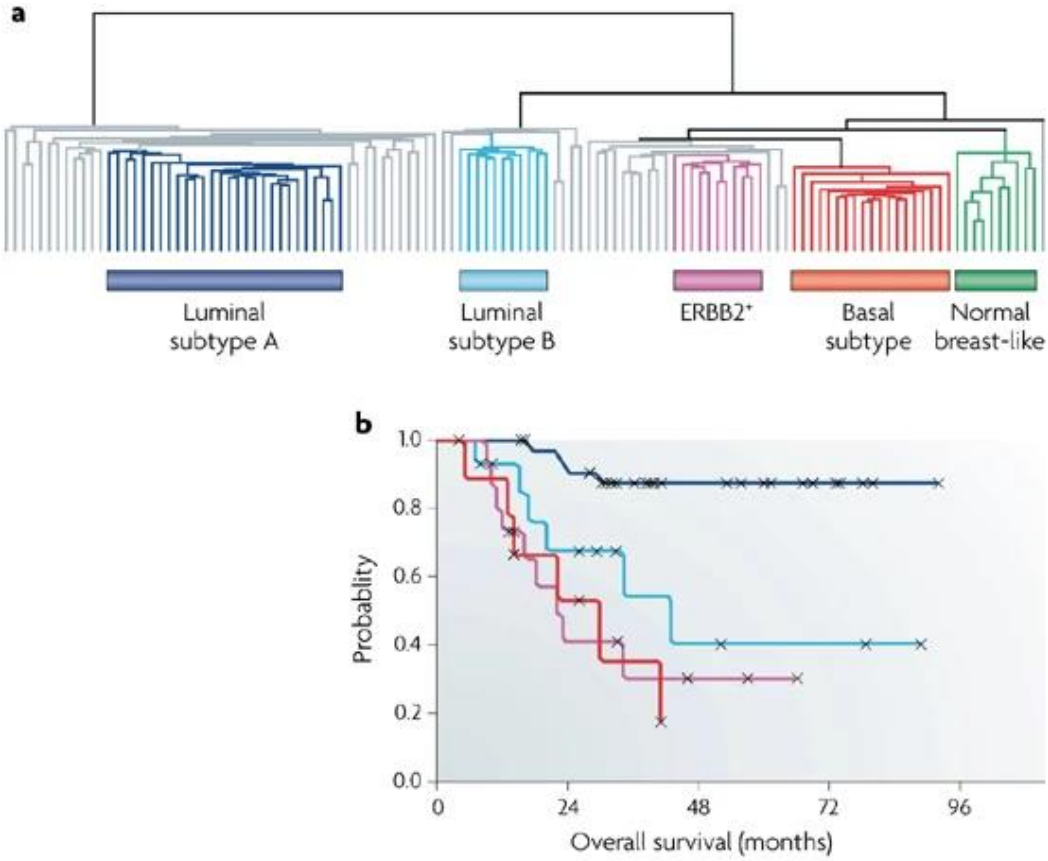

Figure 6: The identification of breast cancer subtypes by molecular profiling. (a) *Dendrogram showing the clustering of 115 breast tumors into 5 different subtypes of carcinoma. Grey branches (approximately 20% of all tested tumors) are tumors that did not correlate with any subtypes. (b) Prognostic outcomes for each subtype of carcinoma are shown as overall survival in months. The ERRB2+ (HER2+) and basal subtypes show the worse prognosis while luminal A tumors show the best prognosis* (Vargo-Gogola & Rosen, 2007).

Insights from studies of intratumoral heterogeneity and cancer stem cells (CSC) challenge the simple binary view of the tumor hierarchy, where a CSC would give rise to a homogenous tumor population and shift the view toward a spectrum of heterogeneous differentiation states and the coexistence of different populations of CSC. These different populations of CSC then give rise to distinct breast cancer subtypes within a single tumor and also implies that breast cancer can interconvert between distinct subtypes upon environmental clues (Nascimento & Otoni, 2020; Yeo & Guan, 2017). The direct clinical implication would be the application of combinations of therapeutic agents most effective for each subtype to minimize the emergence of resistant cells (Yeo & Guan, 2017).

2.2. Extracellular remodeling during breast cancer progression

Cell-ECM contacts are key in the governance of cellular phenotype and molecular functions. The interaction between cell surface receptors and the ECM components and ECM-bound growth factors mediates cell adhesion and cell signaling and therefore regulates cell proliferation, differentiation, migration, and apoptosis (Hastings et al., 2019). Although ECM remodeling is essential and tightly regulated in physiological processes, systemic aberrations of the ECM have been reported regarding tumor progression and metastasis establishment.

2.2.1. Mechanisms of tumorigenic ECM remodeling

2.2.1.1. Changes in the composition of ECM

Although any cell can in principle synthesize and deposit ECM components, the majority of ECM production is mediated by myofibroblasts, which are fibroblasts transformed by pro-inflammatory factors such as TGF-β. Myofibroblasts are fibroblasts that can modify the ECM topology by exerting contractile functions through *de novo* α-smooth muscle actin expression. Sustained production of TGF-β by tumor cells, but also of FGF-2, PDGF, and other various growth factors can attract and over-activate myofibroblasts and other stromal cells (so-called cancer-associated fibroblasts, CAF) (Winkler et al., 2020). A recent study showed that inhibiting CAF-mediated collagen production and deposition reduced breast tumor growth and metastatic spread *in vivo* and breast cancer cell proliferation *in vitro*, illustrating the importance of stromal cells and of the ECM on the tumoral progression (Kay et al., 2022). Furthermore, iron-bound-hyaluronic acid interaction with its cellular receptor CD44 has been shown to promote iron-mediated epigenetic activation of a mesenchymal phenotype *in vitro* (Müller et al., 2020). Tumorigenesis and increased deposition of collagen, fibronectin, and hyaluronic acid in the interstitial ECM results in a fibrotic phenotype characterized by chronic inflammation, fibroblast expansion and activation, and elevated angiogenesis (Auvinen et al., 2000; Kauppila et al., 1998; Pickup et al., 2014; Winkler et al., 2020). This tumorigenic fibrosis, termed desmoplasia, is a common characteristic of breast cancer and is associated with a poor prognosis (Catteau et al., 2019).

2.2.1.2. Changes in organization and post-translational modifications

ECM components undergo post-translational modifications which affect cell-matrix and molecule-matrix interactions. Collagens fibers are extracellularly cross-linked by lysyl oxidases (LOX) and LOX-like (LOXL) enzymes, tissue transglutaminase 2(TG2) mediates the transamidation of glutamine to lysine between fibronectin, HSPG, fibrinogen resulting in a covalent bond between two proteins. These enzymes are frequently overexpressed during cancer progression which results in increased cross-linking and linearization of ECM molecules (Yuzhalin et al., 2018). In normal tissues, the fibers are curly and parallel to the

epithelium and this architecture can protect against tumor initiation by stimulating the expression of cell-cell contact proteins and downregulating mesenchymal genes. During tumor progression in the breast, collagen form bundles of straightened and aligned fibers perpendicular to the tumor edge, and patients showing this architectural modification signature exhibit poor survival (Conklin et al., 2011; Risom et al., 2022). The ECM, especially the heparan sulfate proteoglycans (HSPGs), are a reservoir of growth factors and thus modulate the activity of the pro-proliferation signaling pathways mediated by tyrosine kinase receptors. Endosulfatases 1 and 2 (Sulfs 1/2) modify the ability of HSPGs to bind to growth factors by altering the sulphation pattern of the HSPGs although the molecular mechanisms are yet to be elucidated. Sulf1 inactivation in ovarian cancer and hepatocarcinoma prevents the inhibition of pro-proliferation tyrosine kinase receptor signaling (de Pasquale & Pavone, 2020; Hammond et al., 2014; Lai et al., 2008; Winkler et al., 2020).

2.2.1.3. Degradation of ECM

The extreme versatility of the ECM allows it to participate in critical developmental processes but also in various basic cellular functions through cell-matrix interactions. This pleiotropic aspect requires plasticity and a highly dynamic structure that is assured by the constant remodeling of the ECM by a reciprocal influence of the cellular residents. Stromal and cancer cells secrete zinc-dependent proteases belonging to three different families: matrix metalloproteinases (MMPs), a-disintergin, and metalloproteinase (ADAMs), and a-disintergin and metalloproteinase with thrombospondin (ADAMTs) families. The substrates of these proteases remain elusive, although recent degradomic studies showed that membrane-bound and soluble ADAM10 have different targets (Scharfenberg et al., 2020). The proteolysis of ECM has multiple consequences on tumor progression: replacement of normal ECM with tumor-derived ECM, driver of cell motility and invasion, the release of pro-tumoral growth factors, the revelation of cryptic binding sites for integrins (which activate pro-proliferating signaling pathways) and lastly the production of short bioactive ECM fragments termed matrikines. The role of matrikines is ambiguous, as they can be pro-tumorigenic as well as anti-tumorigenic. For instance, the degradation of elastin can activate the matrix metalloproteinase 14 (MMP14), while the α3 chain released from the cleavage of type IV collagen represses MMP14 (Martinella-Catusse et al., 2001). In breast cancer, trans-membrane MMP14 (also called membrane-type 1 matrix metalloproteinase 1, MT1-MMP) correlates with the progression from ductal carcinoma *in situ* (DCIS) to invasive ductal carcinoma (IDC) (Lodillinsky et al., 2016). The role of matrikines on the regulation of tumor progression should not be taken lightly, as recent evidence points to the fact that myoepithelium disruption was higher in DCIS that do not progress to IDC compared to DCIS having progressed to IDC, suggesting that the degradation of the basement membrane and

potential exposition to matrikines (and immune surveillance) could repress tumor progression (Risom et al., 2022).

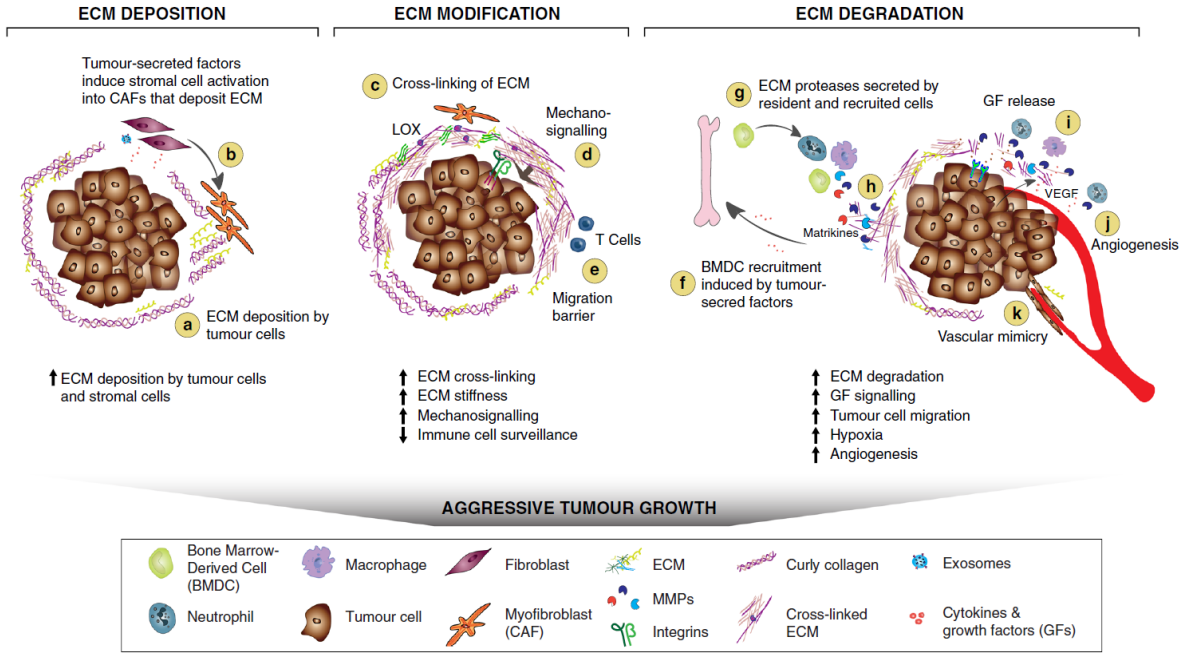

Fig. 6 ECM remodeling in the primary tumor. *(a, b) Tumor-derived factors activate stromal cells which differentiate into cancer-associated fibroblasts (CAFs) leading to the secretion and deposition of large amounts of ECM components along with the cancer cells. © ECM-modifying enzymes such as LOX expressed by tumor cells and CAFs cross-link and align collagen fibers, which increases matrix stiffness around the tumor. (d) Increased matrix stiffness promotes the interaction between ECM components and cell-surface receptors on tumor cells that triggers mechanosignaling mediated by integrins. (f) To sustain a tumorigenic microenvironment, tumor cells and resident immune cells secrete cytokines, chemokines, and growth factors (GFs), which differentiate and recruit bone marrow-derived cells (BMDCs). (g) The BMDCs, CAFs, and tumor cells secrete ECM-degrading proteases, including MMPs, which are cell surface-bound (e.g., trans-membrane MT1-MMP) or secreted (e.g., MMP-9). (h) Proteolytic ECM degradation generates bioactive matrikines and (i) releases matrix-bound GFs. These factors induce pro-tumourigenic ECM signaling that promotes tumor proliferation, migration, invasion, and angiogenesis. (j) These combined changes to the ECM create a hypoxic environment. Neutrophils secrete potent MMP-9 that degrades ECM and releases matrix-bound VEGF that forms a concentration gradient for new angiogenic sprouting. (k) Stimulated by dense ECM, the tumor cells may gain endothelial-like functions and mimic the vasculature that connects to blood vessels.* (Winkler et al., 2020)

2.2.2. Impact of tumorigenic ECM remodeling

2.2.2.1. Rewiring of signaling pathways by ECM remodeling

Integrins, which connect the ECM to the intracellular actin cytoskeleton, are heterodimeric transmembrane receptors. There are 24 integrins in mammals, each composed of one of the 18 α and 8 β subunits that recognize different ECM substrates: laminins (α2β1, α3β1), fibrillar collagens (α1β1, α2β1) and various other ECM proteins containing an RGD motif (α5β1, αvβ3, αvβ5). Activation of integrin starts with a conformational change to an open structure induced by the intracellular recruitment of talin (an adaptor protein that links integrin to the actin cytoskeleton). It is the inside-out signaling part of the integrin signaling pathway. Active integrin can bind to ECM molecules leading to integrin clustering which elicits robust outside-in signaling *via* the activation of focal adhesion kinase (FAK) and SRC family kinases (SFK). As a consequence, the Rho family GTPases, Rac, Rho, and Cdc42 are recruited to the plasma membrane and promote the assembly of pro-migratory structures such as filopodia, lamellipodia, and focal adhesions. Furthermore, FAK phosphorylates EGF, IGF, and VEGF receptor tyrosine kinases (RTK) to prime them for ligand-induced activation of mitogenic signaling such as the mitogen-activated protein kinases (MAPK) or the PI3K/AKT/mTOR pathway. In turn, the RTK induces phosphorylation of FAK. Joint integrin-RTK signaling thus regulates multiple cellular functions such as migration and invasion, proliferation and survival, and metabolic pathways (**Figure 7**) (Cooper & Giancotti, 2019; Z. Sun et al., 2016). ECM stiffness can be sensed by the actin cytoskeleton through integrins which promotes the rearranging and clustering of the focal adhesion proteins (talin, FAK, SRC, actin proteins) and can greatly influence the downstream signaling pathways. Elevated ECM deposition and cross-linking during desmoplasia increase stiffness and combined with integrin overexpression in various cancers, can dramatically alter integrin-mediated signaling and trigger tumor promotion (Deville & Cordes, 2019; Northcott et al., 2018; Z. Sun et al., 2016).

Discoidin Domain Receptors 1 and 2 (DDR1, DDR2) are transmembrane collagen receptors with increased tyrosine kinase activity under a high abundance of collagen in the tumor microenvironment. In breast cancer, the interaction of collagen with DDR1 activated the JAK/STAT3 pathway which led to the manifestation of cancer stem cell traits and drove metastatic growth (Gao et al., 2016).

uPARAP/Endo180 belongs to the mannose receptor family and can bind and internalize collagen through clathrin-mediated endocytosis. Once in the endosomal/lysosomal compartment, collagen is degraded in a process dependent on the lysosomal cysteines proteases. uPARAP is therefore involved in collagen turnover and its expression in the stromal compartment of breast cancer has been proposed to be a potential bad prognostic marker, as mice deficient for the uPARAP gene has lower tumor burden. However, in most studies,

internalization has been demonstrated with solubilized collagen, and therefore the conformation status and the size of the fragments are not clear. Furthermore, mice deficient in uPARAP are relatively healthy, besides minor defects in bone length, which suggest the existence of alternative compensatory mechanisms for collagen internalization *in vivo* (Curino et al., 2005a; East et al., 2003; Engelholm et al., 2003; Nielsen et al., 2017).

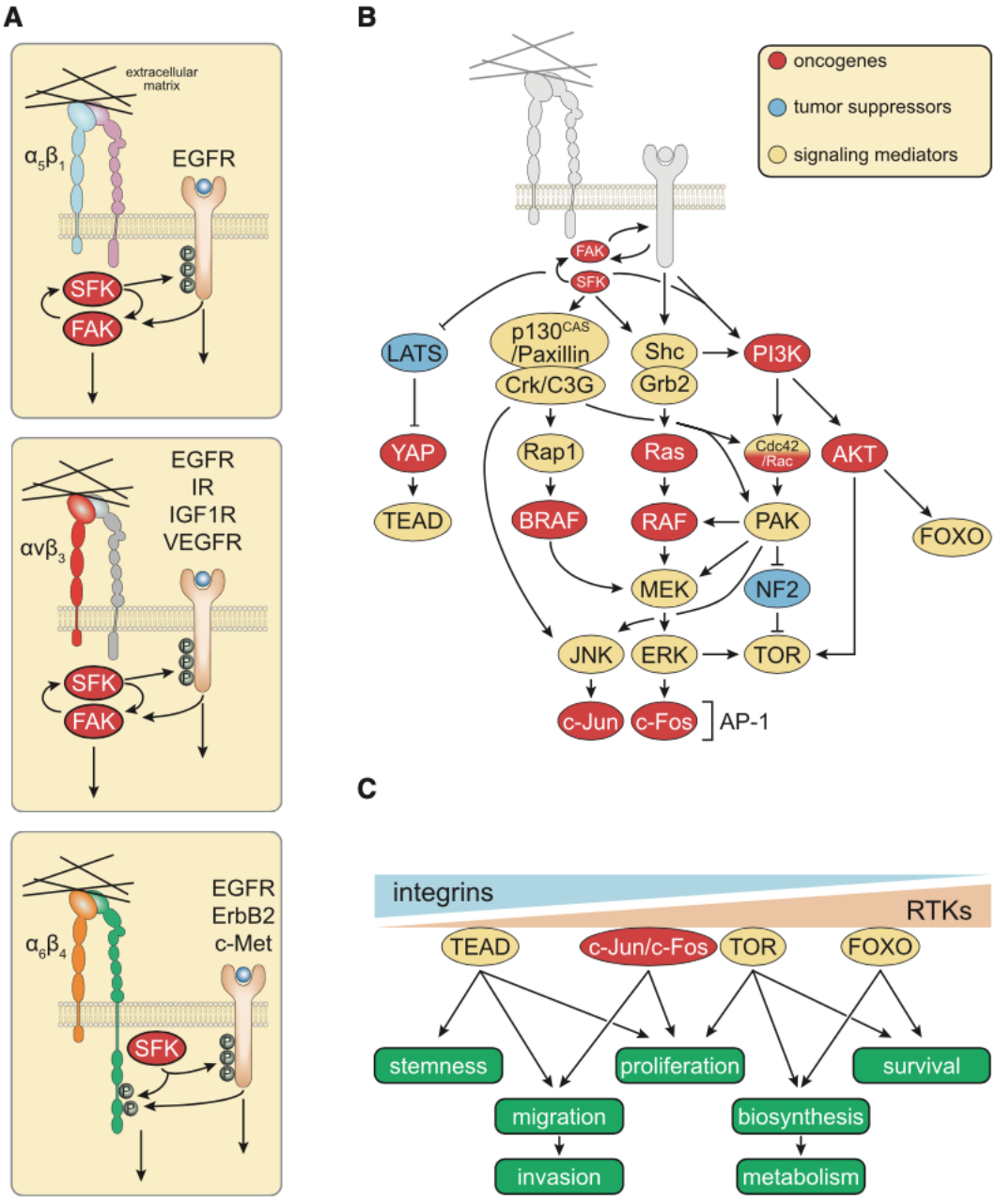

Figure 7: Integrins are bidirectional cell-surface signaling molecules. *(A) Scheme of the joint integrin-RTK signaling pathways occurring at the plasma membrane. FAK and SFK downstream of integrins phosphorylate the P-loop of RTKs and prime them for ligand-induced activation. Conversely, the RTKs also phosphorylate FAK and SFK in a positive feedback loop.*

(B) Signaling pathways induced by downstream joint integrin-RTKs activation. Integrin and RTKs cooperate to activate the PI3K/AKT/TOR, MAPK and the p130/Paxillin pathway to induce nuclear translocation of the transcription factors C-jun, c-Fos as well as Yes-associated protein (YAP) (C) which in turn (co-)activate several critical cellular functions (Cooper & Giancotti, 2019).

2.2.2.2. Tumor cell migration and invasion are supported by ECM remodeling

Promotion of integrin-based focal adhesions by cross-linked collagen induced the invasion of transformed mammary epithelial cells (Levental et al., 2009). Upon TGF-β treatment, breast cancer cells actively secrete WISP1 to directly remodel and linearize collagen fibers promoting cell invasion and spontaneous metastasis formation (Jia et al., 2019).

The basement membrane represents a physical barrier to dissemination and its proteolysis and remodeling promote tumor cell migration in the stroma, which is a clinical sign that the DCIS has evolved to an IDC (Risom et al., 2022b). In breast tumor cells, proteolytic degradation of the basement membrane is mediated by MT1-MMP (Castro-Castro et al., 2016; Lodillinsky et al., 2016). In the interstitial matrix, metalloprotease-mediated degradation of the ECM components opens migratory tracks and reduces mechanical tension on the nucleus, the biggest and stiffest organelle in the cell, therefore activating active migration (Ferrari et al., 2019).

Tumor cells can be located at distant sites from blood vessels and be deprived of nutrients and oxygen. Furthermore, a fibrotic and stiffened ECM can induce the collapse of blood vessels or block blood flow to tumor cells (Jain et al., 2014b). This hypoxic microenvironment induces the activation of hypoxia-inducible transcription factor 1 (HIF-1) which promotes an angiogenic switch, tumor growth, and stromal cell recruitment but also ECM remodeling through regulation of various MMPs (including MT1-MMP) (Muñoz-Nájar et al., 2006; Semenza, 2016). This process restores an (almost) adequate blood flow to the tumor but can also promote metastasis by the dissemination of tumor cells in the vascularization network.

2.3. Breast cancer metastatic program

2.3.1. The epithelial to mesenchymal transition

Approximately 90% of breast cancer deaths are caused by local invasion and distant metastasis of tumor cells. At present, we do not have sufficient knowledge on the transition between a non-invasive lesion (DCIS) to IDC although the epithelial to mesenchymal transition (EMT) has been hypothesized to have a significant role in the switch to an invasive phenotype and the ability to form metastasis (Hanahan & Weinberg, 2011). EMT is a vital process during embryonic development and wound repair wherein epithelial cells lose their epithelial

characteristics and adopt a mesenchymal invasive phenotype. Loss of epithelial integrity is mediated by a cadherin switch where E-cadherin (a protein involved in adherent cell-cell junctions) is transcriptionally downregulated and N-cadherin is upregulated. The EMT is also characterized by a loss of apicobasal polarity in favor of an elongated, migratory-favorable spindle shape morphology with a deep reorganization of the cytoskeleton. Cells also acquire invasive properties mediated by transcriptional upregulation of MMPs (such as MT1-MMP, (Pang et al., 2016)) and genes involved in collagen and fibronectin reorganization (Risom et al., 2022a).

This phenotype is underlined by molecular changes regarding the expression of target genes (**Figure 8)**. The downregulation of E-cadherin in the cadherin switch is accompanied by an increase in the expression of N-cadherin. Loss of E-cadherin destabilizes cell-cell tight and adherent junctions, as well as cell-matrix junctions, and has been shown to be sufficient to promote the progression from DCIS to IDC (Derksen et al., 2006). N-cadherin is also a structural element of adherent junctions but is found in motile and less polarized non-epithelial cells such as neural cells or endothelial cells. Homotypic N-cadherin interactions on opposing cells activates Rac GTPase, which stimulates local actin polymerization and the formation of invasive membrane protrusions (Ouyang et al., 2013; Yap & Kovacs, 2003). N-cadherin expression in tumor cells has been shown to promote collective migration and collective invasion in a 3D ECM (Klymenko et al., 2017; Kuriyama et al., 2016; Mrozik et al., 2018). Furthermore, N-cadherin binds and stabilizes fibroblast growth factor receptors (FGFR) which potentiates the downstream MAPK pathway promoting cell survival and proliferation but also promotes metastasis (Mrozik et al., 2018; Qian et al., 2014; Wheelock et al., 2008). Cell shape and movement are structured by the cytoskeleton which is composed of actin microfilaments, intermediate filaments, and microtubules. Keratins are a type of epithelial-specific intermediate filaments that provide structural support to epithelial cells by linking cell-cell (desmosomes) and cell-matrix (hemidesmosomes) junctions to the plasma membrane and the nucleus. Vimentin is another type of intermediate filament expressed in mesenchymal cells. Overexpression of vimentin in epithelial cells induces morphological change towards a mesenchymal shape and a loss of desmosomes. Keratins are often downregulated during the EMT process, while the expression of vimentin is increased (Datta et al., 2021). Another mesenchymal characteristic accompanying EMT is the upregulation of genes involved in matrix remodeling, such as the synthesis of ECM components (fibronectin, collagen type I) but also matrix digesting proteinases (MMPs). TGF-β-induced EMT in breast cancer cell lines induces the upregulation of MMP-2 and MMP-9 expression and activity (Y.-H. Lee et al., 2008). Recent evidence suggests that MT1-MMP cooperates with TGF-β to trigger SNAIL-induced EMT (Djediai et al., 2021).

EMT is controlled by the SNAIL, ZEB, and basic helix-loop-helix (E47, Twist) families of transcription factors and are under tight regulation by various signaling pathways. TGF-β produced by both stromal and tumoral cells is a potent inducer of EMT by binding to its receptors (type I and II serine-threonine kinases receptors, TBRI and TBRII) at the surface of cancer cells. Activated TBR stimulates the nuclear translocation of the SMAD2/3/4 complex and the transcriptional upregulation of Snail, Slug, and Twist. The Wnt /β-catenin and the TNF-a/NK-kB signaling pathways also play a critical role in the activation of the EMT program by stabilizing the Snail transcription factor. Once activated these transcription factors bind to consensus E-box DNA sequences and downregulate the expression of target genes (Buyuk et al., 2022).

Mesenchymal cells can also undergo the opposite process of EMT, the mesenchymal to epithelial transition (MET), a process thought to support the formation and implantation of metastasis in distance sites. By triggering MET, even highly mesenchymal cells such as the MDA-MB-231 (a triple-negative breast cancer cell line) clustered together *via* the establishment of cell-cell junctions in association with downregulation of vimentin and SNAIL (Jo et al., 2009). EMT is not a binary process in which cells are either 100% epithelial or mesenchymal, but it rather represents a spectrum of distinct hybrid states (**Figure 8).** Primary mammary tumor cells showed diverse states of EMT (defined by their surface markers) with different invasive and metastatic characteristics. Interestingly, cells that exhibited hybrid epithelial-mesenchymal gene expression were most efficient in forming metastases. This existence of distinct EMT states *in vivo* has implications not only for our understanding of cancer biology (tumor heterogeneity, collective cell invasion, metastasis formation) but is also another facet of tumor cells that could explain the resistance to therapy (Pastushenko et al., 2018).

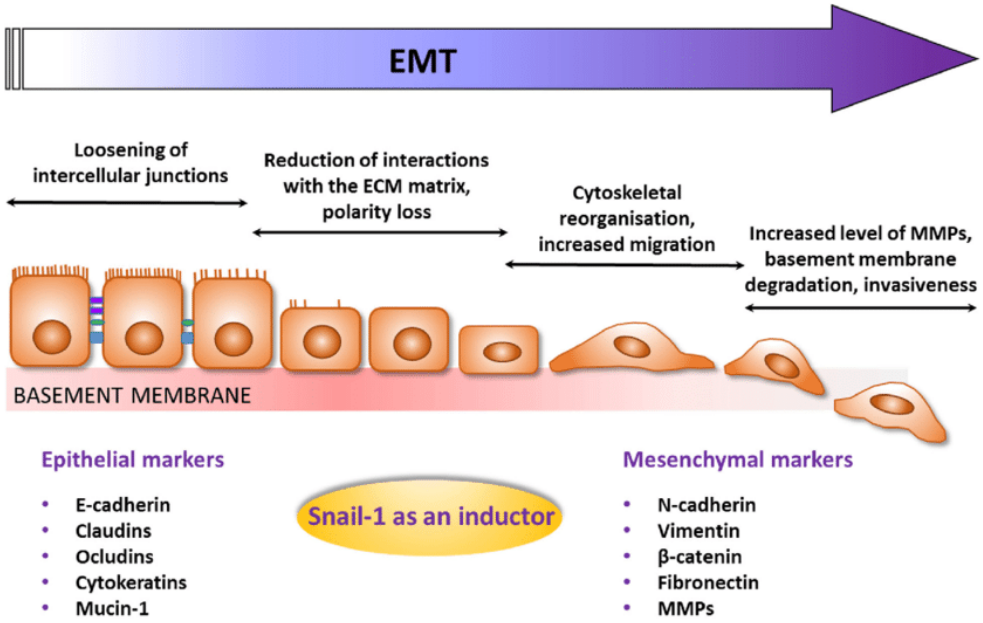

Figure 8: Schematic representation of the phenotypic and molecular modifications during the epithelial to mesenchymal transition. *During EMT reduced E-cadherin expression and deep cytoskeleton reorganization mediated by the activity of transcription factors Snail/ZEB/BHLH induces a loss in cell-cell and cell-matrix adhesions, disrupting the epithelium and favoring a spindle shape phenotype over the typical epithelial apico-basal polarity. Increase in the expression of MMPs potentiates the invasiveness of mesenchymal cells. Note the presence of intermediate states where cells express mesenchymal genes while retaining some epithelial traits* (Wieczorek-szukala & Lewinski, 2021)

2.3.2. Mechanisms of tumor cell invasion

Organs (including tumors) are composed of a variety of cell types influenced by a vastly heterogeneous and ever-changing environment. The characterization of cell migration was historically focused on the migration in 2D models of cell culture. However, migration on surfaces is rather the exception that the rule *in vivo*. The concepts acquired from these studies are important but have now to be applied to 3D models to consider the complexity of organs and tumors. Advances made in live fluorescence imaging allowed us to move into the third dimension and highlighted novel interactions between cell and matrix in the migration process.

Cells adapt to changes in their immediate environment by sampling chemical and physical cues, mostly through the integrin-mediated interactions with the ECM. Focal adhesions are indeed a mechanosensing signaling hub that sense and adapts to mechanical constraints in the ECM. In 2D models, the molecular clutch hypothesis hypothesized by Mitchison and Kirschner is a model explaining how focal adhesions are involved in actin-dependent traction force propagation (**Figure 9**). At the leading edge of the migrating cell, without proper attachment of the focal adhesion to the actin microfilaments, the retrograde flow

of F-actin is greater than the rate of G-actin polymerization, resulting in the absence of cell protrusion. However, engagement of focal adhesions with the actin microfilament significantly reduces local actin retrograde flow, stabilizing and promoting actin polymerization to create protrusions (lamellipodia) by applying forces against the cell membrane. On a 2D substrate, lamellipodia are spread out like a flat pancake with many stress fibers and focal adhesions stabilizing the structure. The cell moves forward over the focal adhesion clutch which serves as a traction force. At the cell rear, the focal adhesions are disassembled to detach the cell from the ECM and recycled back at the front to help in the formation of new membrane protrusions (Doyle et al., 2022; Ridley et al., 2003).

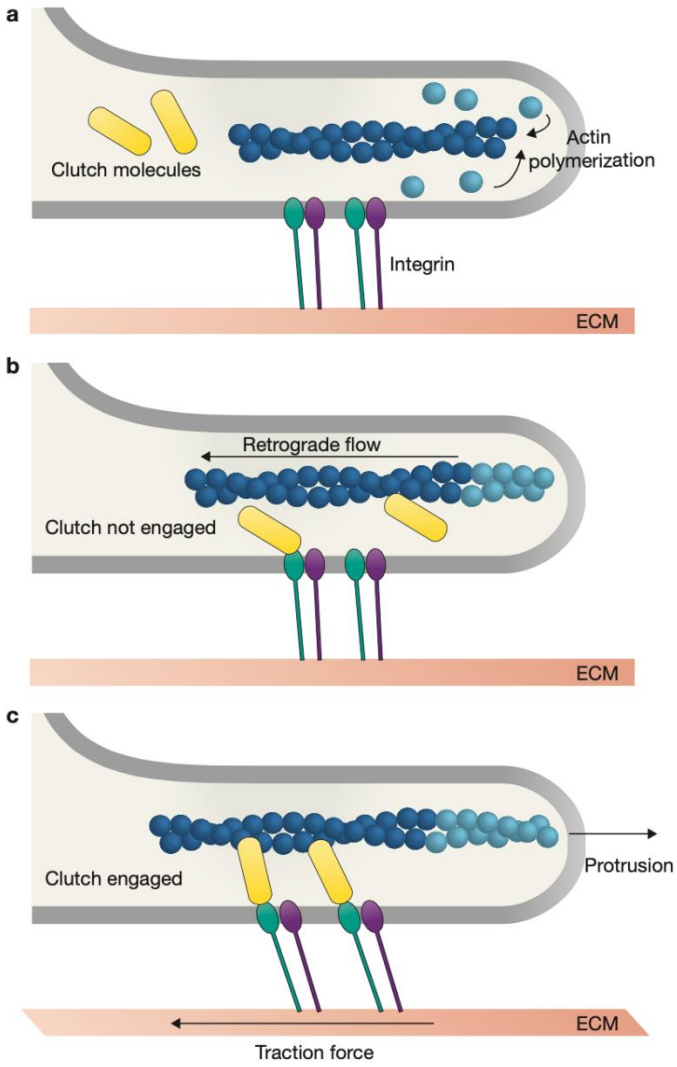

Figure 9: The molecular clutch hypothesis. (a) *G-actin monomers (light blue) are integrated to the F-actin filament (dark blue). Integrins (green and purple) are at the plasma membrane (grey) and engaged with the ECM (orange). (b) If the molecular clutch is not engaged and actin filaments are not connected to the integrins and the ECM, then rapid actin retrograde flow occurs and there are no net protrusion or traction forces on the ECM. (c) Once the clutch is*

engaged, F-actin filaments are stabilized, and the forces generated by actin polymerization led to protrusion and traction force on the ECM. (Case & Waterman, 2015).

The first main mode of 3D cell migration characterized and the most resembling 2D migration is the mesenchymal migration mode in rich 3D environments. Actin polymerization at the leading edge of the cell generates invasive protrusions (the lamellipodia) and integrin-based focal adhesions for ECM anchoring. Contrary to the wide lamellipodia produced in 2D substrate, mesenchymal cells in 3D matrix extrude a protrusion on a straight axis following collagen orientation. Clusters of β1 integrin were found at each site of contact between the cell protrusion and the ECM (**Figure 10**). Through these adhesions and the contractile activity of myosin II, mesenchymal cells apply a constrictive mark (a pre-stain) on the matrix along the protrusion that orients and polarizes the cell (Doyle et al., 2021). Other ECM parameters such as pore sizes or fibril alignment can impede mesenchymal cell migration. Matrix pores too small can impede the passage of the nucleus, the biggest and stiffest organelle of the cell. As such, mesenchymal cells cleave the matrix fibers and expand the matrix pore size to allow the nucleus to go through by secreting soluble MMPs and enriching their invasive protrusions with membrane-bound MMPs, which cleave the fibers ahead of the nucleus and facilitate cell migration (Infante et al., 2018; Wolf et al., 2003, 2007) (**Figure 10**).

Amoeboid migration is the second main 3D cell migration phenotype observed, characterized by extensive actin-based or hydrostatic-mediated cell body deformations (blebs) and low adhesion to the ECM (**Figure 10**). The third and less studied 3D cell migration mode is a hybrid between the two first, termed lobopodial migration. Cells generate lobopodia which are hydrostatic-mediated cell protrusions resembling lamellipodia while pulling on the ECM. The pressure exerted to form the lobopodia structures is generated at the rear of the cell by the nucleus which moves forward like a piston. Cells migrating in a 3D environment show high plasticity and can switch between modes of migration, most likely under the influence of the microenvironment (matrix pore size, fibril alignment, cross-linking, viscoelasticity). For instance, confinement in a low-adherent chamber or MMP inhibition was enough to induce immediate mesenchymal to amoeboid transition (Yamada & Sixt, 2019).

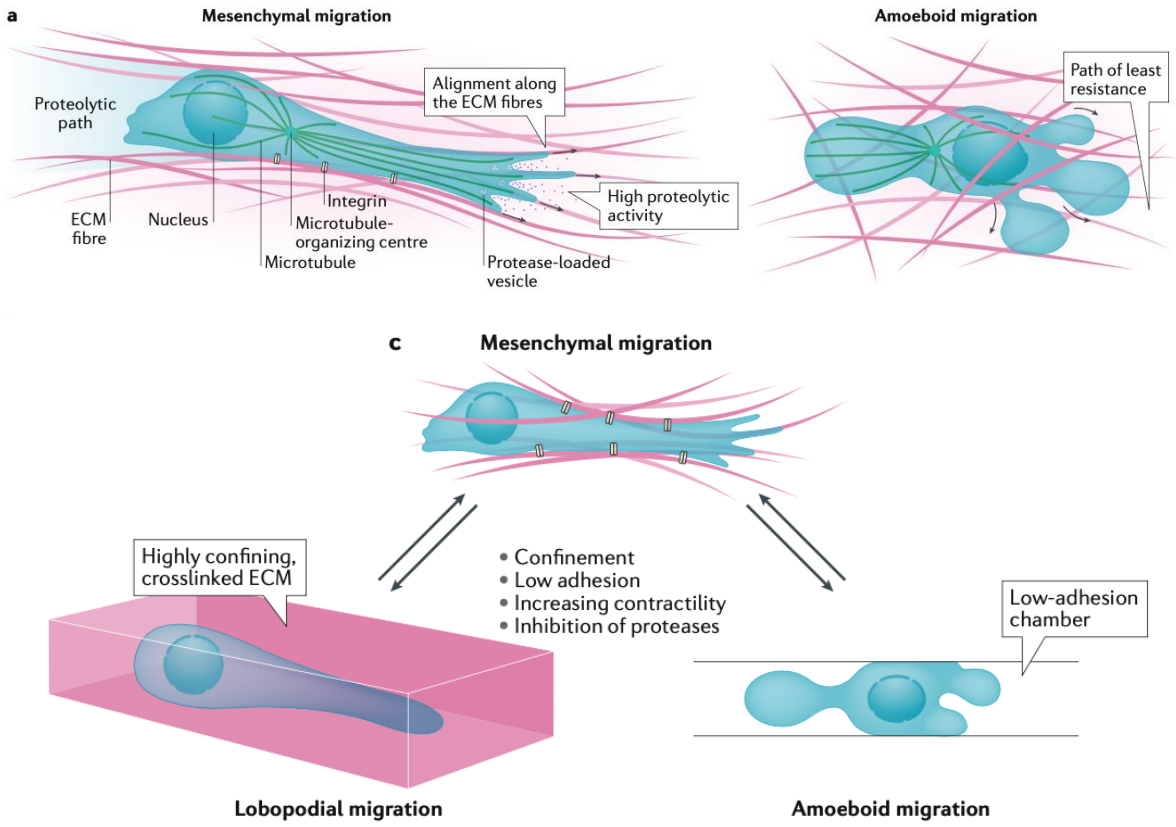

Figure 10: Mesenchymal *vs* amoeboid migration. *(a) Mesenchymal cells are aligned parallel to the ECM tension lines and migrate in the confined environment by degrading the matrix. Amoeboid cells do not degrade the ECM fibers but protrude through the matrix pores and find the path of least resistance. (c) Cell migration is dictated by the environment and for example, various factors such as low-adhesion, confinement, and inhibition of matrix-degrading enzymes can lead to a switch from mesenchymal migration to lobopodial or amoeboid migration* (Yamada & Sixt, 2019).

3. Invadopodia, membrane protrusions mediating matrix proteolysis, and breast cancer invasion

3.1. Invadosomes: good from afar but far from good

3.1.1. An umbrella term for regrouping nearly identical cellular structures

Invadopodia were first observed in 1985 in Rous-sarcoma virus-transformed fibroblasts where several focal adhesion proteins (integrins, α-actinin, vinculin, myosin…) underwent a puzzling reorganization and clustering at the ventral membrane in contact with the substratum. Actin filaments and actin-regulating proteins also re-localized to the same place and formed small actin-rich membrane protrusions which reorganized and degraded the underlying ECM.

Invadosome is a generic term that regroup several structures that are defined as actin-based force-producing cell-ECM contacts that degrade and reorganize the ECM (Cambi & Chavrier, 2021). Invadosomes is thus an umbrella term for regrouping podosomes formed by non-transformed cells and invadopodia found in invasive tumor cells (Cambi & Chavrier, 2021; Paterson & Courtneidge, 2018).

3.1.2. Cut from the same cloth?

Invadosomes are characterized by a force-producing actin core enriched in barbed actin filaments. These filaments are generated by the N-WASP (or related WASP) -mediated activation of the actin nucleator Arp2/3 complex. The protrusions are enriched in matrix metalloproteases such as MT1-MMP in invadopodia and podosomes and confer to the invadosomes an ECM proteolysis activity that contributes to the invasive capacity of these structures.

On glass coverslips and 2D matrices resembling BM, podosomes present a round shape with a diameter of 0.5 to 1 µm. They are characterized by a core of F-actin and associated proteins (WASP/N-WASP, CDC42), and MMPs while β1, β2, and β3 integrins, associated focal adhesion proteins (paxillin, talin, vinculin, α-actinin) and signaling proteins (PI3K, SRC, Pyk2/FAK) are clustered on the periphery of the podosome. Integrin engagement with the substrate stimulates SRC activation *via* PKC resulting in the activation of the CDC42/WASP/Arp2/3 signaling axis and consequent actin polymerization. The resulting protrusion, enriched in MMPs, locally degrades, and invades the matrix within minutes (Linder & Kopp, 2005) (**Figure 11**). However, there is a great diversity in mesoscale podosome morphologies dictated by the cell type in question. Typically, immune, and endothelial cells form clusters of podosomes (or rosettes) that breach the basement membrane during immune infiltration or angiogenesis, while osteoclasts form rings and belts that evolve into a specialized sealing zone during the differentiation period which delimitates the bone-resorbing zone (Linder & Kopp, 2005; van den Dries et al., 2019). Mesoscale organization of the podosome

also depends on the ECM topography as cells in a reconstituted 3D matrix form linear podosomes aligned on the fibers (Cambi & Chavrier, 2021; van den Dries et al., 2019). It should be noted that podosomes also form during pathogenic processes such as excessive podosome-mediated bone degradation resulting in osteoporosis (Guimbal et al., 2019; Vives et al., 2015).

Invadopodia are cancer cell-specific contact sites between the membrane and the ECM fibers. These types of protrusion can last for more than an hour and are characterized by local MT1-MMP-mediated matrix degradation. Invadopodia formed in the breast cancer cell line MDA-MB-231 cultured in a 2D ECM model present a striking resemblance to podosomes with a dotty-like perinuclear distribution. Although the actin organization of podosomes is of a high degree of complexity, the actin meshwork in invadopodia is rather rudimentary with Arp2/3 mediating branched actin polymerization directed on the plasma membrane to exert forces on the substratum. In a 3D environment, the organization of the invadopodia also shifts to a non-protrusive linear structure following type I collagen fibers. The ultrastructure organization of curvilinear invadopodia showed a distinct enrichment in branched actin on the cytosolic side of the plasma membrane in association with the inner side of the curved ECM fiber (**Figure 11**). In a 3D type I collagen matrix environment, invadopodia structures form in a ring-like shape (like barrel hoops) on the cell body ahead of the nucleus and extended to widen the matrix pores in association with MT1-MMP collagenolytic activity (Cambi & Chavrier, 2021; Ferrari et al., 2019; Infante et al., 2018). Invadopodia activity has been shown to promote tumor growth and metastasis formation in breast cancer (Castro-Castro et al., 2016; Eddy et al., 2017; Lodillinsky et al., 2016), showcasing its importance in tumor biology and the therapeutical requirement to further study this invasion mechanism.

3.2. Initiation and formation of invadopodia

Current models derived from adenocarcinoma cells define three stages in invadopodia formation: initiation of a precursor core, stabilization of the invadopodia precursor, and finally maturation of the invadopodia.

3.2.1. Triggering of invadopodium precursor core initiation

Exposure to growth factors was shown to be sufficient to initiate invadopodia formation in adenocarcinoma cells by binding to their respective tyrosine kinase receptors and activation of signaling pathways (PI3K, SRC, JAK/STAT) (Augoff et al., 2020). TGF-β and PDGF were also shown to induce Twist1-dependant invadopodia initiation, linking invadopodia to epithelial to mesenchymal transition (Eckert et al., 2011). The ECM itself is also a potent modulator of invadopodia formation depending on the considered component and topology. The attachment

of integrin α5β1 to fibronectin has been shown to be a potent inducer of invadopodia formation while attachment of integrin α3β1 to laminin was shown to repress it (Beaty & Condeelis, 2014; Murphy & Courtneidge, 2011). While integrin α2β1 integrin and collagen receptor DDR1 are necessary for punctiform invadopodia formation on gelatin, initiation of linear invadopodia does not and relies instead MT1-MMP, showcasing once again the importance of the ECM topology (Ferrari et al., 2019).

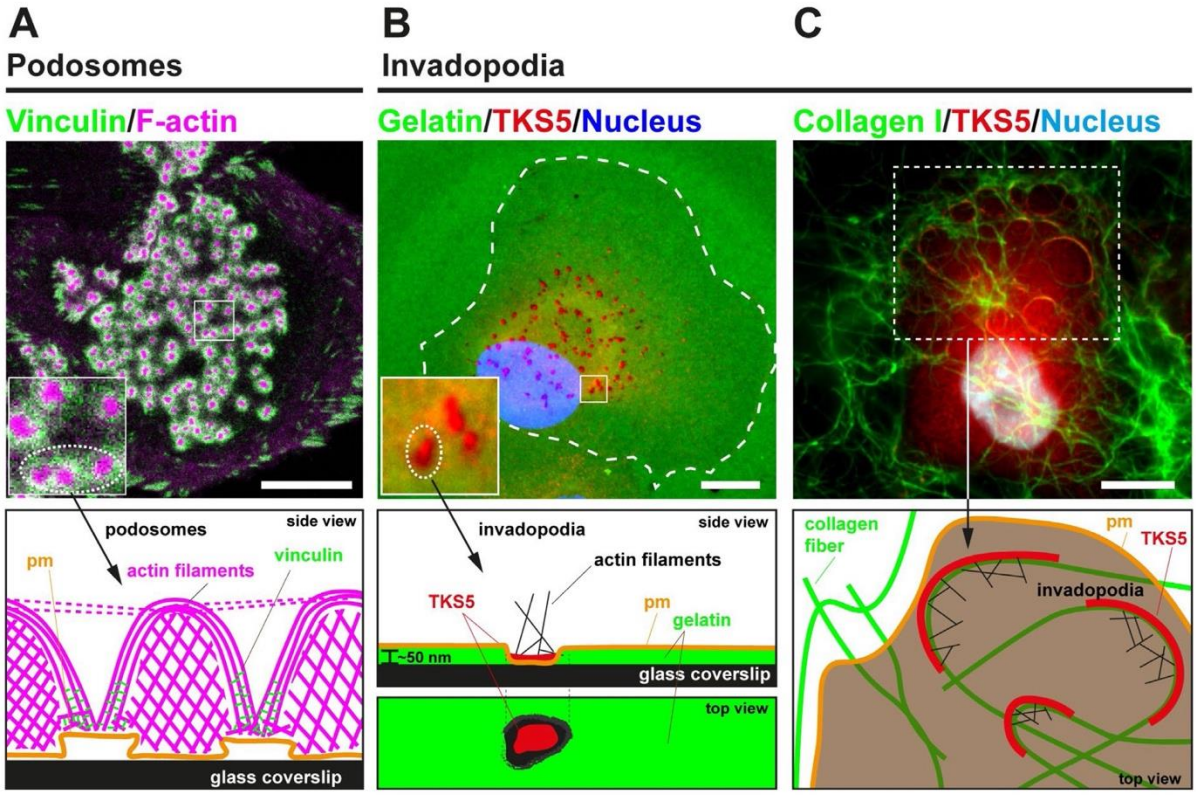

Figure 11: The architecture of actin-rich invadosomes is dictated by the environment. *(A) Immunofluorescence image of vinculin (green) and actin (magenta) forming podosomes at the adherent surface of a human monocyte-derived immature dendritic cell plated on a glass coverslip. The actin architecture of podosomes in a side view is schemed in the lower panel. (B) Immunofluorescence image of the invadopodia marker Tks5 (red) in triple negative breast cancer (TNBC) cells (MDA-MB-231) plated on a 2D matrix (fluorescent cross-linked gelatin, green). The architecture of the punctiform invadopodia (side view and top view) is schemed on the lower panel and show small, branched actin patches associated with Tks5 and deep local ECM degradation. (C) Immunofluorescence image of the Tks5 (red) in MDA-MB-231 cells plated on a thick layer of fluorescently-labeled type I collagen matrix (green). The scheme below shows the linear invadopodia formed alongside the collagen fibers with the actin network*

polymerizing on the curvilinear side. Scale bars, 10 µm. pm, plasma membrane. (Cambi & Chavrier, 2021).

The activation of the PI3K, SRC or CDC42 signaling pathways downstream of integrin engagement and growth factors binding to their receptors is the triggering signal for actin polymerization and invadopodia initiation. N-WASP and Arp2/3 activation downstream of Cdc42 stimulates the formation of a branched actin network (Castro-Castro et al., 2016; Colombero et al., 2021; Monteiro et al., 2013; Zagryazhskaya-Masson et al., 2020) (**Figure 12**). As such, depletion of CDC42 guanine exchange factor FGD1 repressed invadopodia formation (Zagryazhskaya-Masson et al., 2020) similarly to the expression of a dominant negative variant of Cdc42 (di Martino et al., 2014), or silencing of N-WASP (Monteiro et al., 2013). In the same line, actin branch-stabilizing protein cortactin is critical for invadopodia formation. Cortactin undergoes several post-translational modifications such as activatory phosphorylation on tyrosine 421 that triggers the recruitment of Nck1 adaptor protein, N-WASP and cofilin to the invadopodia precursor, thereby promoting the formation and turnover of branched actin filaments (Oser et al., 2010). Actin debranching factors such as coronin 1C also have a role in invadopodia as its depletion reduces the number of invadopodia formed in triple-negative MDA-MB-231 breast cancer cells while high expression in breast cancers is a bad prognostic factor as it correlates with increased invasiveness (Castagnino et al., 2018). The core invadopodium precursor is formed in 15 to 20 seconds and is highly unstable (Eddy et al., 2017).

3.2.2. Stabilization of the invadopodium core precursor

The precise sequence of invadopodium core stabilization remains unknown. However, the recruitment of adaptor protein tyrosine kinase substrate with five SH3 domains Tks5 is crucial for invadopodia core initiation and stabilization as its depletion completely abolishes the formation of invadopodia (Eddy et al., 2017; V. P. Sharma et al., 2013). Due to its fundamental role in invadopodia formation, Tks5 is the most exclusive invadopodia marker identified so far. Tks5 (or FISH) is an adaptor protein coded by the SH3PXD2A gene that forms 3 splice variants. The protein is composed of three main regions: an N-terminal Phox homology (PH) domain that binds to specific membrane phosphoinositides and is present only in the Tks5α isoform, five Src homology 3 (SH3 domains), and multiple proline-rich regions (PRR). Tks5β and Tks5short differ in the number of amino acids present in the N-ter domain. Tks4 is a related protein containing 4 SH3 domains encoded by the SH3PXD2B gene and has a role in invadopodia formation albeit not to the same extent as Tks5 (Zagryazhskaya-Masson et al., 2020).

Activation of the PI3K signaling cascade by growth factors and integrin engagement during invadopodium initiation also leads to the formation of phosphoinositide-3,4-biphosphate (PI(3,4)P2) at the plasma membrane. PI3K phosphorylates phosphoinositide-4,5-biphosphate (PI(4,5)P2) in phosphoinositide-3,4,5-triphosphate (PI(3,4,5)P3) which is then dephosphorylated by 5'-inositol phosphatase SHIP2 to PI(3,4)P2 (V. P. Sharma et al., 2013). Through its PX domain, Tks5 binds to PI(3,4)P2 which brings it closer to the plasma membrane. Tks5 first SH3 domain interacts with CDC42-GEF FGD1, the fourth SH3 domain binds to N-WASP and finally SRC-mediated TKS5 phosphorylation stimulates its interaction with Nck1, allowing the recruitment of Tks5 and stabilization of the invadopodia F-actin core precursor (Oikawa et al., 2008; Stylli et al., 2009; Zagryazhskaya-Masson et al., 2020) (**Figure 12**). 3D super-resolution microscopy (SRM) in MDA-MB-231 cells embedded in a dense fibrillar collagen matrix suggest that at the level of the invadopodia, TKS5α is punctiform and at a 500 nm distance from the plasma membrane while the cortical actin assembly extends further in the invadopodia body (Iizuka et al., 2020).

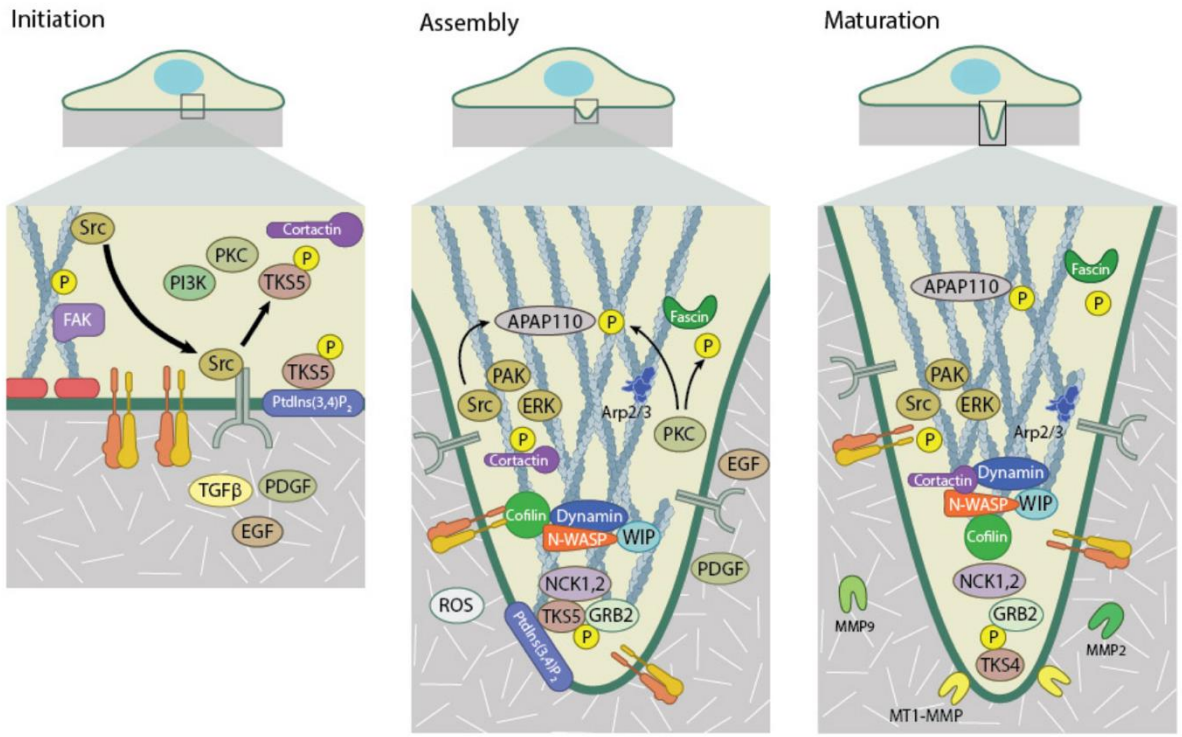

Figure 12: The three stages of invadopodium formation. *Initiation starts with Src activation downstream of integrin and growth factors signaling and leads to the formation of a core actin polymerization complex (N-WASP/Arp2/3/Cofilin/Cortactin) quickly stabilized by Tks5 scaffold protein at the adherent plasma membrane. During the assembly maturation step, branched actin polymerization promotes the formation of an invasive protrusion which stimulates the recruitment of new pools of actin polymerization factors in an auto feedback loop. Maturation*

of the invadopodia consists in the exocytosis and enrichment of matrix degrading enzymes promoting tumor cell invasion (*What Mechanisms Drive Invadopodia Extension? | MBInfo*, n.d.).

3.3. Maturation and disassembly of invadopodia: TKS5, metalloproteases, disassembly

3.3.1. ECM-degrading proteases and their roles in invadopodia maturation

Invadopodia function requires the ECM degradative abilities of proteases (**Figure 12**). Three superfamilies of matrix proteases have been associated with invadopodia so far: the zinc-endopeptidases superfamily containing MMPs and ADAMs proteases, the cathepsin proteases found mainly in endo/lysosomal compartments, and the serine proteases enzymes containing a histidine-serine-aspartate triad in their catalytic domain and cleaving a wide variety of substrates.

Given their critical role in invadopodia ECM-degrading function, the following chapter will be devoted to a detailed description of MMPs (especially MT1-MMP). The ADAMs are a family of transmembrane sheddases proteolytically processing cellular and ECM components and regulating cell behavior (Díaz et al., 2013). Among the 34 members identified up until now, ADAM12 and ADAM19 were found to localize at invadopodia by interacting with Tks5 (Abram et al., 2003), and knockdown of ADAM12 severely reduced invadopodia formation (Eckert et al., 2017).

Due to their main localization in acidic endo/lysosomal compartments, cathepsins were considered for a long time to mediate the bulk degradation of lysosomal proteins. Recent studies found cathepsins in the intracellular milieu influencing cell death and inflammation but also exocytosed in the extracellular environment where they mediate the degradation of ECM proteins (Sobotič et al., 2015). Cathepsins are classified according to the amino acid present in their catalytic site: serine cathepsins (A to G), aspartyl cathepsins (D and E), and cysteine cathepsins (B, C, F, H, K, L, O, S, V, W, Z). Lysosomes containing cathepsin B have been found to fuse with invadosomes and enhance matrix degradation capacities in v-Src-transformed fibroblasts (Tu et al., 2008). Finally, among the diverse serine proteases, seprase (fibroblast activation protein-a, FAPa) and Dipeptidyl peptidase IV (DPP4) are two of the most recognized ECM degrading serine proteases found at invadopodia (Ghersi et al., 2006). Recent work using 3D SRM revealed a close association of cathepsins and MMPs with Tks5α in the invadopodia, a peculiar position as ECM degradation could be expected to be at the advancing tip of the invadopodia. Exosome delivery of these proteases is a hypothesis advanced by the authors to explain their unexpected position in the invadopodia (Iizuka et al., 2020).

3.3.2. Disassembly of the invadopodia

While the formation of the invadopodia has been (and still is) extensively studied (see above), very little is known about the disassembly and the turnover of invadopodia structures. Given the central and fundamental role of the actin dynamics in invadopodia function, studies have focused on the role of actin regulators in the disassembly of the invadopodia. Silencing of RhoG (a GTPase controlling the actin cytoskeleton) has been shown to increase the number of punctiform invadopodia per cell in breast cancer, as well as their lifetime which suggest that RhoG is an inhibitor of invadopodia. RhoG phosphorylates paxillin which destabilizes invadopodia and promotes its disassembly (Badowski et al., 2008; Goicoechea et al., 2017). Several studies pointed to the role of Rac1, another GTPase from the Rho GTPase family and revealed that phosphorylation of cortactin (a critical stabilizer of branched actin) by the Rac1-PAK signaling axis destabilized and dissociated the invadopodia (Moshfegh et al., 2014). However, Rac1 and RhoG effects on invadopodia disassembly seem to be context- and cell-dependent as their activity is required for invadopodia formation in some cell lines while they promote invadopodia disassembly in other (Harper et al., 2010; Lin et al., 2014; Moshfegh et al., 2014; Nakahara et al., 2003). Cell cycle inhibitor $p27^{Kip1}$ (CDKN1B) was also shown to promote PAK activity and subsequent cortactin phosphorylation, which also lead to invadopodia disassembly (Jeannot et al., 2017). A recent study also demonstrated the role of phosphatase SHIP1 in dephosphorylation of cortactin and invadopodia disassembly (Varone et al., 2021).

4. Matrix metalloproteases

Cells are constantly modifying the ECM and assuring its homeostasis by synthesis, degradation, and post-translational modifications of its various components. Matrix remodeling is mediated by specific matrix-degrading enzymes as discussed in previous chapters, including MMPs. Their dysregulation can lead to various diseases, including cancers. This chapter is dedicated to the biology of MMPs with a focus on MT1-MMP, a trans-membrane MMP enriched at invadopodia.

4.1. The biology of matrix metalloproteases and their key role in cell invasion

4.1.1. Common features of MMPs

The discovery of MMPs dates back to 1962 when Gross and Lapierre found a diffusible, soluble principle of the tadpole fin skin that mediated the degradation of a collagen gel and participated in the resorption of the tail during its development (Gross & Lapierre, 1962). MMPs are now known as a diverse endoprotease subfamily of the metzincin enzyme superfamily that have various and critical roles in physiological processes such as embryogenesis, morphogenesis, angiogenesis, and wound repair. More than 20 MMPs with a common structure are expressed in human cells but they differ in their localization: some MMPs are soluble and released in the extracellular space, while some are transmembrane proteases (membrane-tethered MMP, MT-MMP). The first common structural domain of MMPs is the N-terminal signal peptide which varies in length and allows translocation of the nascently translated protease through the ER membrane for secretion. Pro-MMPs are expressed as catalytically inactive zymogens by the interaction of the cysteine thiol group of the prodomain and the Zn^{2+} ion in their active site. Conversion to active MMP required proteolytic cleavage of this prodomain by other MMPs. The third common structural feature is the catalytic domain (about 160 aa) containing the aforementioned zinc ion. To the exception of MMP-7, -23, and -26, all MMPs contain an hemopexin-like domain linked to the catalytic domain by a linker of variable length (the hinge region). MMPs can cleave a vast diversity of proteins (ECM components but also various receptors and other proteases including other MMPs) and the substrate specificity is mediated by the hemopexin-like domain. Subsites within the catalytic domain can also confer a certain degree of substrate specificity (Tallant et al., 2010). Tissue inhibitors of MMPs (TIMPs) are a family of 4 proteins (TIMP-1 to -4) that can selectively inhibit MMPs (but also ADAMs and ADAMTs) by forming a stoichiometric 1:1 complex with MMPs. Their C-terminal domain binds to the hemopexin domain of some MMPs while their N-terminal domain binds and inhibits the catalytic site of MMPs (Bonnans et al., 2014; Laronha & Caldeira, 2020) (**Figure 13**).

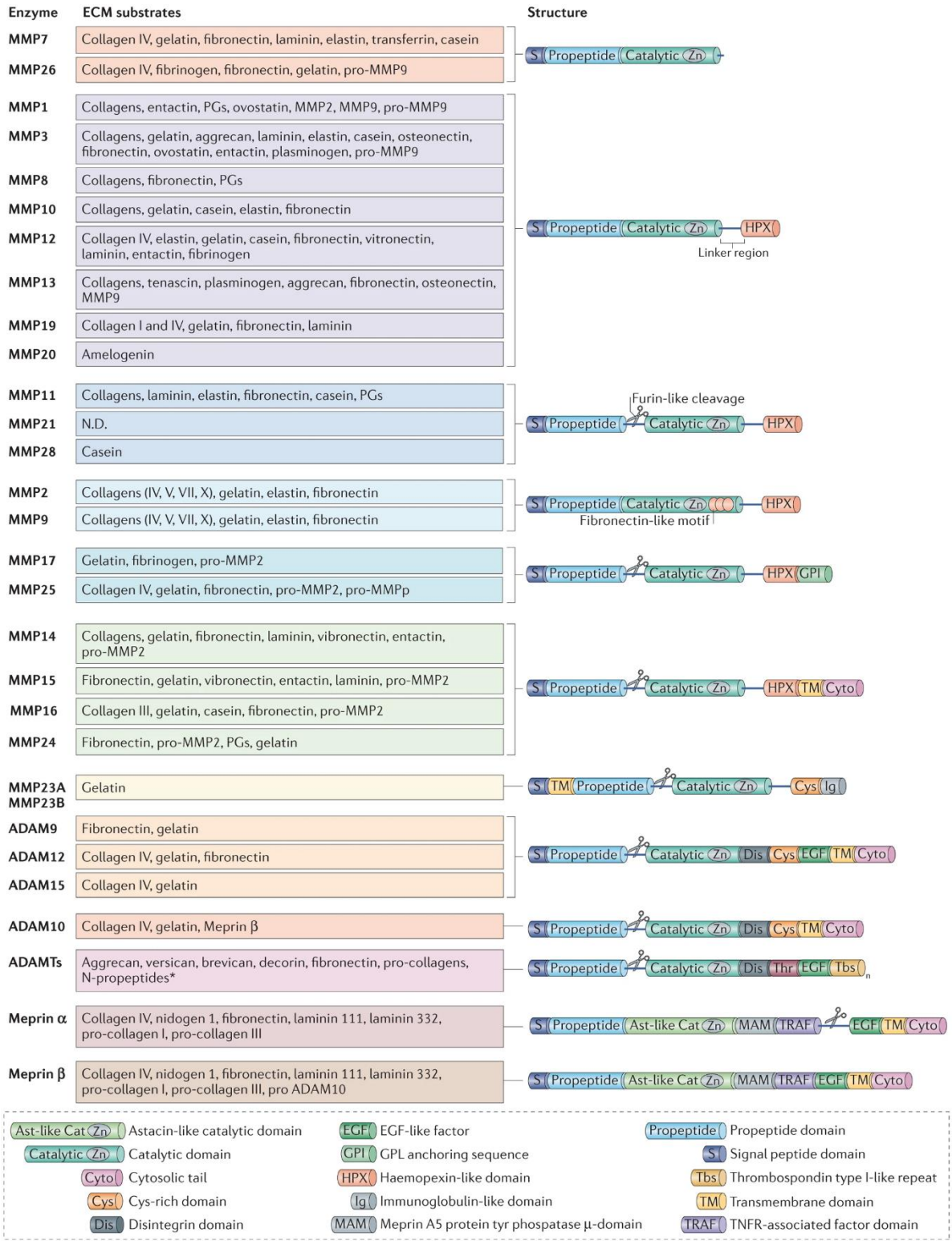

Figure 13: MMPs have a conserved structural core and a wide range of substrates. *MMPs are formed by an N-terminal signal sequence, an inhibitory pro-peptide domain and the Zinc-dependent catalytic domain. Most MMPs have an hemopexin-like domain that determines substrate specificity (see the wide repertoire of ECM substrates for MMPs). Six MMPs have a transmembrane domain (Adapted from* Bonnans et al., 2014).

4.1.2. Soluble MMPs

Most MMPs are soluble and exocytosed in the extracellular milieu. Among them, a subset of MMPs has been found to be upregulated in breast cancer in association with a poor prognosis. Specifically, high expression of MMP-2, -9, -12, -14, and -15 have been defined as adverse factors in mammary tumors (H. Jiang & Li, 2021; Joseph et al., 2020; Lodillinsky et al., 2016; Rossé et al., 2014; Q. M. Wang et al., 2019). *In vitro* assays showed that MMP-9 for instance could degrade type IV collagen and therefore could potentially promote tumor invasion. However, the functional role of these enzymes in tumor progression is complicated at best, as depending on the tumor type, progression can be impaired or stimulated in mice deficient in MMP-2 or MMP-9 (Martin et al., 2008; Pellikainen et al., 2004; Rowe & Weiss, 2009). Furthermore, several lines of evidence implicate MT1-MMP in the activation of pro-MMP-2 *via* the binding of TIMP-2 (Itoh et al., 2001; Rapti et al., 2006; Ries et al., 2007; Strongin et al., 1995).

Finally, recent evidence points to the roles of MMPs in disease progression independently of their proteolytic activity. MMP-1, -2, and -3 were reported to localize at the plasma membrane in different cell types, interacting with and activating various cell receptors through their hemopexin-like domain (integrins, growth factor receptors, …) (Chetty et al., 2010; Conant et al., 2002, 2004; Correia et al., 2013). MMP-9 binds to low-density lipoprotein receptor-related protein (LRP-1) in Schwann cells *via* its hemopexin domain. This interaction has been shown to stimulate the pro-migratory ERK/Akt signaling pathway and promote the migration of Schwan cells in the peripheral nervous system (Hahn-Dantona et al., 2001; Mantuano et al., 2008). These studies fuel the concept of the hemopexin domain emerging as a therapeutical target.

4.2. MT1-MMP: expression, activation zymogen, endocytosis, and exocytosis and traffic regulation

4.2.1. MT-MMPs

Besides soluble MMPs are nine MMPs which are membrane-tethered (MT-MMPs): MMP14 (MT1-MMP), MMP15 (MT2-MMP), MMP16 (MT3-MMP), and MMP24 (MT5-MMP) are anchored to the membrane through a transmembrane domain (TM) followed by a short C-terminal cytoplasmic tail (around 20 amino acids) that serves as a signaling platform, whereas a glycosylphosphatidylinositol (GPI) anchor attaches MMP17 (MT4-MMP) and MMP25 (MT6-MMP) in glycolipid-enriched membrane domains. Their localization therefore confers exquisite control over their dynamics and activity (Turunen et al., 2017). Like their soluble counterparts, MT-MMPs have various and critical roles in physiological and pathological processes. For instance, high stromal expression of MT1-MMP in ovarian cancer was associated with aggressive features (Kamat et al., 2006). Non-invasive COS cells overexpressing MT1-MMP,

MT2-MMP or MT3-MMP acquire basement membrane remodeling and invasive capacities (Hotary et al., 2000). The most extensively studied MT-MMP is MMP14 (or MT1-MMP) due to its pro-invasive role in cancer.

MT1-MMP is synthesized as a 72 kDa zymogen and activated during transport to the plasma membrane by furin-mediated cleavage of its Pro-domain (Remacle et al., 2006; Yana & Weiss, 2000). At the plasma membrane, MT1-MMP can homodimerize through its hemopexin domains which induce auto-activatory proteolysis of the inhibitory N-terminal pro-domain. MT1-MMP has an extensive repertoire of ECM substrates including collagens I to III but also fibronectin, vitronectin, gelatin, laminin 1 and 5, and fibrin. Like many MMPs, MT1-MMP can proteolytically activate other MMPs, such as pro-MMP-2 and pro-MMP-13 (Thakur & Bedogni, 2016). The variety in substrates of MT1-MM actually goes beyond ECM components as demonstrated by mass spectrometry analysis revealing multiple partners of MT1-MMP including members of the tetraspanin family, integrins (α2β1 and αvβ3), and hyaluronic acid receptor CD44 (Gálvez et al., 2002; Grafinger et al., 2021; Marrero-Diaz et al., 2009; Schröder et al., 2013; Suárez et al., 2020a; Thakur & Bedogni, 2016). MT1-MMP-mediated shedding of LDL-1 receptors was also recently shown to accelerate the development of atherosclerosis (Alabi et al., 2021).

MT1-MMP expression is generally low in adults but is found to be re-expressed in cells during specific events, such as in fibroblasts during wound healing or in endothelial cells during angiogenesis (Kang et al., 2019; Quintero-Fabián et al., 2019; Yana et al., 2007). Loss of its collagenolytic activity *in vivo* in mice induces a progressive cranial dysmorphism, dwarfism, osteopenia, osteoclast-mediated arthritis and fibrosis of the soft tissues which eventually led to animal death between 3 and 16 weeks, illustrating the importance of MT1-MMP proteolysis activity in ECM remodeling during development (Holmbeck et al., 1999).

Although gene polymorphism and alterations in gene copy number are relatively rare for MT-MMPs, expression of MT1-MMP is upregulated in various epithelial tumors, especially in invasive breast and prostate carcinoma (Castagnino et al., 2018; Lodillinsky et al., 2016) (**Figure 14**). MT1-MMP and its high collagenolytic activity are also required for the transition from non-invasive to invasive breast tumor in a mice xenograft model (Lodillinsky et al., 2016). Once in the stroma, MT1-MMP is also necessary for the invasion of mesenchymal cells in a three-dimensional type I fibrillary collagen matrix which is resistant to other proteases such as MMP-1, -2, and -8 (Ferrari et al., 2019; Itoh, 2015; Monteiro et al., 2013; Zagryazhskaya-Masson et al., 2020). MT1-MMP has also been implicated in the infiltration and exfiltration of vascular and lymphatic networks which are necessary steps for metastasis formation (Ota et al., 2009; Sabeh et al., 2004).

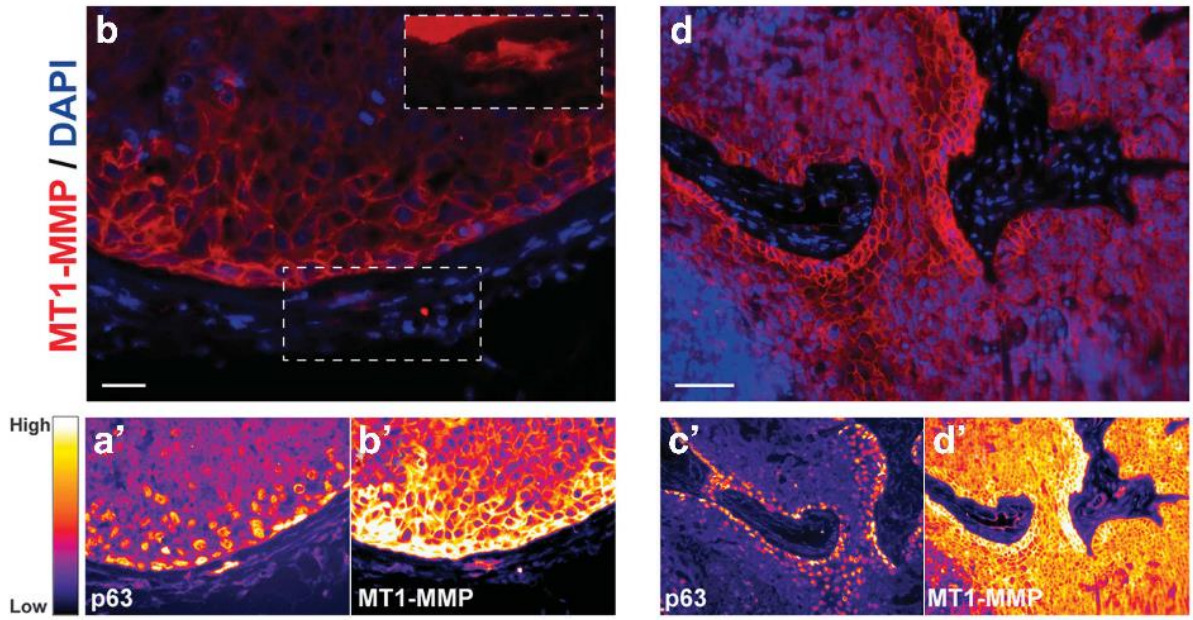

Figure 14: The p63/MT1-MMP axis in breast cancer cell invasion. (a, d) *Sections of intraductal xenografts of DCIS.com tumors immunostained for MT1-MMP (red) or p63 (not shown). Nuclei were stained in blue. (a', b', c', d') Panels show heatmaps of MT1-MMP and p63 expression and emphasizes the increased co-expression of p63 and MT1-MMP on the edge of the tumor* (Adapted from Lodillinsky et al., 2016).

MT1-MMP also functions on other levels to regulate cancer cell growth and invasion such as the shedding of diverse membrane bound receptors. Cleavage of CD44 or of protein tyrosine kinase-7 (PTK7) at the cell surface can lead to cell migration although the mechanisms remain unclear. MT1-MMP also indirectly impinge on cell migration by cleaving laminin 5, releasing the ɣ2 matrikine that binds to and activate the EGF receptor (Knapinska & Fields, 2019; Thakur & Bedogni, 2016).

MT1-MMP is delivered and enriched in invadopodia structures at the invasion front which promotes local, pericellular proteolysis. Binding of MT1-MMP cytoplasmic tail to F-actin is thought to anchor the protease to the invadopodia and creates a tight apposition of MT1-MMP with the ECM components for degradation (Yu et al., 2012). Silencing of MT1-MMP or inhibition of its catalytic activity by the broad metalloproteinase inhibitor GM6001 abolishes the invadopodia expansion and elongation rates, thus preventing the pushing forces normally exerted on the collagen fibers during mesenchymal migration (Ferrari et al., 2019). Due to the unfavorable roles of MT1-MMP activity in many pathological situations as aforementioned, the regulation of the protease cell surface exposure has been extensively studied.

4.2.2. MT1-MMP: example of a regulation of a MT-MMP

4.2.2.1. Regulation of expression and post-translational modifications

An increase in MT1-MMP expression is generally a factor of bad prognosis across a multitude of cancer types. MMP14 gene is located on chromosome 14q11 and, like most other MMPs, consists of 10 exons and nine introns spanning more than 10 kilobases (Lohi et al., 2000). Consensus binding sites for transcription factors include specificity protein 1 (Sp1), early growth response 1 (Egr-1), and NFkB, but contrary to other MMPs, not AP-1, AP-2, no TATA box and no TGF-β inducible element (Haas et al., 1999). Studies investigating the regulation of MT1-MMP expression revealed a vast array of factors controlling MMP14 expression (Alfonso-Jaume et al., 2004; Haas et al., 1999; Lohi et al., 2000). The p53-family transcription factor p63 is necessary for mammary gland development and was reported to induce the overexpression of MT1-MMP thus promoting an invasive program in breast DCIS (Lodillinsky et al., 2016) (**Figure 14**). Recently, interleukin-6/JAK/STAT-mediated activation of p53 was shown to lead to the stimulation of transcription factor Sp1 and a subsequent increase in MT1-MMP expression (Cathcart et al., 2016). On the contrary, transcription factor prospero homeobox 1 (PROX1) is a negative regulator of MT1-MMP expression, as was demonstrated by reduced 3D invasion in spheroids overexpressing PROX1 (Gramolelli et al., 2018).

MT1-MMP is also regulated by biochemical post-translational modifications. The most important one, already explained above is the proteolysis of the N-terminal pro-domain involved in keeping MT1-MMP inactive during the transit in the trans-Golgi compartment. MMPs are also inhibited by natural endogenous proteins and MT1-MMP is no exception. TIMP-2 (and to a lesser extent TIMP-3) is the physiological inhibitor of MT1-MMP and is typically co-expressed with MMP14 during normal or pathological conditions. The N-terminal domain of TIMP-2 binds to the catalytic domain of surface exposed MT1-MMP in a 1:1 molar ratio, leading to the binding of pro-MMP2 to the C-terminal of TIMP-2. The MT1-MMP molecule in the homodimer whose catalytic site is not obstructed by TIMP-2 cleaves the pro-domain of pro-MMP-2, releasing an active, soluble MMP-2 in the extracellular space (Itoh, 2015; Valacca et al., 2015) (**Figure 15**). Interestingly, MT1-MMP/TIMP-2 complex also induces the pro-migratory ERK1/2-AKT pathway although the extracellular context seems to positively or negatively modulate this response (Sounni et al., 2010; Valacca et al., 2015).

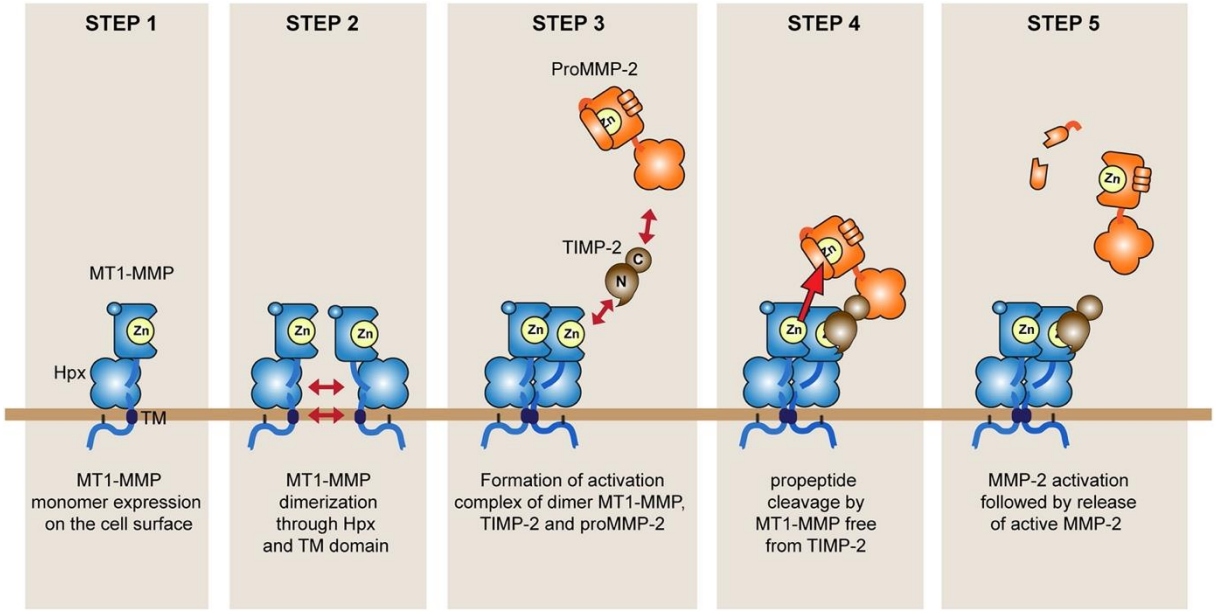

Figure 15: Schematic model of proMMP-2 activation by MT1-MMP. *MT1-MMP is secreted to the plasma membrane where it homodimerizes with another molecule (steps 1 and 2). Endogenous inhibitor TIMP-2 binds one molecule of the homodimer by its N-terminal domain while recruiting pro-MMP-2 by its C-terminal domain (steps 3 and 4). The free MT1-MMP proteolytically activates pro-MMP-2 and frees active MMP-2 (steps 4 and 5)* (Itoh, 2015).

4.2.2.2. Regulation of MT1-MMP trafficking

Endocytosis of MT1-MMP

MT1-MMP is rapidly internalized from the cell surface by clathrin-mediated endocytosis (CME) on the basis of an interaction between the µ2 subunit of adaptor protein 2 (AP-2) and a dileucine motif ($L^{571}L^{572}$) in the cytoplasmic tail of MT1-MMP (Castro-Castro et al., 2016; Ferrari et al., 2019; A. Jiang et al., 2001; Poincloux et al., 2009a; Uekita et al., 2001). The later stage of CME is membrane fission and the formation of an endocytic vesicle, mediated by dynamin-2 GTPase in complex with Endophilin A2 (EndoA2) protein. Recent work illustrated that tyrosine phosphorylation of Endo A2 (Y315) by focal adhesion kinase (FAK)/Src signaling axis alters the formation of dynamin-2/EndoA2 complex and leads to a decrease in MT1-MMP endocytosis rate and increase ECM degradation (Wu et al., 2005). The metastasis-suppressor, nucleoside disphophate kinase (NDPK) NME1 has been shown to interact and fuel dynamin 2 with high levels of GTP requires for CME (Boissan et al., 2014). Silencing of NME1 in MCF10DCIS.com cell line was shown to reduce MT1-MMP internalization rate and increase its surface exposure which was correlated with the acceleration of the switch from DCIS to IDC in a NME1-KO intraductal xenograft model (Lodillinsky et al., 2021) (**Figure 16**).

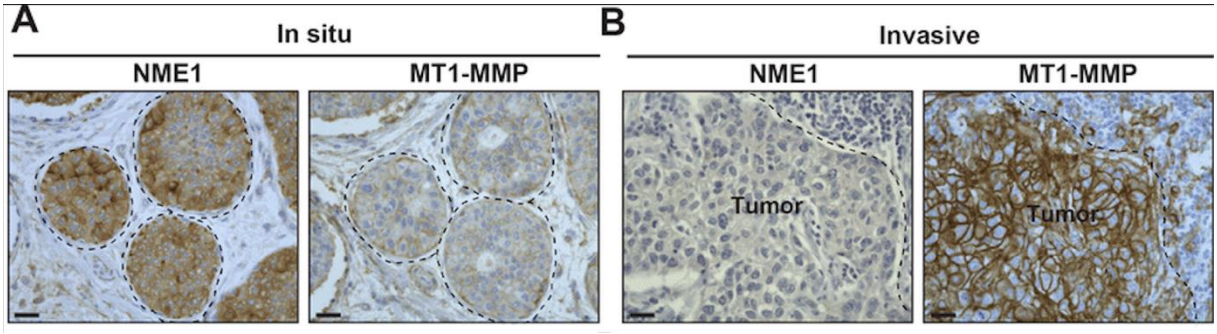

Figure 16: Anti-correlation of NME1 and MT1-MMP in breast tumors. *Immunohistochemistry stainings of NME1 and MT1-MMP on sections of (A) In situ or (B) invasive human breast cancers. Downregulation of NME in invasive tumors inhibits the CME of MT1-MMP and promotes the invasive phenotype* (Adapted from Lodillinsky et al., 2021).

Cargo endocytosis can also occur through flotillins which can, when upregulated, induce caveolin- and clathrin-independent invaginations of the plasma membrane. Upregulation of flotillins in carcinoma and sarcoma cells induced MT1-MMP surface clearance by Rab5-dependant endocytosis and participated in the recycling of MT1-MMP from the plasma membrane to the endolysosomal compartment and its polarized secretion to invadopodia, thus stimulating ECM degradation (Planchon et al., 2018).

Reports documenting the association of phosphorylated caveolin with the cytoplasmic tail of MT1-MMP suggest that surface levels of MT1-MMP could be regulated by caveolae-dependent endocytosis (Annabi et al., 2001; Gálvez et al., 2004; Labrecque et al., 2004; Yamaguchi et al., 2009a). However, there are discrepancies in the several functional studies of caveolae-mediated MT1-MMP endocytosis and its consequences on tumor progression (Castro-Castro et al., 2016; T. M. Williams et al., 2004; Yamaguchi et al., 2009b).

The cytoplasmic tail of MT1-MMP has also been reported to interact with proteins of the ezrin radixin moesin (ERM) family which are organizers of the cell cortical actin and place MT1-MMP in tetraspanin-enriched microdomains (TEM) although the molecular mechanisms of this localization regulation remain to be elucidated (Suárez et al., 2020b).

At the cell surface MT1-MMP is rapidly bound by TIMP-2, which has been shown to promote its internalization. In the acidic endolysosomal compartment, the proteolytically-inactive dimeric complex MT1-MMP/TIMP-2 can be dissociated in order to form an active protease that can be recycled back to the invadopodia (Maquoi et al., 2000; Poincloux et al., 2009b; Zucker et al., 2004).

Exocytosis of MT1-MMP to invadopodia

Delivery of neosynthesized MT1-MMP to invadopodia follows the classic secretion route (ER to Golgi to the plasma membrane). Data also support the notion that MT1-MMP is

rapidly internalized from the invadopodia and stored in the endolysosomal compartment (see above). Upon invadopodia formation, a fraction of endosomal MT1-MMP is exocytosed to the invadopodia.

Extensive studies involved the Rab-7 GTPase-, and soluble N-ethylmaleimide-sensitive factor attachment protein receptors (SNARE) protein VAMP-7-positive late endosomal/lysosomal (LE) compartments in MT1-MMP recycling pathways. These vesicle-associated proteins were found to be critical for the recycling of MT1-MMP to the invadopodia and to breast cancer invasion (Chevalier et al., 2016; Linder & Scita, 2015; Miyagawa et al., 2019; Monteiro et al., 2013; Pedersen et al., 2020a; Rossé et al., 2014; Steffen et al., 2008; K. C. Williams & Coppolino, 2011). Other Rab GTPases such as Rab8, Rab4 and Rab5A have been identified to be important circuitries depending on the tumoral context. Lastly, Rab2A was found to be elevated in breast cancers and was shown to associate with vacuolar protein sorting 39 (Vps39), a key component of the LE. This binary axis controlled post-endocytic trafficking of membrane-bound MT1-MMP, ECM degradation and invasion of breast cancer cells (Kajiho et al., 2016).

LE compartments are characterized by discrete branched actin dots nucleated by WASH and Arp2/3 complex and stabilized by cortactin. Although the functions of these endosomal actin domains are still elusive, they are abolished by silencing of Wiskott-Aldrich syndrome protein and Scar homolog (WASH, a member of WASP family) or of Arp2/3 which disrupts the delivery of endosomal MT1-MMP to invadopodia and inhibits ECM degradation (Castro-Castro et al., 2016; Monteiro et al., 2013). Along the same line, disrupting cortactin phosphorylation (which is necessary for the stabilization of this endosomal actin network) by atypical protein kinase C iota (aPKCι) silencing led to the enlargement of the actin dots and also impaired MT1-MMP trafficking to the endosomes (Rossé et al., 2014). The WASH complex is recruited on the LE compartment by the retromer complex, a heterotrimeric complex composed of Vps35, Vps26, and Vps29 with a crucial role in controlling the sorting and recycling of various transmembrane cargoes. The retromer complex itself is recruited to the LE compartments by Rab7A and the sorting nexin family (SNX) proteins. Super-resolution 3D structured illumination microscopy analysis demonstrated the presence of submicrometric domains of SNX27 and Vps26 at the surface of MT1-MMP-GFP-positive endosomes, and GST pull-down assays confirmed that the cytoplasmic tail of GST-MT1-MMP interacted with SNX27 and Vps26. Disrupting Vps26-SNX27 interaction using an SNX27 mutant showed reduced MT1-MMP surface exposure and ECM degradation, illustrating the role of the retromer-SNX27 axis in the recycling of MT1-MMP and retaining its proteolysis activity. Interestingly, depletion of SNX27 in a breast cancer xenograft model was enough to delay metastasis and prolong survival compared to control (P. Sharma et al., 2020).

The microtubule cytoskeleton network supports the bidirectional mobility of LE using two types of molecular motors that bind vesicles: the dynein/dynactin complex migrating towards the negative end of microtubules (towards the centrosome) and the kinesin protein family migrating towards the positive-end of microtubules (located mostly at the plasma membrane). Kinesins and dynein are controlled by c-Jun N-terminal kinase (JNK)-interacting proteins 3 and 4 (JIP3, JIP4) which are recruited by WASH to MT1-MMP-positive LE (Bowman et al., 2000; Marchesin et al., 2015; Monteiro et al., 2013; Watt et al., 2015). The switching of JIP3 and JIP4 between controlling kinesins or dynein is mediated by the activity of small GTPase Arf6 (Montagnac et al., 2009). Immunohistochemistry (IHC) staining of Arf6 in TNBC revealed an increase of the GTPase at the plasma membrane of tumor cells which was significantly higher in the invasive components of IDC compared to non-invasive components. Similarly, the expression of kinesin-1 subunit KIF5B was increased in high-grade TNBC. Depletion of Arf6, JIP3 or JIP4 in breast cancer cells induced a perinuclear accumulation of MT1-MMP-positive endosomes, a decrease in matrix degradation and an inhibition of invasion in a model of tumor spheroids embedded in 3D fibrillar collagen (Marchesin et al., 2015) (**Figure 17**).

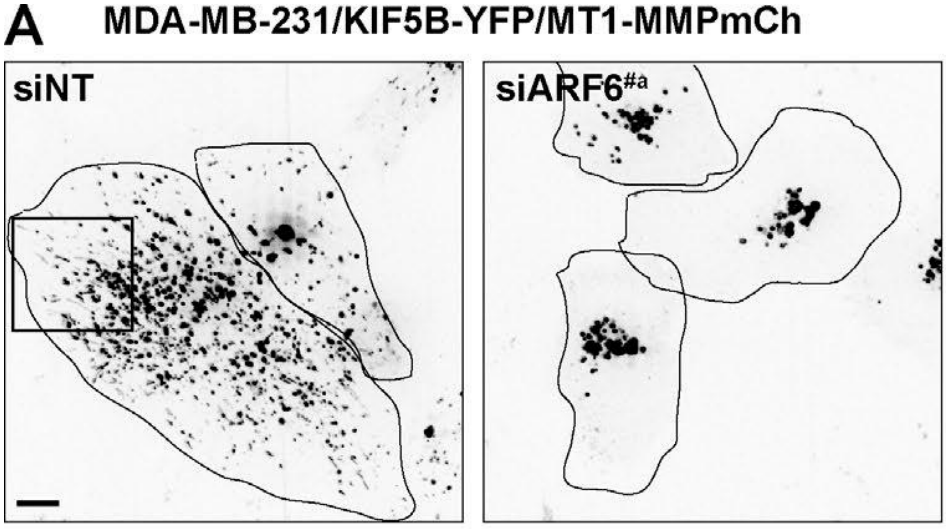

Figure 17: Arf6 controls the positioning of MT1-MMP-positive endosomes. *Inverted still images of mCherry channel of live microscopy of MDA-MB-231 cells expressing KIF5B-YFP and MT1-MMPmCherry and treated with control or Arf6 siRNA. The sur-expression of Kif5B dramatically scattered MT1-MMP-positive endosomes to the cell periphery in control cells, while upon knock-down of Arf6, the endosomes remain perinuclear* (Adapted from Marchesin et al., 2015).

Recent evidence points to a control of the anterograde MT1-MMP-positive LE translocation to the invadopodia by the Protrudin pathway. The transmembrane endoplasmic reticulum (ER) Protrudin protein interacts with endosomal PI(3)P and RAB7 resulting in the formation of ER/LE contact sites. Kinesin-1 is then transferred from Protrudin to endosomal kinesin-1 adaptor

FYCO1. Once the ER/LE contact site is abrogated, the kinesin-1-loaded vesicle translocates and docks to the invadopodia. Depletion of Protrudin in MDA-MB-231 cells impairs MT1-MMP exocytosis and inhibits matrix degradation (Pedersen et al., 2020b).

Endosomal-associated WASH can mediate the recruitment of the exocyst complex, a highly conserved octameric protein complex that tethers secretory vesicles to the cell surface before subsequent membrane fusion mediated by the SNAREs (Mei & Guo, 2018). Silencing of exocyst subunit Exo84 was sufficient to perturb the endosomal actin dots and resulted in perinuclear accumulation of MT1-MMP-positive LE (Sakurai-Yageta et al. 2008)(Monteiro et al., 2013).

Based on these data, a hypothetical model emerged whereby the Protrudin pathway, the retromer, and exocyst complexes mediate the transport and docking of MT1-MMP-positive endosomes to the plasma membrane. Arf6-GTP, enriched in the invadopodia, binds to JIP3 and JIP4 and, together with WASH and SNARE protein (mainly VAMP7) induces the tubulation of the endosomes and subsequent transport of MT1-MMP to the surface (Castro-Castro et al., 2016; Derivery et al., 2009; Monteiro et al., 2013; van Weering et al., 2012). Indeed, live-cell microscopy reveals that the MT1-MMP-positive endosomes remain anchored to the invadopodia for several minutes and that they do not collapse, nor do they fuse completely with the plasma membrane (Monteiro et al., 2013). Detachment of the endosome from the invadopodia is thought to be controlled by hydrolysis of GTP by Arf6 as Arf6 depletion induces a striking perinuclear clustering of MT1-MMP-positive endosomes (Marchesin et al., 2015). Finally, chloride intracellular channel 3 (CLIC3) silencing in breast cancer cells MDA-MB-231 and MCF10DCIS.com cells reduced matrix degradation and invasiveness (Macpherson et al., 2014). The authors found that MT1-MMP recycling from the late endosome/lysosomal compartment to plasma membrane/ECM contact sites in a CLIC3-dependent fashion.

Data also support the notion that exosome exocytosis could be an alternative mechanism whereby MT1-MMP is secreted in the extracellular space (Clancy et al., 2015; Hakulinen et al., 2008). Inward budding of the LE result in the formation of a multivesicular body (MVB) which is a vesicle containing smaller (50 to 100 nm) exosomes positive for docking markers such as Rab27 or CD63 (Ostrowski et al., 2009). Fusion of the MVB with the plasma membrane releases the exosomes in the cell environment. In head and neck squamous carcinoma cells (HNSCC), Rab27a- and CD63- positive endosomes were found in transient association with some invadopodia markers and depletion of Rab27a decreased 2D matrix degradation as well as 3D invasion. The contribution of this alternative exosome-dependent invadopodia function to the cell invasion program compared to the canonical process of LE exocytosis at the invadopodia has yet to be defined and although the idea of an extension of MT1-MMP modes of action is exciting, the depletion of Rab27A has also been shown to reduce the rate of

recycling of MT1-MMP from the plasma membrane and increase matrix degradation (Macpherson et al., 2014).

4.3. In vitro reconstitution of ECM to assess their alteration by invading tumor cells

The importance of the ECM in the most fundamental cellular processes has inspired researchers to develop *in vitro* reconstituted matrices in order to study the impact of the ECM on cell and tissue behavior.

Matrigel is the trade name from Corning Life Science referring to a solubilized basement membrane-like matrix secreted by Engelbreth-Holm-Swarm (EHS) mouse sarcoma cells, a tumor rich in collagen IV, laminin, heparan sulfates and other ECM components found in basement membrane, as well as growth factors. Under temperatures of 22-37°C, Matrigel forms a hydrogel of cross-linked ECM components. As such, Matrigel has been used for more than four decades as a basement membrane-mimicking ECM to study a variety of cell functions *in vitro* but presents severe limitations. Matrigel composition is ill-defined and variable between batches raising uncertainty in cell culture results and reproducibility. It was also reported that collagen IV in Matrigel is not properly cross-linked (Rowe & Weiss, 2008a). Furthermore, at the molecular level batch-dependent but also within a single layer of Matrigel, stiffness variations have been observed which can alter mechanosignaling pathways as well as matrix degradation (Aisenbrey & Murphy, 2020).

Gelatin is produced by heat and enzymatic denaturation of (type I) collagen-rich organic constituents (most often porcine skin). Thus, gelatin molecular composition is very similar to type I collagen although it does not have the complex helicoidal fibrillar organization. Cells plated on a thin layer of fluorescently-labeled cross-linked gelatin develop discrete dot-like 0.5-1 μm diameter F-actin-, cortactin- and Tks5-positive structures located mainly underneath the nucleus. Loss of gelatin fluorescence associated with these cellular structures correspond to matrix degradation (Artym et al., 2011; Cambi & Chavrier, 2021). The thin layer of gelatin is a matrix mimick that has been widely used to monitor the cell matrix-degradation activity. It is also the least expensive, easy to use matrix substratum with high reproducibility. However, to study invasion or migration, this 2D matrix construct is not suitable.

Although bidimensional environments were useful in understanding some cell functions, the aforementioned research shows that the cues from the tridimensional cell environment are major regulators of cell behavior. Type I collagen is the most abundant protein in the stroma and thus collagen extracts have been commonly used as reconstituted ECM. Acid-extracted collagen from rat tail tendon is relatively pure and can re-polymerize at neutral pH into a cross-linked network of fibrillar collagen (Ferrari et al., 2019; Infante et al., 2018; Monteiro et al.,

2013; Zagryazhskaya-Masson et al., 2020). Embedding cells or spheroids in type I collagen to recapitulate a 3D environment is a widespread study to monitor cell invasion capacities (Marchesin et al., 2015) (**Figure 18**). Antibodies have been developed to monitor the cleavage of the collagen fibers allowing the study of the effects of matrix metalloproteases such as MT1-MMP (Ferrari et al., 2019; Lodillinsky et al., 2021; Zagryazhskaya-Masson et al., 2020) (Cf. Annexe 3). Furthermore, the biophysical properties of the reconstituted matrix can be modified by altering the polymerization step and were shown to affect cell behavior. Widening matrix pore sizes by reducing the polymerization temperature was shown to decrease collagen degradation but did not affect the speed of cell invasion compared to control polymerization temperatures, suggesting that matrix pore size can influence the mode of 3D invasion (degradation-dependent mesenchymal invasion *vs* non-degradative amoeboid mode) (Infante et al., 2018).

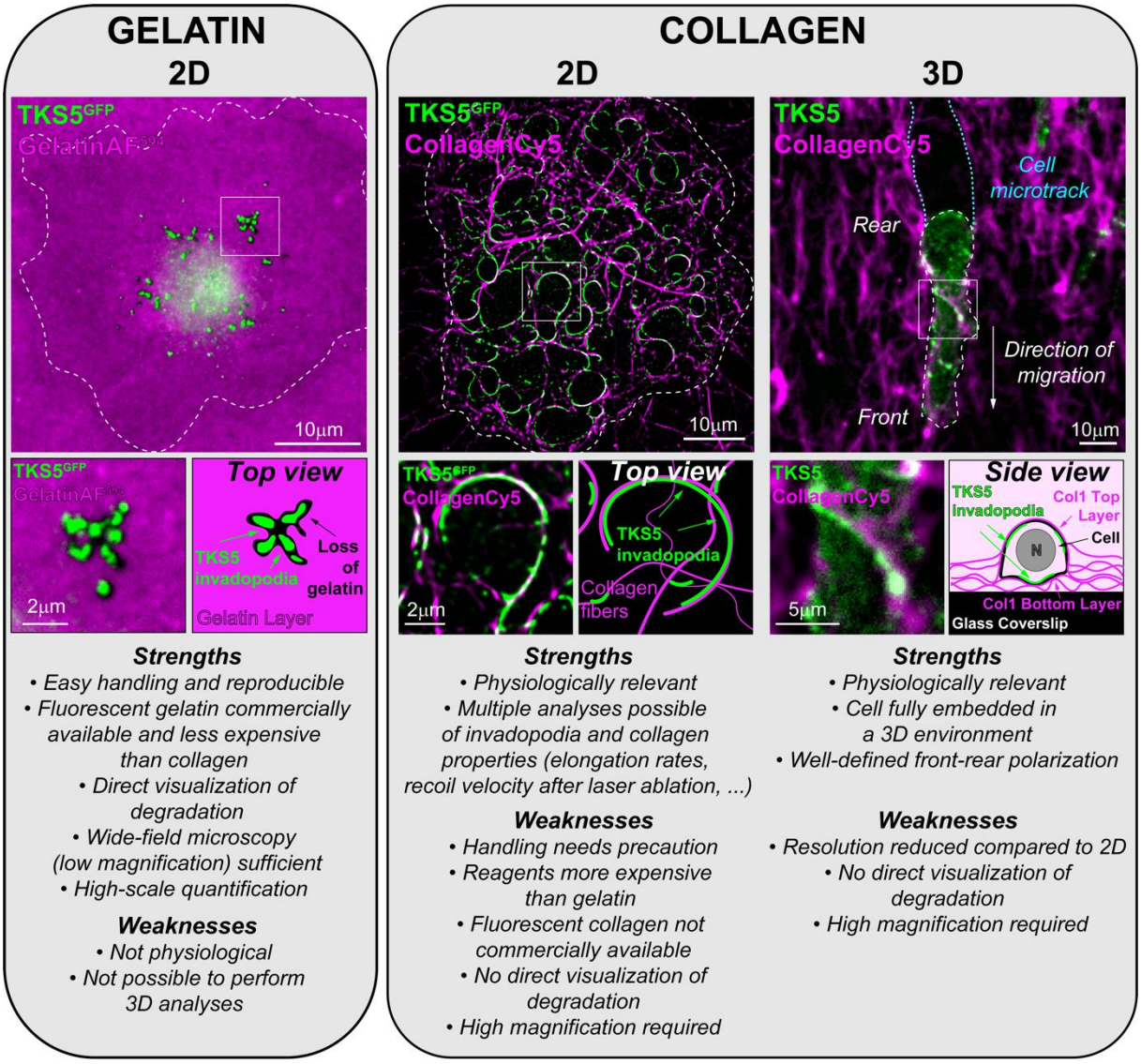

Figure 18: Reconstituted ECM. MDA-MB-231 cells expressing TKS5^{GFP} (green) plated on a fluorescently-labeled matrix (magenta). Matrix is gelatin in the left panel and 2D or 3D fibrillar

type I collagen in the right panel. Higher magnification of the boxed region and schematic representation is shown in the insets. Dotted line, cell contour. The strengths and weaknesses of each matrix are listed.

5. Tumoral metabolic reprogramming and mTOR signaling pathway

5.1. mTOR signaling pathway

5.1.1. The sTORy behind mTOR discovery

The discovery of the TOR (target of rapamycin) pathway begins in 1964 with Geordes Nógrády, a microbiology researcher who was trying to understand how the inhabitants of the Easter Island (also known as Rapa Nui) could walk barefoot on the island without contracting tetanus. He collected soil samples and gave them to Aryest Pharmaceuticals (now Pfizer) where scientists managed to extract a macrolide with antifungal activity from the bacterium *Streptomyces hygroscopicus*, which they aptly named rapamycin in homage to the island. Although this compound was found to have exciting and incredible anti-tumoral properties, its mechanisms of action remained elusive. Research groups led a hunt to characterize the cellular target of rapamycin, including the group of Michael Hall at the Biozentrum of the University of Basel who used genetic screens to identify genes conferring resistance to rapamycin in *Saccharomyces cerevisiae.* He cloned two genes, TOR1 and TOR2 (for Target of Rapamycin), while Stuart Schreiber (Harvard University, USA), David Sabatini (John Hopkins University, USA), and Robert Abraham (Mayo Clinic, USA) managed to find its mammalian counterparts which they aptly termed mammalian TOR, or mTOR ("A Long and Winding STORy," 2017).

5.1.2. The mTOR serine threonine kinase nucleates mTORC1 and mTORC2

5.1.2.1. mTOR kinase

mTOR is a 289-kDa protein exhibiting common ancestry with the members of the phosphoinositide-3 kinase (PI3K)-related kinase (PIKK) family of atypical protein kinases whose members (such as ATM or ATR) are involved in the control of cell cycle, cell growth and DNA damage. However, mTOR has no known lipid substrate but rather possesses a serine/threonine protein kinase activity. Yet, its structure is homologous to the five other mammalian PIKKs, with a multitude of tandemly repeated HEAT motifs in its N-terminal region, a middle FAT (FRAP/ATM/TRRAP) domain thought to mediate interactions in multiprotein complexes and the PIKK catalytic domain in the C-terminal region. The FKBP-rapamycin binding (FRB) domain is located between the FAT and the PIKK regions (Battaglioni et al., 2022; Yang et al., 2013). Rapamycin forms an inhibitory ternary complex with the FK506-binding protein 12 (FKBP12) and the FRB domain of mTOR, an interaction that resulted in the other name of mTOR, FKBP12-rapamycin associated protein (FRAP) (**Figure 19**). mTOR nucleates two distinct complexes, mTORC1 and mTORC2 with distinct inputs and downstream effects, which will be further detailed in the following sections (Battaglioni et al., 2022; Yang et al., 2013).

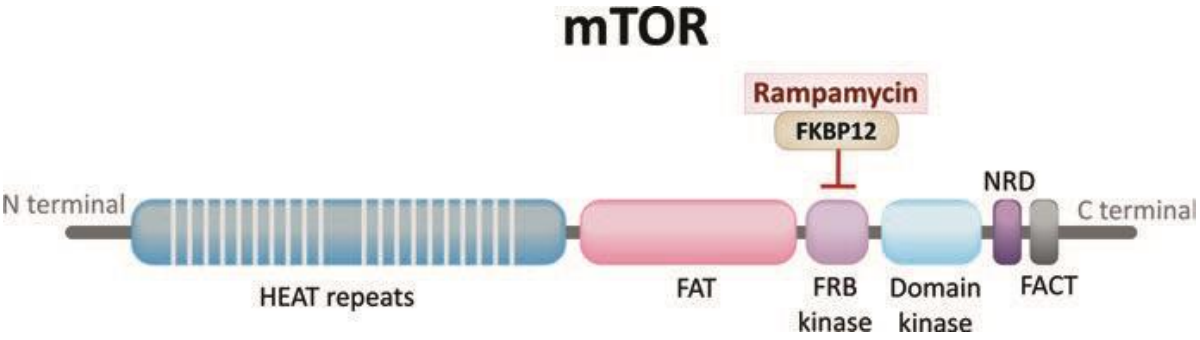

Figure 19: Schematic structure of mTOR kinase. *mTOR presents distinct PIKK kinase domains such as HEAT repeats, interaction-mediating FAT domains, regulatory FRB domain, and catalytic kinase domain* (Ilha et al., 2018).

5.1.2.2. mTORC1

The mTOR protein can form an heterotrimer with mammalian lethal with SEC13 protein 8 (mLST8), and the defining subunit of the mTORC1 complex named regulatory-associated protein of mTOR (RAPTOR). Dimerization of this trimer results in the formation of mTORC1 (Battaglioni et al., 2022). The exact function of mLST8 is unclear as mLST8-knockout embryos die at day 10.5, suggesting that mLST8 may not be critical for mTORC1 function (Guertin et al., 2006). RAPTOR targets mTORC1 to the surface of the lysosomes and is also responsible for binding some substrates of mTORC1 *via* their TOR signaling (TOS) motif (Antonia et al., 2019; Aylett et al., 2016; Schalm et al., 2003). Raptor knock-out mice die at day 3.5, illustrating its importance in mTORC1 function. Proline-rich Akt substrate of 40 kDA (PRAS40) is an endogenous inhibitor of mTORC1 that competes with other substrates by binding the mTOR/RAPTOR complex *via* its TOS motif and inhibits downstream signaling (Battaglioni et al., 2022). The last component of mTORC1 complex is DEP domain-containing mTOR-interacting protein (DEPTOR), a potentially endogenic allosteric inhibitor that binds directly to mTOR. Until recently, the mechanism of action of DEPTOR was elusive but its implication in cancer progression, obesity, and immunodeficiency fueled interest, and recently, two independent studies delivered cues to the mechanism by which DEPTOR regulates mTORC1 activity. A high concentration of DEPTOR could only inhibit half of the mTORC1 kinase activity, suggesting that DEPTOR is a partial inhibitor of mTORC1. Furthermore, cryo-electron microscopy analysis of the mTORC1/DEPTOR complex revealed a bipartite binding mode where the PDZ domain of DEPTOR is anchored to mTOR FAT domain and facilitates the binding of DEPTOR N-terminal tandem DEP domain region (DEPt), thereby hindering mTORC1 activity (Heimhalt et al., 2021; Wälchli et al., 2021). Interestingly, DEPTOR and PRAS40 are both substrates of mTOR and direct phosphorylation reduces their physical

interaction which further activates mTORC1. mTORC1 integrates and responds to growth factors and amino acid signals, energy status, and oxygen levels. In response to these stimuli, active mTORC1 stimulates anabolic processes such as proteins, lipids, nucleic acid and organelles biosynthesis while repressing catabolic processes such as autophagy and lysosomal function, leading to cell growth and proliferation (Laplante & Sabatini, 2012; Yang et al., 2013). As such, mTORC1 is implicated in many diseases, including cancer progression in which mTORC1 signaling is often dysregulated, which justifies the following chapter solely dedicated to understanding the molecular mechanisms controlling mTORC1 signaling.

5.1.2.3. mTORC2

The mTORC2 complex is composed of mTOR, mLST8, DEPTOR, rapamycin-insensitive companion of mTOR (RICTOR), and mammalian stress-activated map kinase-interacting protein 1 (mSIN1). mSIN1 and RICTOR are the defining subunits of mTORC2. mSIN1 contains a CRIM region in the middle of its structure which is important to recruit mTORC2 substrates and a C-terminal phox-homology (PH) domain which inhibits mTOR but is also important to tether mTORC2 to the cell membranes. A recent study demonstrated that mLST8 properly positioned the CRIM domain in mTORC2, revealing a mTORC2-specific function of mLST8. Although the function of RICTOR is unknown, its yeast homolog AVO3 is required for mTORC2 tethering to the plasma membrane (Battaglioni et al., 2022; G. Y. Liu & Sabatini, 2020; Saxton & Sabatini, 2017).

Activation of PI3K in response to growth factors initiates the production of a local pool of PI(3,4,5)P3. The binding of mSIN1 to PI3P *via* its PH domain releases the auto-inhibition on mTOR and recruits mTORC2 to the membrane, bringing it closer to membrane-bound mTORC2 substrates, such as Akt. Phosphorylation of Akt on Ser473 is a potent stimulator of mTORC1. Although mTORC2 was also found on organelles such as the ER, the Golgi apparatus, or mitochondria, it is not yet understood how it is recruited and activated there (Betz & Hall, 2013). mTORC2 is also negatively regulated by mTORC1 in a negative feedback loop. Activated mTORC1 can phosphorylate insulin receptor substrate 1 (IRS1) or growth factor bound-receptor protein 10 (GRB10) which both inhibit insulin signaling but can also indirectly stimulates the phosphorylation of RICTOR and mSIN1, leading to mTORC2 disassembly (Lamming et al., 2012; Sarbassov et al., 2006).

In contrast to mTORC1, for which many upstream signals and cellular functions have been defined (see below), relatively little is known about mTORC2. Three mTORC2 substrates have been extensively studied: AKT, serum- and glucocorticoid-induced protein kinase 1 (SGK1), and protein kinase Calpha (PKCa), which all belong to the AGC kinase family (Baffi et al., 2021). As such, they have similar structures, with a T-loop in their kinase domain and a hydrophobic motif (HM) in their C-terminal region. Full activation of these proteins required two

phosphorylation events on serine threonine residues: one in the HM region by mTORC2 and one in the T-loop region by phosphoinositide-dependent kinase 1 (PDK1). mTORC2 is implicated in cell survival, metabolism, and proliferation mostly *via* AKT. AKT and SGK1 both phosphorylate and inhibit the transcription factors FoxO1 and FoxO3 involved in the control of genes pertaining to stress resistance, metabolism, cell-cycle arrest, and apoptosis. Furthermore, the knock-down of mTORC2 leads to the perturbed actin cytoskeleton. Although the molecular mechanisms have yet to be elucidated, independent studies suggest that mTORC2-mediate control of the actin cytoskeleton *via* phosphorylation of PKCa and paxillin and by promoting GTP loading of RhoA and Rac1 (Fu & Hall, 2020).

5.1.3. Regulation of mTORC1 signaling/Upstream cues

The mTORC1 pathway is a complex signaling network integrating multiple cues. The pathway itself is typically made of several layers or regulatory elements. The first layer consists of the external environmental cues that impact the activity of sensors (which is the second layer). These sensors regulate the third layer made of GTPase activating proteins (GAPs) and guanine nucleotide exchange factors (GEFs). By definition, GEFs and GAPs can modulate the activity of specific GTPase proteins (the fourth and final layer) by promoting the hydrolysis of GTP or exchanging a GDP with a GTP. Finally, the GTPases can activate or repress mTORC1 activity.

5.1.3.1. Growth factors

Growth factors and other mitogens are often considered as proxies for broader metabolic signals and by acting upstream of mTORC1, they regulate cell, tissue, and organ metabolism to respond to diverse local and/or systemic cues. Tyrosine kinase receptors are activated by insulin or other growth factors on the cell surface and stimulate the production of a pool of PI3P *via* the activation of PI3K. PDK1 and AKT both bind to PI3P and phosphorylates AKT is activated by PDK1-mediated phosphorylation on Thr-308.

One of the most important regulators of mTORC1 activity is the tuberous sclerosis complex (TSC) which is composed of TSC tumor suppressors, TSC1 and TSC2, and Tre2-Bub2-Cdc16-1 domain family member 7 (TBC1D7) (Antonia et al., 2019; Dibble et al., 2012; Inoki et al., 2003; Yang et al., 2021). TSC1 acts as a scaffold for TSC2 and TBC1D7 to stabilize the complex while TSC2 acts as a GAP for the Ras homolog enriched in brain (RHEB) GTPase, converting catalytically active Rheb-GTP to inactive Rheb-GDP. Although the mechanisms remain to be defined, data suggest that under growth factor withdrawal, the TSC complex stimulates GTP hydrolysis by lysosomal membrane-bound Rheb, leading to mTORC1 inactivation. Growth factors lead to the phosphorylation of TSC2 by AKT which stimulates the dissociation of TSC from the lysosomal compartment and allows Rheb-GTP loading required

for mTORC1 activity (Demetriades et al., 2016; Menon et al., 2014) (**Figure 20**). Cryo-electron microscopy revealed that Rheb binds distally to the mTOR kinase site and has allosteric effects by realigning amino acids in the kinase active site, leading to its activation (Chao & Avruch, 2019).

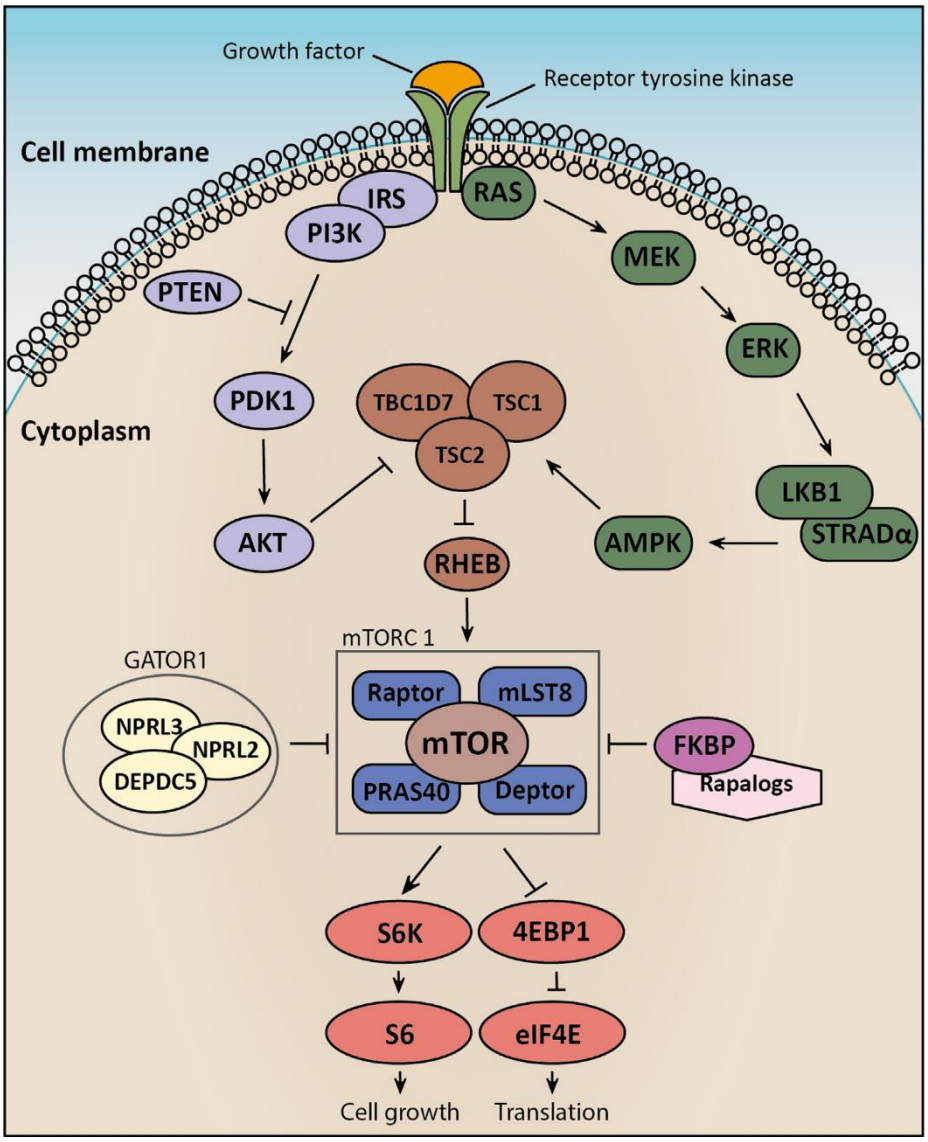

Figure 20: The TSC complex inhibits mTORC1 signaling. *The tuberous sclerosis complex is a heterotrimer of TSC1 scaffolding TSC2 and the Rheb GTPase GAP TBC1D7. Rheb-GTP is a potent activator of mTORC1. Under growth factors starvation, TSC inhibits Rheb by promoting GTP hydrolysis. However, in nutrient repletion conditions, the active Akt phosphorylates and inhibits TSC, leading to Rheb GTP loading and activation of mTORC1 activity* (Moavero et al., 2022).

The importance of TSC in the regulation of cell size and cell growth *via* mTORC1 is illustrated by the tuberous sclerosis complex, a syndrome characterized by mutations in the *TSC1* and *TSC2* genes leading to unrestrained mTORC1 activity and the growth of

hamartomas (brain, kidney, lung, skin, …) (Crino et al., 2006). Mice with *TSC1* mutations had disorganized cerebral cortical layers, thick dermal layer and reduced hypodermal layer of the skin, and enlarged polycystic kidneys (Liang et al., 2014). Interestingly, knock-out of mTORC1 substrate p70 S6 kinase in TSC1 deficient mice reduced cyst formation in the kidney (Bonucci et al., 2020).

5.1.3.2. Nutrient availability

The regulation of mTORC1 by amino acids is mediated by the four Ras-related GTPases (Rag) RagA, RagB, RagC, and RagD. Unlike canonical GTPases, the Rags form obligatory heterodimers (RagA/RagC or RagB/RagD) with an active conformation wherein RagA or RagB are in a GTP-bound state while RagC or RagD are in a GDP-bound state. The binding of GTP to one subunit induces intra- and inter-subunit conformational changes that prevent the dissociation of the prebound GTP while inhibiting the binding of a second GTP to the other subunit (Condon & Sabatini, 2019; Shen & Sabatini, 2018; Takahara et al., 2020). The Rags lack a lipid-targeting signal and are recruited to the lysosomes by the Ragulator complex, consisting of p18 (LAMTOR1), p14 (LAMTOR2), MP1 (LAMTOR3), HBXIP (LAMTOR4) and C7orf59 (LAMTOR5). LAMTOR1 is a critical scaffolding protein as it wraps around the other LAMTORs and anchors the complex to the lysosomal membrane *via* its N-terminal myristoyl and palmitoyl groups (de Araujo et al., 2017). Rags bind to Ragulator *via* their C-terminal roadblock domains and, in their active conformation, recruit mTORC1 to the lysosome where mTORC1 encounters and is activated by Rheb (Egri & Shen, 2021).

mTORC1 senses both cytoplasmic and lysosomal AA concentrations through distinct mechanisms. The GAP activity towards the Rags 1 (GATOR1) complex is a heterotrimer composed of DEP-domain containing-5 (DEPDC5), nitrogen permease related-like 2 (NPRL2) and NPRL3. NPRL2 possesses a poorly characterized GAP activity promoting the inactive RagA(B)^{GDP} conformation thereby inhibiting mTORC1. GATOR2 is another pentameric complex composed of WDR59, WDR24, MIOS, SEH1L, and SEC13 that can bind and completely antagonize GATOR1 through unknown mechanisms (Bar-Peled et al., 2013). The regulation of GATOR1-GATOR2 interaction involves the cytoplasmic leucine sensors Sestrin2 and Sar1B and arginine sensor Castor1. When cytoplasmic leucine and arginine levels fall, Sestrin2 and Castor1 bind and inhibit GATOR2, thereby releasing the inhibition on GATOR1. (Saxton, Chantranupong, et al., 2016; Saxton, Knockenhauer, et al., 2016) (**Figure 21 and 22**). Interestingly, Sar1B binds leucine with a higher affinity than Sestrin2 and thus requires lower levels of leucine to release GATOR2. Sar1B and Sestrin2 bind GATOR2 on distinct sites, suggesting a possible interplay between Sar1B and Sestrin2 (Battaglioni et al., 2022; J. Chen et al., 2021). The large KICSTOR complex, consisting of the proteins KPTN, ITFG2, C12orf66, and SZT2, tethers GATOR1 to the lysosome and is required for RagA/B and mTORC1

inhibition (Wolfson et al., 2017). Finally, the S-adenosylmethionine (SAM) sensor upstream of mTORC1 (SAMTOR) is an activator of GATOR1. High levels of SAM are directly sensed by SAMTOR and lead to the dissociation of SAMTOR-GATOR1, thereby inhibiting GATOR1 and activating mTORC1 (**Figure 22**). GTP loading on RagB is also promoted by alpha-ketoglutarate produced during glutaminolysis (Battaglioni et al., 2022).

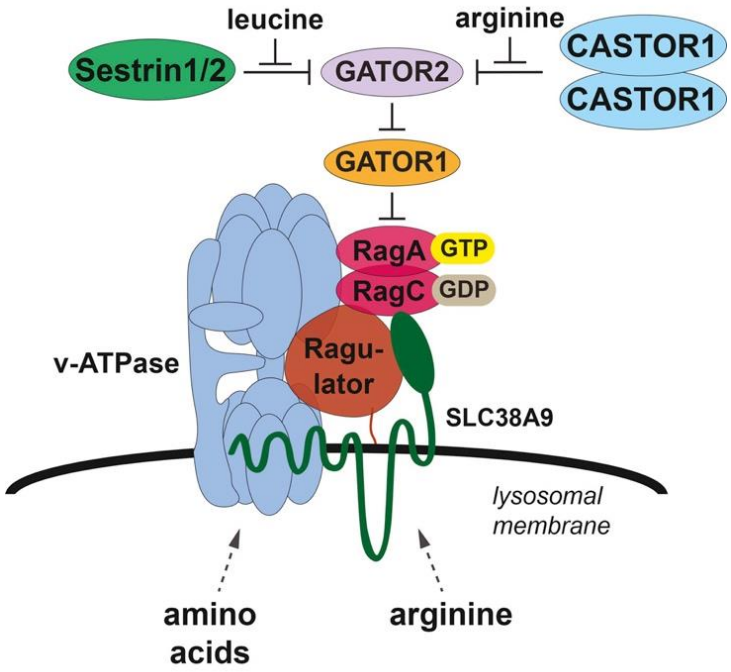

Figure 21: GATOR-mediated regulation of mTORC1 activity. *GATOR1 complex promotes the inactive RagA^{GDP} conformation through its GAP activity. GATOR1 is inhibited by a physical interaction with GATOR2. Under leucine or arginine starvation the association of GATOR1 and 2 is disrupted by Sestrin1/2 and Castor1 which bind GATOR2 thereby promoting GATOR1-mediated mTORC1 inactivation. Leucin inhibits Sestrin1/2 while arginine binds to Castor1, lifting the inhibition of GATOR2 and stimulating mTORC1 activity. Lysosomal arginine is also sensed by SLC38A9 transmembrane protein which is a GEF for RagA and promotes the binding of GTP to RagA and the activation of mTORC1 activity* (Chantranupong et al., 2016).

The folliculin (FLCN) protein contains a differentially expressed in normal and neoplastic cells (DENN) domain that places it within a family of proteins with GEF activity for Rab GTPases (Schmidt & Linehan, 2018). In fact, FLCN rather acts as a GAP for RagC and RagD thereby controlling mTORC1 activity. FLCN is in a heterodimeric complex with either FLCN-interacting proteins 1 or 2 (FNIP1/2). A dimer of this heterodimer results in an active FLCN-FNIP complex (Shen et al., 2019). FLCN loss-of-function mutation in Birt–Hogg–Dubé syndrome results in a non-canonical dimer of RagA^{GTP}-RagC^{GTP} that paradoxically promotes

hyperactivation of mTORC1 (Napolitano et al., 2020). Structural data support the notion that only the RagA(B)^{GTP} conformation is necessary for mTORC1 recruitment to the lysosome with a lesser contribution of the nucleotide-binding state of RagC(D), which could be consistent with data why mTORC1 would not be inactivated in a of RagA^{GTP}-RagC^{GTP} conformation (Lawrence et al., 2019; Wada et al., 2016).

The Ragulator complex is critical for anchoring the Rag GTPases to the lysosomal membrane, but they also possess a GEF activity. Early experiments suggested that Ragulator was a GEF for RagA and RagB, but recent biochemical studies have demonstrated that Ragulator relieves GTP from RagC upon AA stimulation. Solute carrier family 38 member 9 (SLC38A9) is a lysosomal multipass transmembrane protein with a large cytoplasmic N-terminal domain binding to the Rag-Ragulator complex. Data from enzymatic kinetic assays based on purified proteins suggest that SLC38A9 is a sensor for lysosomal arginine and acts as a GEF for RagA^{GDP}, effectively catalyzing the release of GDP and loading of GTP on RagA. Interestingly, even if SLC38A9 is activated by lysosomal amino acids, the absence of cytoplasmic arginine or leucine would result in the activation of GATOR1 and conversion of RagA^{GTP} to a GDP-bound form. This futile cycle would prevent mTORC1 activation without sufficient amino acids (Shen & Sabatini, 2018).

It is widely accepted that the Rag and Rheb GTPases define the two arms of a two-pronged mechanism that converge to activate mTORC1, wherein the Rags recruit mTORC1 to the lysosomal surface where it encounters Rheb which licenses the kinase activity of mTOR (**Figure 22**). Along this line, a recent study reported that low growth factors and reduced PI3K/AKT activity were sufficient to reduce mTORC1 activity but not to dissociate mTORC1 from the lysosome. In these conditions, local production of PI(3,4)P2 in the lysosomal membrane recruited 14-3-3ɣ proteins which bind and inhibited Raptor (Marat et al., 2017). However, interconnections in these two (AA and growth factors) signaling branches have been reported. Under AA starvation, TSC2 was shown to be recruited by the inactive Rag GTPases and mediate the inhibition of mTORC1 activity by stimulating the hydrolysis activity of Rheb^{GTP}. Cells lacking TSC2 and deprived of amino acids retained partial mTORC1 activity and mTORC1 lysosomal localization. Therefore, to completely dissociate TSC from the lysosomes and full activate mTORC1, both amino acids and growth factors must be present (Demetriades et al., 2014).

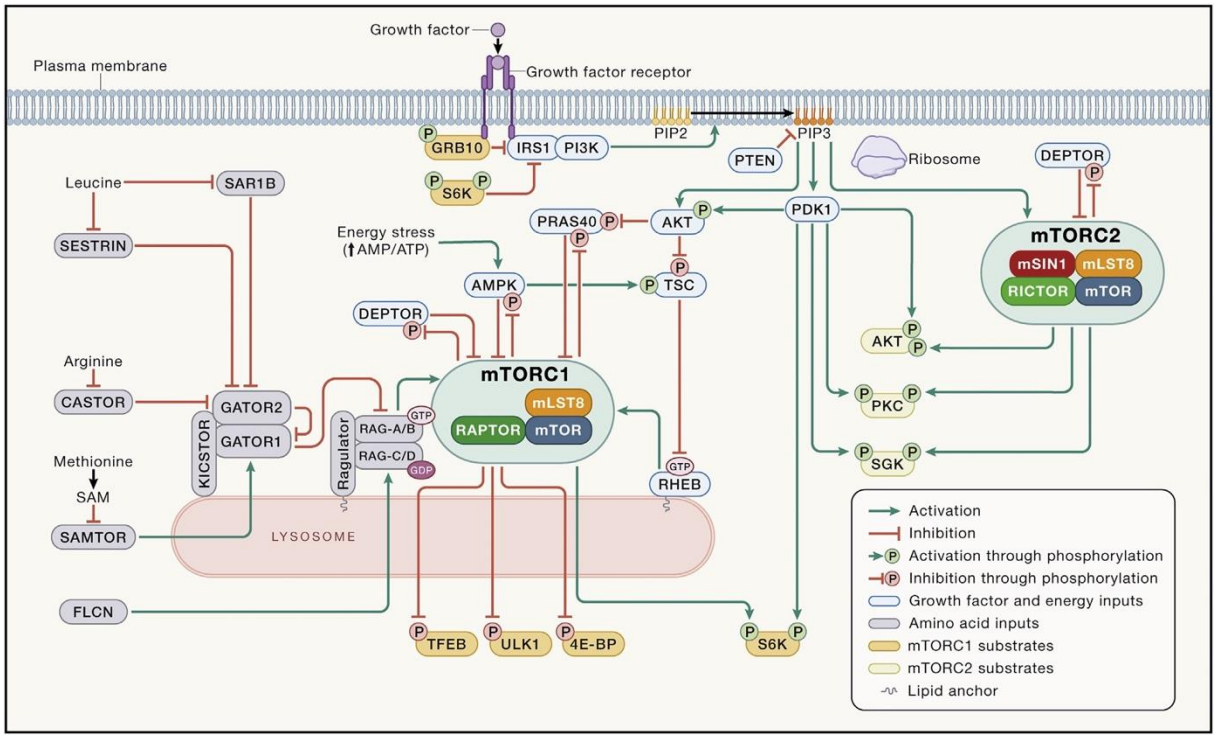

Figure 22: Schematic representation of mTOR signaling pathway. *Upstream of mTORC1, growth factors regulate the PI3K/AKT/TSC/Rheb pathway while amino acids regulate the GATOR/Rags, Ragulator-SLC38A9/Rags, and FLCN/Rags pathway. Rags recruit mTORC1 to the late endosome/lysosome membrane where it encounters Rheb. Rheb activates the kinase activity of mTORC1. mTORC1 phosphorylates downstream effectors 4E-BP1 and S6K promoting mRNA translation, ULK1 to repress autophagy, and TFEB to repress the expression of lysosomal genes* (Battaglioni et al., 2022).

5.1.3.3. Cholesterol

Cholesterol is an essential building block for membrane biogenesis, and rapidly proliferating cells rely on enhanced cholesterol synthesis and uptake to sustain their growth. The lysosome is the residing site of low-density lipoproteins (LDL) carrying cholesterol and fatty acids. Cholesterol is exported from the lysosome by the specific sterol transport system composed of the Niemann-Pick C1 (NPC1) and NPC2 proteins. NPC1 knock-out triggers a massive accumulation of cholesterol in endolysosomes, illustrating the importance of NPC proteins in cholesterol clearance. Recently, it was shown that cholesterol is one of the nutrient inputs sensed by SLC38A9 and which controlled mTORC1 activity. Cholesterol in the lysosomal membrane is sensed by the cholesterol recognition amino acids consensus (CRAC) domain of SLC38A9 which mediates mTORC1 recruitment and activation through the Rags. On the other hand, cholesterol depletion in HEK293T cells by methyl-beta-cyclodextrin (MCD) repressed mTORC1 signaling in NPC1 WT cells, but not in NPC KO cells where mTORC1 was hyperactive. Further experimental work is required to understand how mTORC1 is hyperactive

in NPC KO cells, where cholesterol cannot reach the limiting membrane (and therefore SLC38A9). Nonetheless, there seems to be a machinery which couples cholesterol in the endolysosomes to the regulation of mTORC1 signaling (Castellano et al., 2017; Davis et al., 2020).

5.1.3.4. Energy and oxygen availability

Under hypoxia or low energy levels, several factors converge towards the activation of the TSC axis to inhibit mTORC1. Energy production levels, transcribed by the intracellular AMP:ATP and ADP:ATP ratios modulate the activity of the AMP-activated protein kinase (AMPK). AMPK is an inhibitor of energy-consuming cellular processes and as such is a potent repressor of mTORC1. Active AMPK phosphorylates TSC2 at Thr1271 and Ser1387 to promote the GAP activity towards Rheb, thereby inhibiting mTORC1 activity. AMPK also phosphorylates and inhibits the mTORC1 component RAPTOR on Ser722 and Ser792 (Battaglioni et al., 2022; van Nostrand et al., 2020) (**Figure 22**).

Molecular oxygen is critical for intracellular bioenergetics and is consumed during a multitude of biochemical reactions. Cells develop quick adaptative strategies to cope to decreased levels of oxygen (hypoxia). A growing body of evidence suggests that hypoxia (1% O2) is sufficient to decrease mTORC1 activity. For instance, gestational hypoxia in the fetal lung impairs mTORC1 activity and leads to vascular damage that could result in pulmonary disease in later life (Mundo et al., 2021). The molecular mechanisms have yet to be elucidated but it was recently shown that hypoxia rapidly repressed TORC1 signaling in the adipose tissue of *Drosophilia* larvae by TSC-mediated inhibition of Rheb (B. Lee et al., 2019). The stress response REDD1 gene was also shown to mediate the activation of TSC upon hypoxia (Brugarolas et al., 2004). Other results suggest that hypoxia results in energy depletion and ultimately leads to the activation AMPK and subsequent inhibition of mTORC1 (L. Liu et al., 2006).

5.1.3.5. Spatial positioning of lysosomes

Work done over the last decade has modified our perception of the lysosome as the unglamorous “trash can organelle” of the cell and it is now widely recognized and appreciated that the lysosome is in fact a metabolic signaling hub with a critical role in coordinating the metabolic cues converging on the cell. By being tethered on the lysosome (or on the yeast vacuole), mTORC1 can gauge nutrient levels and modulate its activity in consequence. It becomes now apparent that the activity of mTORC1 is controlled both by the levels of amino acids in the lysosome lumen but also by the position of the lysosomes. Conversely, mTORC1 activity can control the activity, biogenesis and distribution of the lysosomes and this will be reviewed in Chapter V section 1.3.4.

In nutrient-replete conditions, active mTORC1 is tethered to dispersed lysosomes while starvation represses mTORC1 activity and induces a perinuclear clustering of the late endosomal/lysosomal compartment. Overexpression of kinesin members KIF1B and KIF2 induced lysosomal dispersion in starved cells which correlated with increased mTORC1 activity. Dispersed lysosomes also enhanced the rescue of mTORC1 activity during refeeding. Therefore, lysosomal distribution seems to modulate the intensity of mTORC1 signaling response to nutrients (Korolchuk et al., 2011). Recent work implicated the kinesin exchange between ER-anchored Protrudin and lysosomal FYCO1 protein to regulate lysosomal positioning and mTORC1 activity. Under starvation conditions, low PI(3)P on the lysosomal membrane prevents the recruitment of PI(3)P-binding proteins FYCO1 and Protrudin and represses the ER/lysosome contacts. Upon refeeding, AA promotes Rag-mediated recruitment of mTORC1 to the lysosomal membrane and Vps35-mediated production of PI(3)P. Lysosomal PI(3)P recruits FYCO1 and binds Protrudin, facilitating the kinesin exchange between Protrudin and FYCO1. Lysosomes loaded with kinesin-1 are translocated on microtubules towards the cell periphery (Hong et al., 2017). mTOR-loaded lysosome dispersion to the cell periphery is thought to be necessary for mTORC1 full activation as some of its upstream regulators such as AKT are recruited and activated at the plasma membrane (Demetriades et al., 2014). Genome-wide small interfering RNA (siRNA) screening also revealed that Rap1 GTPase deletion led to the expansion of the lysosomal compartment and enhancing the lysosomal surface for mTORC1 association, which resulted in mTORC1 hyperactivation. When AA were limited, Rap1 decreased lysosomes number and confined them to the perinuclear area. Although the AA signaling factors upstream of Rac1 are unknown, this work suggest that Rap1 is a regulator of the lysosomal system (Mutvei et al., 2020).

Lysosomes are also connected to kinesin-1 KIF5 and kinesin-3 KIF1 proteins by the octameric BLOC-1-related complex (BORC) and the small GTPase Arl8 (Farías et al., 2017; Guardia et al., 2016; Pu et al., 2015). Silencing of lyspersin2, a BORC subunit, provoked a perinuclear clustering of the lysosomes. Recent studies revealed that BORC also interacts with LAMTOR2 from the Ragulator complex, an interaction that controlled lysosomal positioning (Pu et al., 2017). This study revealed that silencing Ragulator subunits shifted lysosomes to the periphery both in nutrient-replete and starved cells, when Raptor KD did not, which suggests that Ragulator can control lysosome positioning independently of mTORC1 activity. Further exploration is required but it would seem as nutrient starvation would cause a change in the interaction between Ragulator and BORC, inhibiting BORC and lysosome dispersal.

5.1.4. Downstream effectors of mTORC1

A comprehensive survey of the literature has recently revealed that mTORC1 can phosphorylate at least 56 substrates (which is possibly a gross underestimation), sometimes on multiple positions, with a marked preference for serine residues over threonine (90 vs. 14 sites, respectively). Interestingly, most of these phosphorylation events were inhibitory. This survey had strict criteria and omitted datasets that lacked follow-up and actual confirmation, and which did not reveal direct phosphorylation by mTORC1. Surprisingly, most of the targets lack a TOS, RAIP, or any other mTOR recognition motif which suggests they may bind to mTOR in an idiosyncratic way. When grouped according to their functions, three major clusters emerged: translation, protein turnover (mainly autophagy), and lipid and glucose metabolism (Battaglioni et al., 2022).

5.1.4.1. Cap-dependent mRNA translation

Although most AGC kinases are substrates of mTORC2, p70-S6 kinase 1 (S6K1) and likely S6K2, are the only members of the AGC kinase family that are mTORC1 substrates. S6K1 is a serine/threonine kinase which phosphorylates and activates the ribosomal S6 protein and the translation regulators elongation factor 2 (eF2) kinase and eukaryotic translation initiation factor subunit 4B (eIF-4B), promoting the 5'-cap binding of eIF-4F. S6K1 also phosphorylates and inhibits eIF-4B inhibitor programmed cell death protein 4 (PDCD4). S6K1 is also involved in the negative feedback of mTOR by phosphorylating mSIN1, or the insulin receptor substrat 1 (IRS1) thereby inhibiting insulin signaling (Barilari et al., 2017). S6K1 possesses a TOS motif and an autoinhibitory C-terminal domain which is phosphorylated on multiple sites upon mitogen signaling. Phosphorylation of the inhibitory loop relaxes the structure of the kinase, allowing phosphorylation on Thr389 in the hydrophobic motif (HM) region and Ser371 in the turn motif by mTORC1. PDK1 also phosphorylates Ser229 in the T-loop of the catalytic domain. All three phosphorylations are necessary for the full activation of S6K1 (Keshwani et al., 2011). S6K1 is one of the major regulators of cell size downstream of mTORC1 as mice null for S6K1 (but not S6K2) have small cells in metabolic tissue (Ohanna et al., 2005; Pende et al., 2000; Sarbassov et al., 2005). S6K1 depletion phenocopies the modifications observed during dietary restrictions, suggesting that S6K1 activity is sensitive and modulated by nutrient availability in the cell.

eIF-4E-binding proteins (4E-BPs) are encoded by three different genes but are similarly regulated by mTORC1 signaling by sequential phosphorylation events. 4E-BP1 binds to Raptor *via* its C-terminal TOS motif which stimulates phosphorylation on residues Thr37 and Thr46 by mTOR, triggering a change of conformation of 4E-BP1. This steric modification allows for binding of the N-terminal RAIP motif to Raptor, which promotes phosphorylation of residues Ser65 and Thr70. The priming phosphorylations reduce the affinity of 4E-BP1 with their

partners eIF-4E by 100-fold. However, it is not sufficient for dissociation and the second round of phosphorylation is required for the complete release. Interestingly, only the late phosphorylation sites are inhibited by rapamycin treatment because of the conformational hindrance induced by the binding of rapamycin-FKBP12 to mTOR (Böhm et al., 2021; Gingras et al., 1999, 2001). eIF-4E recruits 40S ribosome subunits to the 5' of cap-ended mRNA and, together with eIF4G and eIF4F, form the eIF4 complex which stimulates translation (Dawson et al., 2020).

5.1.4.2. Promotion of lipogenesis

Lipids are required for membrane biogenesis and to sustain cell growth. Under PI3K/AKT control, mTORC1 drives *de novo* lipid synthesis through regulation of the transcription factors sterol regulatory element binding protein 1 and 2 (SREBP 1/2) and peroxisome proliferator-activated receptor-γ (PPARγ). The SREBPs belong to the family of basic helix-loop-helix-leucine zipper (bHLH-zip) transcription factors and control the expression of metabolic genes involved in fatty acid and cholesterol biosynthesis. Inactive SREBPs precursors reside in the endoplasmic reticulum (ER). Upon insulin stimulation (SREBP1) or cholesterol depletion (SREBP2), SREBPs bud from the ER and are transported to the Golgi where site-1 protease (S1P) and S2P cleave the N-terminus of SREBP (nSREBP). nSREBP translocates to the nucleus and induces the expression of target genes (Ferré & Foufelle, 2007; Han & Wang, 2018; Horton et al., 2002).

During feeding, rapamycin treatment was shown to inhibit nSREBP nuclear translocation and the expression of lipogenic genes suggesting that mTORC1 controls lipogenesis *via* regulation of SREBPs localization (Porstmann et al., 2008). Further research demonstrated that mTORC1 controlled SREBPs localization in an S6K-dependent and S6K-independent manner. How S6K is involved in lipogenesis remains unclear. Independently of S6K, mTORC1 phosphorylates and inactivates CREB regulated transcription coactivator 2 (CRCT2) which is an inhibitor of SREBPs budding from the ER (Han et al., 2015; Han & Wang, 2018). mTORC1 also phosphorylates and prevents the nuclear translocation of Lipin-1, a phosphatidic acid phosphatase required for glycerolipid biosynthesis. In the nucleus, Lipin-1 promotes the association of SREBPs with the nuclear matrix, thereby preventing its association with target genes (Han & Wang, 2018; Peterson et al., 2011) (**Figure 23**).

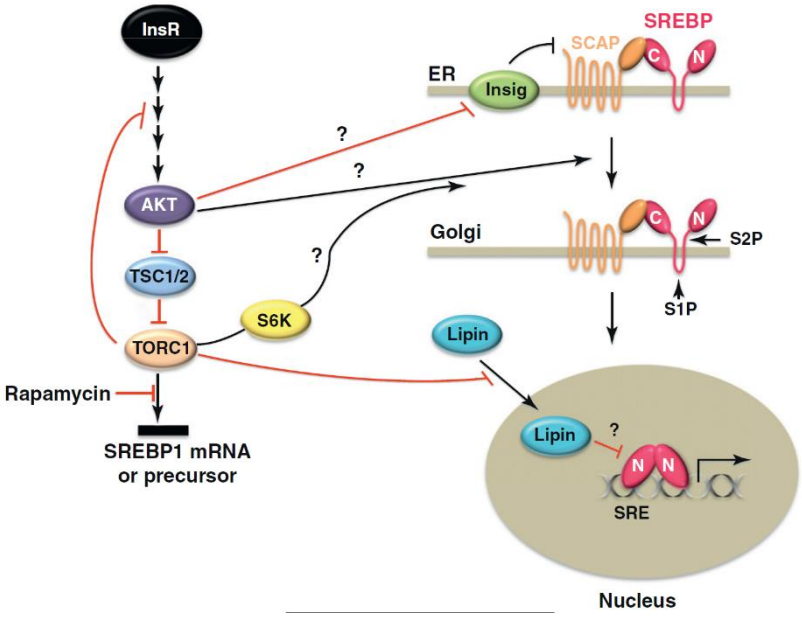

Figure 23: Model for SREBP-regulated maturation. *The precursor SREBP is sequestrated in the ER membrane in a complex with cholesterol-bound SCAP and Insig. Low cholesterol or insulin signaling (through AKT and mTORC1) dissociates this repressive complex and induces the translocation of SCAP/SREBP to the Golgi apparatus where SREBPs are proteolytically activated by the S1P/S2P enzymes. The mature SREBP N-terminal fragment (N) is released and rapidly enters the nucleus where it activates target genes. mTORC1 phosphorylates and inhibits SREBPs repressor Lipin-1. Red and black arrows indicate inhibitory and stimulatory actions. The question marks indicate the mechanism for the effects still need to be defined* (Jeon & Osborne, 2012).

5.1.4.3. Protein catabolism

Autophagy

Autophagy is a process of nutrient stress-induced cellular self-digestion conserved in all eukaryotic organisms in which cytoplasmic components are engulfed and degraded in an acidic double-membraned organelle. Broken-down components are then recycled to sustain cell growth, proliferation, and survival under nutrient adverse conditions. Autophagy is thereby regulated by nutritional cues and under the control of mTOR and AMPK kinases.

The molecular processes of autophagy have been researched and described in detail. An isolation membrane buds out from the ER and envelopes a portion of the cytoplasm containing damaged organelles and macromolecules, and forms the autophagosome, a double-membraned vesicle. Lysosomes fuse with the autophagosomes, and lysosomal hydrolases break down cytoplasm-derived materials into constituent amino acids or fatty acids that are delivered back to the cytoplasm, enabling their subsequent reuse in metabolic processes (Hosokawa et al., 2009; G. Y. Liu & Sabatini, 2020). Initial work studying the

regulation of autophagy revealed a set of over 30 autophagy-related (Atg) genes involved in every step of the autophagy process. The yeast complex Atg1-Atg13-Atg17 is hyperphosphorylated by TOR in nutrient-rich conditions and hypophosphorylated under starvation conditions which coincide with autophagy initiation. In mammals, unc-51-like autophagy-activating kinase 1 (ULK1) and ULK2 are Atg1 homologs. No mammalian homolog of Atg17 exists but 200-kDa FAK family kinase-interacting protein (FIP200) was proposed as a counterpart to form a ULK1-Atg13-FIP200 complex initiating phagosome formation (Hosokawa et al., 2009). In nutrient-rich conditions, mTORC1 phosphorylates and inhibits ULK1 on Ser758 (Hosokawa et al., 2009) and ATG13 on Ser258 (Puente et al., 2016), consequently blocking autophagy initiation. Interestingly, active ULK1 phosphorylates Raptor to hinder substrate recognition, further inhibiting mTORC1 and promoting autophagy. By binding to the homotypic fusion and vacuole protein sorting (HOPS) complex, UV radiation resistance-associated gene product (UVRAG) modulates Rab7 activity to promote autophagosome maturation and fusion with lysosomes. UVRAG is kept inactive by the association with RUN domain Beclin 1-interacting and cysteine-rich-containing protein (RUBICON), an interaction promoted by mTORC1-mediated phosphorylation on Ser498 of UVRAG (Young-Mi Kim & Hwa Jung, 2015).

Glucose starvation also promotes autophagy by AMPK-mediated mTORC1 inactivation. AMPK also phosphorylates ULK1 on multiple sites to promote its activity. mTORC1-mediated phosphorylation of ULK1 on Ser758 disrupts the association of AMPK and ULK1, further demonstrating the antagonistic roles of mTORC1 and AMPK in the regulation of energy homeostasis (Battaglioni et al., 2022; Kim et al., 2011). Finally, novel findings link mTORC2 to autophagy where AKT- and SGK1-mediated phosphorylation of Foxo1/3A transcription factors downstream of mTORC2 inhibits autophagy initiation and cargo degradation (Aspernig et al., 2019; Deleyto-Seldas & Efeyan, 2021; J. Zhao et al., 2007)

Lysosomal metabolism

Cells constantly regulate the number and activity of the lysosomal compartment in response to their energetic needs. Lysosomes are acidic organelles specialized in the degradation of contents/cargoes received from the secretory, endocytic, autophagic, and phagocytic pathways due to lysosomal hydrolases which degrade proteins, lipids, nucleic acids, and polysaccharides. Mutation in lysosome function can result in a lysosomal storage disease (LSD) characterized by the intraluminal accumulation of undegraded contents. Patients with LSD present a multi-systemic phenotype often associated with early-onset neurodegeneration (Ballabio, 2016). Therefore, a cellular program coordinating lysosomal activity under nutrient cues is plausible. Lysosomal proteins tend to have coordinated expression and promoter analysis revealed that a little less than 100 lysosomal genes share a

highly enriched 10 base pair motif, the so-called Coordinated Lysosomal Expression and Regulation (CLEAR) element (Sardiello et al., 2009). This CLEAR element overlaps the CACGTG E-box, a target of the members of the microphthalmia–transcription factor E (MiT/TFE) subfamily of bHLH factors. Among the four members of the MiT/TFE family (MITF, TFEB, TFE3, and TFEC), TFEB has emerged as a master regulator of lysosomal biogenesis and functions by binding the CLEAR element, thereby controlling the expression of this entire specific gene network and demonstrating that lysosomes are globally regulated on the transcriptomic level. As such, overexpression of TFEB has been shown to increase the number of lysosomes and the levels of lysosomal enzymes, but also enhanced the fusion of autophagosomes with lysosomes and the degradation of the autophagic cargo, indicating that TFEB also controls autophagy (Palmieri et al., 2011; Sardiello et al., 2009; Settembre et al., 2011, 2013).

Lysosomes are also involved in lysosomal exocytosis, a process required for plasma membrane repair, bone resorption, and antigen presentation. Lysosomes are displaced on microtubules towards the cell periphery and dock to the plasma membrane. So far, only KIF5B has been shown to be exclusively associated with lysosomes for their peripheral transport (Cardoso et al., 2009). The Arf-related Arl8 GTPase is associated with lysosomes and recruits the BORC complex to link kinesins to lysosomes, but also salmonella-induced filaments A (SifA) and Kinesin-Interacting Protein (SKIP), also known as Pleckstrin Homology Domain-Containing Family M Member 2 (PLEKHM2), which recruit kinesin-1 to lysosomes (Tancini et al., 2020). As described above, the Protrudin-FYCO1 is also required to dock lysosomes to kinesins during ER-endosomes/lysosomes contacts (Raiborg et al., 2015). Docking of the lysosome to the plasma membrane occurs by the tethering of vesicle-associated membrane protein 7 (VAMP7) on the lysosomal membrane to syntaxin-4 and synaptosome-associated protein of 23 kDa (SNAP23) on the plasma membrane, which are members of the N-ethylmaleimide-sensitive factor attachment receptor (SNARE) family (Rao et al., 2004). The fusion step between the membranes requires the local release of calcium from the ER or the lysosomes themselves through the lysosomal cation channel transient receptor potential mucolipin 1 (TRPML1) also called mucolipin 1 (MCOLN1). Interestingly, TFEB overexpression was shown to induce lysosomal exocytosis by enhancing the expression of MCOLN1 and subsequent cytoplasmic release of lysosomal calcium (Medina et al., 2011) (**Figure 25**).

TFEB is a transcription factor, and its activity thus depends on its localization which is mainly regulated by phosphorylation. In most cell types, mTORC1 and extracellular signal-regulated kinase 2 (ERK2) are the main kinases known to phosphorylate TFEB. Under nutrient replete conditions, mTORC1 phosphorylates TFEB on Ser142 and Ser211 which are docking sites for 14-3-3 regulatory proteins that subsequently sequestrate and inactivate TFEB to the cytoplasm (Martina et al., 2012; Roczniak-Ferguson et al., 2012; Settembre et al., 2011, 2012).

These phosphorylation marks also induce STUB-1-mediated ubiquitination and degradation of TFEB (Sha et al., 2017). Starvation inhibits mTORC1 and *de novo* phosphorylation of TFEB. Interestingly, nutrient depletion also activates MCOLN1 independently of mTORC1 activity, and the released calcium activates the phosphatase calcineurin which in turn dephosphorylates TFEB and promotes its nuclear translocation (Medina et al., 2015b). In a feedback loop, TFEB then promotes the expression of lysosomal genes, including MCOLN1. A recent study also showed that the activation of the MCOLN1-TFEB axis also happens upon bacterial sensing in dendritic cells (Bretou et al., 2017). mTORC1- and ERK-mediated phosphorylation on Ser142 is also a priming event for GSK3B-mediated phosphorylation on Ser138, which is required for exportin CRM1 biding and efficient TFEB nuclear export (Li et al., 2018; Napolitano et al., 2018) (**Figures 24 and 25**).

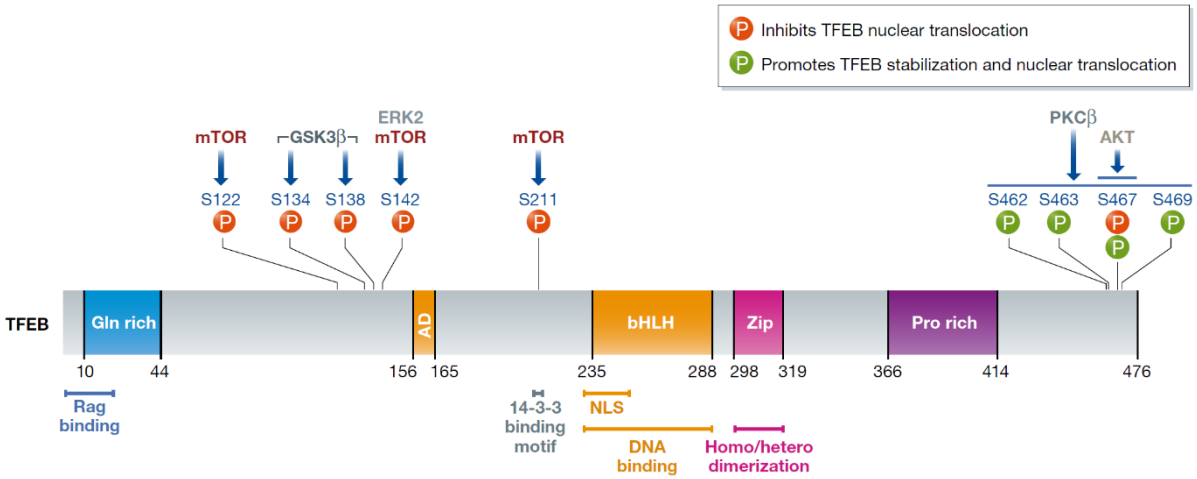

Figure 24: Scheme of TFEB structure and phosphorylation sites. (Puertollano et al., 2018)

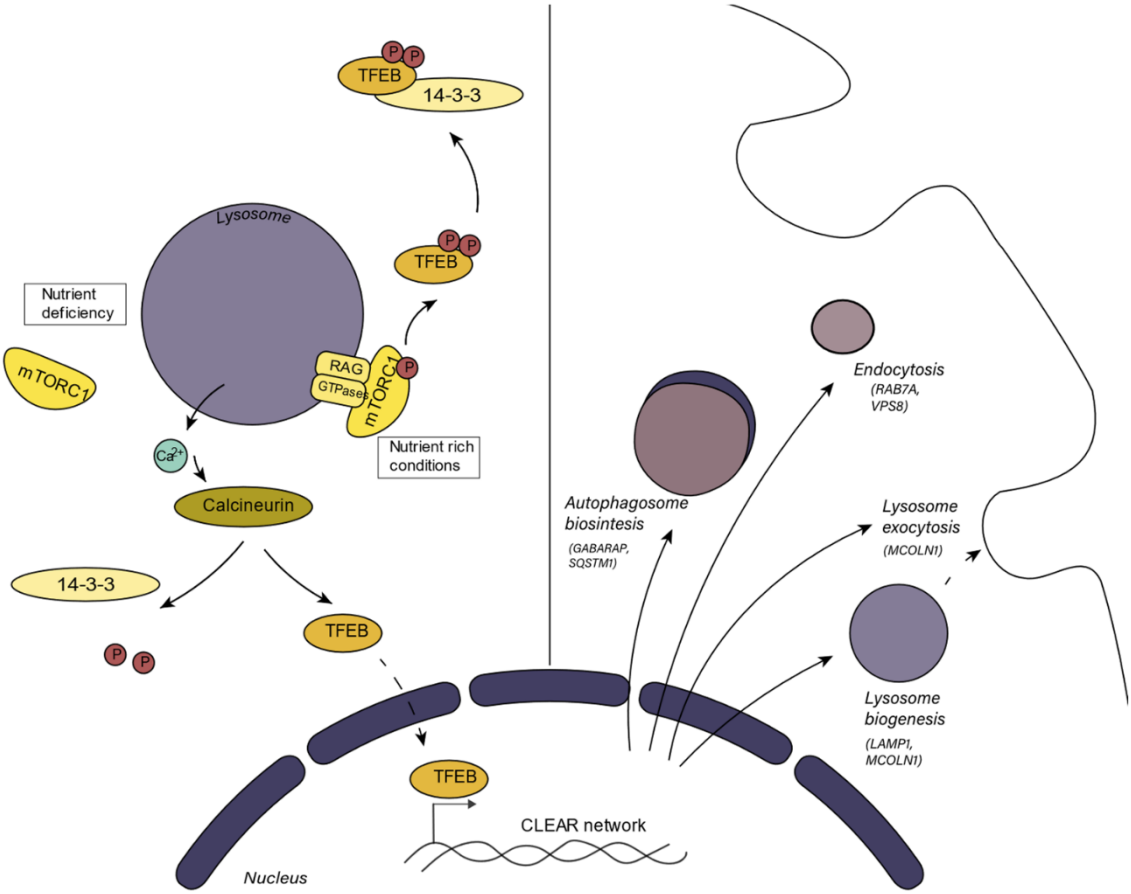

Figure 25: Schematic overview of TFEB regulation and functions. *In nutrient-rich conditions, mTORC1-mediated phosphorylations on TFEB are bound by the regulatory proteins 14-3-3 thus sequestrating TFEB in the cytoplasm. Starvation inhibits mTORC1 and promotes lysosomal Ca2+ release through MCOLN1 channel which activates calcineurin phosphatase. Dephosphorylation of TFEB leads to nuclear translocation and the expression of genes involved in lysosomal biogenesis (LAMP1), lysosomal exocytosis (MCOLN1) and other lysosomal-related processes* (Guerrero-Navarro et al., 2022).

TFEB lack a TOS motif and is recruited to the lysosomes by RagC/D in their GDP-bound conformation (Malta et al., 2017; Martina & Puertollano, 2013; Napolitano et al., 2020). Thereby, loss of RagC/D GAP, FLCN/FNIP, results in RagC/D^{GTP} accumulation, constitutive nuclear localization of TFEB independently of the cell nutrient status, and hyperactivation of mTORC1 by TFEB-mediated increase in RagD transcription. Constitutive hyperactivation of mTORC1 promotes kidney cysts and renal cell carcinoma (Malta et al., 2017; Napolitano et al., 2020).

mTORC1 has also been involved in unconventional protein secretion (UPS) through its substrate GRASP55 (Nüchel et al., 2021). Proteins involved in UPS are cargos without a signal peptide or transmembrane domain which are secreted by stressed cells. The Golgi reassembly

stacking protein (GRASP) family is composed of GRASP55 and GRASP65, two proteins involved in the maintenance of Golgi structure and function. mTORC1 phosphorylates GRASP55 at the Golgi while dephosphorylation of GRASP55 induced by nutrient starvation or rapamycin treatment promotes its re-localization to LC3B-positive autophagosomes and multi-vesicular bodies which drives UPS of several cargo, including MMP-2 but also other proteins involved in focal adhesions and cell junctions. This work revealed a previously unknown relationship between mTORC1 signaling and surfactome and secretome modifications in stressed cells.

5.2. Microenvironment-induced metabolic stress

5.2.1. Solid tumors are starved and hypoxic

As described above, tumors are heterogeneous entities presenting non-uniform genetic and phenotypic features. This heterogeneity can be driven by the tumoral microenvironment which co-evolves with the tumor and influences tumor progression. Despite their mind-boggling complexity in many aspects of their biology, tumoral tissues, like all tissues, still require a constant supply of nutrients and oxygen to sustain their rapid expansion. To allow tumor progression and propagation, the induction of a tumoral microvasculature - an angiogenic switch - is thus necessary to perfuse the ever-growing tumor mass. Angiogenesis (the sprouting of new blood vessels) is a physiological process tightly regulated by a balance between pro- and anti-angiogenic factors. This balance is completely lost during tumoral progression, and normal vessel quiescence is inhibited, resulting in the constant elongation of blood vessels. The architecture of the tumor vasculature is thus quite distinct from a physiological network, with irregular shapes, excessive dilatation, twists and turns, and sometimes dead ends (Bergers & Benjamin, 2003). However, rampant cell proliferation remains disproportionately increased relative to blood vessel sprouting which leads to large areas of the tumors devoid of functional blood vessels. Assessment of the vasculature landscape, blood perfusion, and oxygen supply in a computational approach based on 3D imaging of whole orthotopic breast tumor xenografts confirmed the presence of large avascular areas within the tumor as well as wide inter-vessel distances and small vascular lengths. Furthermore, analysis of the distributions of blood flow rates and intravascular oxygenation revealed that a large subpopulation of tumor vessels was inadequately perfused and under-oxygenated (Stamatelos et al., 2019) (**Figure 26**). Additionally, TGF-β-induced ECM stiffening during tumor progression impairs the progression of vascular morphogenesis and provokes an increase in interstitial pressure that compresses blood vessels and impedes blood flow (Helmlinger et al., 1997; Jain et al., 2014a; Saini et al., 2018). In breast tumors, the median partial pressure of oxygen was measured at 10 mmHg while it reached 65 mmHg in normal breast tissues (Vaupel et al., 2007). An elegant fate-mapping study established that hypoxia

was first detected in early DCIS lesions in an MMTV mice model that develop spontaneous tumors. Furthermore, experiments on MDA-MB-231 spheroids revealed that cells escape the hypoxic core and are found at the invasive front. Consequently, *in vivo* post-hypoxic tumor cells had a distinct potential to form lung micro and macrometastasis (Godet et al., 2019) (**Figure 27**).

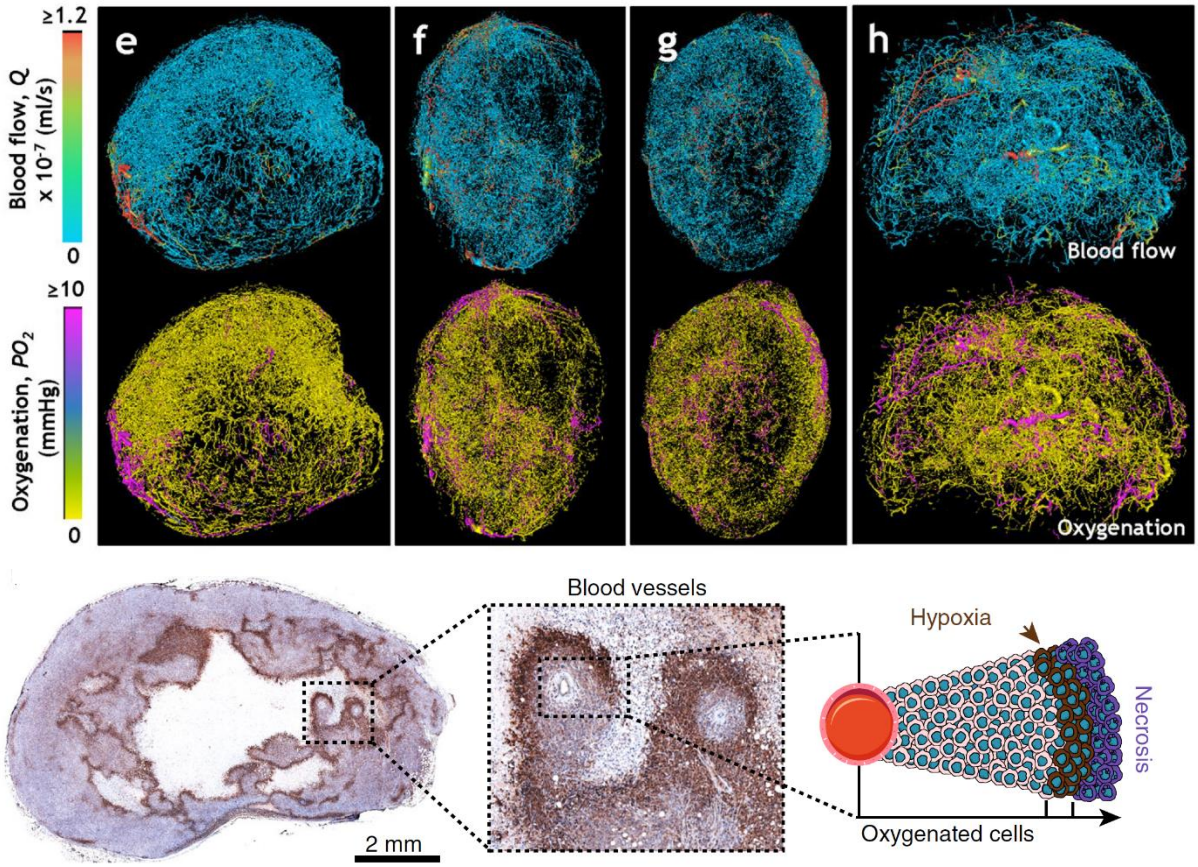

Figure 26: Tumors are poorly vascularized and hypoxic *Top panel shows a 3D-based computational representation of blood flow and partial pressure of oxygen in whole orthotopic breast tumor xenografts showing large areas of the tumors with severely limited blood flow (blue regions) and highly hypoxic (yellow regions). The bottom panel is a cross-section of a mice mammary tumor stained with Hypoxyprobe. The inset shows two blood vessels surrounded by cancer cells with a radial gradient of Hypoxyprobe staining illustrating that the farther the cells are from the blood vessel, the more hypoxic they are* (Adapted from Godet et al., 2019 and Stamatelos et al., 2019).

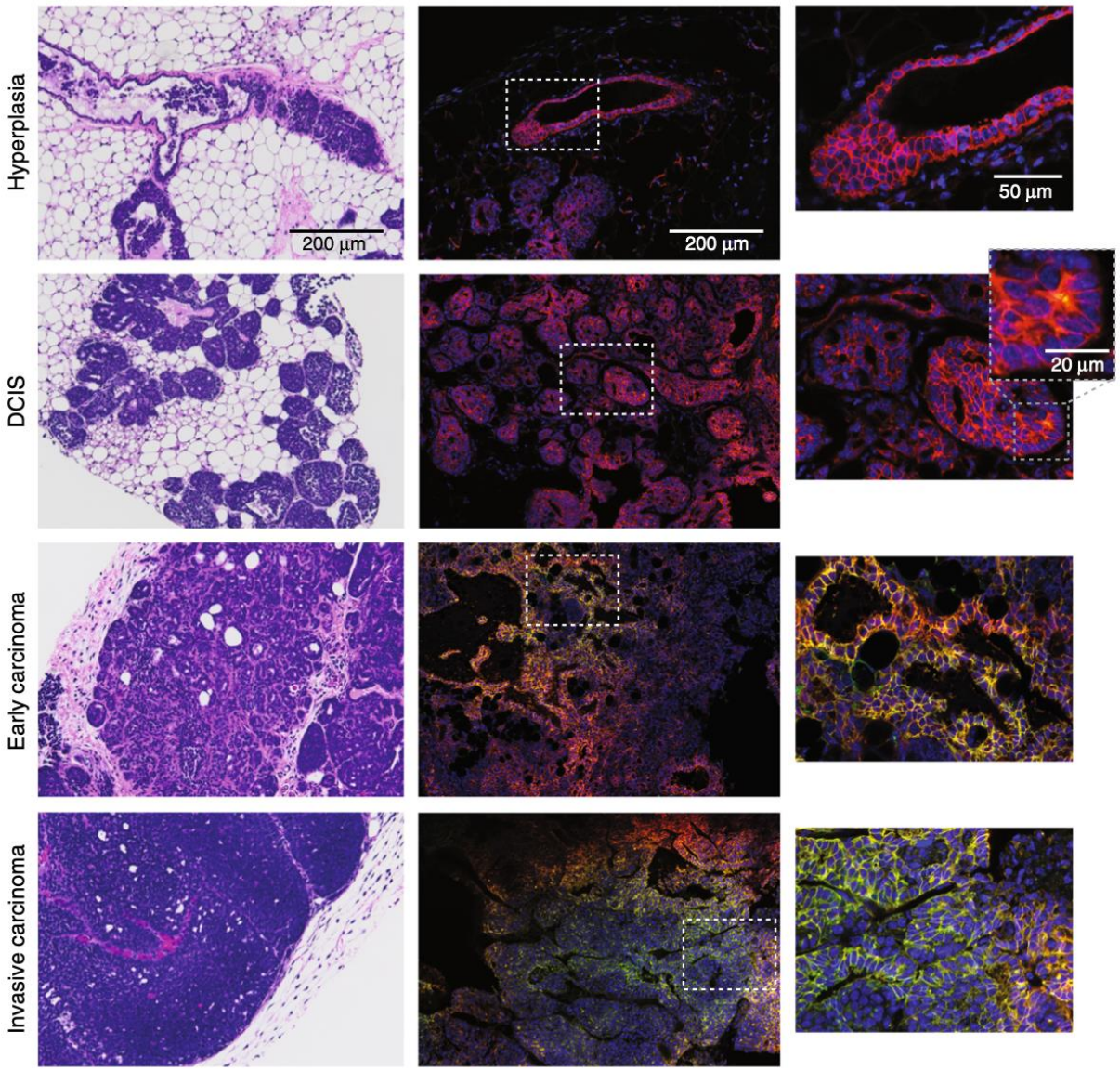

Figure 27: Hypoxia drives tumor cell invasion and metastasis. *Cross-sections of different stages of mice breast tumors to ductal carcinoma to invasive carcinoma stained for hematoxylin and eosin (left). The mice were designed to develop spontaneous tumors in which cells would permanently switch from tdTomato (red staining) to GFP (green staining) under hypoxic conditions. The first detection of hypoxia was in DCIS lesion* (Godet et al., 2019).

Nutrients follow the same trend as oxygen and metabolomic research has shown that several metabolites (glutamine and cytidine, glucose, and TCA cycle-related phosphorylated glucose-derivatives) were severely depleted in solid tumors such as pancreatic ductal adenocarcinoma, compared to normal adjacent tissues (Kamphorst et al., 2015). These results were also found in organotypic microfluidic breast cancer models (Ayuso et al., 2018). The intraductal niche is therefore a source of nutrient and hypoxic stress for cancer cells which can

be circumvented and be drivers of progression towards invasive phenotypes (Godet et al., 2019)

5.2.2. Dysregulation of PI3K/AKT/mTOR and consequences for sustain growth and proliferation in an hypovascularized tumor environment

Due to its role in cell growth and proliferation, hyperactivation of mTORC1 signaling is frequently found across several tumor types, including breast cancer. Aberrant activation of mTOR rarely results from mutation of the kinase itself, but rather from the accumulation of oncogenic mutations in upstream signaling components such as the PI3K/AKT and Ras/Raf/MEK/ERK (MAPK) pathways. Gain-of-function mutations of PI3KCA are found in one-third of breast cancers, and mutations of PI(3,4,5)P3 3'-phosphatase PTEN (Phosphatase and Tensin Homolog deleted on Chromosome 10) are detected in half of breast cancers, leading to hyperactivated AKT and mTORC1 (Carbognin et al., 2019). Mutations in PI3KCA are more common in hormone receptor-positive (HR+) luminal A and HER2+ subtypes (45% and 39% of cases respectively). In contrast, alterations of PI3KCA appear in only 9% of TNBC cases. However, PTEN downregulation was more prevalent in TNBC than in HR+ tumors and was associated with lower disease-free survival (Prvanović et al., 2021). Endogenous inhibitors of mTORC1 signaling such as TSC1/2 and FLCN are tumor suppressors found to be inactivated in the familial cancer syndrome TSC and in Birt-Hogg-Dube hereditary cancer syndrome (Napolitano et al., 2020).

A growing body of evidence points to the central role of 4E-BP1/eIF4E downstream of mTORC1 in tumor progression. eIF4E is able to selectively enhance the translation of mRNA products of several oncogenes and cancer-promoting factors such as c-Myc, Cyclin D1, VEGF, and MMP9 and was shown to be upregulated in many carcinomas, including breast cancer. mTORC1-mediated phosphorylation and inhibition of 4E-BP1 also promote eIF4E activity. However, non-phosphorylated 4E-BP1 has been shown to act as a tumor promoter under cellular stress induced by the microenvironment such as starvation. These observations suggest that in hypovascularized areas and under starvation, mTORC1 is inactivated and the repression on 4E-BP1 is abolished. Consequently, 4E-BP1 can highjack the translation machinery to promote the expression of pro-survival and pro-angiogenic genes (Musa et al., 2016).

In a progressive effort to understand and characterize cell heterogeneity within a tumor, a growing body of evidence suggests that mTORC1 is not hyperactivated everywhere within a single tumor. Starvation and hypoxia lead to an inhibition of mTORC1 within the tumor core and in cells distanced from blood vessels (Gerdes et al., 2018; Risom et al., 2022b). Autophagy has dual roles in tumor initiation, acting both as a tumor suppressor by preventing the accumulation of damaged molecules and organelles, and as an oncogenic pathway that

promotes cell survival and growth in transformed cells. Autophagy defects such as loss of autophagy initiators beclin-1 or atg7, lead to susceptibility to metabolic stress, ROS production, and subsequent genetic instability thus promoting tumorigenesis. Autophagy inhibition can also lead to the formation of cytoplasmic aggregates and phase separation of autophagy receptors (*i.e.*, p62 and neighbor of BRCA1 (NBR1)) which sequesters and activates oncogenic key signaling components such as MAP3K3 from the MAPK pathway (Marsh et al., 2020, 2021; D. Sun et al., 2018; Zaffagnini et al., 2018). On the other hand, autophagy confers stress resistance to transformed breast cells, especially in hypoxic and nutrient-depleted microenvironments, or in response to ECM detachment during the metastatic process (Espina et al., 2010; Sharifi et al., 2016). Metastatic tumor recurrence can occur years after the removal of the primary tumor by the outgrowth of quiescent circulating cancer cells upon microenvironmental inputs. Autophagy has been shown to be critical for the survival of dormant breast tumor cells and genetic or pharmacological inhibition of autophagy inhibits the switch from dormancy to growth and lessens the lung metastatic burden (Vera-Ramirez et al., 2018). Triple-negative breast cancers exhibit higher levels of autophagy than other subtypes and express more autophagy-related genes (including Beclin-1, LC3A and LC3) which are markers of poor prognosis (Bertozzi et al., 2021; Espina et al., 2010; Overgaard et al., 2009; H. Zhao et al., 2013). Knock-down of LC3 and Beclin-1 in TNBC cell lines induced apoptosis, migration, and invasion (Hamurcu et al., 2018) Clinical evidence suggest that TNBC are more hypoxic compared to non-TNBC and that constitutive increased autophagy promotes survival in this oxygen-deficient environment (O'Reilly et al., 2015).

5.2.3. Mode of action of some inhibitors of mTOR signaling and clinical use

Targeting the hyperactivated PI3K/AKT/mTORC1 pathway has therefore generated significant interest for cancer therapy.

Rapamycin confers a gain of function of FKB12 which then allosterically inhibits mTORC1 (see above). mTORC2 is insensitive to short-term treatment with rapamycin because RICTOR hides the FRB domain of mTOR. However, chronic treatment can diminish mTORC2 activity as rapamycin could bind to neosynthesized mTOR and therefore inhibit the formation of *de novo* mTORC2. At the time of its discovery, Rapamycin treatment was considered a promising target for anticancer therapy. However, rapamycin has poor solubility and pharmacokinetics. Some rapamycin analogs (rapalogs) have been approved for cancer treatment. Temserolivus (Pfizer) was the first one approved for treatment of advanced-stage renal cell carcinoma in 2007. The rapalog Everolimus (Novartis) is also used in combination with hormonal therapies for the treatment of metastatic HR+ HER2-negative breast cancer as it improved progression-free survival (Bachelot et al., 2012; Baselga et al., 2012). However, the efficacy of Everolimus

(alone or in combinational treatment) remains modest compared to what was expected, probably due to incomplete inhibition of the phosphorylation of 4E-BP1 (Laplante & Sabatini, 2012). As such, small ATP-competitive mTOR inhibitors abolishing even 4E-BP1 phosphorylation were developed. Their results were promising, as they can impair cell growth and proliferation but also induce apoptosis. (Y. Chen et al., 2018; J. jie Shi et al., 2018; H. Wang et al., 2020). mTORC1 inhibits AKT and the insulin growth factor signaling in a negative feedback loop. Inhibiting mTORC1 relieves AKT inhibition and could paradoxically stimulate cell growth and proliferation. Dual inhibition of PI3K and mTOR are considered a good combinatory treatment to circumvent this issue (Wu et al., 2022).

5.2.4. Scavenging of extracellular molecules to sustain growth and proliferation in an hypovascularized tumor environment

Cancer cells can bypass the bloodstream and harvest nutrients by scavenging macromolecules directly from the tumor microenvironment. Scavenging is defined as the uptake of macromolecules synthesized by other cells in the tumor microenvironment and further broken down in lysosomes into elemental building blocks used for ATP production, anabolic processes, and cell growth. By definition, scavenging is the opposite of autophagy wherein cells recycle their own components, however due to the mass conservation law, cells cannot grow indefinitely on a strict autophagy regime (Finicle et al., 2018). Scavenging pleases every palate, and a diversity of extracellular molecules can be scavenged, including ECM components, serum albumin, apoptotic and necrotic debris. Therefore, different scavenging strategies are employed by cancer cells to overcome nutrient limitations.

Like breast DCIS, pancreatic ductal adenocarcinomas (PDACs) are typically characterized by nutrient and oxygen limitations due to poor perfusion and high interstitial pressure. Activating mutations in K-Ras are the most frequent oncogenic drivers of PDACs (95% of cases) and promote a metabolism relying heavily on glutamine-derived glutamate to fuel the tricarboxylic acid (TCA) cycle. Mutation of K-Ras also stimulates the scavenging of extracellular proteins by constitutively activating macropinocytosis, an actin-dependent non-selective uptake mechanism of extracellular components. Macropinocytosed proteins are further degraded in lysosomes and provide amino acids, including glutamine, to starved cancer cells (Commisso et al., 2013; Davidson et al., 2017; Kamphorst et al., 2015; Olivares et al., 2017). Scavenging of ECM proteins such as collagens and fibronectin, which represent the majority of the tumoral microenvironment biomass, has also been reported in ovarian and pancreatic cancers (Nazemi & Rainero, 2020; Olivares et al., 2017). Starving PDAC cells of glucose or glutamine also induce internalization and lysosomal degradation of collagens I and IV. Collagen-derived proline is transported in the mitochondria through the transporter

PRODH1 and converted to glutamate, then to TCA substrate alpha-ketoglutarate. Feeding starved PDACs cells with soluble collagen or proline promotes both survival and proliferation (Olivares et al., 2017). Solid tumors, and especially PDACs, are characterized by an exceptional metabolic plasticity and can use a diversity of macromolecules as nitrogen donors for glutamine and nucleotide synthesis (Fendt et al., 2020; Gouirand et al., 2022; Tsai et al., 2021). Few studies have reported that mTORC1 activity represses intralysosomal degradation of scavenged molecules (Palm et al., 2015) and that mTOR inhibition upon starvation promotes scavenging, restores the intracellular amino acid balance, and drives the proliferation of starved cancer cells (Finicle et al., 2018; Kamphorst et al., 2015; Nofal et al., 2017). Conversely, mTORC1 activity is rescued in starved cells upon supplementation with albumin in a dose-dependent manner. The catabolism of albumin restored the amino acid levels in these cells, preventing cell death (Nofal et al., 2017; Palm et al., 2015; Palm & Thompson, 2017). Scavenging has therefore the potential to greatly influence tumor progression and has gathered quite the attention over the last few years as a potential druggable pathway (Finicle et al., 2018).

WORKING HYPOTHESIS AND OBJECTIVES

It is widely accepted that invasive cancer cells form MT1-MMP-enriched, actin-based plasma membrane/ECM contact sites called invadopodia, which focally degrade matrix tissues, enabling cell penetration and dissemination. Most of the studies focused on the cellular signals affecting invadopodia formation and function such as the activation of integrins and tyrosine kinase receptors or by cell cycle regulators. However, the influence of the ever-changing tumoral microenvironment on invadopodia dynamics and plasticity remains elusive (Masi et al., 2020). Due to tumor growth rate and limited blood supply, the tumor microenvironment is often hypoxic and deprived of nutrients (including glucose and amino acids/AA). In addition, increased ECM stiffness can further impede the perfusion and nutriment supply of the tumor and can trigger the rewiring of the tumor metabolism to support tumor survival and proliferation. A growing body of evidence points out that under nutrient-limiting conditions, normal and transformed cells can internalize ECM molecules to restore the AA balance which promotes survival and proliferation. However, the molecular mechanisms underlying ECM proteolysis prior to internalization remain largely overlooked.

The cell response to nutrients is controlled by the kinase mTOR which nucleates two distinct complexes, mTORC1, and mTORC2. Under AA replete conditions, mTORC1 is activated on the surface of lysosomes and it phosphorylates several target proteins including p70S6 Kinase 1 (S6K) and eukaryotic translation initiation factor 4E (eIF4E)-binding protein 1 (4E-BP1), promoting protein and lipid anabolism. In addition, active mTORC1 represses autophagy by phosphorylating and inhibiting the autophagy regulator, ULK 1, and the transcription factor EB (TFEB), which regulates the expression of genes for lysosomal biogenesis and the autophagy machinery. In starved cells, mTORC1 is repressed which promotes the degradation of autophagic cargo and exogenous macromolecules to restore the AA balance and prevent a metabolic and energetic crisis (Commisso et al., 2013; Kamphorst et al., 2015; Nofal et al., 2017; Palm et al., 2015). However, the cross-talk between the mTOR signaling pathway and ECM degradation and uptake of proteolytic products to support cancer cell growth are still poorly understood.

Prior results of Dr Cecilia Colombero, a post-doctoral fellow in the host lab showed that MDA-MB-231 breast cancer cells deprived of growth factors (GF) and AA (EBSS buffer) for up to 60 min massively degraded fibrillary type I collagen with a 10-fold increase compared to cells cultured in a complete medium. This increase in gelatino- and collagenolysis was abolished by genetic depletion of MT1-MMP or TKS5, suggesting that invadopodia mediate a strong ECM degradation in response to starvation. Additionally, EBSS treatment repressed mTORC1 activity as assessed by the phosphorylation of S6K and 4E-BP1. Supplementing AA to EBSS partially restored mTORC1 activity and importantly, reduced by 50% the starvation-

induced ECM degradation. Based on these findings, we hypothesized that nutrient starvation and mTORC1 repression could promote ECM breakdown and possibly internalization in breast cancer cells to support their proliferation and survival.

I addressed the plasticity of the invadopodia-mediated ECM degradation in response to the nature and amount of nutrients in the microenvironment. I also dissected the molecular mechanisms by which starvation and mTOR signaling altered the dynamics of the invadopodia components to support the increased ECM degradation.

Working closely with Sandra Antoine-Bally, an engineer in the host lab, we used fluorescence microscopy to image breast (MDA-MB-231) and pancreatic (Bx-PC3) cancer cells and monitored their ECM degradative capacities in response to nutrient levels/availability. We showed that mTORC1 repression by nutrient starvation (EBSS buffer) or pharmacological inhibition (rapamycin) induced a massive degradation of fibrillar type I collagen or gelatin. Furthermore, restoring mTORC1 activity in starved cells by genetic ablation of TSC or by supplementing the EBSS buffer with albumin or free AA partially rescued mTORC1 activity which abolished half of the starvation-induced collagen degradation. We recapitulated the effect of starvation on ECM degradation in *ex vivo* TNBC patient-derived xenografts (PDX) explants embedded in collagen. Altogether, these results were consistent with direct control of ECM degradation by mTORC1 activity. Mechanistically, we showed that short-term nutrient starvation greatly impeded clathrin-mediated endocytosis as it increased the density and the lifetime of clathrin-coated pits (CCPs) at the plasma membrane of starved cells. These CCPs coincided with MT1-MMP and were in close association with TKS5. These results suggest that in nutrient-starved cells, MT1-MMP is sequestrated in arrested CCPs which supports ECM degradation. These discoveries were published in an article presented in the next section and in which I share co-first authorship (see **Article 1**).

Based on this first demonstration of a link between mTOR and the invadopodia machinery, I have started to dissect the mechanisms by which mTORC1 signaling may influence the invadopodia response in nutrient-replete conditions. I used a siRNA-based approach to systematically knock down (KD) the main components of the mTORC1 pathway and investigated their effect on gelatin degradation and mTORC1 activity. In addition, I made use of different pharmacological inhibitors known to interfere with mTOR signaling. Consistent with our previous findings, siRNA-mediated downregulation of mTORC1 (*e.g.*, siRagC or siRaptor), enhanced matrix degradation. Interestingly, KD of folliculin (FLCN) had no effect on mTORC1 activity as expected but massively induced matrix degradation. This dissociation between mTORC1 activity and matrix proteolysis pointed to a potential role of TFEB which translocates in the nucleus in FLCN-depleted cells, independently of mTORC1 activity (Napolitano et al., 2020, 2022). In addition, TFEB induces lysosomal exocytosis (Medina et al., 2011; Palmieri et al., 2011) and we hypothesized that enhanced lysosomal exocytosis may

increase MT1-MMP delivery to the invadopodia to support/fuel ECM degradation. We first showed that TFEB was necessary for the ECM degradation response induced by silencing RagC, Raptor or FLCN as well as by treatment with mTOR-inhibitors. Live-cell microscopy of MDA-MB-231 stably expressing MT1-MMP tagged with super ecliptic pHLuorin revealed that MT1-MMP exocytosis rates were increased in siRagC cells, consistent with an increase of endogenous MT1-MMP at the plasma membrane levels as assessed by surface labeling. Furthermore, using particle image velocimetry to quantify $TKS5^{GFP}$-based invadopodia by live cell microscopy, we could show that siRagC-treated cells displayed invadopodia with increased velocimetry compared to control cells; this increased invadopodia dynamics was abolished by concomitant TFEB KD. Treatment of *ex vivo* TNBC patient-derived xenografts (PDX) with mTOR drugs such as Everolimus or Torin-1 also increased massive matrix degradation. Increased invadopodia activity and ECM degradation have been shown to promote tumor cell invasion. We tested the invasion capacities of these highly degradative cells by using a spheroid-based assay and showed that KD of RagC enhanced the invasion of MDA-MB-231 multicellular spheroids as well as spheroids of MCF10DCIS.com cells. Altogether, we propose that mTOR, through TFEB regulation, controls the invadopodia response by promoting MT1-MMP exocytosis from the endolysosomal compartments, eliciting a surge in matrix degradation. We show that the enhanced matrix degradation response allows cancer cells to efficiently remodel and invade the surrounding ECM environment. These results are presented in a second manuscript to be submitted for publication

In the appendix section, I also included an in-press manuscript that I wrote together with Pedro Monteiro, a post-doctoral fellow in the host lab, in which we review the main experimental procedures to assess the formation and activity of invadopodia in cell in culture in different ECM environments.

ARTICLE 1

mTOR repression in response to amino acid starvation promotes ECM degradation through MT1-MMP endocytosis arrest

Cecilia Colombero[1, *], David Remy[1, *], Sandra Antoine-Bally[1], Anne-Sophie Macé[2], Pedro Monteiro[1], Nadia ElKhatib[3], Margot Fournier[1], Ahmed Dahmani[4], Elodie Montaudon[4], Guillaume Montagnac[3], Elisabetta Marangoni[4], and Philippe Chavrier[1, ±]

[1] Institut Curie, PSL Research University, CNRS UMR 144, 75005, Paris, France

[2] Institut Curie, PSL Research University, Cell and Tissue Imaging Facility (PICT-IBiSA), 75005, Paris, France

[3] INSERM U1279, Gustave Roussy Institute, Université Paris-Saclay, Villejuif, France

[4] Institut Curie, PSL Research University, Translational Research Department, 75005, Paris, France

* These authors contributed equally

± Corresponding author, e-mail: philippe.chavrier@curie.fr

Published in Advanced Sciences: 11th July 2021

ADVANCED SCIENCE Open Access
www.advancedscience.com

mTOR Repression in Response to Amino Acid Starvation Promotes ECM Degradation Through MT1-MMP Endocytosis Arrest

*Cecilia Colombero, David Remy, Sandra Antoine-Bally, Anne-Sophie Macé, Pedro Monteiro, Nadia ElKhatib, Margot Fournier, Ahmed Dahmani, Elodie Montaudon, Guillaume Montagnac, Elisabetta Marangoni, and Philippe Chavrier**

Under conditions of starvation, normal and tumor epithelial cells can rewire their metabolism toward the consumption of extracellular proteins, including extracellular matrix-derived components as nutrient sources. The mechanism of pericellular matrix degradation by starved cells has been largely overlooked. Here it is shown that matrix degradation by breast and pancreatic tumor cells and patient-derived xenograft explants increases by one order of magnitude upon amino acid and growth factor deprivation. In addition, it is found that collagenolysis requires the invadopodia components, TKS5, and the transmembrane metalloproteinase, MT1-MMP, which are key to the tumor invasion program. Increased collagenolysis is controlled by mTOR repression upon nutrient depletion or pharmacological inhibition by rapamycin. The results reveal that starvation hampers clathrin-mediated endocytosis, resulting in MT1-MMP accumulation in arrested clathrin-coated pits. The study uncovers a new mechanism whereby mTOR repression in starved cells leads to the repurposing of abundant plasma membrane clathrin-coated pits into robust ECM-degradative assemblies.

1. Introduction

Metabolic reprogramming is a hallmark of cancer cells, which adapt their nutritional strategies to match their elevated metabolic needs.[1,2] In certain microenvironments including in poorly perfused tumors, free nutrients such as amino acids (AAs) can be limiting, and extracellular proteins are used as alternative resources.[3–7] Recent studies found that in desmoplastic microenvironments, pancreatic and breast cancer cells can internalize proteolytic extracellular matrix (ECM) fragments such as peptides derived from fibronectin and type I collagen, which accounts for most of the extracellular biomass in these tumors.[8–11] Degradation of ECM-derived peptides in lysosomes contributes to AA supply that fuels the tumor metabolism and supports tumor survival and proliferation.[10–12] In addition, high collagen density has been linked with metabolism rewiring in breast cancer cells.[7,13] However, the mechanism underlying ECM breakdown under nutrient-depleted conditions is unknown.

The cell response to nutrients is controlled by the kinase mechanistic target of rapamycin (mTOR), which assembles into distinct protein complexes known as mTOR Complex 1 and 2 (mTORC1 and -2).[14] Only mTORC1 is sensitive to acute treatment by the anticancer drug, rapamycin.[14] Under AA replete conditions, mTORC1 localizes to the lysosome surface and phosphorylates several substrates including S6K and 4E-BP1, promoting protein translation and cell growth. Upon AA starvation, mTORC1 is inactivated inducing autophagy, cellular catabolism, and translation shut down.[14] Dysregulation of the PI3K/Akt/mTOR signaling pathway is linked with breast

C. Colombero, D. Remy, S. Antoine-Bally, A.-S. Macé, P. Monteiro, M. Fournier, P. Chavrier
Institut Curie
PSL Research University
CNRS UMR 144, Paris 75005, France
E-mail: philippe.chavrier@curie.fr

The ORCID identification number(s) for the author(s) of this article can be found under https://doi.org/10.1002/advs.202101614

DOI: 10.1002/advs.202101614

A.-S. Macé
Cell and Tissue Imaging Facility (PICT-IBiSA)
Institut Curie
PSL Research University
Paris 75005, France

N. ElKhatib, G. Montagnac
Gustave Roussy Institute
Université Paris-Saclay
INSERM U1279
Villejuif 94805, France

A. Dahmani, E. Montaudon, E. Marangoni
Translational Research Department
Institut Curie
PSL Research University
Paris 75005, France

cancer initiation and progression and regional heterogeneity in immunohistochemical profiles of phosphorylated (p)-mTOR and its downstream signaling effectors, pS6K, and p4E-BP1 have been described in relation with metabolic alterations.[15,16]

The protease-dependent invasion program of tumor cells is mediated by invadopodia, which are F-actin-, cortactin-based cell–matrix contacts that enzymatically degrade and push confining ECM fibers aside to allow cell movement.[17–20] The scaffolding protein, TKS5, plays a pivotal role in the assembly and surface accumulation of the trans-membrane matrix metalloproteinase and collagenase, MT1-MMP, to invadopodia.[20–23] Here, we investigated the mechanism of ECM degradation under conditions of nutrient scarcity in relation with mTOR signaling. Our findings uncover a novel mechanism that leads to the repurposing of the invadopodial MT1-MMP/TKS5 axis. This program, which is controlled by mTOR signaling, inhibits the endocytic clearance of MT1-MMP and triggers its accumulation in arrested plasma membrane clathrin-coated pits (CCPs) to actively degrade the collagen matrix in an AA-depleted environment.

2. Results

2.1. Starvation of Tumor Cells Stimulates Invadopodia-Mediated Pericellular Matrix Degradation

MDA-MB-231 cells were selected as a model of breast cancer cells known for producing a robust invadopodial response at matrix contact sites.[20] When plated on fluorescently labeled gelatin for 60 min in complete medium (CM), several gelatin degradation spots were visible underneath the cells, which coincided with punctate invadopodia positive for TKS5 (endogenous or overexpressed GFP-tagged protein) located underneath or in the vicinity of the nucleus (**Figure 1a** and Figure S1a, Supporting Information). The consequences of starvation on ECM degradation were assessed by culturing cells in AA- and serum-depleted medium (EBSS). Starvation robustly increased the degradation of gelatin by MDA-MB-231 cells (Figure 1a,b and Figure S1a, Supporting Information). This response was abolished by treatment with the broad-spectrum MMP inhibitor, GM6001 (Figure 1b). Increased gelatinolysis correlated with a 4-5-fold increase in the density of matrix-degradative TKS5-positive structures, which were reduced in size as compared with those in cells incubated in CM (Figure 1c,d). Analysis of the invadopodia distribution along a cell centroid-to-periphery axis (0-1 position) revealed that invadopodia were homogeneously scattered throughout the entire adherent cell surface in starved cells in contrast to their typical central localization in cells in replete conditions (Figure 1e). In order to exclude that association of TKS5-positive dotty structures with degradation spots was by chance due to the high structure density in starved cells, TKS5 positions were randomly scrambled 5000 times, and the association of TKS5-positive structures with degradation spots was calculated for each scrambled image (Figure S1b,c, Supporting Information). The observed association values exceeded all those calculated for randomly scrambled images ruling out that TKS5 association with degradation spots was random (Table S5, Supporting Information).

Cells were embedded within a 3D fibrillar collagen network, the main component of interstitial ECM tissue, and stained with a Col1-¾C antibody that recorded collagen cleavage cumulated over the incubation period. Similar to the gelatinolysis response, collagen cleavage by starved cells was strongly enhanced as compared to replete conditions (Figure 1f,g). Although the association of the invadopodia components, cortactin, and TKS5, with cleaved fibers was visible irrespective of nutrient availability, invadopodia occupied a much larger portion of the cell surface and were more fragmented in starved cells (Figure 1h and Figure S1d, Supporting Information). MT1-MMP can be inhibited by tissue inhibitors of metalloproteinases (TIMPs), including TIMP-2 which is present in tissues and biological fluids including serum.[24] EBSS medium was supplemented with increasing amount of recombinant TIMP-2 from two independent sources. Only at the dose of 2 μg mL^{-1} (i.e., 20-200-fold TIMP-2 concentration in CM, not shown),[24] was recombinant human TIMP-2 capable of fully repressing collagenolysis (Figure S1e, Supporting Information). These data show that the absence of TIMP-2 in EBSS condition does not account for the observed changes in matrix degradation by starved cells. Moreover, it is likely that TIMP-2 concentration is reduced in tumors embedded within a dense collagen-rich desmoplasia lowering vascularization.

As reported, silencing of MT1-MMP or TKS5 inhibited collagen cleavage in MDA-MB-231 cells in replete conditions (Figure S1f,g, Supporting Information).[23] Depletion of MT1-MMP or TKS5 also abolished collagenolysis in starved cells (Figure 1i). MT1-MMP was similarly required for induction of gelatinolysis in EBSS (Figure S1h, Supporting Information). Induction of collagenolysis upon starvation and MT1-MMP and TKS5 dependency were seemingly observed in pancreatic adenocarcinoma Bx-PC3 cells, which expressed levels of the main invadopodia components similar to breast MDA-MB-213 cells (Figure S2a,d, Supporting Information). Collectively, these findings indicate that increased matrix degradation by AA-depleted cells is mediated by a MT1-MMP and TKS5-dependent mechanism in breast and pancreatic tumor cells.

We compared the capacity of cells to remodel collagen fibers in nutrient replete or deplete environments by live cell imaging. $TKS5^{GFP}$-positive invadopodia in cells in replete conditions were highly dynamic and were able to push aside and bundled the contacted collagen fibers (Figure 1j and Movie S1, Supporting Information).[20] In contrast, fragmented and mostly static TKS5-positive structures were visible in AA-starved cells with the little remodeling of the underlying fibers over time (Figure 1k and Movie S2, Supporting Information). These observations demonstrate that tumor cells switch from a potent matrix remodeling and invasive mode in replete conditions typical of disseminating cells, to an exclusive matrix degradation and possibly nutrient sourcing program in nutrient-scarce conditions.

2.2. Induction of the MT1-MMP Collagenolytic Response Upon Starvation of TNBC PDX Explants

To generalize these findings to a model close to the human disease, we used cells obtained from triple-negative breast cancer patient-derived xenografts (PDX).[25,26] Cells isolated from several independent PDXs were cultured *ex vivo* in a 3D type I collagen gel in AA-replete or depleted conditions and their collagenolytic activity was assessed (**Figure 2a**). PDX-derived cells were primarily composed of cytokeratin-8-positive carcinoma cells and

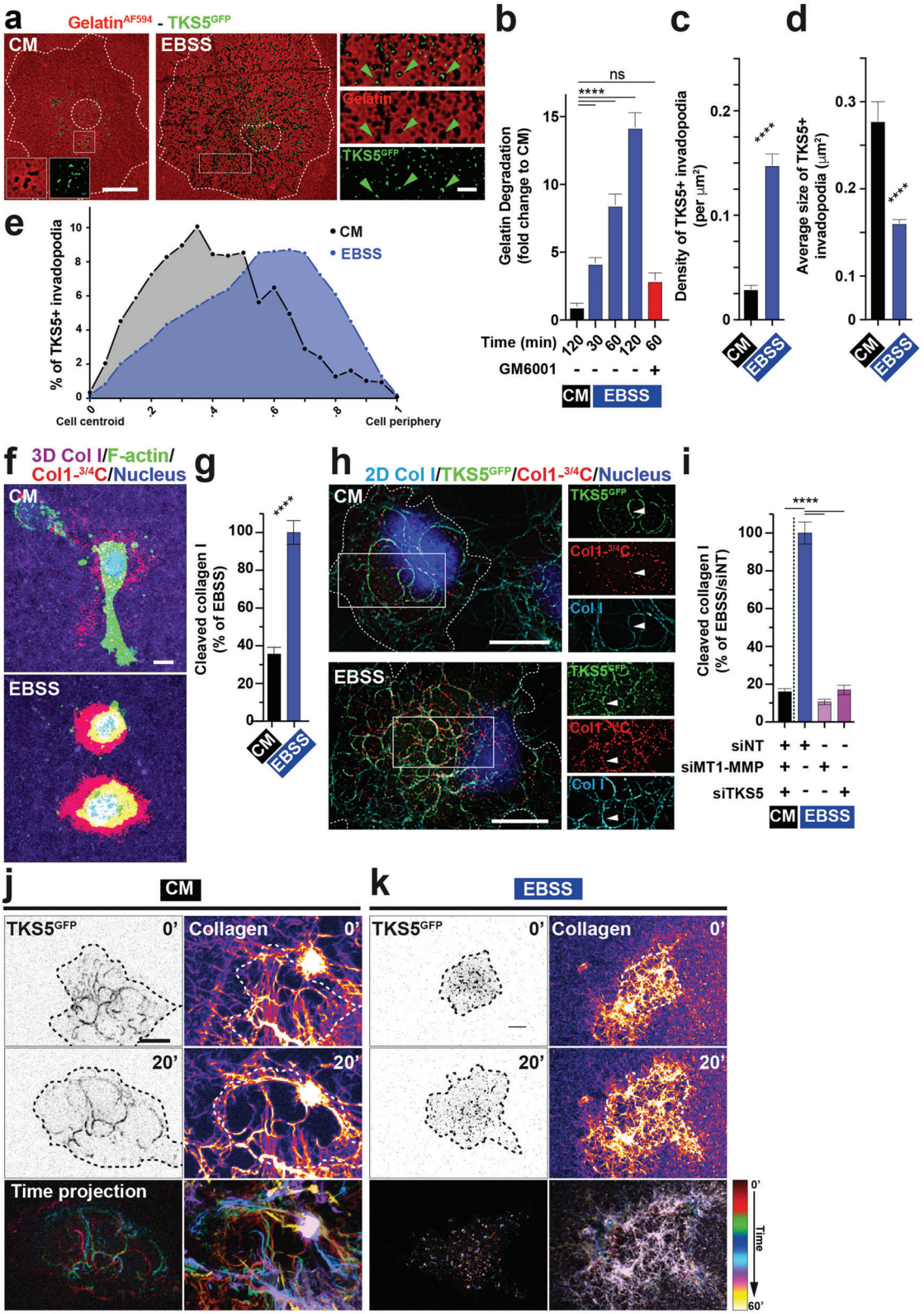

Figure 1. Enhanced matrix degradation and requirement for MT1-MMP and TKS5 in AA- and serum-starved cells. a) Deconvoluted images showing MDA-MB-231 cells expressing TKS5^{GFP} (green) plated on fluorescently-labeled gelatin (red) for 60 min in CM or EBSS starvation medium depleted for AAs and serum. Higher magnification of the boxed region is shown in the insets. Dotted lines, cell and nucleus contour. Scale bars, 10 μm, 2 μm (insets). b) Gelatin degradation by MDA-MB-231 cells cultured in the indicated conditions. c) Mean density of TKS5-positive invadopodia ± SEM

fibroblasts, the latter being identified based on their characteristic spindle-shaped morphology (not shown). In five out of eight PDXs, overnight incubation in EBSS resulted in a strong induction of pericellular collagen degradation as compared to the complete medium (Figure 2b,c). Moreover, treatment with GM6001 inhibited collagenolysis supporting the conclusion that stimulation of ECM degradation requires MMP activity in starved PDXs (Figure 2d). Starvation of the PDXs correlated with reduced phosphorylated 4E-BP1 (Ser65) level as a proxy for mTORC1 kinase activity as compared to conditions of nutrient sufficiency (Figure 2d). Additionally, we found a correlation between the intensity of the starvation-induced collagenolytic response with MT1-MMP, and to some extent TKS5, expression levels in PDX (for instance compare the response of $TKS5^{Low}$ and $MT1\text{-}MMP^{Low}$ HBCx-66, HBCx-92 and HBCx-172 and $MT1\text{-}MMP^{High}$ HBCx-4B and HBCx-60 PDXs, Figure 2e,f). Collectively, these data support the conclusion that nutrient scarcity enhances collagenolysis in breast PDXs in relation with the TKS5/MT1-MMP axis.

2.3. Regulation of the Collagenolytic Response by mTOR Signaling

mTOR is the master regulator of the cell's response to nutrient and AA availability.[14] As expected, mTORC1 activity was strongly repressed in cells cultured for 1 h in EBSS as compared to CM as shown by the reduction in phosphorylated S6K (Thr389) and p4E-BP1 levels (**Figure 3a**,e,h). Replenishment of EBSS with free AAs similar to their concentration in CM (see Table S4, Supporting Information) partially restored mTORC1 activity (Figure 3a), and was correlated with a 50–60% reduction of collagen cleavage by MDA-MB-231 cells as compared to EBSS (Figure 3b). These findings indicated that nutrient scarcity, in particular the lack of free AAs, strengthens the collagenolytic activity of breast MDA-MB-231 tumor cells, and that the absence of serum components accounted for ≈50% of the response. In addition, it has been shown that oncogenic Ras mutations promote macropinocytic uptake of extracellular proteins such as serum albumin, which are catabolized in lysosomes and serve as an AA source to sustain cancer cells' metabolic needs.[3,4,27] We observed that supplementing EBSS with 3% bovine serum albumin (BSA) partially restored pS6K levels in agreement with the mutated *KRAS* status of MDA-MB-231 cells (Figure 3c, and Figure S3a, Supporting Information),[28,29] and resulted in a ≈60% reduction of collagen cleavage as compared to EBSS alone (Figure 3d). Alltogether, these data suggest a correlation between mTORC1 activity and ECM degradation, i.e., mTORC1 inhibition correlates with the induction of matrix degradation by breast tumor cells.

In agreement with this assumption, we observed that inhibition of mTORC1 activity by acute rapamycin treatment of cells grown in nutrient-replete conditions (CM) (Figure 3e, and Figure S3b–d, Supporting Information), resulted in a ≈2.5-4-fold increase in collagen or gelatin degradation (Figure 3f and Figure S3e, Supporting Information). In contrast, collagenolysis was only marginally increased upon rapamycin treatment in EBSS (Figure 3f), in conjunction with the fully repressed mTORC1 status in starved cells (Figure 3e, and Figure S3b–d, Supporting Information). Interestingly, reduced collagenolysis upon EBSS supplementation with free AAs was abolished in cells treated with rapamycin in parallel with fully repressed mTORC1 activity (Figure 3a,b). mTORC1 integrates convergent AA-sensing signals from Rag and signaling inputs from Rheb GTP-binding proteins on endolysosomes.[14] The TSC complex (TSC1, TSC2, and TBC1D7), which acts as a GTPase activating protein (GAP) for Rheb, is recruited to the endolysosomes by Rag GTPases upon AA removal causing Rheb inactivation.[30] Expectedly, we observed a redistribution of mTOR from perinuclear vesicular compartments in CM to a diffuse cytosolic mTOR staining along with the disappearance of p4E-BP1 and pS6K signals in starved cells consistent with endolysosome dissociation and repression of mTOR (Figure 3g,h). In agreement with previous observations,[30] we found that starved cells silenced for TSC2 and TBC1D7 subunits failed to completely inactivate mTORC1 as shown by residual mTOR association with perinuclear membrane compartments and detection of pS6K and p4E-BP1 signal (Figure 3g,h). TSC2 and TBC1D7 knockdown led to approximately twofold reduction of gelatinolysis in EBSS that strongly correlated with some persistence of active mTOR on perinuclear endolysosomes (Figure 3g,i). Collectively, these data are consistent with a direct control of ECM degradation by mTORC1 activity.

In order to further strengthen the interplay between mTORC1 activity and the ECM degradation response, autophagy levels were investigated in starved cells in the absence or presence of type I collagen by staining for the autophagy marker, LC3.[31] As expected, LC3-positive vesicular structures increased upon starvation of MDA-MB-231 cells cultured on plastic as compared to replete conditions (Figure 3j,k). Interestingly, autophagy was significantly reduced in starved cells cultured in the presence of type I collagen, and this effect was partially abrogated upon MMP inhibition by GM6001 treatment (Figure 3j,k). All together, these results confirm that AA scarcity represses mTORC1 activity leading

(invadopodia μm^{-2}). d) Mean size of TKS5-positive invadopodia ± SEM (μm^2). e) Mean percentage distribution of TKS5-positive invadopodia according to their cell center-to-cell periphery (0-1) position in MDA-MB-231 cells cultured in the indicated conditions. f) MDA-MB-231 cells embedded in a 3D collagen I gel (magenta) for 6 h in the indicated medium and stained for cleaved collagen (red); F-actin (green); nucleus (blue). Scale bar, 10 µm. g) Collagen degradation by MDA-MB-231 cells cultured in CM or EBSS media normalized to EBSS value. h) Deconvoluted images showing MDA-MB-231 cells expressing $TKS5^{GFP}$ cultured on a fibrillar type I collagen network (cyan) for 60 min in indicated medium and stained for $TKS5^{GFP}$ (green), cleaved collagen fibers (red), and nucleus (blue). Higher magnification of boxed regions is shown in the insets. Arrowheads, $TKS5^{GFP}$-positive invadopodia. Scale bar, 10 µm. i) Collagen degradation by MDA-MB-231 cells treated with the indicated siRNAs. j,k) MDA-MB-231 cells expressing $TKS5^{GFP}$ were cultured on fluorescently-labeled type I collagen in CM or EBSS medium and imaged over time (1 image min^{-1}) by video microscopy (see Movies S1 and S2, Supporting Information). The first and 20^{th} images of representative time-lapse sequences are displayed in the upper left row showing $TKS5^{GFP}$-positive invadopodia using an inverted grayscale lookup table. The upper right row shows the collagen network using a Fire lookup table. The dotted lines underline the cell contour. The bottom row displays color-coded time projections of seven images at 10-min intervals showing the dynamics of $TKS5^{GFP}$-positive invadopodia and the remodeling of type I collagen fibers over time.

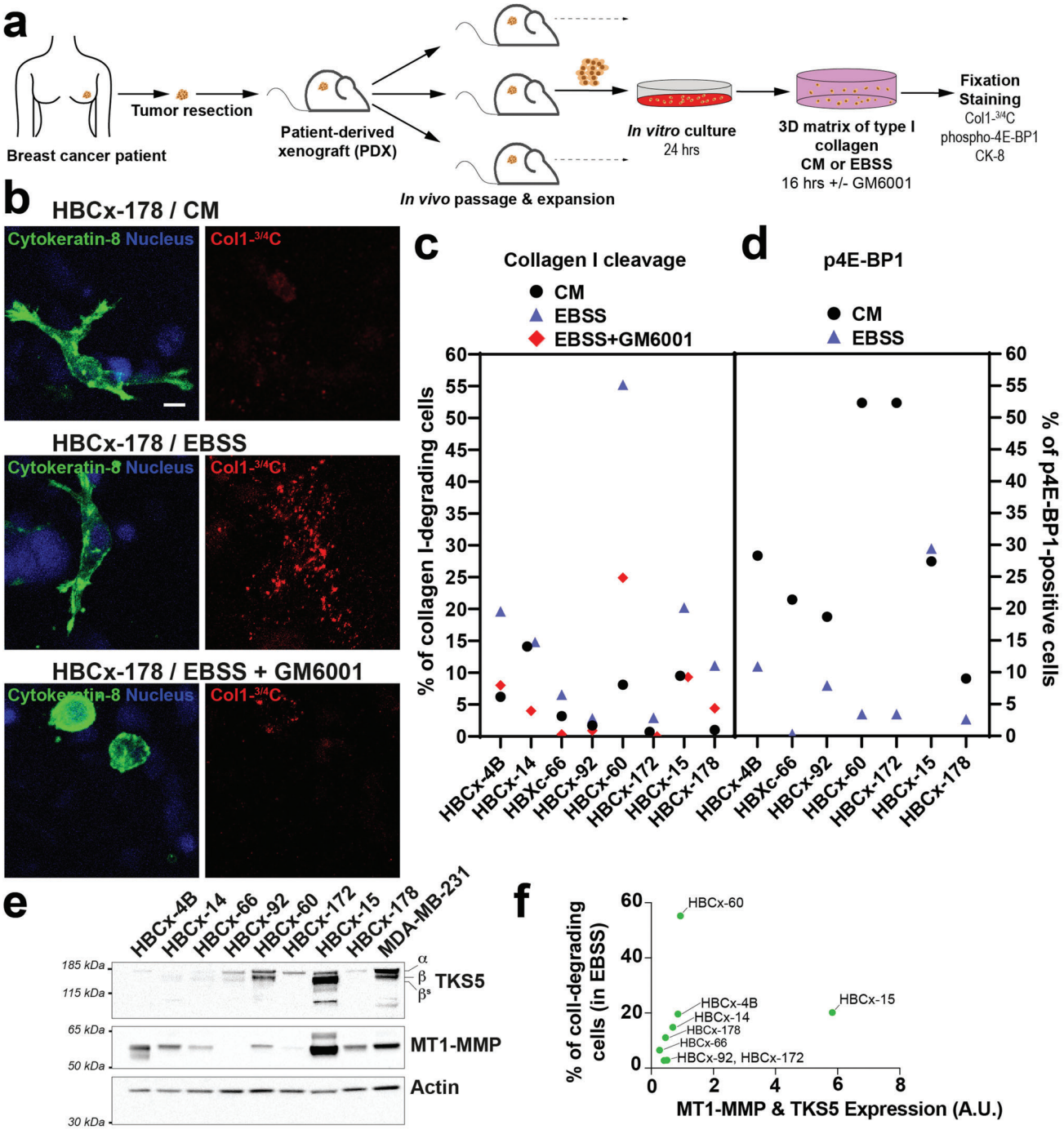

Figure 2. Induced collagenolysis in starved TNBC PDX ex vivo. a) Scheme depicting the preparation and analysis of breast cancer-derived PDX explants. b) PDX cells embedded in type I collagen in the indicated culture conditions were fixed and epithelial breast tumor cells were stained for Cytokeratin-8 (green) and cleaved collagen (red). DAPI-stained nuclei are shown in blue. Scale bar, 10 µm. c) Collagen cleavage by epithelial breast tumor cells derived from PDXs cultured in CM or EBSS medium in the presence or absence of GM6001. d) Levels of phosphorylated (p)4E-BP1 in epithelial breast tumor cells derived from PDXs cultured in CM or EBSS medium. e) Representative western blots of TKS5 and MT1-MMP expression in the PDX-derived cells grown in complete medium. Actin was used as a loading control. Molecular weights are in kDa. f) Levels of MT1-MMP and TKS5 expression in PDXs normalized to F-actin based on immunoblotting analysis show in panel d were summed up (*x*-axis) and plotted vs. the percentage of collagen degrading-cells (*y*-axis) for each starved PDX.

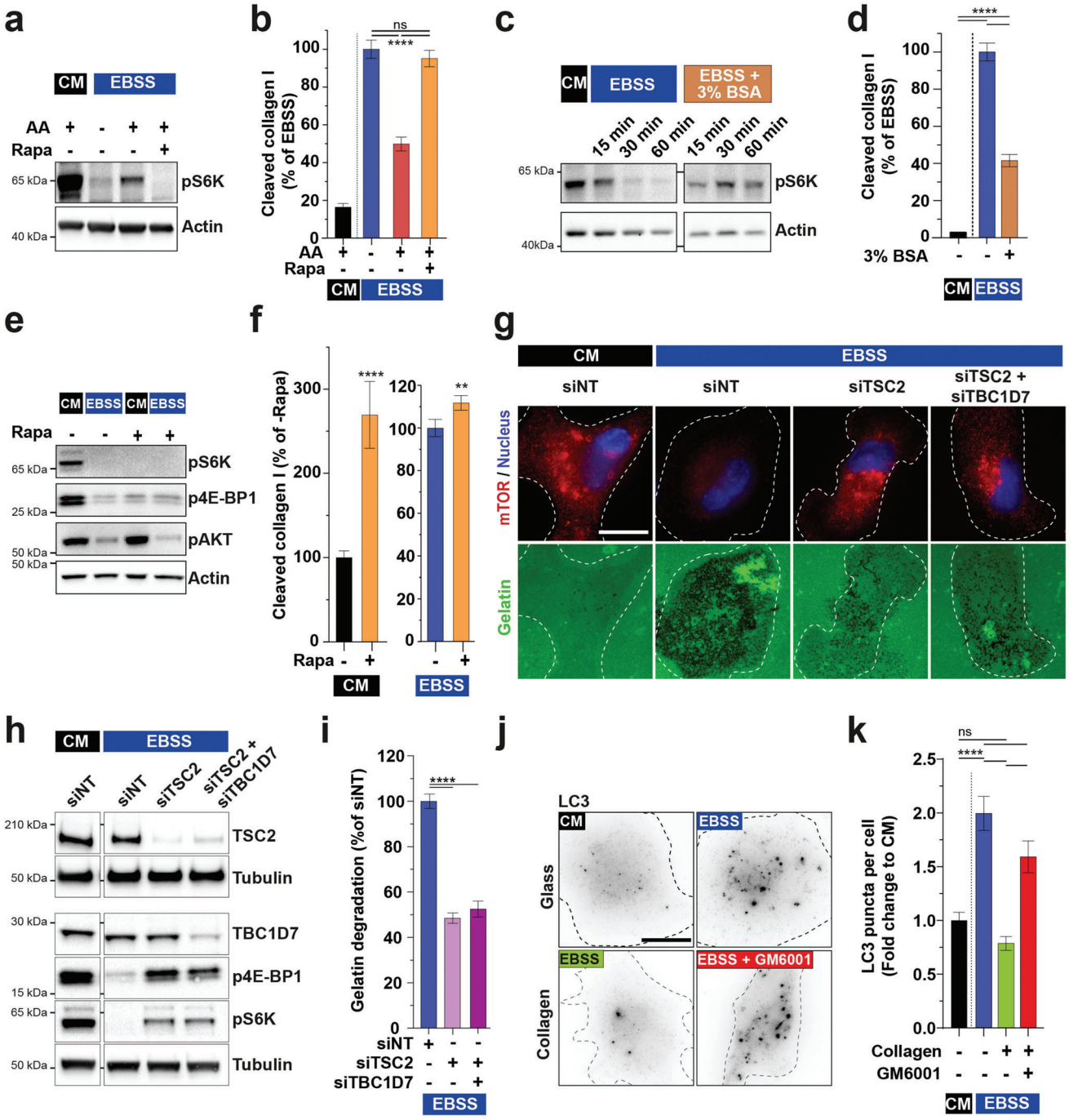

Figure 3. Regulation of ECM degradation by mTORC1. a,b) Phosphorylated (p)S6K (Thr389) in MDA-MB-231 cells incubated for 60 min in CM or EBSS medium supplemented with AA in the presence or absence of rapamycin. Actin was used as a loading control (panel a). Collagen cleavage by MDA-MB-231 cells incubated in the indicated conditions (panel b). c) Levels of pS6K in MDA-MB-231 cells incubated for the indicated period of time in CM or EBSS medium supplemented with 3% BSA. d) Collagen cleavage by MDA-MB-231 cells incubated for 60 min in the indicated medium. e) Immunoblots of total and phosphorylated S6K, 4E-BP1 (Ser65), and AKT (Ser473) in MDA-MB-231 cells incubated for 60 min in the indicated medium in the presence of mTOR inhibitor, rapamycin, or with the corresponding vehicle with actin used as a loading control. f) Collagen cleavage by MDA-MB-231 cells incubated for 60 min in indicated medium with or without rapamycin. g) MDA-MB-231 cells treated with the indicated siRNAs, were plated on fluorescently-labeled gelatin (green) for 60 min in CM or EBSS starvation medium. Cells were fixed and analyzed by immunofluorescence staining for mTOR (red). The cell contour is shown with a dotted line. Scale bar, 10 µm. h) Immunoblots of TSC2, TBC1D7, p4E-BP1, and pS6K in MDA-MB-231 cells incubated for 60 min in the indicated medium. Tubulin was used as a loading control. i) Gelatin degradation by MDA-MB-231 cells cultured in the indicated conditions. j,k) Quantification of autophagy LC3 puncta in MDA-MB-231 cells cultured in the indicated conditions normalized to the mean value in cells grown in CM medium on plastic ± SEM. Scale bar, 10 µm.

to the induction of autophagy and show that the autophagy response is inhibited by type I collagen in the presence of active MMP (presumably MT1-MMP). These data suggest that collagen breakdown by MT1-MMP may produce AA resources,[10–11] which restore some level of mTOR activity leading to the downmodulation of the autophagy response in starved MDA-MB-231 cells.

2.4. Endocytic Arrest and CCP Retention of MT1-MMP in Starved Cells

Total levels of MT1-MMP remained steady for at least 6 h in starved cells suggesting some redistribution of a preexisting pool to support the increase in collagenolysis (Figure S4a, Supporting Information). The influence of nutrient availability on the distribution of MT1-MMP was analyzed. Confirming previous observations, MT1-MMP fused with a GFP variant (pHLuorin)-tag localized predominantly in perinuclear late endosomes/lysosomes from which it can recycle to plasma membrane invadopodia (**Figure 4a**,b).[32] In addition, in cells grown in replete conditions, MT1-MMP was detected in plasma membrane accumulations in association with the underlying collagen fibers (i.e., invadopodia, Figure 4a). In contrast, MT1-MMP had an extensive dotty-like surface distribution in cells cultured in EBSS (Figure 4b). Endocytic CCPs cover the entire cell surface and display an archetypical dotty distribution. Moreover, the LLY^{573} motif in the carboxy-terminal tail of MT1-MMP is known to interact with the clathrin adaptor AP-2 complex involved in MT1-MMP surface clearance (see below).[33] Counterstaining for the α-adaptin subunit of AP-2 revealed that MT1-MMP-positive puncta were in close proximity to CCPs in starved cells (Figure 4b). Additionally, we noticed a 1.6-fold increase in the density of CCPs at the plasma membrane of starved cells as compared to cells grown in CM (Figure 4c).

Similarly, we observed a striking association of gelatin degradation spots and AP-2-positive CCPs in cells plated on fluorescently-labeled gelatin matrix grown in EBSS medium (Figure 4d, right panel and Figure S4b,c, Supporting Information). MT1-MMP punctate accumulations also coincided with the degradation spots (Figure S4d, Supporting Information). All together, accumulations of TKS5 (Figure 1a), AP-2 (Figure) and MT1-MMP (Figure S4d, Supporting Information) in association with a prominent dotty matrix degradation pattern appear as a strong emerging feature of starved cells.

Constitutive endocytosis of the transferrin (Tfn)-receptor is mediated by clathrin and AP-2 and can be readily monitored using fluorophore-conjugated Tfn. We followed the decay of Tfn^{AF546} from α-adaptin-positive CCPs overtime in cells cultured in CM or EBSS as a quantification of clathrin-mediated endocytosis (CME). While CCP-associated Tfn^{AF546} rapidly decayed in cells incubated in CM medium in the absence of fluorescent ligand, the intensity of receptor-bound Tfn^{AF546} associated with CCPs remained almost constant over the 10 min pulse in EBSS (Figure 4e,f). Internalized Tfn^{AF546} rapidly reached EEA1-positive early endosomes in cells incubated in nutrient-replete conditions, while the amount of Tfn^{AF546} detected in early endosomes was much lower in starved cells consistent with the reduction in Tfn uptake (Figure 4g). Additionally, we followed the dynamics of μ-$adaptin^{mCh}$-positive CCPs by TIRF-M and found approximately twofold increase in the percentage of stable CCPs (lifetime > 295 s) in EBSS versus CM conditions (Figure 4h and Movie S3, Supporting Information), in agreement with the observed increase in CCP density and reduced CME flux. Interestingly, TIRF-M also revealed some association between CCPs and $TKS5^{GFP}$-positive puncta that formed in their vicinity (Figure 4j and Movie S3, Supporting Information). Similar to stable CCPs in starved cells, adjacent $TKS5^{GFP}$-positive puncta also appeared to be long-lived (Figure 4i, and Movie S3, Supporting Information). Finally, we found that under conditions of endocytic arrest in starved cells, the induction of gelatinolysis was abrogated by α-adaptin knockdown (Figure 4j and Figure S4e, Supporting Information). This was in sharp contrast to the silencing of clathrin heavy chain that did not significantly impair matrix degradation nor AP-2 cluster formation (Figure 4j). All together, these observations highlight the requirement for the clustering of surface-exposed MT1-MMP to sustain the starvation-induced ECM degradation response through a mechanism, which, likely, involves the interaction of MT1-MMP with AP-2 in arrested CCPs (see Figure S4f, Supporting Information).[33]

3. Discussion and Conclusion

We show that depletion of extracellular AAs and serum to replicate conditions of nutrient scarcity in a collagen-rich microenvironment elicits a robust cancer cell-autonomous collagenolytic response, exceeding by one-order-of-magnitude the ECM-degradative activity of invasive breast and pancreatic cell lines and breast PDXs. The pericellular ECM-degradation response to starvation is triggered by mTOR inactivation and we identified the key invadopodia components, TKS5 and MT1-MMP, as major players. In contrast to its association to dynamically forming invadopodia at ECM contact sites typical of invasive cells under nutrient-replete conditions,[19–20] surface-exposed MT1-MMP accumulates at arrested CCPs in cells in a nutrient-scarce environment. Intriguingly, we observed some association between dynamic TKS5-positive assemblies and CCPs, which is enhanced upon starvation. Interestingly, several CME regulators including inositol 5-phosphatase, SHIP2, and its product, phosphatidylinositol 3,4-bisphosphate (PI(3,4)P2), the F-BAR domain proteins, CIP4 and FBP17, the Arp2/3 complex activator, N-WASP, and cortactin are known TKS5 interactors involved in invadopodia formation, suggesting that related mechanisms operate at CCPs and invadopodia.[23,34–36] Interaction of TKS5 with stable CCPs in conjunction with MT1-MMP clustering based on binding to the AP-2 clathrin-adaptor complex is probably key to the repurposing of CCPs into powerful ECM-degradative assemblies.

A dual role for collagenolytic invadopodia has been found during tumor cell invasion.[20] On the one hand, limited proteolysis of individual collagen molecules by invadopodial MT1-MMP can soften the fibrils to facilitate cell passage during confined invasion.[20] On the other hand, invadopodia can generate outward forces to push collagen fibers aside using the energy of actin polymerization.[20,37] Although CCPs have been found to form in association with and can grab collagen fibers,[38] actin-based forces generated at CCPs are inwardly oriented to facilitate the budding of endocytic clathrin-coated vesicles.[39] Thus, it is unlikely that CCPs could exert pushing forces on matrix fibers. It is more plausible that the approximately 10-fold increase in

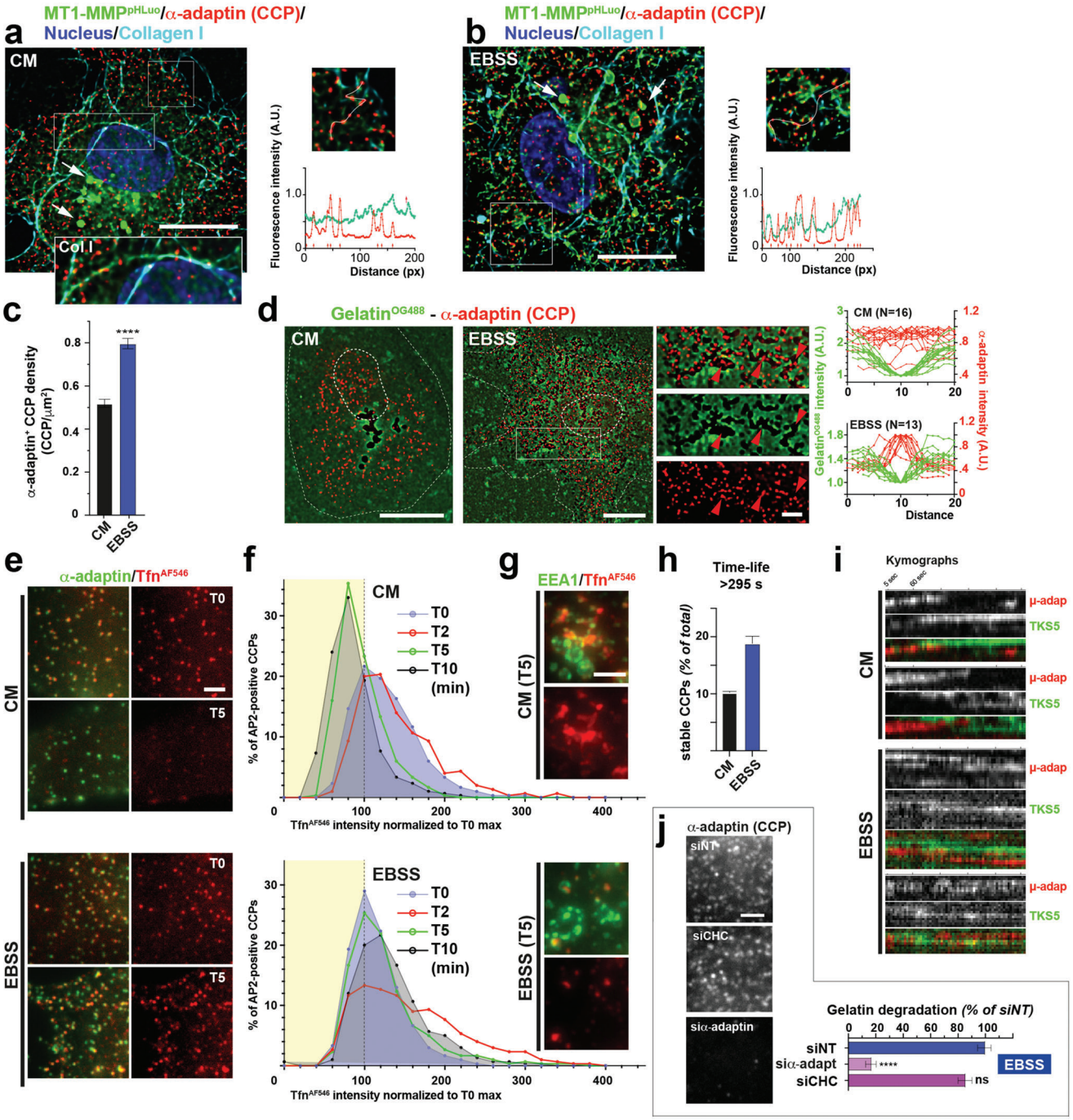

Figure 4. Starvation induces MT1-MMP endocytic arrest. a,b) Deconvoluted images showing the distribution of MT1-MMP^{pHLuorin} (green) and α-adaptin-positive CCPs (red) in MDA-MB-231 cells cultured on fibrillar type I collagen (cyan) in the indicated medium. DAPI-stained nuclei are shown in blue. White arrows, fluorescence signal of MT1-MMP^{pHLuorin} in endolysosomes visible after cell fixation. Inset shows higher magnification of the boxed region. Scale bar, 10 μm. Right panels, intensity profile (linescan) of α-adaptin and MT1-MMP^{pHLuorin} signals (red arrows, CCPs). c) Mean density of α-adaptin-positive CCPs ± SEM (CCP μm^{-2}). d) Deconvoluted images showing the distribution of α-adaptin-positive CCPs (red) in cells plated on fluorescently-labeled gelatin (green) in indicated medium. Dotted lines, cell and nucleus contour. Scale bars, 10 μm; 2 μm (insets). Red arrowheads, CCP associated with gelatin degradation spots. Right panels, linescan intensity profiles of α-adaptin (red) and gelatin fluorescence in degraded areas. e) Fluorescence signal of Tfn^{AF546} (red) associated with α-adaptin-positive CCPs (green) in cells cultured in the absence of labeled Tfn in the indicated medium. Scale bar, 2 μm. f) Kinetics of Tfn^{AF546} uptake in MDA-MB-231 cells incubated in the indicated medium. g) Internalization of Tfn^{AF546} (red) in EEA1-enriched endosomes (green) is reduced upon cell starvation. Scale bar, 2 μm. h) Percentage of stable CCPs ± SEM (lifetime > 295 s). i) Kymographs showing CCP and TKS5 dynamics in cells expressing μ-adaptin^{mCh} and TKS5^{GFP} plated on unlabeled gelatin in the indicated medium. Cells were imaged by TIRF-M every 5 s for 5 min. j) Gelatinolysis by starved cells silenced for α-adaptin or CHC. Right panels show α-adaptin-positive CCPs in the different cell populations. Scale bar, 2 μm.

collagenolysis under nutrient restriction conditions leads to the fragmentation of ECM fibers facilitating their internalization and incorporation in the cell metabolism.[10–12] It is thus tempting to speculate that MT1-MMP-rich CCPs in starved cells have limited impact on tumor cell invasion, rather transforming the entire plasma membrane into an ECM-degradative surface and promoting a vigorous nutrient sourcing program.

Earlier studies in cell lines and in drosophila and mouse models revealed that genetic or pharmacological inhibition of mTOR kinase impedes endocytosis, similar to the observations.[40–43] Other reports highlighted that nutrient scarcity and mTORC1 inhibition stimulate the nutritional use of extracellular proteins and that combined mTORC1 and -2 inhibition induces macropinocytosis, the main route for extracellular protein uptake by cancer cells.[3–5,11,27,44] Collectively, despite mechanistic details that are missing, these data point to some opposite effects of starvation and mTOR inhibition on the downmodulation of CME and activation of macropinocytic (or related phagocytic) uptake, which could cooperate in the production and internalization of ECM fragments by tumor cells. The study suggests the extreme capacity of cancer cells to rewire their nutritional plans and metabolism for survival and growth in adverse conditions by repurposing an ECM proteolysis machinery. It also underscores potential limitations of anti-mTOR therapeutic strategies as mTOR inhibition can unleash the ECM-degradative potential of carcinoma cells.

Supporting Information

Supporting Information is available from the Wiley Online Library or from the author.

Acknowledgements

The authors thank G. Martin for expert technical expertise and Drs. M. Pende, H. Stenmark, C. Raiborg, and S. J. Weiss and members of P.C. lab for helpful comments during the preparation of this manuscript. C.C. was supported by a grant from the Cancéropôle Région Ile-de-France (2016-2-APD-04-ICR-1) to P.C. This work was supported by a donation from Mr. T. Paulsen (InvaCell Project), by Fondation ARC pour la Recherche contre le Cancer (PGA1 RF20170205408) and Fondation Ruban Rose (Prix Avenir 2018) and by institutional support from Institut Curie and Centre National pour la Recherche Scientifique to P.C. The funders had no role in study design, data collection and analysis, decision to publish or preparation of the manuscript. The experimental protocol and animal housing were in accordance with institutional guidelines and with the recommendations of the French Ethics Committee (Agreement B75-05-18, France).

Conflict of Interest

The authors declare no conflict of interest.

Author Contributions

C.C. and D.R. contributed equally to this work. C.C. and D.R.: conceptualization, investigation, methodology, validation, formal analysis, manuscript editing. S.A-B., P.M., and N.E.: methodology, investigation, validation, analysis. A.-S.M.: image processing and analysis. M.F., A.D., and E.M.: methodology. G.M.: supervision of TIRF-M analysis. E.M.: supervision of PDX experiments. P.C.: conceived the study, conceptualization, validation, visualization, drafting of the manuscript, funding acquisition, supervision, and project administration.

Data Availability Statement

Data available on request from the authors.

Keywords

breast cancer, clathrin-mediated endocytosis, extracellular matrix, invadopodia, MT1-MMP, mTOR, starvation

Received: April 20, 2021
Revised: June 7, 2021
Published online: July 11, 2021

[1] D. Hanahan, R. A. Weinberg, *Cell* **2011**, *144*, 646.
[2] B. T. Finicle, V. Jayashankar, A. L. Edinger, *Nat. Rev. Cancer* **2018**, *18*, 619.
[3] C. Commisso, S. M. Davidson, R. G. Soydaner-Azeloglu, S. J. Parker, J. J. Kamphorst, S. Hackett, E. Grabocka, M. Nofal, J. A. Drebin, C. B. Thompson, J. D. Rabinowitz, C. M. Metallo, M. G. Vander Heiden, D. Bar-Sagi, *Nature* **2013**, *497*, 633.
[4] J. J. Kamphorst, M. Nofal, C. Commisso, S. R. Hackett, W. Lu, E. Grabocka, M. G. Vander Heiden, G. Miller, J. A. Drebin, D. Bar-Sagi, C. B. Thompson, J. D. Rabinowitz, *Cancer Res.* **2015**, *75*, 544.
[5] M. Nofal, K. Zhang, S. Han, J. D. Rabinowitz, *Mol. Cell* **2017**, *67*, 936.
[6] M. V. Recouvreux, C. Commisso, *Front. Endocrinol.* **2017**, *8*, 261.
[7] M. Nazemi, E. Rainero, *Front. Oncol.* **2020**, *10*, 239.
[8] M. W. Pickup, J. K. Mouw, V. M. Weaver, *EMBO Rep.* **2014**, *15*, 1243.
[9] E. Rainero, J. D. Howe, P. T. Caswell, N. B. Jamieson, K. Anderson, D. R. Critchley, L. Machesky, J. C. Norman, *Cell Rep.* **2015**, *10*, 398.
[10] O. Olivares, J. R. Mayers, V. Gouirand, M. E. Torrence, T. Gicquel, L. Borge, S. Lac, J. Roques, M. N. Lavaut, P. Berthezene, M. Rubis, V. Secq, S. Garcia, V. Moutardier, D. Lombardo, J. L. Iovanna, R. Tomasini, F. Guillaumond, M. G. Vander Heiden, S. Vasseur, *Nat. Commun.* **2017**, *8*, 16031
[11] S. M. Davidson, O. Jonas, M. A. Keibler, H. W. Hou, A. Luengo, J. R. Mayers, J. Wyckoff, A. M. Del Rosario, M. Whitman, C. R. Chin, K. J. Condon, A. Lammers, K. A. Kellersberger, B. K. Stall, G. Stephanopoulos, D. Bar-Sagi, J. Han, J. D. Rabinowitz, M. J. Cima, R. Langer, M. G. Vander Heiden, *Nat. Med.* **2017**, *23*, 235.
[12] T. Muranen, M. P. Iwanicki, N. L. Curry, J. Hwang, C. D. DuBois, J. L. Coloff, D. S. Hitchcock, C. B. Clish, J. S. Brugge, N. Y. Kalaany, *Nat. Commun.* **2017**, *8*, 13989.
[13] B. A. Morris, B. Burkel, S. M. Ponik, J. Fan, J. S. Condeelis, J. A. Aguirre-Ghiso, J. Castracane, J. M. Denu, P. J. Keely, *EBioMedicine* **2016**, *13*, 146.
[14] G. Y. Liu, D. M. Sabatini, *Nat. Rev. Mol. Cell Biol.* **2020**, *21*, 183.
[15] X. F. Ding, L. F. Li, X. L. Zhou, L. N. Guo, M. M. Dou, Y. Y. Chi, S. X. Wu, Y. N. Zhang, Z. Z. Shan, Y. J. Zhang, F. Wang, Q. X. Fan, J. Zhao, T. W. Sun, *PLoS One* **2017**, *12*, e0170302.
[16] D. Mossmann, S. Park, M. N. Hall, *Nat. Rev. Cancer* **2018**, *18*, 744.
[17] D. A. Murphy, S. A. Courtneidge, *Nat. Rev. Mol. Cell Biol.* **2011**, *12*, 413.
[18] F. Sabeh, R. Shimizu-Hirota, S. J. Weiss, *J. Cell Biol.* **2009**, *185*, 11.
[19] E. Infante, A. Castagnino, R. Ferrari, P. Monteiro, S. Aguera-Gonzalez, P. Paul-Gilloteaux, M. J. Domingues, P. Maiuri, M. Raab, C. M. Shanahan, A. Baffet, M. Piel, E. R. Gomes, P. Chavrier, *Nat. Commun.* **2018**, *9*, 2443.
[20] R. Ferrari, G. Martin, O. Tagit, A. Guichard, A. Cambi, R. Voituriez, S. Vassilopoulos, P. Chavrier, *Nat. Commun.* **2019**, *10*, 4886.
[21] D. F. Seals, E. F. Azucena Jr., I. Pass, L. Tesfay, R. Gordon, M. Woodrow, J. H. Resau, S. A. Courtneidge, *Cancer Cell* **2005**, *7*, 155.

[22] V. P. Sharma, R. Eddy, D. Entenberg, M. Kai, F. B. Gertler, J. Condeelis, *Curr. Biol.* **2013**, *23*, 2079.
[23] A. Zagryazhskaya-Masson, P. Monteiro, A. S. Mace, A. Castagnino, R. Ferrari, E. Infante, A. Duperray-Susini, F. Dingli, A. Lanyi, D. Loew, E. Genot, P. Chavrier, *J. Cell Biol.* **2020**, *219*, e201910132.
[24] T. Hayakawa, K. Yamashita, E. Ohuchi, A. Shinagawa, *J. Cell Sci.* **1994**, *107*, 2373.
[25] A. Bruna, O. M. Rueda, W. Greenwood, A. S. Batra, M. Callari, R. N. Batra, K. Pogrebniak, J. Sandoval, J. W. Cassidy, A. Tufegdzic-Vidakovic, S. J. Sammut, L. Jones, E. Provenzano, R. Baird, P. Eirew, J. Hadfield, M. Eldridge, A. McLaren-Douglas, A. Barthorpe, H. Lightfoot, M. J. O'Connor, J. Gray, J. Cortes, J. Baselga, E. Marangoni, A. L. Welm, S. Aparicio, V. Serra, M. J. Garnett, C. Caldas, *Cell* **2016**, *167*, 260.
[26] F. Coussy, L. de Koning, M. Lavigne, V. Bernard, B. Ouine, A. Boulai, R. El Botty, A. Dahmani, E. Montaudon, F. Assayag, L. Morisset, L. Huguet, L. Sourd, P. Painsec, C. Callens, S. Chateau-Joubert, J. L. Servely, T. Larcher, C. Reyes, E. Girard, G. Pierron, C. Laurent, S. Vacher, S. Baulande, S. Melaabi, A. Vincent-Salomon, D. Gentien, V. Dieras, I. Bieche, E. Marangoni, *Int. J. Cancer* **2019**, *145*, 1902.
[27] W. Palm, Y. Park, K. Wright, N. N. Pavlova, D. A. Tuveson, C. B. Thompson, *Cell* **2015**, *162*, 259.
[28] X. Liu, D. Ghosh, *Int. J. Nanomed.* **2019**, *14*, 6589.
[29] V. Jayashankar, A. L. Edinger, *Nat. Commun.* **2020**, *11*, 1121
[30] C. Demetriades, N. Doumpas, A. A. Teleman, *Cell* **2014**, *156*, 786.
[31] X. Wen, D. J. Klionsky, *Semin. Cancer Biol.* **2020**, *66*, 3.
[32] V. Marchesin, A. Castro-Castro, C. Lodillinsky, A. Castagnino, J. Cyrta, H. Bonsang-Kitzis, L. Fuhrmann, M. Irondelle, E. Infante, G. Montagnac, F. Reyal, A. Vincent-Salomon, P. Chavrier, *J. Cell Biol.* **2015**, *211*, 339.
[33] R. Poincloux, F. Lizarraga, P. Chavrier, *J. Cell Sci.* **2009**, *122*, 3015.
[34] F. Nakatsu, R. M. Perera, L. Lucast, R. Zoncu, J. Domin, F. B. Gertler, D. Toomre, P. De Camilli, *J. Cell Biol.* **2010**, *190*, 307.
[35] M. J. Taylor, D. Perrais, C. J. Merrifield, *PLoS Biol.* **2011**, *9*, e1000604.
[36] P. Saini, S. A. Courtneidge, *J. Cell Sci.* **2018**, *131*, jcs203661.
[37] E. Dalaka, N. M. Kronenberg, P. Liehm, J. E. Segall, M. B. Prystowsky, M. C. Gather, *Sci. Adv.* **2020**, *6*, eaax6912.
[38] N. Elkhatib, E. Bresteau, F. Baschieri, A. L. Rioja, G. van Niel, S. Vassilopoulos, G. Montagnac, *Science* **2017**, *356*, eaal4713.
[39] C. Hinze, E. Boucrot, *Biochem. Soc. Trans.* **2018**, *46*, 565.
[40] L. Pelkmans, E. Fava, H. Grabner, M. Hannus, B. Habermann, E. Krausz, M. Zerial, *Nature* **2005**, *436*, 78.
[41] K. M. Hennig, J. Colombani, T. P. Neufeld, *J. Cell Biol.* **2006**, *173*, 963.
[42] E. M. Gleixner, G. Canaud, T. Hermle, M. C. Guida, O. Kretz, M. Helmstadter, T. B. Huber, S. Eimer, F. Terzi, M. Simons, *Cell Rep.* **2014**, *8*, 10.
[43] F. Grahammer, S. K. Ramakrishnan, M. M. Rinschen, A. A. Larionov, M. Syed, H. Khatib, M. Roerden, J. O. Sass, M. Helmstaedter, D. Osenberg, L. Kuhne, O. Kretz, N. Wanner, F. Jouret, T. Benzing, F. Artunc, T. B. Huber, F. Theilig, *J. Am. Soc. Nephrol.* **2017**, *28*, 230.
[44] R. K. Srivastava, C. Li, J. Khan, N. S. Banerjee, L. T. Chow, M. Athar, *Proc. Natl. Acad. Sci. USA* **2019**, *116*, 24583.

ADVANCED SCIENCE
Open Access

Supporting Information

for *Adv. Sci.*, DOI: 10.1002/advs.202101614

mTOR repression in response to amino acid starvation promotes ECM degradation through MT1-MMP endocytosis arrest

*Cecilia Colombero, David Remy, Sandra Antoine-Bally, Anne-Sophie Macé, Pedro Monteiro, Nadia ElKhatib, Margot Fournier, Ahmed Dahmani, Elodie Montaudon, Guillaume Montagnac, Elisabetta Marangoni, and Philippe Chavrier**

Supporting Information

mTOR repression in response to amino acid starvation promotes ECM degradation through MT1-MMP endocytosis arrest

Cecilia Colombero, David Remy, Sandra Antoine-Bally, Anne-Sophie Macé, Pedro Monteiro, Nadia ElKhatib, Margot Fournier, Ahmed Dahmani, Elodie Montaudon, Guillaume Montagnac, Elisabetta Marangoni, and Philippe Chavrier[*]

Supplementary Experimental Section

Cell culture, transfection and siRNA treatment. Human MDA-MB-231 breast adenocarcinoma cells obtained from ATCC (ATCC HTB-26) were grown in L-15 medium (Sigma-Aldrich) supplemented with 15% fetal calf serum (FCS) and 2 mM Gln (ThermoFisher Scientific) at 37°C in 1% CO_2. The human pancreas adenocarcinoma cell line Bx-PC3 obtained from ATCC (ATCC CRL-1687) was grown in RPMI-1640 medium (ThermoFisher Scientific) supplemented with 10% fetal calf serum at 37°C in 5% CO_2. Both cell lines were routinely tested for mycoplasma contamination. MDA-MB-231 cells stably expressing TKS5^{GFP} or MT1-MMP^{pHLuorin} were generated by lentiviral transduction.[1] For transient expression, MDA-MB-231 cells were transfected with the plasmid constructs using AMAXA nucleofection (Lonza) and analyzed by live cell imaging 48 h after transfection. For starvation experiments, cells were cultured in EBSS medium (ThermoFisher Scientific) supplemented with MEM Vitamins (Gibco, composition in Table S1, Supporting Information) at 37°C in 5% CO_2. For siRNA treatment, except for α-adaptin and clathrin heavy chain (CHC), we used SMARTpool reagents consisting of a mix of four individual siRNAs used at lower concentration in order to reduce potential off-target effects (see Table S2, Supporting Information, for a list of siRNAs used for this study). Cells were treated with the indicated SMARTpool mix (50 nM final concentration) using Lullaby (OZ Biosciences) according to manufacturer instructions and analyzed after 72 hrs of treatment. For silencing of α-adaptin and CHC, cells were treated twice with the siRNA (50 nM final concentration) at 48 hrs interval and analyzed 120 hrs after initial treatment.

Antibodies and drugs. The source of commercial antibodies used for this study are listed in Table S3 (Supporting Information). The source and working concentration of drugs used in this study are listed in Table S4 (Supporting Information).

Polymerization of type I collagen gel. A type I collagen polymerization mix was prepared on ice by adding 25 µM HEPES (final concentration) to a 2.2 mg mL^{-1} acidic-extracted type I collagen solution (Corning) and pH was adjusted to 7.5 with 0.34 N NaOH. When required for microscopic visualization of the collagen network, 2 to 5% of a ~2 mg mL^{-1} solution of AlexaFluor 647-conjugated type I collagen was added to unlabeled collagen in the polymerization mix. When required, drugs were added to the appropriate final concentration in the polymerization mix (see Table S4, Supporting Information). Polymerization was started by incubation at 37°C in a humidified chamber (CO2 cell incubator).

Co-immunoprecipitation of MT1-MMP^{phLuorin}-bound proteins. Cells stably expressing MT1-MMP^{pHLuorin} from two 100-mm dishes (3×10^6 cells per dish plated the day before) were pulled and lysed in 500 µl of lysis buffer (50 mM Tris-HCl, pH 7.5, 150 mM NaCl, 0.5 mM EDTA, 10 mM $MgCl_2$, 10% glycerol, 60 mM β-glucoside, 1% NP-40, Protease inhibitor cocktail tablets (Roche #11873580001) and phosphatase inhibition cocktail 2 (Sigma Aldrich #P5726) for 15 min at 4°C. Lysates were centrifuged at 17,700 x g for 10 min at 4°C. 50 µl of the supernant was kept as input and the rest was added to 30 µl of equilibrated control magnetic agarose beads (ChromoTek #bmab20) for 30 min at 4°C under mild rotation. The precleared lysate was then incubated with 30 µl of magnetic agarose beads coupled to anti-GFP nanobodies (GFPTrap; ChromoTek #gtma20) for 1 hr at 4°C under mild rotation. The beads were washed with washing buffer A (lysis buffer without β-glucoside and with 0.7% NP-40), followed by two washes with washing buffer B (without β-glucoside and

NP-40). Proteins bound to the beads were immediately heated at 95°C for 10 min in Laemmli Sample Reducing buffer (63 mM Tris/HCl, pH 6.8, 2% sodium dodecyl sulfate (SDS), 5% glycerol, 2% β-mercaptoethanol, 0.005% bromophenol blue) and stored at −20°C.

Western blot analysis. Cells treated under the indicated conditions were lysed in lysis buffer containing 50 mM Tris HCl (pH 8.0), 137 mM NaCl, 1% triton X-100, 10 mM MgCl2, 10% glycerol, Protease inhibitor cocktail tablets (Roche #11873580001) and phosphatase inhibition cocktail 2 (Sigma Aldrich #P5726). Lysates were centrifuged at maximum speed (17,700 x g) for 30 min at 4°C. 4x Laemmli Sample Reducing buffer was added and samples were heated for 10 min at 95°C and analyzed by SDS-polyacrylamide gel electrophoresis (PAGE) on NUPAGE 3-8% Tris-acetate or 4-12% Tris-glycine gels (ThermoFisher Scientific). Proteins were transferred on a nitrocellulose membrane using the iBlot2 Dry Blotting System (Invitrogen). After incubating the membranes in 5% BSA or 5% skimmed milk in TBS (Interchim #UPU75132)-Tween 1%, proteins were detected by immunoblotting analysis with the indicated antibodies (see Table S3, Supporting Information). Antibodies were detected using the Enhanced Chemiluminescence reagent (ECL, Amersham RPN2232) on the ChemiDoc MP Imaging System (Bio-Rad).

Quantification of pericellular collagenolysis. To measure pericellular collagenolysis on a thin layer of type I collagen gel, a 18-mm diameter glass coverslip was layered with 200 µl of the ice-cold 2.2 mg mL^{-1} AlexaFluor 647(AF^{647})-labeled type I collagen polymerization mix as described above. Excess collagen solution was removed by pipette aspiration to leave a thin smear of collagen solution on the glass coverslip. After 3 min of polymerization at 37°C, the collagen gel was gently washed in PBS and $7x10^4$ cells were added and incubated for 1 at 37°C in CM or EBSS

medium in the presence or in the absence of AA supplements or drugs as indicated. Cells were pre-extracted with 0.1% Triton X-100 in 4% PFA in PBS for 90 sec at 37°C and fixed in 4% PFA in PBS for 20 min at 37°C. Coverslips were treated with 1% BSA in PBS for 30 min at room temperature then incubated with Col1-¾C and anti-cortactin antibodies diluted in 1% BSA in PBS for 2 hrs at 4°C. After three washes with PBS at 4°C, samples were counterstained with Cy3-conjugated anti-rabbit IgG and A488-conjugated anti-mouse IgG antibodies for 60 min at 4°C, extensively washed in PBS and mounted in Prolong-DAPI mounting medium (Invitrogen). Images were acquired with a wide-field microscope (Eclipse 90i Upright; Nikon) using a 100x Plan Apo VC 1.4 oil objective and a cooled interlined charge-coupled device (CCD) camera (CoolSnap HQ^2; Roper Scientific). A z-dimension series of images was taken every 0.2 µm by means of a piezoelectric motor (Physik Instrumente). The system was steered by Metamorph software. Deconvolution was processed by Nikon NIS-Elements software (3D-deconvolution module; Lucy-Richardson algorithm).

For quantification of pericellular collagenolysis in a 3D collagen network, 40 µl of a $6x10^4$ cells/mL cell suspension in the 2.2 mg mL^{-1} type I collagen polymerization mix was added on top of a 12-mm diameter glass coverslip and polymerization was performed for 30 minutes at 37°C. The indicated culture medium was added and samples were incubated for 6 hrs at 37°C. Samples were fixed, permeabilized and stained with Col1-¾C antibody as described above except that samples were counterstained with Phalloidin-Alexa488 to visualize cell shape. Image acquisition was performed with an A1R Nikon confocal microscope with a 40x NA 1.3 oil objective using high 455 sensitivity GaASP PMT detector and a 595 +/- 50 nm band-pass filter. Quantification of Col1-¾C signal (cleaved collagen) was performed with a

homemade ImageJ macro. Acquired z-planes were projected using maximal intensity projection in Fiji and Col1-¾C signal was determined using the thresholding command excluding regions <50-px to avoid non-specific signal. Col1-¾C signal area was normalized to the total cell surface (thin layer) or to the number of nuclei in field (3D network) and values normalized to control cells.

Fluorescent gelatin degradation assay. MDA-MB-231 cells were plated for 1 to 5 hrs on Oregon Green 488 (OR^{488}) or AF^{594}-conjugated cross-linked gelatin (Invitrogen) in EBSS or CM medium in the presence or absence of rapamycin as previously described.[2] Cells were pre-extracted with 0.1% Triton X-100 in 4% PFA in PBS for 90 sec at 37°C and fixed in 4% PFA in PBS for 20 min at 37°C and then stained with the indicated antibodies or with fluorescently-labeled phalloidin to stain F-actin. Cells were imaged with a 100x objective on a wide-field microscope equipped with a piezoelectric motor as above. For quantification of degradation, the area of degraded matrix (black pixels) measured with the threshold command of ImageJ was divided by the total cell surface and values were normalized to control cells. The regions of interest delimiting the gelatin degradation were saved for further analysis, such as the assessment of AP-2 association (see below). Linescans were performed using Fiji software. Deconvolution was processed by Nikon NIS-Elements software (3D-deconvolution module; Lucy-Richardson algorithm).

Quantification of invadopodia parameters. $7x10^4$ MDA-MB-231 cells stably expressing TKS5-GFP were plated on top of a coverslip coated with AF^{405}- or AF^{594}-conjugated gelatin and incubated for 1 hr in CM or EBSS medium. After fixation and permeabilization, cells were stained with anti-GFP antibodies. TKS5 positive structures were detected using the threshold command of ImageJ set with constant upper and lower threshold values. TKS5-positive structures outside of the regions of

degraded gelatin were eliminated from the analysis. The distance of the invadopodia to the cell centroid was measured on ImageJ with a homemade macro. Briefly, a line was created between the cell centroid and the invadopodia, then extended to the nearest cell periphery point. The reported distance is the distance between the invadopodia and the cell centroid normalized by the distance between the cell periphery and the cell centroid.

Quantification of CCP density. $7x10^4$ MDA-MB-231 cells were plated on top of a coverslip coated with gelatin^{OR488} and incubated for 1 hr in CM or EBSS medium. After fixation and permeabilization, cells were stained with α-adaptin as described above. CCPs in the entire cell were detected using the Find Maxima command of ImageJ and the number of detected CCPs was divided by the area of the cell. CCPs positions were saved for further analysis (see below).

Randomization of AP-2 distribution over gelatin degradation spots. To measure the association of α-adaptin positive CCPs with gelatin degradation spots, CCPs and degradation spots were detected as described above and their positions as well as the position of all pixels inside the cell (total pixels) defined by their X and Y coordinates were saved. For each CCP, (X, Y) positions were randomly drawn from all pixels of the cell, effectively changing the position of CCPs inside the cell in a random fashion (see Figure S3B, Supporting Information). This randomization procedure was performed 5,000 times per cell and the number of CCPs associated with gelatin degradation was measured each time. The true value of CCP association with gelatin degradation was calculated and compared to the randomized values. Synthetic images displaying cell contour (white line), degradation spots (black) and associated CCPs (red crosses) were generated with ImageJ. This procedure was

repeated for ten independent cells with *p*-values ranging from 0 to 0.0142 (mean *p*-value = 0.001).

Tfn uptake assay. $7x10^4$ MDA-MB-231 cells plated on a 18-mm diameter glass coverslip were incubated overnight at 37°C in CM. Cells were washed twice with PBS before incubation in EBSS or CM medium for 1 hr at 37°C, then transferred on ice and washed twice with ice-cold EBSS or L15 medium supplemented with 1% BSA and 20 mM HEPES pH 7.5. Coverslips were incubated with 20 µg mL^{-1} of AF^{546}-conjugated Tfn (ThermoFisher) in the same medium for 1 hr at 4°C. Cells were fixed with 4% PFA in PBS or incubated in pre-heated CM or EBSS for 2, 5 or 10 min at 37°C before fixation. After permeabilization with 0.1% Triton X-100 in PBS for 15 min, samples were incubated with anti-α-adaptin (overnight at 4°C) or with anti-EEA1 antibodies (1 hr at room temperature), and then counterstained with AF488-conjugated anti-mouse antibodies (1 hr at room temperature). Stacks of images were acquired with a wide-field microscope (Eclipse 90i Upright; Nikon) steered by Metamorph software as described above. For analysis, the plane corresponding to the plasma membrane was selected. CCPs positive for α-adaptin in a selected region were detected and segmented using the manual threshold command of ImageJ. The regions of interest (ROI) were saved and copied on the Tfn image. The mean intensity of Tfn inside each ROI was measured and a frequency histogram was generated with a normalization to T0.

Quantification of LC3-positive puncta. $7x10^4$ MDA-MB-231cells were plated on collagen-coated or on non-coated 18-mm diameter glass coverslips as previously described and incubated for 4 at 37°C in CM or in EBSS medium. Cells were fixed with 4% PFA in PBS for 10 min and permeabilized with 0.05% saponin (Sigma-Aldrich) in PBS for 10 min. Samples were blocked in PBS with 0.05% saponin and

5% FCS for 30 min at room temperature and stained with anti-LC3 and anti-p4E-BP1 antibodies for 2 hrs at room temperature. After three washes, samples were counterstained with Cy3-conjugated anti-mouse IgG and Alexa488-conjugated anti-rabbit IgG antibodies and mounted in Prolong-DAPI medium. Image acquisition was performed by wide-field microscopy as previously described. Quantification of LC3-positive vesicles was performed by maximal orthogonal projection of the series of optical sections (the distance between two sections is 0.2 µm). Cells were manually delimited using the p4E-BP1 signal while LC3 signal was denoised and thresholded to detect LC3-positive autophagic vesicles. Detected spots were counted and saved for visual verification. No manual correction was done. The average number of LC3-positive puncta per cell was normalized to the value in CM-treated cells set to 1.

Dynamics of TKS5- and µ-adaptin-positive structures by live cell total internal reflection fluorescence microscopy (TIRF-M). MDA-MB-231 cells transfected with GFP-tagged TKS5 and mCherry-tagged µ-adaptin were plated in CM or EBSS on glass bottom dishes (Ibidi Corporation) layered with unlabeled cross-linked gelatin as previously described. Simultaneous dual color TIRF-M sequences were acquired with an inverted microscope (Eclipse-Ti-E, Nikon) equipped with a 100x PlanApo TIRF objective (1.47 NA), a TIRF arm, an image splitter (DV; Roper Scientific) installed in front of the EMCCD camera (Photometrics) and a temperature controller. GFP and m-Cherry were excited with 491- and 561-nm lasers, respectively (50 mW, Gataca Systems) and fluorescent emissions were selected with bandpass and longpass filters (Chroma Technology Corp). The system was driven by Metamorph. For quantification of CCP dynamics, CCP lifetime was measured using the TrackMate plugin of FIJI.[3] At least 300 CCPs from at least 6 cells per condition and per

experiment were tracked from three independent experiments. Data are expressed as mean lifetime ± sem.

Ex-vivo **culture of TNBC patient-derived xenografts.** Breast cancer patient derived xenografts were obtained from triple-negative breast tumors and generated as described.[4] After surgical excision of the tumor xenograft, tumor cells were dissociated in DMEM/F12 medium supplemented with collagenase and hyaluronidase (SIGMA-Aldrich, 1X final) in 10 mM HEPES, 7.5% BSA Fraction V (Gibco), 5 µg mL^{-1} insulin (SIGMA-Aldrich) and 50 µg mL^{-1} gentamycin (GIBCO) for 1 hr at 37°C on a rotating wheel at 180 rpm as previously described.[5] Samples were washed with DMEM/F12 medium and digested with 0.25% of trypsin (Gibco) for 2 min at 37°C. Trypsin was neutralized in HBSS medium (Invitrogen) supplemented in 10 mM HEPES and 2% FCS. Then, samples were treated with dispase (5 UI mL^{-1}, StemCell Technologies) and DNAse I (1mg mL^{-1} in DMEM, Sigma for 2 min at room temperature and then incubated in neutralization buffer supplemented with NH_4Cl (0.8%, StemCell Technologies) to remove red blood cells. After filtration through a 40 µm Cell Strainer (Corning), tumor cells were plated in a 25-cm^2 cell-culture flask for 16 hrs at 37°C in DMEM/F12 medium supplemented with 10% FCS. For the pericellular collagenolysis assay, non-attached PDX tumor cells in the culture supernatant were resuspended in a 2,2 mg mL^{-1} collagen I solution as described above and incubated for 16 hrs in CM or EBSS medium with or without GM6001. After fixation with PFA 4% for 20 min and permeabilization with Triton 0.1% in PBS for 5 min, samples were stained with Col1-¾C and anti-Keratin-8 (K8) antibodies (2 hrs at 4°C) or anti-phospho-4E-BP1 and anti-Keratin-8 antibodies (1 hr at 4°C), counterstained with fluorescently labeled secondary antibodies and mounted. Image

acquisition was performed with an A1R Nikon confocal microscope as described above.

Statistics and reproducibility. All data are presented as mean ± S.E.M. from at least three independent experiments except indicated otherwise. GraphPad Prism software was used for statistical analysis. Data were tested for normal distribution using the D'Agostino-Pearson normality test and nonparametric tests were applied otherwise. One-way ANOVA, Kruskal-Wallis or Mann-Whitney tests were applied as indicated in the figure legends and are summarized in Supplemental Table 5. Statistical significance was defined as *, $P<0.05$; **, $P<0.01$; ***, $P<0.001$; ****, $P<0.00001$; ns, not significant.

Supplementary Figure legends

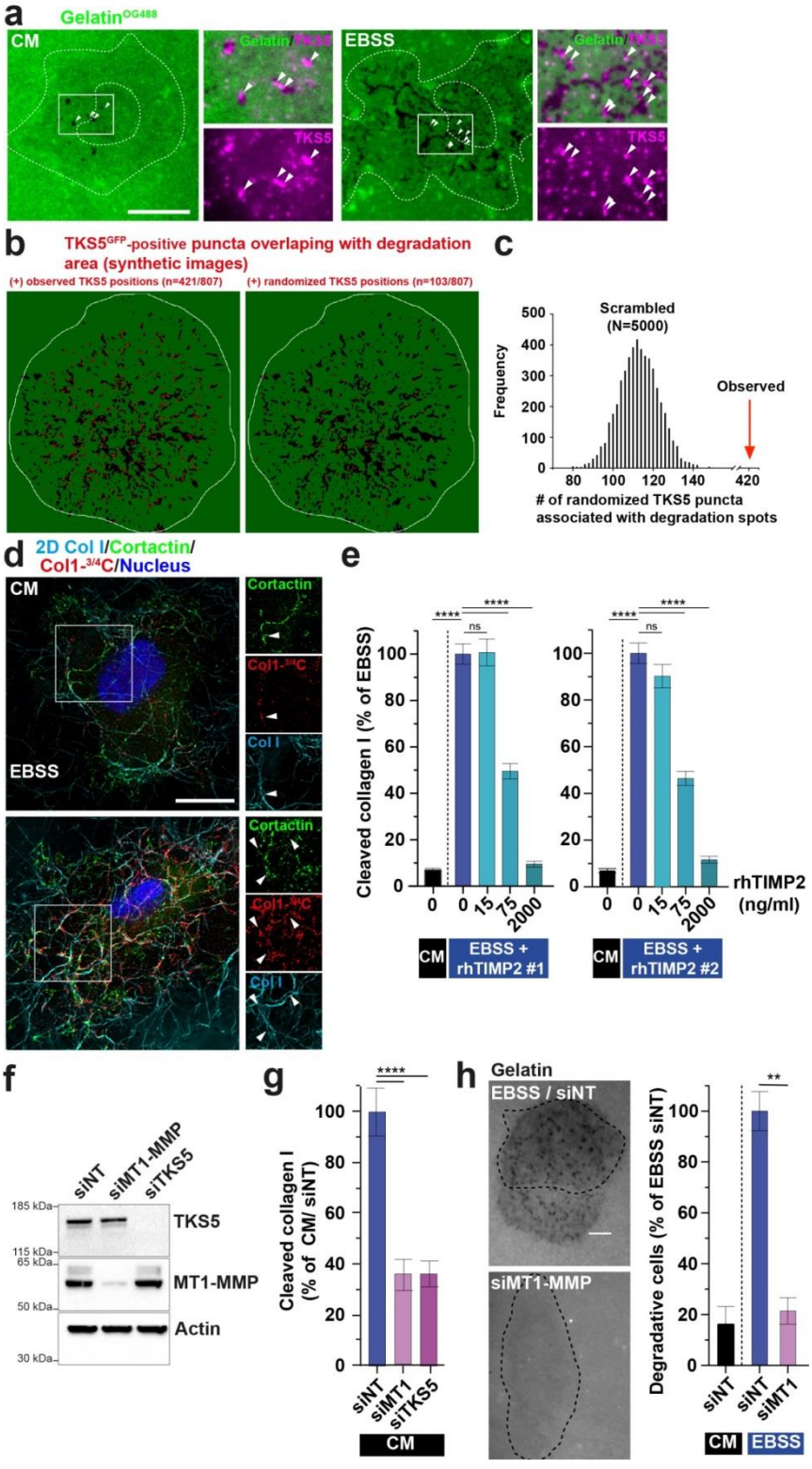

Figure S1. Matrix degradation by starved cells. (a) MDA-MB-231 cells plated on fluorescently-labeled gelatin (green) for 60 min in CM or EBSS starvation medium depleted for AAs and serum and stained for TKS5 (magenta). Higher magnification of

boxed regions is shown in the insets. Arrowheads, TKS5-positive invadopodia; dotted lines, cell and nucleus contour. Scale bar, 10 µm. **(b)** Synthetic images showing virtual TKS5-positive invadopodia (depicted as red crosses) overlapping with the mask representing the degraded zones of gelatin (black spots over a green background). In the left image, the position of TKS5-positive structures corresponds to their observed position in the original microscopy image (see Figure 1A, EBSS). The right image corresponds to one of the 5,000 scrambled images generated by randomization of CCP positions on the mask of the degradation zones. **(c)** $TKS5^{+}$ invadopodia were scrambled 5,000 times and the histogram shows the number of randomized $TKS5^{+}$ invadopodia associated with gelatin degradation spots. The true unscrambled value (n=422) exceeds the randomized values, indicating high statistical confidence in non-random association of $TKS5^{+}$ invadopodia with degradation areas (see also Supplemental Table 5). **(d)** Deconvoluted images showing MDA-MB-231 cells cultured on a fibrillar type I collagen network (cyan) for 60 min in indicated medium and stained for cortactin (green); cleaved collagen fibers (red); nucleus (blue). Scale bar, 10 µm. Higher magnification of boxed regions is shown in the insets. Arrowheads, cortactin-positive invadopodia. **(e)** Collagen cleavage by MDA-MB-231 cells incubated for 60 min in CM or EBSS medium supplemented with 15, 75 or 2000 ng mL^{-1} recombinant human TIMP2 protein from two independent suppliers (rhTIMP2#1 and #2). **(f)** Representative western blots of MT1-MMP and TKS5 expression with actin as loading control in MDA-MB-231 cells treated with indicated siRNAs. **(g)** Collagen cleavage by MDA-MB-231 cells knocked-down for MT1-MMP or TKS5 or treated with a non-targeting siRNA and cultured in CM. **(h)** MDA-MB-231 cells knocked-down for MT1-MMP or treated with a non-targeting (siNT) siRNA were plated on fluorescently-labeled gelatin in CM or EBSS

medium for 2 hrs. The cell contour is shown with a black dotted line. Scale bar, 10 µm. The graph shows the gelatin degradation normalized to the degradation of cells grown in EBSS medium ± SEM.

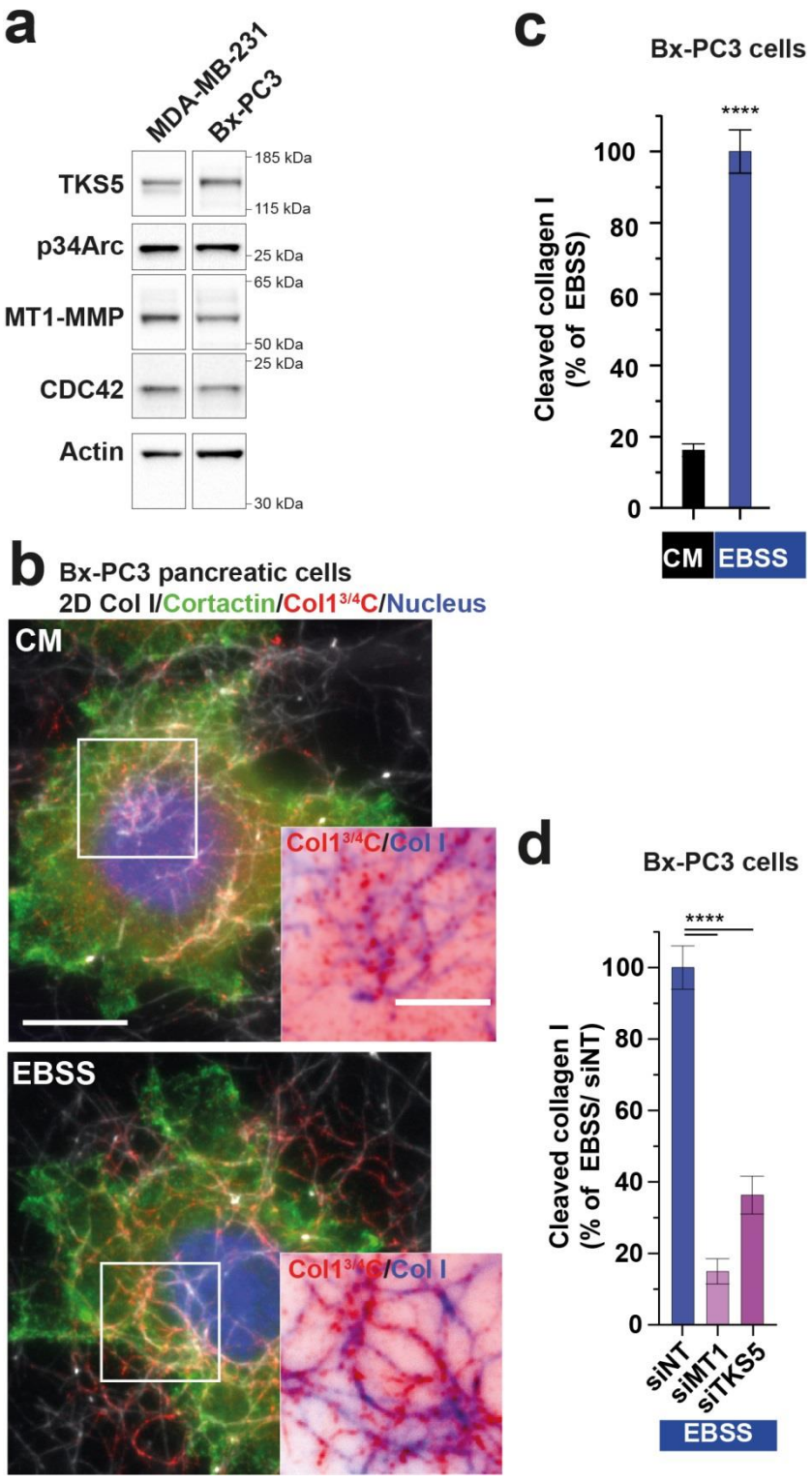

Figure S2. AA starvation induces matrix degradation in pancreatic Bx-PC3 tumor cells. (a) Comparison of the expression of key invadopodia components by immunoblotting analysis in MDA-MB-231 and Bx-PC3 cell lysates with actin as loading control. Molecular weights are in kDa. **(b)** Pancreatic ductal adenocarcinoma Bx-PC3 cells were cultured on a layer of fibrillar type I collagen (gray) for 60 min in indicated medium and stained for cortactin (green) and cleaved collagen I (Col1-¾C, red). Scale bar, 10 µm. Insets, higher magnification of boxed regions using inverted lookup tables (collagen fibers are in blue, cortactin or Col1-¾C signal is in red). Scale bar, 5 µm. **(c)** Collagen cleavage by Bx-PC3 cells was measured by Col1-¾C neoepitope staining and normalized to mean value of cells starved in EBSS ± SEM. **(d)** Collagen cleavage by Bx-PC3 cells knocked-down for MT1-MMP or TKS5 or treated with a non-targeting siRNA and cultured in EBSS medium.

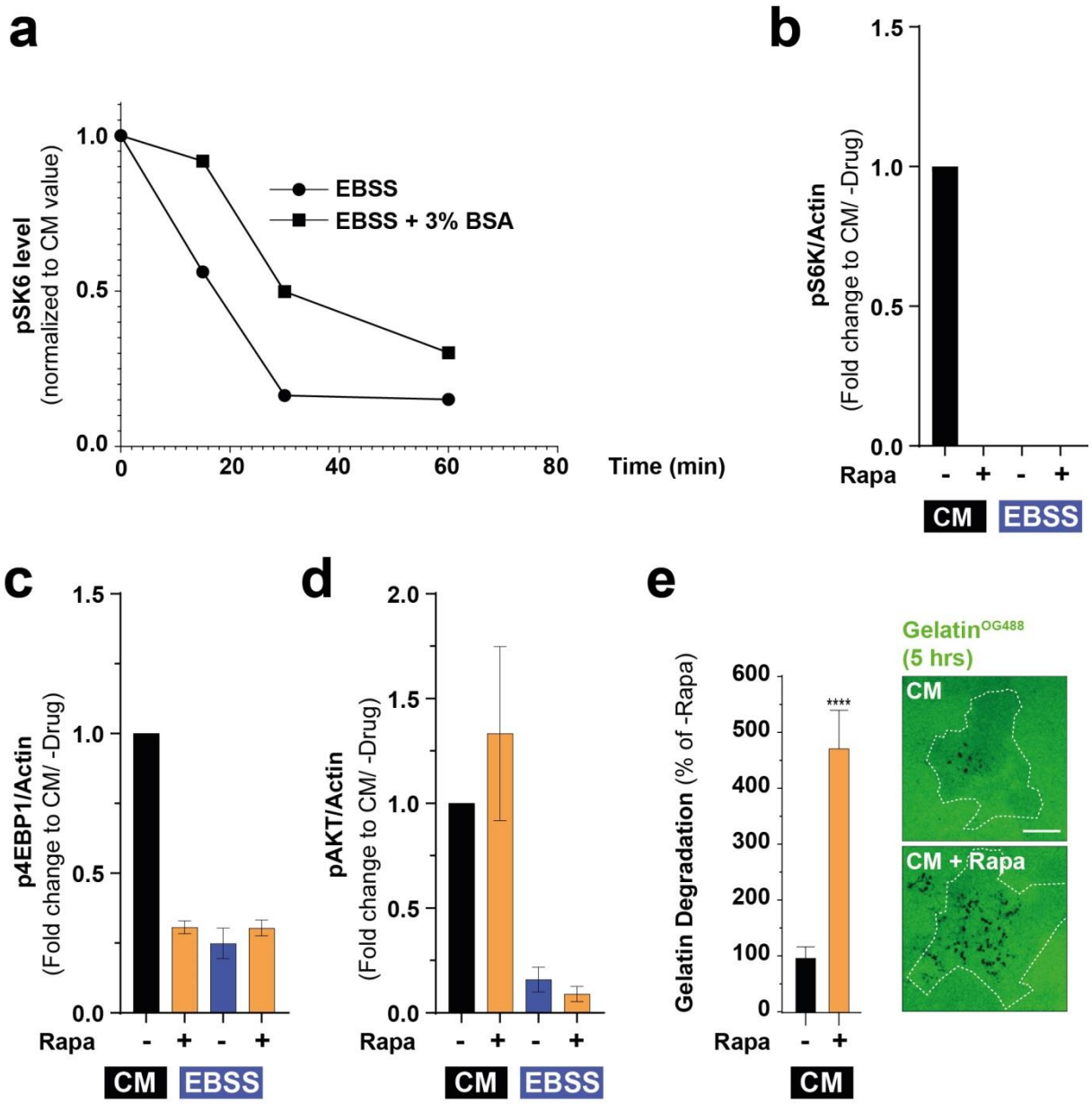

FIGURE S3

Figure S3. Phosphorylation of mTOR substrates in cells treated with rapamycin. (a) Levels of phosphorylated S6K in MDA-MB-231 cells cultured in EBSS medium in the absence or presence of 3% BSA normalized to pSK6 levels in CM medium from two independent experiments (see Figure 3C). **(b-d)** Levels of phosphorylated (p)S6K (panel A), p4E-BP1 (panel B) or pAKT (panel C) normalized to actin levels in MDA-MB-231 cells cultured in CM or EBSS medium in the presence

or absence of rapamycin from three independent experiments (see Figure 3E). **(e)** Gelatin degradation by MDA-MB-231 cells incubated for 5 hrs in CM with or without rapamycin. Scale bar, 10 µm.

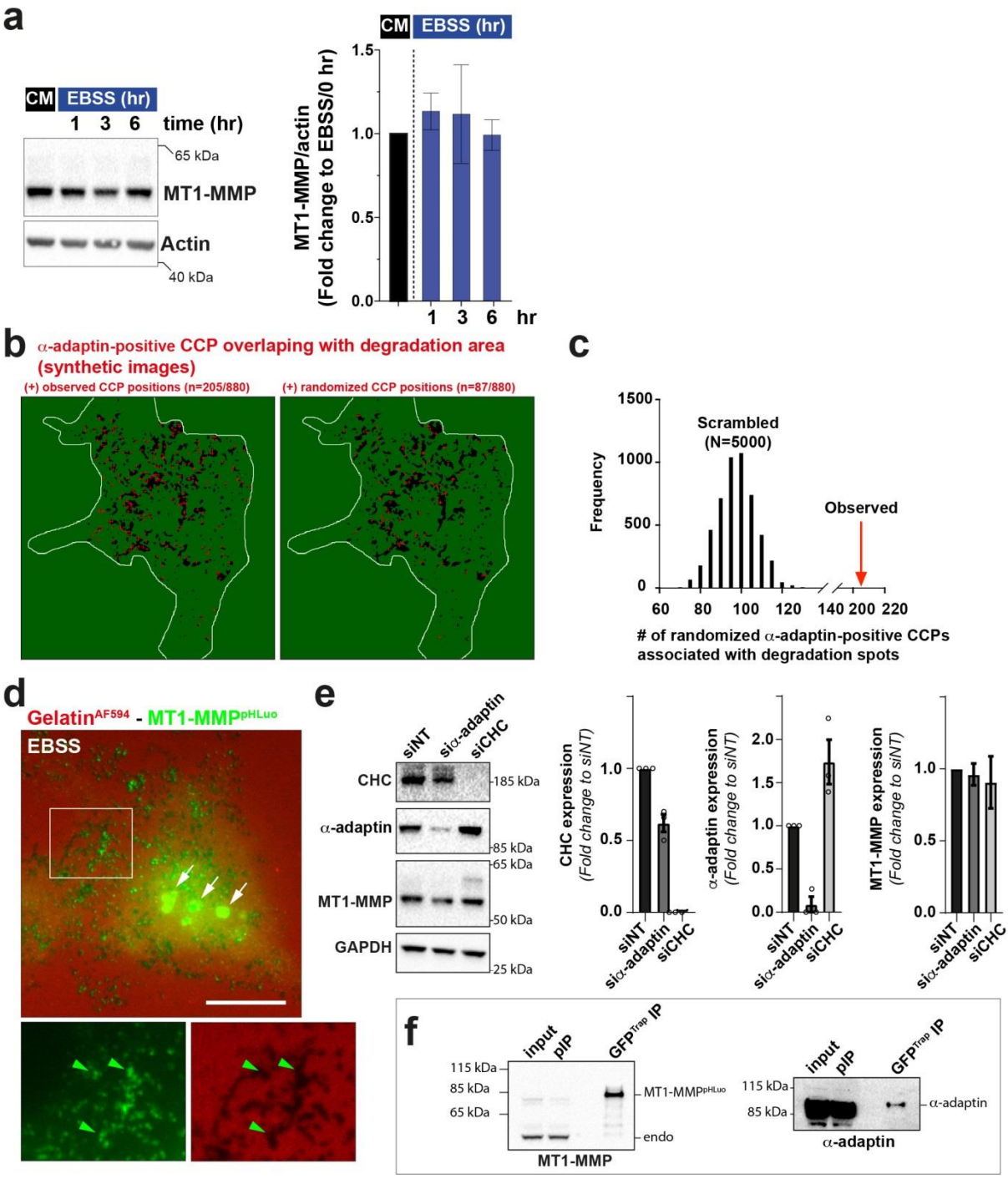

Figure S4. Matrix degradation correspond to MT1-MMP accumulation in arrested CCPs. (a) MT1-MMP levels analyzed by western blot, normalized to actin in MDA-MB-231 cells incubated in the indicated medium for the indicated periods of

time. Representative immunoblots are shown in the right panels. Molecular weight in kDa. **(b)** Synthetic images showing virtual CCPs (depicted as red crosses) overlapping with the mask representing the degraded zones of gelatin (black spots over a green background). In the left image, the position of CCPs corresponds to their observed position in the original microscopy image (see Figure 4D, EBSS). The right image corresponds to one of the 5,000 scrambled images generated by randomization of CCP positions. **(c)** $TKS5^{+}$ invadopodia were scrambled 5,000 times and the histogram shows the number of randomized $TKS5^{+}$ invadopodia associated with gelatin degradation spots. The true unscrambled value (n=422) exceeds the randomized values, indicating high statistical confidence in non-random association of $TKS5^{+}$ invadopodia with degradation areas (see also Supplemental Table 5). **(d)** MDA-MB-231 cells expressing MT1-$MMP^{pHLuorin}$ were plated on AF^{594}-labeled gelatin for 60 min. White arrows, fluorescence signal of MT1-$MMP^{pHLuorin}$ in endolysosomes. Green arrowheads point to the accumulation of MT1-$MMP^{pHLuorin}$ in association with gelatin degradation areas. Scale bars, 10 µm. **(e)** Representative western blots of CHC, α-adaptin or MT1-MMP expression with GAPDH as loading control in MDA-MB-231 cells treated with indicated siRNAs. Molecular weights are in kDa. Quantification of protein expression based on three (α-adaptin and CHC) or two (MT1-MMP) independent experiments. **(f)** Lysates of MDA-MB-231 cells expressing MT1-$MMP^{pHLuorin}$ were immunoprecipitated with GFP antibodies (GFP^{Trap} IP). Total lysate before (input) and after immunoprecipitation (pIP) was loaded as control. Bound proteins were analyzed with MT1-MMP and α-adaptin antibodies Equal loading was controlled using GAPDH antibody (not shown).

Supplementary Table Legends

Table S1. Medium composition

Vitamin mix

Component	MEM Vitamin Solution 100 X (g/L)	L-15 Medium (g/L)
Choline Chloride	0.1	0.001
Folic Acid	0.1	0.001
Myo-Inositol	0.2	0.002
Niacinamide	0.1	0.001
D-Panthothenic Acid * ½Ca	0.1	0.001
Pirydoxal.HCl	0.1	0.001
Riboflavin	0.01	0.0001
Thiamine*HCl	0.1	0.001

Amino acid mix composition

Amino Acid	RPMI-1640 50 X (g/L)	L-15 Medium (g/L)
L-Alanine	-	0.225
L-Arginine (free base)	10.0	0.5
L-Asparagine	2.84	0.25
L-Aspartic Acid	1.0	-
L-Cystine	2.5	0.12
L-Glutamic Acid	1.0	0.3
Glycine	0.5	0.2
L-Histidine	0.75	0.25
Hydroxy-L-Proline	1.0	-
L-Isoleucine	2.5	0.125
L-Leucine	2.5	0.125
L-Lysine	2.0	0.094
L-Methionine	0.75	0.075
L-Phenylalanine	0.75	0.125
L-Proline	1.0	-
L-Serine	1.5	0.2
L-Threonine	1.0	0.3
L-Tryptophan	0.25	0.02
L-Tyrosine	1.16	0.3
L-Valine	1.0	0.1

Table S2. siRNAs used in this study

siRNA	**Company**	**Targeted sequence** (5'-to-3')
MT1-MMP *SMARTpool*	Horizon Discovery L-004145-00-0005	GGAUGGACACGGAGAAUUU GGAAACAAGUACUACCGUU GGUCUCAAAUGGCAACAUA GAUCAAGGCCAAUGUUCGA
TKS5 *SMARTpool*	Horizon Discovery L-006657-00-0005	ACAAUAACCUCAAAGAUGU GGACGUAGCUGUGAAGAGA CGACGGAACUCCUCCUUUA GGAUAAGUUUCCCAUUGAA
α-adaptin	Merck Millipore	AAGAGCAUGUGCACGCUGGCCA
Clathrin Heavy Chain (CHC)	Elkhatib et al., Science 2017	GCUGGGAAAACUCUUCAGATT
Non-Targeting	Horizon Discovery D-001810-01	UGGUUUACAUGUCGUACUAA
siTSC2 *SMARTpool*	Horizon Discovery L-003029-00-0005	GCAUUAAUCUCUUACCAUA CGAACGAGGUGGUGUCCUA GGAAUGUGGCCUCAACAAU GGAUUACCCUUCCAACGAA
siTBC1D7 *SMARTpool*	Horizon Discovery L-021140-00-0005	GGAAGAUAGUGUCGACUGU UUACAGAGGGUUUGGGAUA CCAUUAAAUACCAAGUAC CGCCCAAACUUCCUUAUGA

Table S3. Commercial antibodies and immunolabeling reagents used in this study.

Antigen	Company	Type (species)
Collagen type I cleavage site (Col1–$^{3/4}$C) *IF*	ImmunoGlobe (0217-050)	Polyclonal (Rabbit)
Cortactin *IF*	Merck (clone 4F11, 05-180)	Monoclonal (mouse)
MT1-MMP (MMP14) *IF, WB*	Merck (clone LEM-2/15.8, MAB3328)	Monoclonal (mouse)
TKS5 (SH3PXD2A) *IF, WB*	Novus Biologicals (NBP1-90454)	Polyclonal (rabbit)
Paxillin *IF*	BD Transduction Laboratories (610052)	Monoclonal (mouse)
GFP *IF*	Abcam (ab13970)	Polyclonal (chicken)
mTOR *IF*	Cell Signaling TECHNOLOGY (2983S)	Monoclonal (rabbit)
TSC2 *WB*	Cell Signaling TECHNOLOGY (4308S)	Monoclonal (rabbit)
TBC1D7 *WB*	Cell Signaling TECHNOLOGY (1494S)	Monoclonal (rabbit)
LC3 *IF*	MBL (clone 4E12 M152-3)	Monoclonal (mouse)
LC3 *WB*	Cell Signaling TECHNOLOGY (2775S)	Polyclonal (rabbit)
Alpha adaptin 2 (AP2) *IF*	Abcam (ab2730)	Monoclonal (mouse)
Alpha adaptin 2 (AP2) *WB*	Abcam (ab2807)	Monoclonal (mouse)
Early Endosome Antigen 1 (EEA1)	BD Transduction Laboratories (610457)	Monoclonal (mouse)
Phospho-4E-BP1 (Ser65) *IF, WB*	Cell Signaling TECHNOLOGY (clone D9G1Q 13443S)	Polyclonal (rabbit)
Phospho-(p70)S6 Kinase (Thr389) *WB*	Cell Signaling TECHNOLOGY (9205)	Polyclonal (rabbit)
Phospho-AKT (Ser473) *WB*	Cell Signaling TECHNOLOGY (4060)	Polyclonal (rabbit)
(p70)S6 Kinase *WB*	Cell Signaling TECHNOLOGY (clone 49D7 2708)	Monoclonal (rabbit)
AKT *WB*	Cell Signaling TECHNOLOGY (9272)	Polyclonal (rabbit)
β1 integrin *WB*	Gift from C. Albiges-Rozo	Polyclonal (rabbit)
Cytokeratin-8 *IF*	DSHB	Monoclonal (rat)
Actin *WB*	Sigma-Aldrich (clone AC-15 A1978)	Monoclonal (mouse)
GAPDH *WB*	Santa Cruz Biotechnology (25788)	Polyclonal (rabbit)

Alpha tubulin *WB*	Sigma-Aldrich (T-9026)	Monoclonal (mouse)
HRP-conjugated anti-rabbit IgG	Sigma (A0545)	Goat
HRP-conjugated anti-mouse IgG	Jackson ImmunoResearch (115-035-062)	Goat
Alexa Fluor 488 Phalloidin	Molecular Probes (A12379)	
Anti-rabbit Alexa488	Molecular Probes (A21206)	Goat
Anti-rabbit Cy3	Molecular Probes (A21206)	Donkey
Anti-chickenAlexaFluor488	Molecular Probes (A11039)	Donkey
Anti-mouse Cy3	Jackson ImmunoResearch (715-165-151)	Donkey
Anti-rat Alexa488	Molecular Probes (A21208)	Donkey

Table S4. Chemicals and reagents used in this study

Reagent	Company	Reference	Vehicle	Dilution
RPMI 1640 amino acids solution	Sigma-Aldrich	R7131	Medium	1/100
Bovine serum albumin solution 30%	ThermoFischer Scientific	A7284	Medium	3%
GM6001	Merck Millipore	CC1100	Ethanol	40 µM
Rapamycin	Tocris Biotechne	1292	Ethanol	20 nM
Recombinant human tissue inhibitor of metalloproteinase (rhTIMP-2)	- R&D Systems (rhTIMP-2#1) - Sigma-Aldrich (rhTIMP-2#2)	971-TM-010 SRP3174	Medium	15, 75 or 2000 ng/mL
Transferrin from human serum, Alexa Fluor™ 546 Conjugate	Invitrogen	11530766	Medium	20 µg/ml

Table S5. Analyzed variables and statistics used in this study.

Table S5. Analyzed variables and statistics used in this study.

Figure	Conditions	Mean	SEM	n	N	p value	Test
1-b **Gelatin degradation** *(fold change to CM)*	**CM**	**1**	**0.2**	**42**	2	**-**	K-W
	EBSS 30 min	4.2	0.4	42		<0.00001	
	EBSS 60 min	8.5	0.8	53		<0.00001	
	EBSS 120 min	14.2	1.1	42		<0.00001	
	EBSS + GM6001 60 min	2.9	0.6	42		ns	
1-c **Density of TKS5+ invadopodia** *(per µm²)*	**CM**	**0,03**	**0,003**	**51**	3	**-**	M-W
	EBSS	0,15	0,011	54		<0.00001	
1-d **Average size of TKS5+ invadopodia** *(µm²)*	**CM**	**0,23**	**0,022**	**51**	3	**-**	M-W
	EBSS	0,11	0,004	54		<0.00001	
1-e **Distance of TKS+ invadopodia to the centroid** *(µm)*	**CM**	**0,408**	**0,006**	**1172**	3	**-**	M-W
	EBSS	0,544	0,003	6850		<0.00001	
1-g **Cleaved collagen I** *(% of EBSS)*	CM	35.7	3.5	59	3	<0.00001	M-W
	EBSS	**100**	**6.2**	**54**		**-**	
1-i **Cleaved collagen I** *(% of EBSS/siNT)*	CM siNT	16.1	1.0	57	3	<0.00001	K-W
	EBSS siNT	**100**	**5.9**	**63**		**-**	
	EBSS siMT1	10.6	1.4	62		<0.00001	
	EBSS siTKS5	17.0	2.5	59		<0.00001	
3-b **Cleaved collagen I** *(% of EBSS)*	CM	16.3	1.1	87	4	<0.0001	K-W
	EBSS	**100**	**4.1**	**90**		**-**	
	EBSS + AA	53.8	3.1	93		<0.0001	
	EBSS + AA + Rapa	97.0	3.9	98		ns	
3-d **Cleaved collagen I** *(% of EBSS/-BSA)*	CM	2.6	0.4	91	3	<0.00001	K-W
	EBSS	**100**	**4.8**	**95**		**-**	
	EBSS+BSA	41.5	3.3	95		<0.00001	
3-f **Cleaved collagen I**	**CM**	**100**	**8.0**	**90**	4	**-**	M-W

(% of - Rapa)	CM + Rapa	269.4	39.6	92		<0.00001	
	EBSS	**100**	**4.0**	**64**	3	**-**	M-W
	EBSS + Rapa	111.8	3.4	67		0.0065	
3-i **Gelatin degradation (% of siNT)**	**EBSS siNT**	**100**	**3.2**	**68**	3	-	K-W
	EBSS siTSC2	48.5	2.3	56		<0.0001	
	EBSS siTSC2 + siTBC1D7	52.5	3.5	44		<0.0001	
3-k **LC3 puncta per cell** *(Fold change to CM)*	**CM - CollagenI**	**1.0**	**0.1**	**78**	3	**-**	K-W
	EBSS 4hrs - CollagenI	2.0	0.2	102		<0.00001	
	EBSS 4hrs +CollagenI	0.8	0.1	87		ns	
	EBSS 4hrs +CollagenI +GM6001	1.6	0.1	88		NA	
	EBSS 7hrs - CollagenI	2.1	0.2	104		<0.00001	
	EBSS 7hrs +CollagenI	0.8	0.1	101		ns	
	EBSS 7hrs +CollagenI +GM6001	1.4	0.1	94		NA	
4-c **alpha-adaptin+ CCP density** *(CCP/µm²)*	CM	0.52	0.02	41	4	-	M-W
	EBSS	0.8	0.02	60		<0.0001	
4-f **% of AP2-positive CCPs (CM)**	T0	100	NA	4459	3	NA	NA
	T2	120		2955			
	T5	80		1923			
	T10	80		1925			
4-F **% of AP2-positive CCPs (EBSS)**	T0	100	NA	5827	3	NA	NA
	T2	100		3614			
	T5	100		3776			
	T10	120		2121			
4-h **Stable CCPs** *(% of total)*	CM	10.2	0.2	607	2	NA	NA
	EBSS	19.9	1.3	365			
4-j **Gelatin Degradation** *(% of EBSS siNT)*	**EBSS siNT**	**100**	**5.0**	**54**	3	**-**	K-W
	EBSS siα-adaptin	17.0	4.1	50		<0.0001	
	EBSS-siCHC	85.6	5.1	48		n.s.	

Supplementary Figure	Cell	Mode of randomized values	Min-Max of randomized values	True value	p-value
S1-b **Randomization of TKS5 positions**	1	225	195-264	323/733	0
	2	174	140-214	308/804	0
	3	445	64-120	218/468	0
	4	555	495-630	670/435	0
	5	243	201-288	518/824	0
	6	158	124-200	349/1038	0
	7	94	68-124	335/886	0
	8	46	28-64	160/325	0
	9	112	80-142	421/807	0
	10	68	44-88	210/605	0

Supplementary Figure	Condition	Mean	SEM	n	N	p value	Stat.
S1-e **Cleaved collagen I** *(% of EBSS/-rhTIMP2)* Left	CM	6.9	0.9	46	3	<0.00001	K-W
	EBSS	**100**	**4.4**	**85**		**-**	
	EBSS+15 ng/mL	100.6	5.8	82		ns	
	EBSS+75 ng/mL	49.5	3.3	80		<0.00001	
	EBSS+2000 ng/mL	9.5	1.2	77		<0.00001	
S1-e **Cleaved collagen I** *(% of EBSS/-rhTIMP2)* Right	CM	6.9	0.9	46	2	<0.00001	K-W
	EBSS	**100**	**4.4**	**85**		**-**	
	EBSS+15 ng/mL	90.2	5.0	49		ns	
	EBSS+75 ng/mL	46.4	3.0	52		<0.00001	
	EBSS+2000 ng/mL	11.6	1.5	41		<0.00001	
S1-g **Cleaved collagen I** *(% of CM/ siNT)*	**CM siNT**	**100**	**9.4**	**57**	3	**-**	K-W
	CM siMT1	35.8	6.2	43		<0.00001	
	CM siTKS5	36.2	4.9	45		<0.00001	
S1-h **Degradative cells** *(% of EBSS/ siNT)*	CM siNT	16.1	1.5	43	3	NA	M-W
	EBSS siNT	**100**	**5.9**	**63**		**-**	
	EBSS siMT1	10.6	1.4	62		0.0015	
S2-c **Cleaved collagen I** *(% of EBSS)*	CM	16.3	1.8	67	3	<0.00001	M-W
	EBSS	**100**	**6.1**	**88**		**-**	
S2-d **Cleaved collagen I** *(% of EBSS/ siNT)*	**EBSS siNT**	**100**	**6.0**	**96**	3	**-**	K-W
	EBSS siMT1	15.0	3.5	84		<0.00001	
	EBSS siTKS5	36.3	5.3	70		<0.00001	
S3-a **pS6K level**	EBSS T0	1.0	NA	NA	2	NA	NA
	EBSS T15	0.56					

(normalized to CM value)	EBSS T30	0.16					
	EBSS T60	0.15					
	EBSS + BSA T0	1.0					
	EBSS + BSA T15	0.92					
	EBSS + BSA T30	0.50					
	EBSS + BSA T60	0.30					
S3-b **pS6K/Actin** *(Fold change to CM/ -Drug)*	**CM**	**1**	**0**	NA	3	NA	NA
	Others	0	4.0				
S3-c **p4E-BP1/Actin** *(Fold change to CM/ -Drug)*	**CM**	**1**	**0**	NA	3	NA	NA
	CM + Rapa	0.3	0.02				
	EBSS	0.2	0.05				
	EBSS + Rapa	0.3	0.03				
S3-d **pAKT/Actin** *(Fold change to CM/ -Drug)*	**CM**	**1**	**0**	NA	3	NA	NA
	CM + Rapa	1.3	0.4				
	EBSS	0.2	0.06				
	EBSS + Rapa	0.1	0.04				
S3-e **Gelatin Degradation** *(fold change to CM)*	**CM**	**100.0**	**17.4**	**53**	2	**-**	M-W
	CM + Rapa	472.0	68.0	54		<0.0001	
S4-a **MT1-MMP/Actin** *(Fold change to EBSS/0 hr)*	**CM**	**1.0**	**0**	NA	2	**-**	K-W
	EBSS 1h	1.0	0.1			ns	
	EBSS 3hrs	0.8	0.3			ns	
	EBSS 6hrs	0.9	0.1			ns	

Supplementary Figure	**Cell**	**Mode of randomized values**	**Min-Max of randomized values**	**True value**	**p-value**
S4-c **Randomization of AP2 positions**	1	20	05-40	46/350	0
	2	41	16-63	91/641	0
	3	40	20-64	61/514	0
	4	50	27-74	127/442	0.0016
	5	40	20-65	54/394	0
	6	59	34-92	118/703	0.0142
	7	117	83-153	165/682	0
	8	98	63-133	204/880	0
	9	61	36-88	143/879	0
	10	51	30-77	112/575	0

Supplementary Figure	**Condition**	**Mean**	**SEM**	**n**	**N**	**p value**	**Stat.**
S4-e **CHC expression**	**siNT**	**1.0**	**0**	-	3	NA	NA
	siα-adaptin	0.6	0.06				

(Fold change to siNT)	siCHC	0	0				
S4-e**α-adaptin expression** *(Fold change to siNT)*	**siNT**	**1.0**	**0**	-	3	NA	NA
	siα-adaptin	0.1	0.1				
	siCHC	1.7	0.3				
S4-e **MT1-MMP expression** *(Fold change to siNT)*	**siNT**	**1.0**	**0**	-	2	NA	NA
	siα-adaptin	0.9	0.07				
	siCHC	0.9	0.2				

SEM (standard error of the mean); n, sample number; N, number of independent experiments; ns, not significative; NA, not available.

Data were tested for normal distribution using the D'Agostino-Pearson normality test and nonparametric tests were applied otherwise.

Non-parametric tests: K-W, Kruskal-Wallis test; M-W, Mann-Whitney

Parametric tests: One-Way ANOVA

Statistical significance was defined as *, P <0.05; **, P <0.01; ***, P <0.001; ****, P <0.00001; ns, not significant.

Supplementary Movie Legends

Movie S1: TKS5 localizes to highly dynamic matrix fiber-remodeling elongated invadopodia in cells grown in nutrient-replete conditions. Shown is a MDA-MB-231 cell expressing TKS5^{GFP} (green). The cell is plated on a layer of fibrillar collagen (magenta) and is grown in nutrient-replete conditions. Images were acquired every 1 min for 60 min. The last sequence of the movie are still images of the time projection of seven frames separated by a 10-min interval with the different time points represented with the indicated pseudocolor coding. In nutrient-proficient medium, cells form dynamic elongated TKS5-positive invadopodia in association with the underlying collagen fibers that are actively remodeled.

Movie S2: TKS5 localizes to punctate, mostly static, structures in starved cells. Shown is a MDA-MB-231 cell grown in nutrient-replete conditions and plated on a layer of fibrillar collagen (magenta). The cell expresses TKS5^{GFP} (green). Images were acquired every 1 min for 60 min. The last sequence of the movie is a time projection of seven frames separated by a 10-min interval with the different time points represented with the indicated pseudocolor coding. Starved cells form static TKS5-positive puncta with minimal displacement of the underlying matrix fibers.

Movie S3: CCP and TKS5 dynamics in nutrient replete and deplete conditions. Shown is the dynamics of plasma membrane TKS5^{GFP} (green) and CCPs labeled with μ-adaptin^{mCherry} (red) in MDA-MB-231 cells plated on cross-linked gelatin in CM (upper panel) or EBSS medium (lower panel). Images were acquired every 5 s for 5 min by TIRF-M. In nutrient-replete conditions (CM), large and static TKS5^{GFP}-positive

invadopodia form and TKS5 shows some transient association with CCPs, contrasting with long-lasting TKS5 interaction with CCPs observed in starved cells (yellow arrows). Scale bar, 2 µm.

Supplementary references

[1] R. Ferrari, G. Martin, O. Tagit, A. Guichard, A. Cambi, R. Voituriez, S. Vassilopoulos, P. Chavrier, *Nat Commun* **2019**, *10* (1), 4886, https://doi.org/10.1038/s41467-019-12930-y.

[2] M. Sakurai-Yageta, C. Recchi, G. Le Dez, J. B. Sibarita, L. Daviet, J. Camonis, C. D'Souza-Schorey, P. Chavrier, *J Cell Biol* **2008**, *181* (6), 985, https://doi.org/10.1083/jcb.200709076.

[3] J. Y. Tinevez, N. Perry, J. Schindelin, G. M. Hoopes, G. D. Reynolds, E. Laplantine, S. Y. Bednarek, S. L. Shorte, K. W. Eliceiri, *Methods* **2017**, *115*, 80, https://doi.org/10.1016/j.ymeth.2016.09.016.

[4] F. Coussy, L. de Koning, M. Lavigne, V. Bernard, B. Ouine, A. Boulai, R. El Botty, A. Dahmani, E. Montaudon, F. Assayag, L. Morisset, L. Huguet, L. Sourd, P. Painsec, C. Callens, S. Chateau-Joubert, J. L. Servely, T. Larcher, C. Reyes, E. Girard, G. Pierron, C. Laurent, S. Vacher, S. Baulande, S. Melaabi, A. Vincent-Salomon, D. Gentien, V. Dieras, I. Bieche, E. Marangoni, *International journal of cancer* **2019**, *145* (7), 1902, https://doi.org/10.1002/ijc.32266.

[5] A. Bruna, O. M. Rueda, W. Greenwood, A. S. Batra, M. Callari, R. N. Batra, K. Pogrebniak, J. Sandoval, J. W. Cassidy, A. Tufegdzic-Vidakovic, S. J. Sammut, L. Jones, E. Provenzano, R. Baird, P. Eirew, J. Hadfield, M. Eldridge, A. McLaren-Douglas, A. Barthorpe, H. Lightfoot, M. J. O'Connor, J. Gray, J. Cortes, J. Baselga, E. Marangoni, A. L. Welm, S. Aparicio, V. Serra, M. J. Garnett, C. Caldas, *Cell* **2016**, *167* (1), 260, https://doi.org/10.1016/j.cell.2016.08.041.

ARTICLE 2

TFEB activation in response to mTOR repression promotes ECM degradation by inducing lysosomal exocytosis of MT1-MMP at invadopodia

David Remy[1], Sandra Antoine-Bally[1], Sophie Grouard de Toqueville[1], Anne-Sophie Macé[2], Adèle Berlioz[1], Ahmed Dahmani[3], Elodie Montaudon[3], Ludivine Morisset[3], Elisabetta Marangoni[3], and Philippe Chavrier[1, ±]

[1] Institut Curie, PSL Research University, CNRS UMR 144, 75005, Paris, France

[2] Institut Curie, PSL Research University, Cell and Tissue Imaging Facility (PICT-IBiSA), 75005, Paris, France

[3] Institut Curie, PSL Research University, Translational Research Department, 75005, Paris, France

± Corresponding author, e-mail: philippe.chavrier@curie.fr

In preparation

Results

mTORC1 repression stimulates invadopodia-mediated matrix degradation in breast cancer cells

To dissect the molecular mechanisms underlying invadopodia-mediated matrix degradation, we systematically knocked-down regulatory elements of the mTORC1 pathway in MDA-MB-231 cells and measured their gelatinolytic activity. MDA-MB-231 cells transfected with control siRNA and plated for 6 h in complete medium on fluorescently-labeled cross-linked gelatin showed punctiform cortactin staining associated with dark gelatin degradation spots underneath the cell body, which is characteristic of invadopodia-mediated pericellular matrix degradation (Figure 1A). Control cells showed robust association of mTOR-rich puncta with CD63-positive late endosome/lysosomal compartment as well as high levels of phosphorylation of S6K and 4E-BP1 (Figure 1C and Extended Figure 1A). As reported, the silencing of transmembrane matrix metalloprotease, MT1-MMP, or invadopodia scaffold protein, TKS5, abolished gelatin degradation with no detectable modification in p-S6K and p-4E-BP1 levels (Figures 1A, B and Extended Figures 1A, B) (Colombero et al., 2021). Silencing of Regulatory-associated protein of mTOR (RAPTOR) lead to a strong reduction in the levels of p-S6K and p-4E-BP1 and mTOR association with CD63-positive endolysosomes, as well as a concomitant 10-fold increase in gelatin degradation. Conversely, KD of RAPTOR Independent Companion Of MTOR Complex 2 (RICTOR) had no effect on p-S6K and p-4E-BP1 and on matrix degradation compared to control conditions (Figures 1B, C and Extended Figures 1A, B). These results suggest that the matrix degradation program is promoted by mTORC1 repression, not by mTORC2.

We systematically knocked-down some essential regulatory elements of the mTORC1 pathway and assessed their effects on gelatin degradation. We found that silencing of RagA, RagC and Rheb GTPases also lead to a marked inhibition of mTORC1 activity based on the lack of phosphorylation of p-S6K and p-4E-BP1 proxies, and a significant increase in matrix degradation (Figures 1A-C and Extended Figures 1A, B). As expected, Rheb silencing reduced p-S6K and p-4E-BP1 levels and gelatin degradation, although it did not affect mTOR recruitment to the endolysosomes (Extended Figure 1C, (Kim & Guan, 2019; Sancak et al., 2008, 2010)). Surprisingly, KD of RagB or RagD in MDA-MB-231 had no effect on mTORC1 activity, suggesting that the RagA/RagC heterodimer is probably the major Rag complex regulating mTORC1 activity in MDA-MB-231 cells. Interestingly, RagB or RagD KD did not impact matrix degradation (Figure 1B, C and Extended Figures 1A, B). We similarly investigated the role of regulatory Rag GTPase activating proteins (GAPs) and guanine

exchange factors (GEFs). As expected, silencing of NRPL2 and DEPDC5, two subunits of the RagA-GAP GATOR1 complex, had no effect on mTORC1 activity (Bar-Peled et al., 2013; Pal et al., 2018) and did not affect gelatin degradation as compared to control cells (Figure 1B and Extended Figures 1A, B). Solute carrier family 38 member 9 (SLC38A9) is a lysosomal-resident protein mediating the lysosomal efflux of several essential amino acids that are then sensed by mTORC1 through Sestrin proteins (Wyant et al., 2017). In addition, SLC38A9 has been proposed to act as a GEF for RagA (Shen & Sabatini, 2018). Along this line, KD of SLC38A9 repressed mTORC1 activity and it stimulated a robust matrix degradation response (Figure 1B and Extended Figures 1 A, B). Cyclin-dependent kinase inhibitor 1B (CDKN1B or $p27^{Kip1}$, referred here to p27) has been shown to repress mTORC1 activity in MEFs by interfering with the structural integrity of the RAGULATOR Rag-GEF complex (Nowosad et al., 2020). Surprisingly, we observed that $p27^{Kip1}$ KD in MDA-MB-231 cells repressed the phosphorylation of S6K but not of 4E-BP1 (Figure 1B, C and Extended Figures 1A, B). However, p27 KD increased gelatin degradation as previously described (Figure 1B, Jeannot et al., 2017). Then, we analyzed the consequences of the concomitant silencing of RagC or Raptor and invadopodial TKS5. Loss of TKS5 completely abolished the matrix degradation induced by the KD of RagC or Raptor alone, confirming that the matrix proteolysis response induced upon mTORC1 repression is mediated by the invadopodia (Figure 1D).

In a next set of experiments, we tested if pharmacological inhibition of mTORC1 could also induce matrix degradation. MDA-MB-231 cells were treated overnight with Rapamycin or Torin-1 and plated for 6 hrs on gelatin. We observed a strong increase in gelatin degradation compared to vehicle-treated cells, similar to the response of mTORC1-depleted cells (Figures 1E, F). Taken together, these results demonstrate that the repression of mTORC1 activity stimulates a robust invadopodia-mediated matrix degradation program in MDA-MB-231 cells.

Folliculin (FLCN) is a RagC/RagD GAP, which maintains these Rag GTPases in their active GDP-bound conformation on the lysosomal membrane. FLCN-mediated activation of RagC is known to play a determinant role in recruitment, mTORC1-mediated phosphorylation, and subsequent inhibition of Transcription Factor EB (TFEB) at the lysosomal surface (Meng & Ferguson, 2018; Napolitano et al., 2020). In FLCN-depleted cells, mTORC1 can no longer phosphorylate TFEB, which can translocate in the nucleus as an active transcription factor (Napolitano et al., 2020, 2022). Interestingly, we found that FLCN KD had no effect on mTORC1 activity but induced a robust ECM degradation response (Figures 1B, C and Extended Figure 1A, B). All together, these data suggested a potential role in TFEB nuclear translocation and activation in the matrix degradation program induced downstream of mTORC1 repression that we sought to address in more detail.

TFEB activation is required for ECM degradation upon mTORC1 repression.

We first monitored the localization of $TFEB^{GFP}$ in MDA-MB-231 cells and found that in contrast to a mostly cytoplasmic localization in control cells in nutrient-replete conditions, cells KD for RagC, Raptor or FLCN displayed a prominent nuclear localization of $TFEB^{GFP}$ coinciding with an increase in ECM degradation (Figures 2A, B and Extended Figure 2A). TFEB activation is known to control lysosomal biogenesis and upregulation of lysosome-residing proteins, such as CD63 (Palmieri et al., 2011). Along this line, we found that CD63-positive vesicles were increased in cells KD for RagC, Raptor, or FLCN compared to control cells (Extended Figure 2B). Altogether, these data suggested that TFEB became activated in these cells and promoted the expected transcriptional changes.

Next, the role of TFEB in the regulation of the matrix degradation program induced upon mTORC1 repression was investigated. Strikingly, concomitant KD of TFEB (double KD, DKD cells) abolished the induction of gelatinolysis by RagC, Raptor, or FLCN single KD (Figure 2C and Extended Figure 2A). In contrast, TFEB KD did not affect gelatinolysis, indicating that TFEB did not contribute significantly to the basal matrix degradation response in MDA-MB-231 cells in nutrient-replete conditions. In addition to TFEB, MDA-MB-231 cells express the related TFE3 transcription factor (Extended Figure 2D). Matrix degradation induced upon RagC KD was not abolished by concomitant TFE3 depletion, suggesting that TFE3 does not contribute to ECM degradation in response to mTORC1 repression (Extended Figures 2C, D).

We then sought to generalize these findings using the MCF10DCIS.com human breast cancer cell line, a model of ductal carcinoma *in situ* (Miller et al., 2000). We found that KD of RagC reduced the levels of p-S6K and p-4E-BP1 and induced a strong nuclear localization of TFEB in these cells (Extended Figures 3A-C). Additionally, RagC KD in MCF10DCIS.com induced a robust degradation of fibrillar type I collagen that was abolished upon concomitant depletion of TFEB (Figure 2D). Furthermore, mTORC1 repression using Torin-1, Rapamycin, or the Rapamycin analog, Everolimus, induced a strong nuclear localization of $TFEB^{GFP}$ in MDA-MB-231 cells (Extended Figures 2E-G), and TFEB KD fully abolished the drug-induced gelatin degradation response (Figure 2E). Similar results were found in the MCF10DCIS.com (Extended Figures 3D, E). Taken together, these results suggest that mTORC1 repression induces a massive matrix degradation response in several breast cancer cell lines, which depends on TFEB function. Transient overexpression of TFEB has been shown to mediate transcriptional changes as increased lysosomal biogenesis, peripheral lysosome trafficking, and exocytosis (Medina et al., 2011). We show that overexpression of $TFEB^{GFP}$ in MDA-MB-231 cells promotes a strong collagen degradation response as compared to control GFP-expressing cells (Figure 2F). The ability of TFEB to bind to DNA requires two conserved Ile243 and Arg248 residues in the b-Helix-Loop-Helix domain (Vu et al., 2021). Ala substitution of

Ile243 and Arg248 in TFEB (IR-TFEB^{GFP}) effectively abolished TFEB's capacity to promote collagenolysis as compared to wild-type TFEB^{GFP} (Figure 2F). Finally, we tested the effect of Apilimod, a drug known to inhibit PIKfyve and the production of phosphatidylinositol 3,5-bisphosphate on endolysosomes, and impedes mTORC1 interaction with TFEB, leading to its nuclear translocation and constitutive activation while maintaining normal mTORC1 activity (Hasegawa et al., 2022). Treatment of MDA-MB-231 cells with Apilimod induced a strong nuclear translocation of TFEB (Figure 2G), and a dramatic increase in gelatin degradation, which was abolished by TFEB KD (Figure 2H). As previously described, p-S6K and p-4E-BP1 levels were unaffected in the presence of Apilimod (Extended Figure 2I). Taken together, these results point to a stimulation of the ECM degradation program in breast cancer cells upon TFEB activation in response to mTORC1 repression. This response requires TFEB DNA binding capacity and probably involves TFEB's transcriptional activity and is independent of the phosphorylation status of other key mTORC1 phosphorylation substrates including S6K and 4E-BP1.

TFEB activation stimulates MT1-MMP exocytosis at invadopodia.

Surface level of MT1-MMP results from a balance of exocytosis and endocytosis events and directly influence pericellular matrix degradation (Castro-Castro et al., 2016; Lodillinsky et al., 2021; Poincloux et al., 2009b). TFEB upregulates genes encoding lysosomal proteins and promotes lysosomal biogenesis and exocytosis (Medina et al., 2011). We hypothesized that upon mTORC1 repression, TFEB activation could lead to increased exocytosis of MT1-MMP at the plasma membrane to support enhanced ECM degradation. Plasma membrane MT1-MMP levels were assessed by surface antibody labeling and confocal microscopy. KD of RagC in MDA-MB-231 cells resulted in a 1.5-fold increase in surface MT1-MMP, which was abolished in DKD cells (Figure 3A, B and Extended Figure 4A). The influence of RagC KD and TFEB activation on MT1-MMP delivery to invadopodia was assessed by live cell microscopy of MDA-MB-231 cells expressing MT1-MMP^{pHLuorin} plated on fibrillar type I collagen (Monteiro et al., 2013; Poincloux et al., 2009b). In control cells, the MT1-MMP^{pHLuorin} signal was detected in endolysosomal vesicles in the vicinity of underlying collagen fibers and accumulated at fiber-plasma membrane contact sites. Based on earlier work, we know that MT1-MMP^{pHLuorin}-positive vesicles correspond to endolysosomes that fused with and remained tethered to the PM (through a thin tubular membrane stem visible in Supplemental Movie 1 and in the gallery in Figure 3E), with their lumen opened to the extracellular milieu (Monteiro et al, 2012; Marchesin et al., 2015). MT1-MMP^{pHLuorin} green flashes thus correspond to exocytic events of MT1-MMP that then accumulates at invadopodial PM-matrix contact sites. As previously described, a majority of MT1-MMP^{pHLuorin} endolysosomes remained at the same position for several minutes

and correspond to the above-described tethered vesicles (Figures 3 C-E and Supplemental Video 1, (Marchesin et al., 2015; Monteiro et al., 2013)). RagC KD lead to a 3-fold increase in the number of MT1-MMP exocytic events and 1.5-fold increase in the number of long-lived endosomes (MT1-MMP^{pHLuorin} endolysosomes with a fluorescent signal stable for the duration of the acquisition, *i.e.,* 14 min) (Figures 3C-E and Supplemental Video 2). Taken together, these results suggest that mTORC1 repression promotes the exocytosis of endolysosomal-resident MT1-MMP at invadopodia to support an increase in ECM degradation. Of note, immunoblotting analysis revealed that RagC KD resulted in a 1.5-fold increase in total levels of MT1-MMP in MDA-MB-231 cells, which was abolished in DKD cells (Extended Figure 4A, B). Collectively, these data suggest that MT1-MMP, and possibly other key invadopodia components, may be under transcriptional control by TFEB and part of the CLEAR gene network in breast cancer cells.

TFEB activation in response to mTORC1 repression stimulates invadopodia dynamics.

Invadopodia are dynamic structures used by cancer cells to remodel the ECM. In particular, invadopodia have been shown to act through a dual activity by controlling proteolytic cleavage and softening of the matrix fibers and generation of actin-based forces that push the fibers aside. We sought to investigate if increased matrix degradation upon mTORC1 repression also involved changes in invadopodia dynamics. First, we found that invadopodia formation increased by 70% in RagC KD cells compared to control cells, and not in DKD cells (Figure 3F). In addition, using a Particle Image Velocimetry (PIV)-based analysis to monitor the movement and direction of TKS5^{GFP}-labeled invadopodia structures, we observed that the expansion speed of the invadopodia was significantly increased by 23% upon RagC silencing compared to control cells (Figures 3G, H and Supplemental Videos 3, 4). Interestingly, this increase was abolished in DKD cells (Figure 3H). Increased dynamics of invadopodia upon RagC silencing conferred to the cells the ability to push the collagen fibers aside faster than control cells (Extended Figure 4).

Concomitant MT1-MMP KD or treatment with matrix metalloprotease inhibitor GM6001 also abolished the enhanced dynamics in RagC KD cells which suggest that increased invadopodia velocity is mediated by the TFEB-mediated surge in MT1-MMP exocytosis rates (Figure 3G and Extended Figure 4C).

mTORC1 repression stimulates breast tumor cell invasion through 3D type I collagen.

We investigated the consequence of TFEB activation on the capacity of breast cancer cells to invade through a 3D type I collagen matrix using a MDA-MB-231 multicellular spheroid-

based assays. Compared to control spheroids, silencing of RagC lead to a 40% increase in invasion of the spheroids through the collagen which was accompanied by a 2.5-fold increase in collagen degradation (Figure 4A-C). Similarly, KD of RagC in MCF10DCIS.com cells induced a 30% increase in invasion (Figure 4D-E). Taken together, these results suggest the existence of a proteolytic-based matrix invasion program that is induced upon mTORC1 repression.

mTORC1 repression induces a collagenolytic invasion program in TNBC patient-derived xenografts.

Long-term-established breast cancer cell lines may fail to recapitulate the behavior of primary cells (Ben-David et al., 2019). For the generalization of our findings to models closer to the disease, we used patient-derived xenografts (PDX) from primary TNBC tumors which are clinically relevant for the analysis of tumor response to drugs (Coussy et al., 2019). Cancer cells were isolated and dissociated from TNBC PDXs and cultured in vitro in a 3D type I collagen matrix in the presence of mTOR inhibitors including rapamycin, Torin-1, and Everolimus, which is used in clinics to treat breast cancer patients (Du et al., 2018; Miricescu et al., 2020). We measured the effects of mTORC1 repression on collagenolysis by PDX cells by staining with the Col¾-C1 antibody (Annex 3 and (Colombero et al., 2021; Ferrari et al., 2019; Monteiro et al., 2013)). Remarkably, all drugs induced a significant increase in ECM degradation in all three tested PDXs, with some variability in the intensity of the drug response depending on the PDX (Figures 5A, B and Extended Figures 5A-C). Levels of MT1-MMP expressed in those PDX was assessed by immunoblotting and compared to those of MDA-MB-231 cells and MCF10DCIS.com cells (Extended Figure 5D). All tested TNBC PDX expressed MT1-MMP at varying levels. In contrast, the only HER2+ PDX we tested did not express MT1-MMP and did not degrade collagen in control or in mTOR-repressed conditions (data not shown). Interestingly, we observed an increased expression of MT1-MMP in 2 out of 3 PDXs upon Everolimus treatment compared to control, confirming results found in MDA-MB-231 silenced for RagC (Extended Figure 5D). We also generated PDX organoids (PDXO) that mimicked solid tumors and were used to visualize the impact of mTORC1 repression on the potential to remodel and invade through the collagen gel. PDXOs were embedded in the 3D collagen gel for three days (d3), and drug or vehicle treatment was applied for four days (d7). At d3, PDXOs were relatively small and homogeneous in size and there was little pericellular collagen cleavage and minimal cell invasion through the matrix. After 7d in vehicle-treated conditions, the size of PDXOs increased as compared to d3 as cells proliferated. Some cells escaped the PDXO and invaded the collagen gel but overall, PDXO remained intact (Figure 5C). In contrast, Everolimus treatment stimulated a strong pericellular degradation of collagen

at the edge of the PDXO, which was abolished by concomitant treatment with GM6001 (Figure 5C). Furthermore, we observed a higher propensity of Everolimus-treated cells to escape the PDXO as compared to control PDXs (Figure 5C). As expected, the PDXOs were also smaller as compared to controls as mTORC1 repression is known to inhibit cell proliferation (Hatem et al., 2016). Altogether, these observations support the conclusion that mTORC1 repression by clinically used inhibitors in TNBC PDXs stimulates MT1-MMP-mediated collagenolysis and invasion.

Methods

Cell culture, transfection, and siRNA treatment. Human MDA-MB-231 breast adenocarcinoma cells obtained from ATCC (ATCC HTB-26) were grown in L-15 medium (Sigma-Aldrich) supplemented with 15% fetal calf serum (FCS) and 2 mM glutamine (ThermoFisher) at 37°C in 1% CO_2. The MCF10DCIS.com cell line was purchased from Asterland and grown in DMEM-F12 supplemented with 15% horse serum (ThermoFisher) at 37°C in 5% CO2. MDA-MB-231 cells stably expressing TKS5^{GFP} or MT1-MMP^{pHLuorin} were generated by lentiviral transduction (Ferrari et al., 2019; Monteiro et al., 2013). All cell lines were routinely tested for mycoplasma contamination. For transient expression, MDA-MB-231 cells were transfected with plasmid constructs using Lipofectamine 3000 (ThermoFisher) for 24 h according to the manufacturer's instructions (see Table S1). Briefly, 50,000 cells were plated in a 24-well plate and incubated with a mixture of Lipofectamine 3000, p3000 reagent, and 0.75 µg of DNA. Fresh growth medium was added after 4 h. For RNA interference, MDA-MB-231 cells were treated with indicated SMARTpool siRNA (Dharmacon) using Lullaby reagent (OZ Biosciences) and analyzed 72 h later (see Table S1). Briefly, 40,000 cells were seeded in a 24-well plate in complete medium and immediately incubated with a mixture of OPTI-MEM, Lullaby, and siRNA for a final siRNA concentration of 50 nM. Cells were analyzed 72 h later or when required, collected 48 h later for plasmid transfection using Lipofectamine 3000 as described above.

Antibodies and drugs. The source and working concentrations of commercial antibodies and drugs used for this study are listed in Table S2 and Table S3 respectively.

Fluorescent gelatin degradation assay. MDA-MB-231 cells treated with siRNA or drugs were plated on Oregon Green 488 (OG^{488})-conjugated cross-linked gelatin (ThermoFisher) as previously described (Remy et al., 2022) (Colombero et al., 2021). For cortactin staining, cells were pre-extracted with 0.1% Triton X-100 in 4% PFA in PBS for 90 sec at 37°C and fixed in 4% PFA in PBS for 30 min at 37°C. For mTOR and CD63 staining, cells were fixed after 3 h on gelatin in 4% PFA in PBS for 30 min and permeabilized with 0.1% Triton X-100 in PBS or 15 min. After extensive washes and 1h blocking in 10% FCS in PBS, samples were stained with appropriate antibodies or with fluorescently-labeled Phalloidin to stain F-actin. Images were acquired with a wide-field microscope (Eclipse 90i Upright; Nikon) using a 100x Plan Apo VC 1.4 oil objective and a cooled interlined charge-coupled device (CCD) camera (CoolSnap HQ^2; Roper Scientific). A z-dimension series of images was taken every 0.2 µm by means of a piezoelectric motor (Physik Instrumente). The system was steered by Metamorph software. To quantify degradation, the area of the degraded matrix (black pixels) measured with the threshold command of ImageJ was divided by the total number of nuclei in the field, and values

of this degradation index (DI) were normalized to the mean DI of control cells. The Convert.AI (NIS Elements Software) was trained to automatically, and without bias, segmentate gelatin degradation. Z-stacks were processed with the Extended Depth of Field (EDF) plug-in to obtain a unidimensional image of the gelatin degradation. For the training phase, Convert.AI was fed with 50 annotated EDF pictures and provided 16-bit pictures of the gelatin degradation. On these pictures, the area of degradation area was obtained automatically with a home-made macro using the AutoThreshold (MaxEntropy dark) and Analyze particle functions of Fiji. When required, linescans were performed using Fiji software. mTOR association with endolysosomes was quantified using a homemade Fiji macro as previously described (Priya and al., 2022). Briefly, z-planed were projected (maximal intensity) on a selected subset of stacks was performed and cells were manually drawn. Independent masks of the CD63-positive vesicles and mTOR-positive structures were created using the AutoThreshold and Analyze Particles commands of Fiji excluding regions <50px to avoid background signals. The CD63 mask was enlarged by 7px and the total area of mTOR-vesicles encompassed within this enlarged mask was divided by the cell area. Values were normalized to the mean ratio of control cells.

Polymerization of type I collagen gel. A type I collagen polymerization mix was prepared as previously described (Remy and al., 2022) by adding 25 µM HEPES (final concentration) to a 2.2 mg/mL acidic-extracted type I collagen solution (Corning) and adjusting pH to 7.5 with 0.34 N NaOH. For microscopic visualization of the collagen network, 5% of a ~2 mg/mL solution of AlexaFluor 647-conjugated type I collagen was added to unlabeled collagen in the polymerization mix. When required, drugs were added to the appropriate final concentration in the polymerization mix (see Table S3). Polymerization was started by incubation at 37°C in a humidified chamber (CO_2 cell incubator).

Quantification of pericellular collagenolysis. To measure pericellular collagenolysis on a thin layer of type I collagen gel, an 18-mm diameter glass coverslip was layered with 200 µl of the ice-cold 2.2 mg/mL Alexa Fluor 647-labeled type I collagen polymerization mix as previously described (Remy and al., 2022). *Excess collagen solution was removed by pipette aspiration to leave a thin smear of collagen solution on the glass coverslip. After 2"20 min of polymerization at 37°C, the collagen gel was gently washed in PBS to stop the reaction.* 70,000 siRNA- or drug-treated MCF10DCIS.com cells were plated and incubated for 4 h at 37°C in CM supplemented with drugs if required. Cells were pre-extracted with 0.1% Triton X-100 in 4% PFA in PBS for 90 sec at 37°C and fixed in 4% PFA in PBS for 20 min at 37°C. Coverslips were treated with 10% FCS in PBS for 30 min at room temperature then incubated with Col1-¾C and anti-cortactin antibodies diluted in 1% FCS in PBS for 2 hrs at 4°C. After three washes with PBS at 4°C, samples were counterstained with Cy3-conjugated anti-rabbit IgG and A488-

conjugated anti-mouse IgG antibodies for 60 min at 4°C, extensively washed in PBS, and mounted in Prolong-DAPI mounting medium (Invitrogen). Images were acquired with a wide-field microscope as described above. Quantification of Col1-¾C signal (cleaved collagen) was performed with a homemade ImageJ macro (Remy and al., 2022). For visualization purposes, images were deconvoluted using the Nikon NIS-Elements software (3D-deconvolution module; Lucy-Richardson algorithm).

Multicellular tumor spheroid invasion assays. MDA-MB-231 and MCF10DCIS cells were transfected with 50 nM of siRNA by nucleofection (Kit V, Lonza) and plated in 6-well plates. The day after, cells were collected and transfected again with 50 nM of siRNA by Lullaby reagent as described above. Multicellular spheroids were prepared immediately after with the hanging droplet method (Kelm et al., 2003). After 3 days, spheroids were embedded in a 40 µL drop of 2.2 mg/mL fluorescently-labeled type I collagen and left to polymerize for 90 min at 37°C. Spheroids were fixed immediately in 4% PFA in PBS (T0) or left to grow in a complete medium for two days before fixation (T2). Samples were either stained with DAPI and Phalloidin-Alexa488 or permeabilized and stained with Col1-¾C antibody as described above, and then counterstained with Phalloidin-Alexa488. Image acquisition was performed with a spinning-disk microscope (Inverted Eclipse Ti-2, Nikon) equipped with a W1 Yokogawa Spinning head using a 4X objective and an ORCA-Flash4.0 V2 sCMOS camera (Hamamatsu) for a wide field of view and a large dynamical range. A z-dimension series of images were taken every 4 µm by means of a Nano z500-N piezoelectric motor (Mad City Labs). The system was steered by NIS Elements software.

For quantification of the invasion, stacks were projected along the z-axis and the background intensity of phalloidin was measured as a reference value. The mean spheroid diameter was measured using a homemade ImageJ macro. Briefly, the intensity profile along a line centered on the spheroid was measured. The intersections between this profile and the background value were computed on each side of the line. The diameter was defined as the distance between these two intersections. To account for the imperfect symmetry of the spheroid, the line was rotated from 0 to 180° with a 5° step and the diameters computed as described above were averaged. The diameter of each T2 spheroid was normalized to the mean T0 diameters.

To record the Col1-¾C signal (cleaved collagen) on the entire spheroid, an Apo LWD 20X water objective was used to acquire a 3x3 mosaic with a 10% overlap stitch between images. For each frame, a z-dimension series of images were taken every 2 µm using. To quantify the Col1-¾C signal, the frames were isolated and projected along the z-axis using maximal intensity projection in Fiji. Col1-¾C signal was determined using the thresholding command

excluding regions <50-px to avoid non-specific signal. Col1-¾C signal area was ratioed to the number of nuclei in the field and values were normalized to the mean DI of the control cells.

Western blot analysis. Cells treated under the indicated conditions were washed once with PBS and then collected in 4x Laemmli Sample Reducing buffer and heated for 10 min at 95°C or collected in a homemade lysis buffer (Colombero et al., 2021). Samples were analyzed by SDS-polyacrylamide gel electrophoresis (PAGE) on 4-12% Tris-glycine gels (ThermoFisher Scientific). Proteins were transferred on a nitrocellulose membrane using the iBlot2 Dry Blotting System (Invitrogen). After incubating the membranes in 5% BSA or 5% skimmed milk in TBS (Interchim #UPU75132)-Tween 1%, proteins were detected by immunoblotting analysis with the indicated antibodies (see Table S2). Antibodies were detected using the Enhanced Chemiluminescence reagent (ECL, Amersham RPN2232) on the ChemiDoc MP Imaging System (Bio-Rad).

MT1-MMP surface staining. Cells treated with indicated siRNA for 72 h were surface labeled with mouse monoclonal anti-MT1-MMP primary antibodies (clone 2D7) diluted in complete medium for 30 min at 4°C. After extensive washes with complete medium and once with PBS, cells were fixed in 4% PFA in PBS. To ensure surface labeling, all solutions were ice-cold and the cells were kept on ice during all incubation steps. Samples were counterstained with Alexa Fluor 488-conjugated anti-mouse IgG secondary antibodies and Cy5-conjugated Phalloidin to visualize cell shape. Image acquisition was performed with a confocal spinning-disk microscope (Inverted Eclipse Ti-2, Nikon) equipped with a W1 Yokogawa Spinning head using a 60X water objective and an ORCA-Flash4.0 V2 sCMOS camera (Hamamatsu) for a wide field of view and a large dynamical range. A z-dimension series of images were taken every 0.2 µm by means of a Nano z500-N piezoelectric motor (Mad City Labs). The system was steered by NIS Elements software. Cells were delimited using the Phalloidin signal and the mean intensity of MT1-MMP at the plasma membrane was measured and normalized to the mean intensity of MT1-MMP in control cells.

MT1-MMPpHLuorin exocytosis. MDA-MB-231 MT1-MMP^{pHLuorin} cells treated with siRNA were plated on glass bottom dishes (MatTek Corporation) layered with a thin layer of fluorescently-labeled polymerized type I collagen (Remy et al., 2022). Cells were imaged by confocal spinning disk microscopy (one images every 20 sec). The number and lifetime of MT1-MMP^{pHLuorin} exocytic events (*i.e.,* GFP flashes) were measured per minute and per cell.

Particle Image Velocimetry of TKS5^{GFP}-positive invadopodia. MDA-MB-231 TKS5^{GFP} cells treated with siRNA were plated on glass bottom dishes (MatTek Corporation) layered with a thin layer of fluorescently-labeled polymerized type I collagen and imaged by confocal spinning disk microscopy (one image/min). To analyze the displacement of TKS5-positive invadopodia,

we used an open-source PIV (particle image velocimetry) MATLAB code, named PIVLab (Thielicke & Sonntag, 2021). To reduce background noise effects, we measure the velocimetry on one region of interest per cell, of identical size for all cells. Quantification of $TKS5^{GFP}$-positive invadopodia and color-coded time projections were described elsewhere (Colombero et al., 2021).

Nuclear translocation of TFEB. MDA-MB-231 transiently expressing TFEB-GFP or wild-type MCF10DCIS.com cells were treated with siRNA for 72 h of with mTOR drugs for 16 h as described above. Cells were then fixed with 4% PFA in PBS for 20 min. After permeabilization with 0.1% Triton X-100 in PBS for 10 min and blocking with 10% FCS in PBS for 1 h, MDA-MB-231 samples were stained with anti-mTOR, anti-CD63, and anti-GFP primary antibodies and counterstained with AF488-conjugated anti-chicken, Cy3-conjugated anti-rabbit, and AF647-conjugated anti-mouse secondary antibodies. MCF10DCIS.com samples were stained with anti-TFEB and anti-CD63 primary antibodies and counterstained with Cy3-conjugated anti-rabbit, and AF647-conjugated anti-mouse secondary antibodies as well as Phalloidin-AF488. Samples were mounted in Prolong DAPI for nucleus visualization. A z-dimension series of images were taken on confocal spinning-disk microscopy as described above. Quantification of the nuclear translocation of TFEB in cells positive for TFEB-GFP was done using a homemade ImageJ macro. Briefly, cells were manually delimited based on the GFP channel (cytoplasm mask) and a nucleus mask was created using the AutoThreshold and Analyze Particles functions of Fiji. The mean intensity of GFP in the nucleus mask was divided by the mean intensity of GFP in the cytoplasm mask and plotted as such. CD63-positive vesicles were detected using the AutoThreshold and Analyze Particles commands of Fiji excluding regions <50px to avoid background signals and the total area was divided by the cell area. Values were normalized to the area ratio of control cells.

***Ex-vivo* culture of TNBC patient-derived xenografts.** Breast cancer patient-derived xenografts were obtained from triple-negative breast tumors and generated as described (Coussy et al., 2019). After surgical excision of the tumor xenograft, tumor cells were dissociated in DMEM/F12 medium supplemented with 1 mg/mL collagenase (Roche) and hyaluronidase (Merck, 1000 U/mL) in 10 mM HEPES, 7.5% BSA Fraction V (ThermoFisher Scientific), 5 µg/mL insulin (Merck) and 50 µg/mL gentamycin (ThermoFisher Scientific) for 1h at 37°C on a rotating wheel at 180 rpm as previously described (Bruna et al., 2016). Samples were washed with DMEM/F12 medium and digested with 0.25% of trypsin (ThermoFisher Scientific) for 2 min at 37°C. Trypsin was neutralized in HBSS medium (ThermoFisher Scientific) supplemented in 10 mM HEPES and 2% FCS. Then, samples were treated with 5mg/mL dispase in HBSS (Roche) and 1 mg/mL DNAse I in DMEM (Merck) for 2 min at room temperature and then incubated in neutralization buffer supplemented with NH_4Cl (0.8%,

StemCell Technologies) to remove red blood cells. After filtration through a 40 µm Cell Strainer (Corning), tumor cells were plated in a 25-cm^2 cell-culture flask for 16h at 37°C in DMEM/F12 medium supplemented with 10% FCS. For the pericellular collagenolysis assay, non-attached PDX tumor cells in the culture supernatant were resuspended in a 2.2 mg/mL collagen I solution as described above and incubated for 16 hrs in CM supplemented with indicated drugs. After fixation with PFA 4% for 30 min at 37°C and permeabilization with Triton 0.1% in PBS for 15 min, samples were blocked with 1% BSA/PBS (60 min, RT), stained with Col1-¾C antibodies (2 hrs at 4°C) and counterstained with fluorescently labeled secondary antibodies and Phalloidin (60 min at 4°C). After extensive washes, samples were incubated for 5 min with 1mg/mL DAPI (Sigma) before mounting the coverslips in Prolong-DAPI mounting medium (ThermoFisher Scientific). Image acquisition was performed with a spinning-disk microscope (Inverted Eclipse Ti-2, Nikon) equipped with a W1 Yokogawa Spinning head using a 60X water objective and an ORCA-Flash4.0 V2 sCMOS camera (Hamamatsu) for a wide field of view and a large dynamical range. A z-dimension series of images were taken every 0.5 µm by means of a Nano z500-N piezoelectric motor (Mad City Labs). The system was steered by NIS Elements software.

For PDX organoids (PDXOs), the protocol was similar to the one for single-cell suspension, except that samples were treated with collagenase/hyaluronidase for 30 min at 37°C instead of 60 min. Furthermore, dispase treatment was omitted to keep cell junctions intact. At the filtration step on the Cell Strainer, we recovered the large objects (i.e., the organoids) that were not filtered by washing the Cell Strainer with 5 mL of DMEM/F12 over a Falcon tube. Finally, to eliminate the single cells from the organoid suspension, samples were centrifuged briefly (1 500 rpm, 2-5 sec) and the supernatants containing single cells were discarded. This last step was repeated 3 times. To count the organoids, 5 50 µL drops of the organoid suspension were plated on a Petri dish to count them by microscopic observations. Organoids were embedded in 40 µL drops of type I collagen drops as described above for 3 days (d3) in complete medium. After 3 days, ¼ of the samples were fixed and the rest was incubated with the indicated drugs for 4 more days (d7). Media was changed at d4 and d6. Samples were fixed at d7 with 4% PFA/PBS (30 min, 37°C), permeabilized with 0.5% Triton X-100/PBS (15 min, RT), and blocked with 1% BSA/PBS (60 min, RT). Samples were stained with Col1-¾C antibodies (16 hrs, 4°C) and then counterstained with secondary antibodies and Phalloidin (60 min, RT). After extensive washes, samples were incubated for 5 min with 1mg/mL DAPI (Sigma) before mounting the coverslips in Prolong-DAPI mounting medium (ThermoFisher Scientific). Image acquisition was performed with a spinning-disk microscope (Inverted Eclipse Ti-2, Nikon) equipped with a W1 Yokogawa Spinning head using a 40X water objective and an ORCA-Flash4.0 V2 sCMOS camera (Hamamatsu) for a wide field of view and a large dynamical

range. A z-dimension series of images were taken every 0.5 µm by means of a Nano z500-N piezoelectric motor (Mad City Labs). The system was steered by NIS Elements software.

Statistics and reproducibility. All data are presented as mean ± S.E.M. from at least three independent experiments except indicated otherwise. GraphPad Prism software was used for statistical analysis. Data were tested for normal distribution using the D'Agostino-Pearson normality test and nonparametric tests were applied otherwise. One-way ANOVA, Kruskal-Wallis or Mann-Whitney tests were applied as indicated in the figure legends and are summarized in Supplemental Table 4. Statistical significance was defined as *, $P<0.05$; **, $P<0.01$; ***, $P<0.001$; ****, $P<0.00001$; ns, not significant.

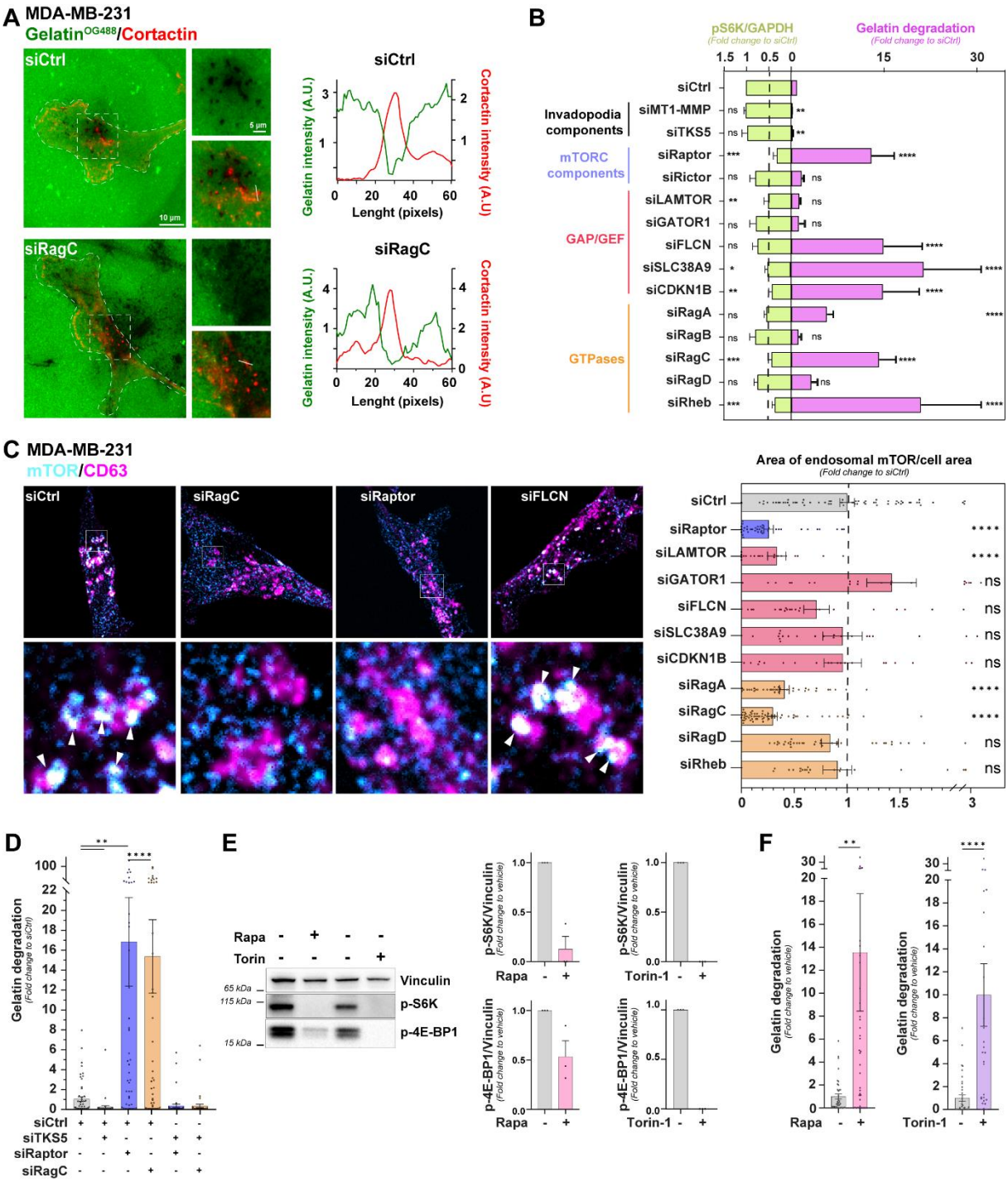
A MDA-MB-231
Gelatin OG488/Cortactin
siCtrl
siRagC
Gelatin intensity (A.U.)
Cortactin intensity (A.U)
Lenght (pixels)
B
pS6K/GAPDH
(Fold change to siCtrl)
Gelatin degradation
(Fold change to siCtrl)
Invadopodia components
mTORC components
GAP/GEF
GTPases
siCtrl
siMT1-MMP
siTKS5
siRaptor
siRictor
siLAMTOR
siGATOR1
siFLCN
siSLC38A9
siCDKN1B
siRagA
siRagB
siRagC
siRagD
siRheb
C MDA-MB-231
mTOR/CD63
siCtrl
siRagC
siRaptor
siFLCN
Area of endosomal mTOR/cell area
(Fold change to siCtrl)
D
Gelatin degradation
(Fold change to siCtrl)
siCtrl
siTKS5
siRaptor
siRagC
E
Rapa
Torin
65 kDa
115 kDa
15 kDa
Vinculin
p-S6K
p-4E-BP1
p-S6K/Vinculin
(Fold change to vehicle)
p-4E-BP1/Vinculin
(Fold change to vehicle)
Rapa
Torin-1
F
Gelatin degradation
(Fold change to vehicle)

Figure 1

Figure 1. mTORC1 repression in breast cancer cells promotes invadopodia-mediated extracellular matrix degradation. (A) MDA-MB-231 cells were treated with indicated siRNA and plated on fluorescently-labeled gelatin for 6 h. Higher magnification of the boxed region is shown in the insets. Dotted lines, cell contour. Graphs show intensity profiles (linescans) of gelatin and cortactin signals. (B) Quantification of gelatin degradation (pink bars) and p-S6K in cells treated with indicated siRNAs. (C) MDA-MB-231 KD for indicated siRNAs and showing the association of mTOR and CD63. Higher magnification of the boxed regions is shown in the insets. The graph shows the association of mTOR with CD63-positive vesicles per cell. (D) Gelatin degradation by MDA-MB-231 cells treated with indicated siRNAs. (E) Immunoblots and quantification of p-S6K and p-4E-BP1 in wild-type MDA-MB-231 cells treated with indicated drugs. (F) Gelatin degradation by cells as in (E).

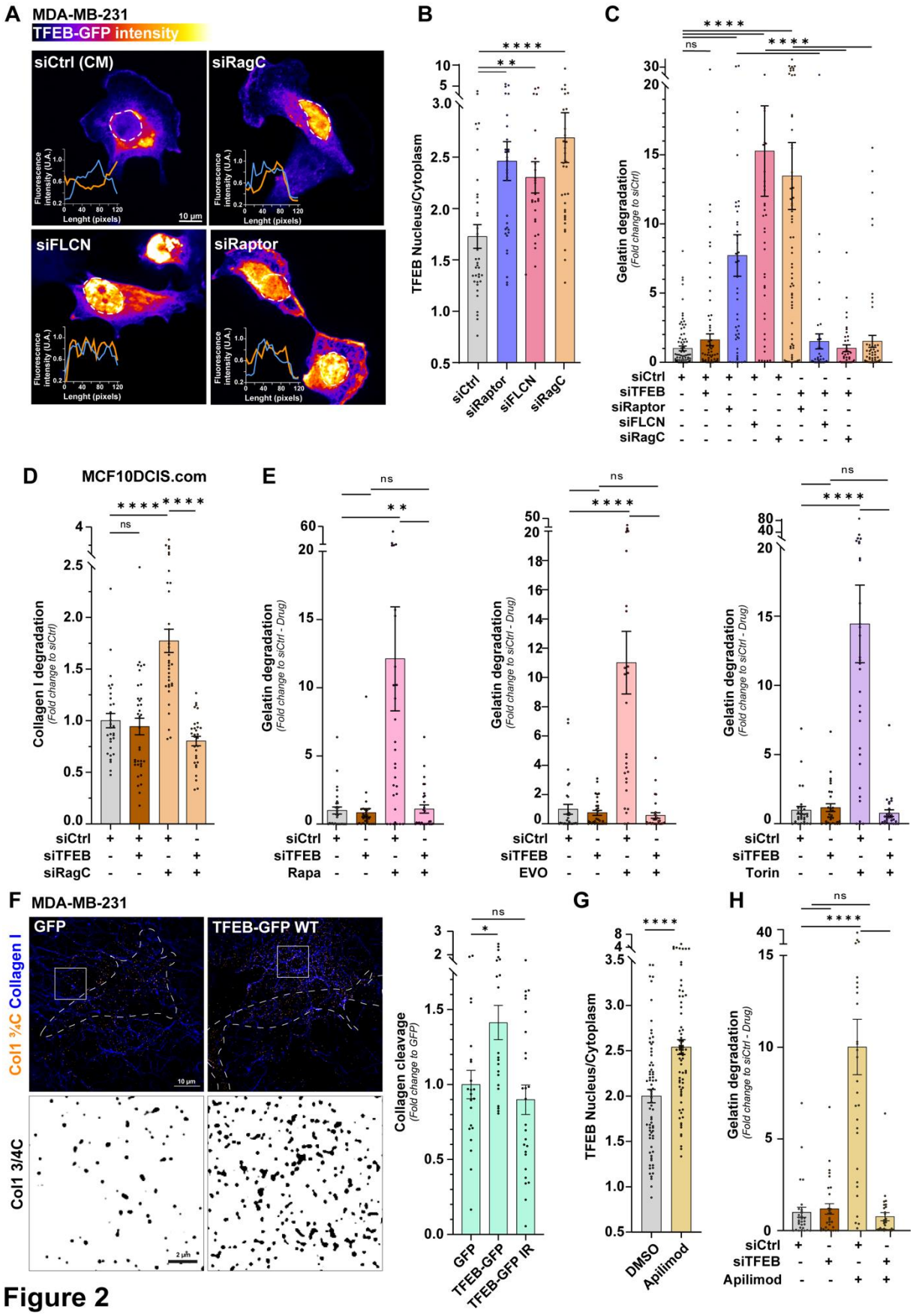
A
MDA-MB-231
TFEB-GFP intensity
siCtrl (CM)
siRagC
siFLCN
siRaptor
Fluorescence intensity (U.A.)
Lenght (pixels)
10 µm
B
TFEB Nucleus/Cytoplasm
siCtrl
siRaptor
siFLCN
siRagC
C
Gelatin degradation
(Fold change to siCtrl)
ns
siCtrl
siTFEB
siRaptor
siFLCN
siRagC
D
MCF10DCIS.com
Collagen I degradation
(Fold change to siCtrl)
siRagC
E
Gelatin degradation
(Fold change to siCtrl - Drug)
Rapa
EVO
Torin
F
MDA-MB-231
GFP
TFEB-GFP WT
Col1 ¾C Collagen I
Col1 3/4C
2 µm
Collagen cleavage
(Fold change to GFP)
GFP
TFEB-GFP
TFEB-GFP IR
G
TFEB Nucleus/Cytoplasm
DMSO
Apilimod
H
Gelatin degradation
(Fold change to siCtrl - Drug)
Apilimod

Figure 2

Figure 2. TFEB activity is required for matrix degradation upon mTORC1 repression. (A) Confocal pictures showing the localization of TFEB-GFP (LUT Fire) in MDA-MB-231 cells treated with indicated siRNAs. Graphs show intensity profiles (linescans) of TFEB-GFP and DAPI. (B) Quantification of the mean intensity ratio of TFEB-GFP between the nucleus and the cytoplasm in MDA-MB-231 cells treated with indicated siRNA. (C) Gelatin degradation by MDA-MB-231 cells treated with indicated siRNAs. (D) Collagen degradation by MCF10DCIS.com cells treated with indicated siRNAs. (E) Gelatin degradation by MDA-MB-231 cells silenced for TFEB (or control siRNA) and treated with indicated drugs. (F) Deconvoluted images showing MDA-MB-231 cells transiently expressing GFP or wild-type TFEB-GFP, cultured on a fibrillar type I collagen network (blue) for 4 h and stained for cleaved collagen fibers (orange). Insets show higher magnification of Col1 ¾C1 in boxed regions as Gray inverted LUT. Dotted lines, cell contour. Graph show collagen cleavage by MDA-MB-231 cells transiently expressing indicated constructs. (G) Quantification of the mean intensity ratio of TFEB-GFP between the nucleus and the cytoplasm in MDA-MB-231 cells treated with Apilimod or vehicle (DMSO). (H) Gelatin degradation by MDA-MB-231 cells silenced for TFEB (or control siRNA) and treated with Apilimod or DMSO.

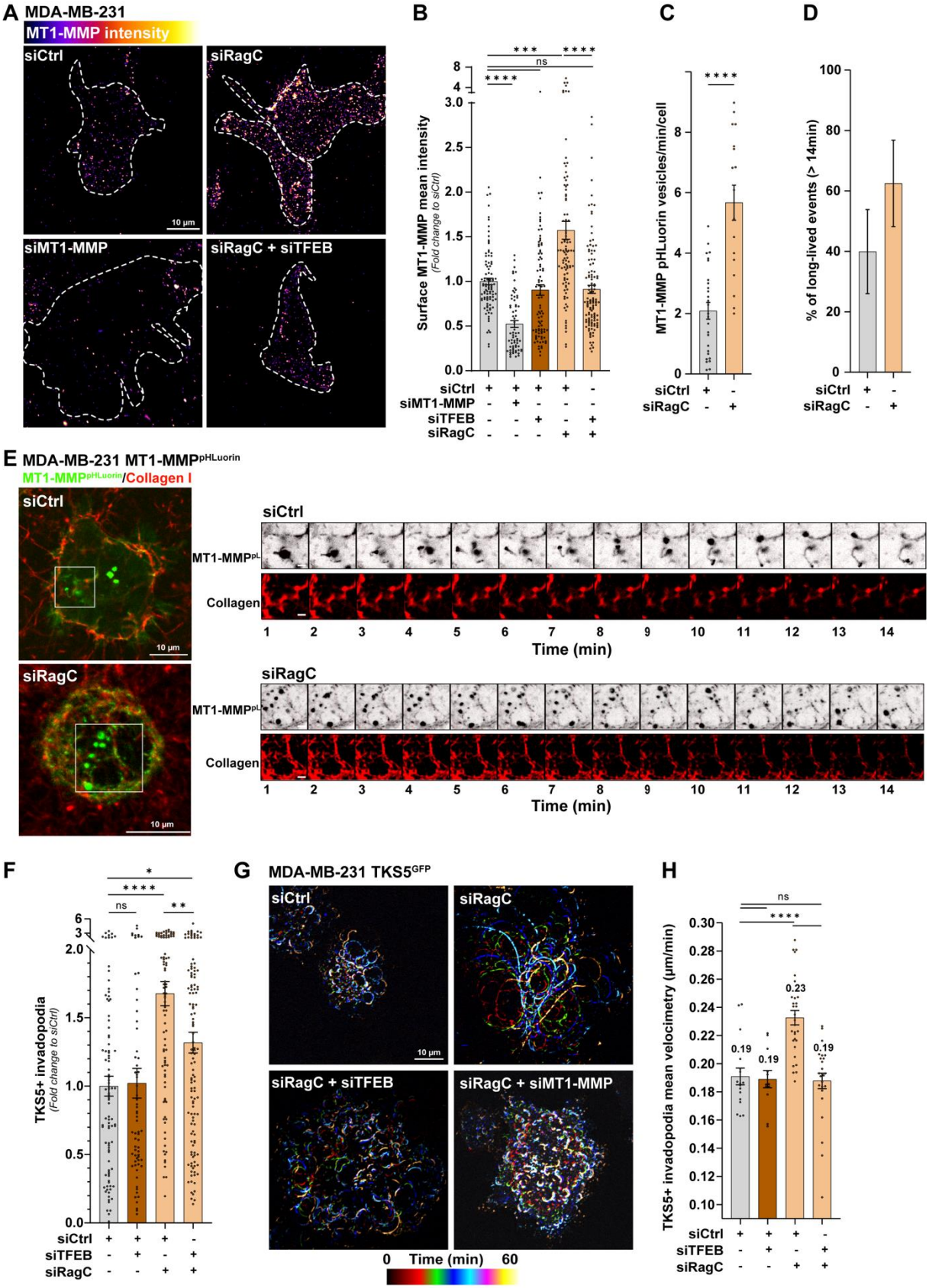
A MDA-MB-231
MT1-MMP intensity
siCtrl
siRagC
siMT1-MMP
siRagC + siTFEB
10 µm
B
Surface MT1-MMP mean intensity
(Fold change to siCtrl)
siCtrl
siMT1-MMP
siTFEB
siRagC
C
MT1-MMP pHLuorin vesicles/min/cell
D
% of long-lived events (> 14min)
E MDA-MB-231 MT1-MMPpHLuorin
MT1-MMPpHLuorin/Collagen I
MT1-MMPpL
Collagen
Time (min)
F
TKS5+ invadopodia
(Fold change to siCtrl)
G MDA-MB-231 TKS5GFP
siRagC + siTFEB
siRagC + siMT1-MMP
0 Time (min) 60
H
TKS5+ invadopodia mean velocimetry (µm/min)

Figure 3

Figure 3. Active TFEB promotes MT1-MMP exocytosis and invadopodia dynamics. Confocal images showing the surface staining of endogenous MT1-MMP (LUT Fire) in MDA-MB-231 cells treated with indicated siRNAs. (B) Quantification of the mean intensity of surface MT1-MMP per cell in MDA-MB-231 cells treated with indicated siRNAs. (C, D) Quantification of (C) the number of MT1-MMP^{pHLuorin} exocytic events per minute per cell and (D) the percentage of exocytic events stable for 14 min or more in MDA-MB-231 cells stably expressing MT1-MMP^{pHLuorin} and treated with control siRNA or siRagC. (E) Stills from representative time-lapse sequences of MDA-MB-231 MT1-MMP^{pHLuorin} treated with control siRNA or siRagC cultured on fluorescently-labeled type I collagen (red). The right panel shows a gallery of non-consecutive frames (1 image per min) from the time-lapse sequence (Movies S1 and S2) and shows the dynamics of the exocytosis of MT1-MMP^{pHLuorin} vesicles (inverted Gray LUT) on the collagen fibers (red). (F) Quantification of TKS5^{GFP}-positive invadopodia in MDA-MB-231 cells stably expressing TKS5^{GFP} treated with indicated siRNAs. (G) Color-coded time projections of seven images at 10-min intervals showing the dynamics of TKS5^{GFP}-positive invadopodia. (H) Mean velocimetry of TKS5^{GFP}-positive invadopodia in MDA-MB-231 cells stably expressing TKS5^{GFP} treated with indicated siRNA measured with PIVLab.

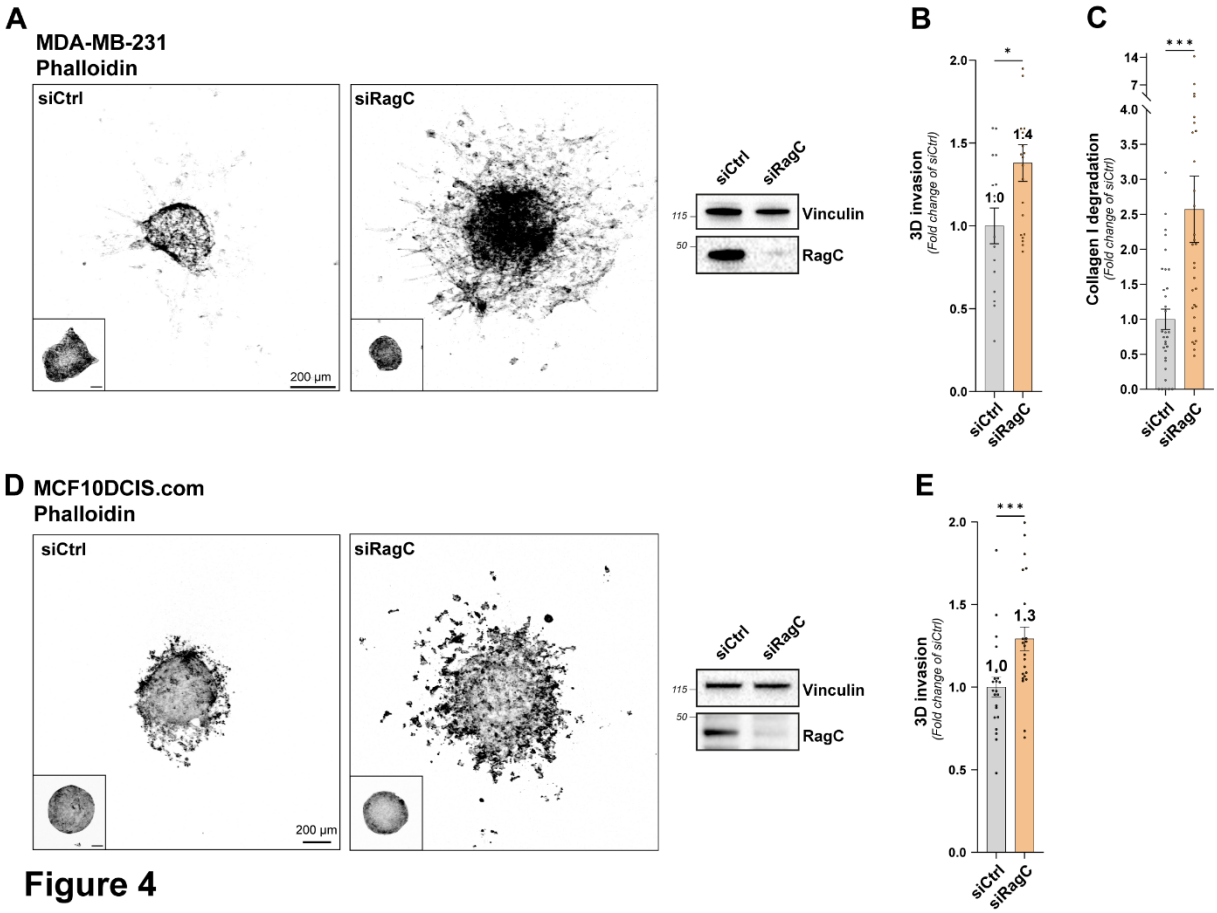
A
MDA-MB-231
Phalloidin
siCtrl
siRagC
200 µm
siCtrl
siRagC
115
50
Vinculin
RagC
B
3D invasion
(Fold change of siCtrl)
*
1.0
1.4
siCtrl
siRagC
C
Collagen I degradation
(Fold change of siCtrl)
***
siCtrl
siRagC
D
MCF10DCIS.com
Phalloidin
siCtrl
siRagC
200 µm
siCtrl
siRagC
115
50
Vinculin
RagC
E
3D invasion
(Fold change of siCtrl)
***
1.0
1.3
siCtrl
siRagC

Figure 4

Figure 4. mTORC1 repression promotes cell invasion. (A) MDA-MB-231 cells were treated with control or RagC siRNA and embedded as multicellular spheroids in 3D type I collagen. Spheroids were fixed and stained with Phalloidin and are shown in Gray inverted LUT. Insets show spheroids fixed after 45 min in type I collagen as controls. Immunoblots show depletion of RagC. (B, C) Quantification of (B) invasion and (C) collagen cleavage (see Methods). (D, E) MCF10DCIS.com were treated and embedded as spheroids as in (A) and 3D invasion was quantified.

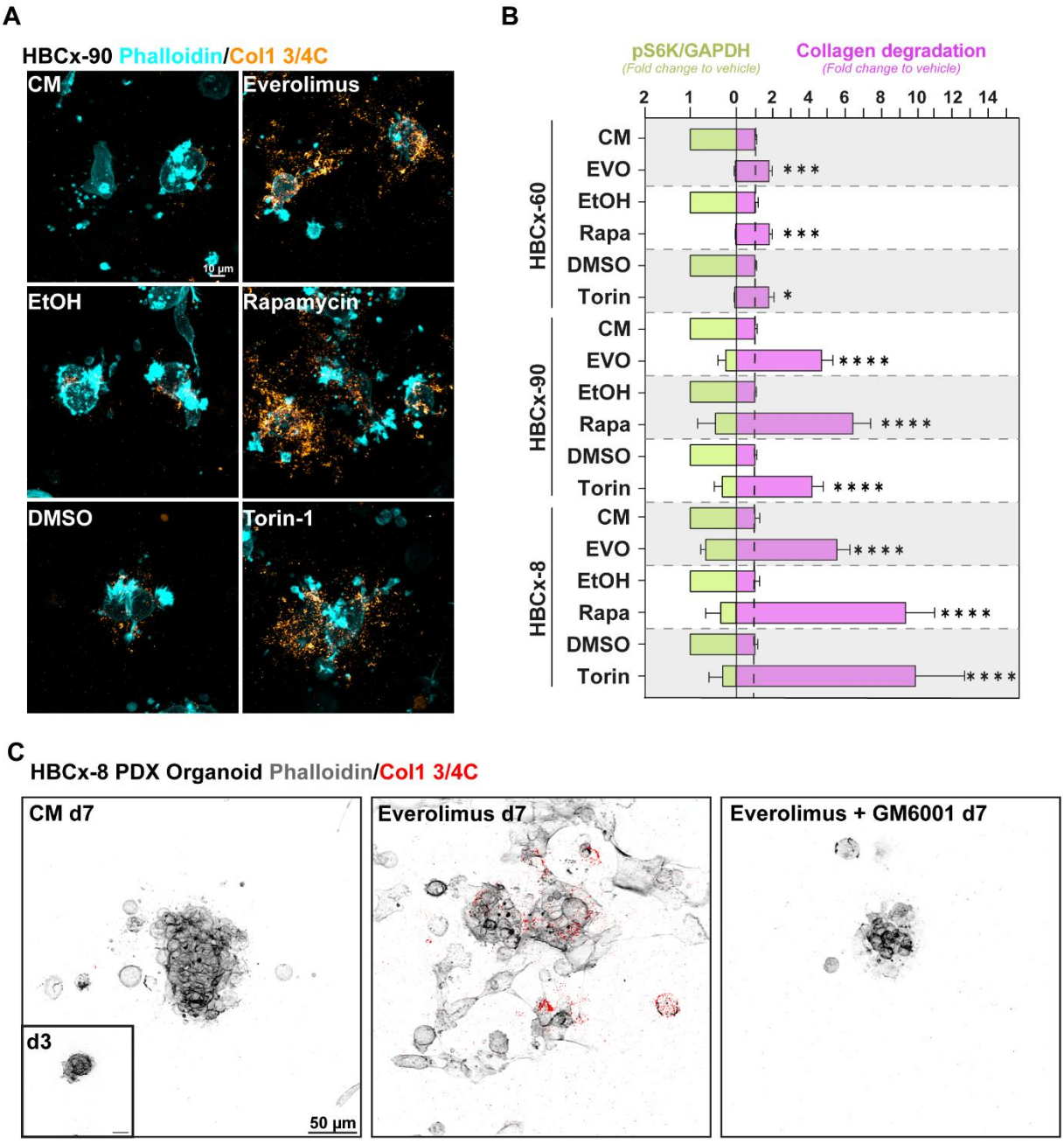
A
HBCx-90 Phalloidin/Col1 3/4C
CM
Everolimus
EtOH
Rapamycin
DMSO
Torin-1
10 µm
B
pS6K/GAPDH
(Fold change to vehicle)
Collagen degradation
(Fold change to vehicle)
2 1 0 2 4 6 8 10 12 14
HBCx-60
HBCx-90
HBCx-8
CM
EVO
EtOH
Rapa
DMSO
Torin
***
*
****
C
HBCx-8 PDX Organoid Phalloidin/Col1 3/4C
CM d7
d3
50 µm
Everolimus d7
Everolimus + GM6001 d7

Figure 5

Figure 5. mTORC1 inhibition unleashes a collagenolysis-dependent invasion program in TNBC PDX. (A) TNBC PDX cells were embedded in fibrillar type I 3D collagen and cultured with indicated mTORC1 inhibitory drugs or appropriate vehicles for 16 h and stained for F-actin (Phalloidin, cyan) and pericellular collagen cleavage (Col1-¾C, orange). Pictures are representative examples of PDX HBCx-90. (B) Quantification of collagen degradation (pink) and p-S6K in PDXs HBCx-60, HBCx-90 and HBCx-8 treated with indicated drugs or appropriate vehicles. Quantification is based on 3 independent experiments per condition and per PDX. (C) HBCx-8 PDXs were cultured as organoids (PDXOs) and embedded in 3D type I fibrillar collagen for 3 days in complete medium (d3, inset) before adding indicated drugs for 4 more days (d7). Samples were stained for F-actin (Phalloidin, gray inverted LUT) and collagen cleavage (Col1-¾C, red). PDXOs treated with Everolimus degrade and invade more compared to control PDXOs and PDXOs treated with a combination of Everolimus and GM6001.

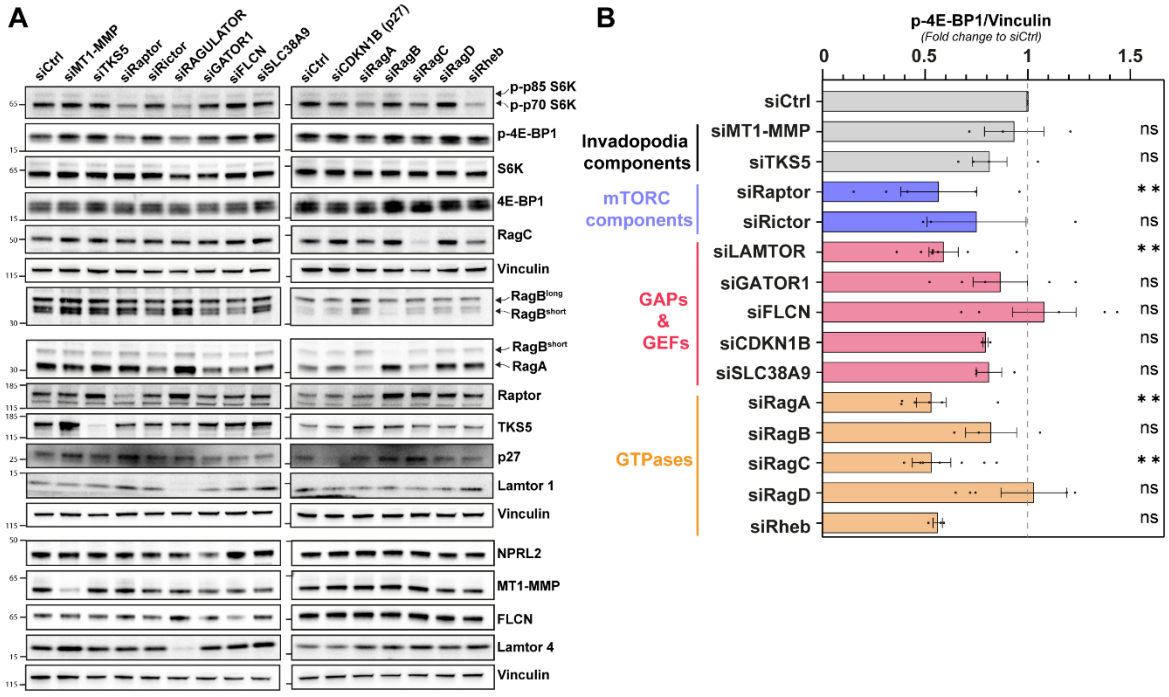

Extended Figure 1

Extended Figure 1. Regulation of mTORC1 signaling. (A, B) Immunoblots showing levels of p-S6K and p-4E-BP1 (quantified in (B)) as well as the depletion of the siRNA targets. Inactivation of the Ragulator complex was mediated by silencing subunits Lamtor1 and Lamtor4. Inactivation of the GATOR1 complex was mediated by silencing both DEPDC5 and NRPL2 subunits. (C) Immunoblots showing levels of p-S6K and p-4E-BP1 and the depletion of Raptor, RagC and TKS5 in MDA-MB-231 cells treated with indicated siRNAs.

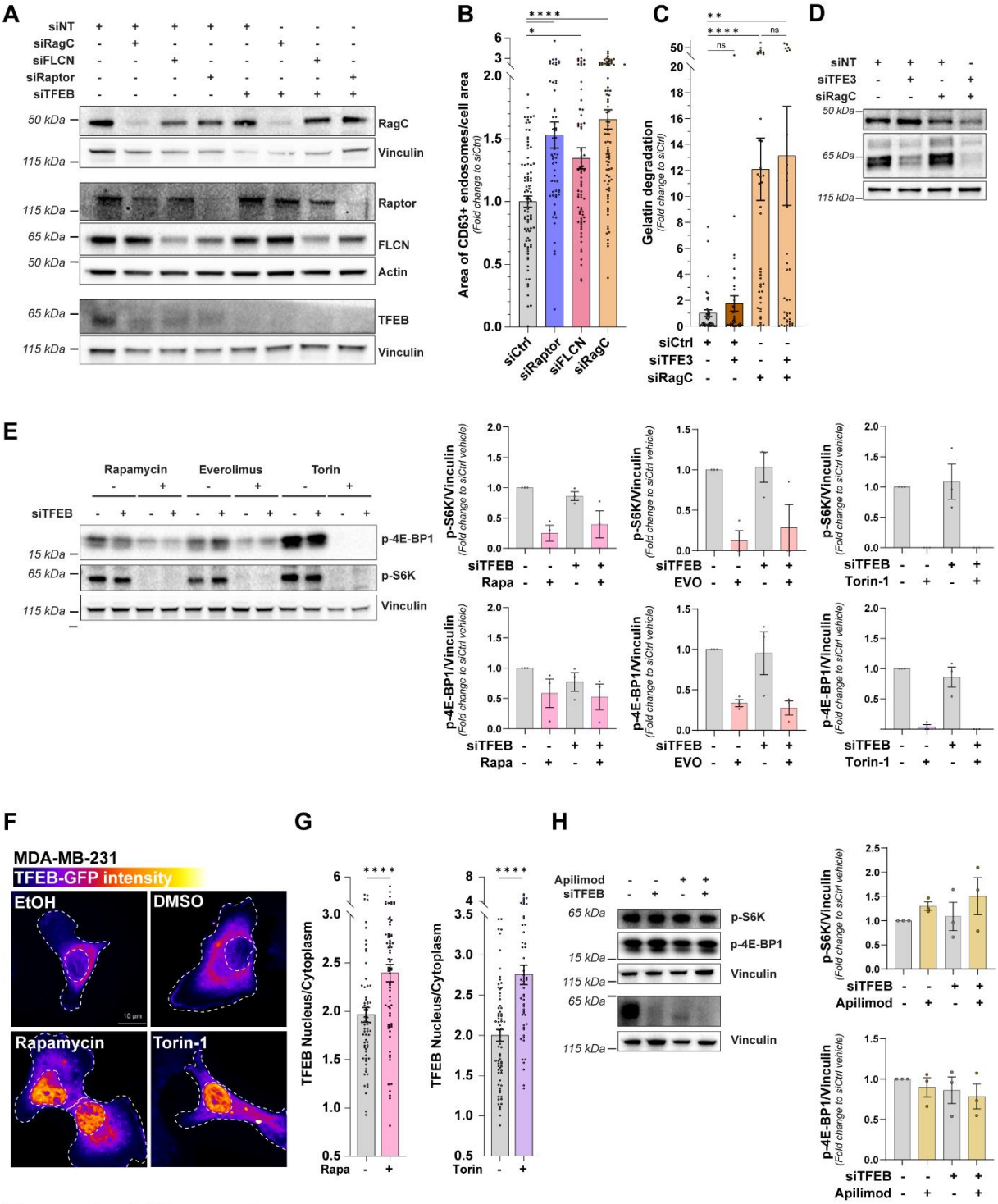

Extended Figure 2

Extended Figure 2. mTORC1 repression promotes TFEB activity. (A) Immunoblots showing the depletion of siRNA targets. (B) Quantification of CD63-positive vesicles in MDA-MB-231 cells treated with indicated siRNAs. (C) Gelatin degradation by MDA-MB-231 cells treated with indicated siRNAs. (D) Immunoblots showing the depletion of RagC and TFE3 in cells treated as in (C). (E) Immunoblots showing the levels of p-S6K and p-4E-BP1 (quantified in the graphs) in MDA-MB-231 cells treated with control or TFEB siRNA and cultured with indicated drugs or appropriate vehicles. (F, G) Confocal pictures and quantification showing the nuclear translocation of TFEB-GFP in MDA-MB-231 treated with Rapamycin or Torin-1. TFEB-GFP is shown as LUT Fire. (H) Luciferase assay, TBD (I) Immunoblot showing the levels of p-S6K and p-4E-BP1 (quantified in the graph) in MDA-MB-231 cells treated with control or TFEB siRNA and cultured with Apilimod or DMSO.

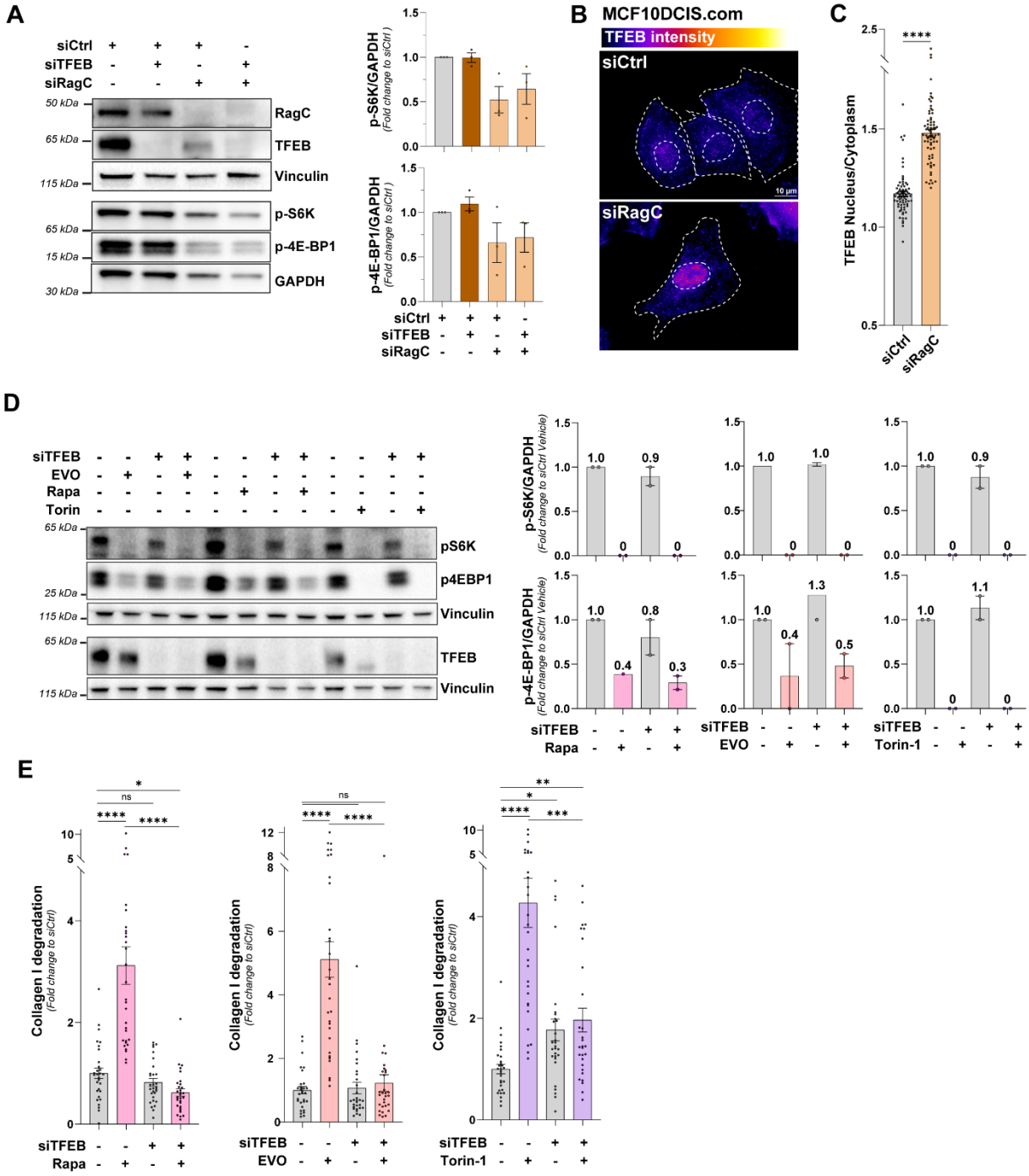

Extended Figure 3

Extended Figure 3. mTORC1 repression and TFEB activation promote ECM degradation in MCF10DCIS.com cells. (A) Immunoblots showing the depletion of RagC and TFEB and the levels of p-S6K and p-4E-BP1 (quantified in the graphs) in MCF10DCIS.com treated with indicated siRNAs. (B, C) Confocal pictures and quantification showing the nuclear translocation of TFEB-GFP in MCF10DCIS.com cells treated with control or RagC siRNA. TFEB-GFP is shown as LUT Fire. (D) Immunoblots showing the levels of p-S6K and p-4E-BP1 (quantified in the graphs) in MCF10DCIS.com cells treated with control or TFEB siRNA and cultured with indicated drugs or appropriate vehicles. (E) Quantification of collagen degradation by MCF10DCIS.com cells treated with control or TFEB siRNA and cultured with indicated drugs or appropriate vehicles.

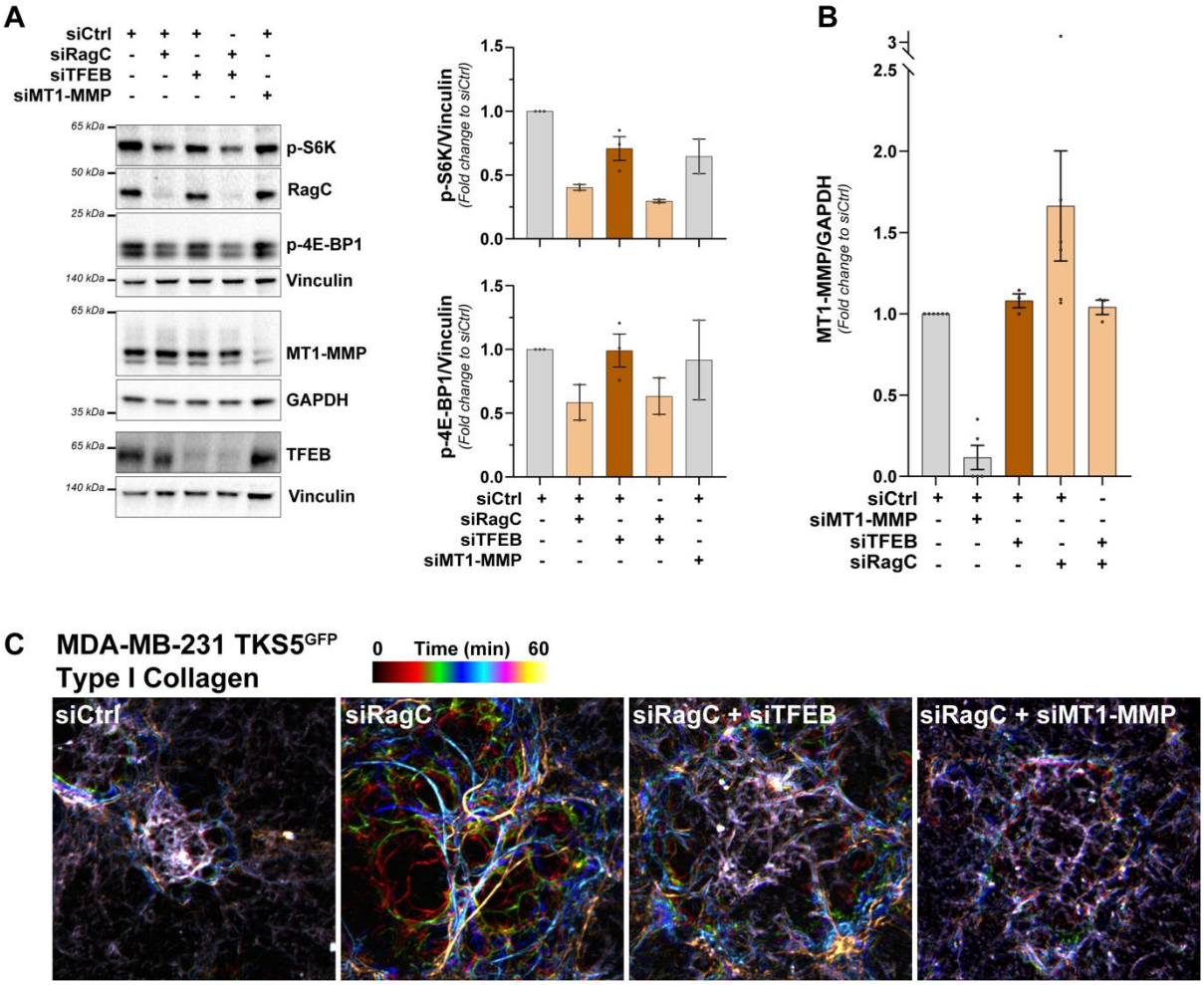
A
siCtrl + + + - +
siRagC - + - + -
siTFEB - - + + -
siMT1-MMP - - - - +
65 kDa
p-S6K
50 kDa
RagC
25 kDa
p-4E-BP1
140 kDa
Vinculin
65 kDa
MT1-MMP
GAPDH
35 kDa
65 kDa
TFEB
140 kDa
Vinculin
p-S6K/Vinculin
(Fold change to siCtrl)
1.5
1.0
0.5
0.0
p-4E-BP1/Vinculin
(Fold change to siCtrl)
1.5
1.0
0.5
0.0
siCtrl + + + - +
siRagC - + - + -
siTFEB - - + + -
siMT1-MMP - - - - +
B
MT1-MMP/GAPDH
(Fold change to siCtrl)
3
2.5
2.0
1.5
1.0
0.5
0.0
siCtrl + + + + -
siMT1-MMP - + - - -
siTFEB - - + - +
siRagC - - - + +
C
MDA-MB-231 TKS5GFP
Type I Collagen
0 Time (min) 60
siCtrl
siRagC
siRagC + siTFEB
siRagC + siMT1-MMP

Extended Figure 4. TFEB activation promotes invadopodia dynamics. (A, B) Representative immunoblots showing the levels of p-S6K and p-4E-BP1 (quantified in the graph) and of siRNA targets in MDA-MB-231 cells treated with indicated siRNAs. MT1-MMP expression normalized to GAPDH is quantified in (B). (C). Color-coded time projections of seven images at 10-min intervals showing the rearrangement of fluorescently labeled fibrillar type I collagen by MDA-MB-231 cells treated with indicated siRNAs.

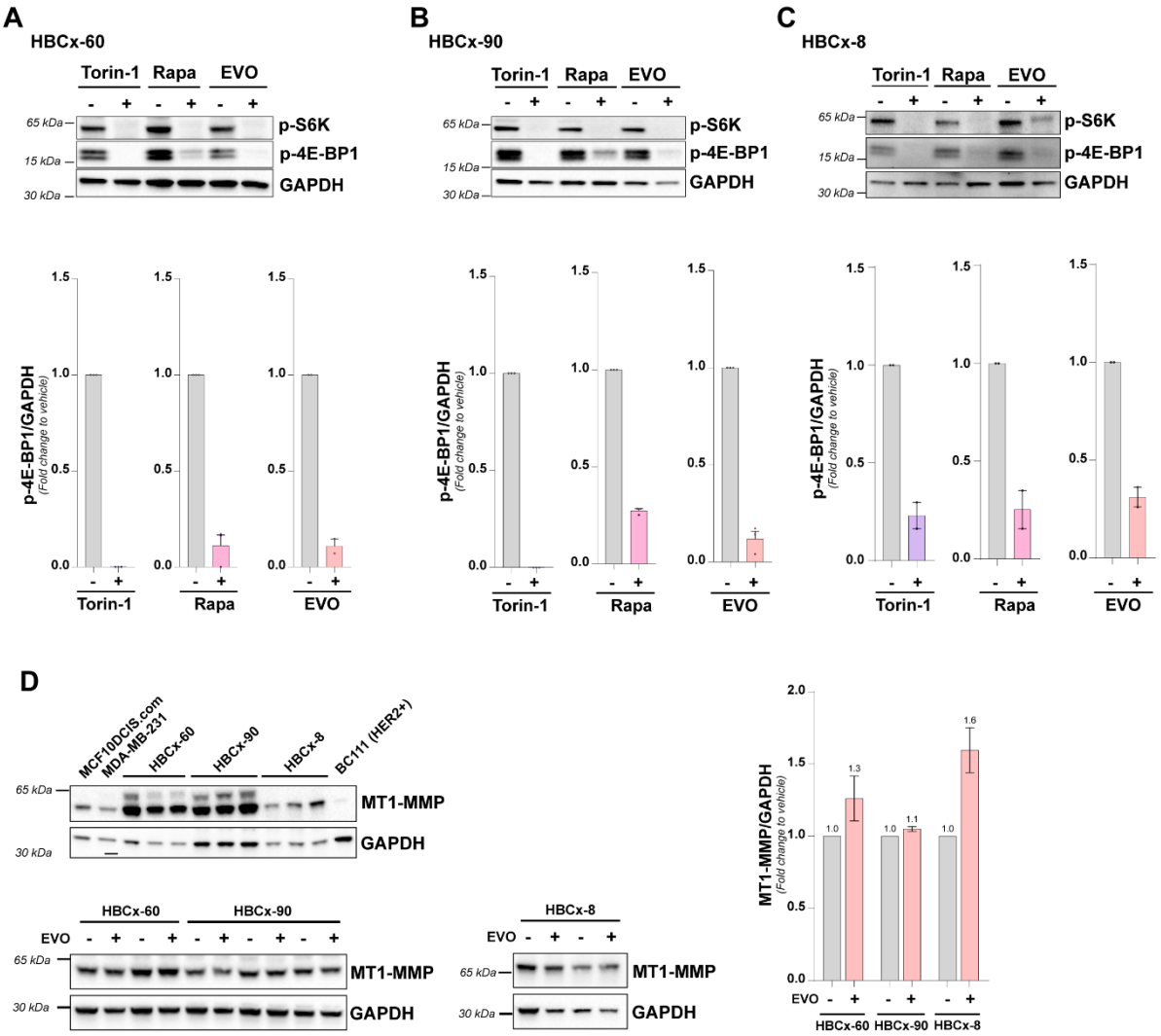

Extended Figure 5

Extended Figure 5. Pharmacological treatment of TNBC PDX with mTORC1 drugs. (A-C) Representative immunoblots showing the levels of p-S6K and p-4E-BP1 (quantified in graphs) in indicated TNBC PDX treated with indicated drugs. (D) Representative immunoblots and associated quantifications of MT1-MMP in PDXs treated with Everolimus or control, with GAPDH as a loading control. MT1-MMP in MDA-MB-231 and MCF10DCIS.com cell lines were used as a reference. The BC111 is a HER2+ breast PDX as a negative control.

Table S1: siRNA used in this study

siRNA	Reference	Targeted sequence
Non-targeting	D-001810-01	UGGUUUACAUGUCGUACUAA
ATG5	L-004374-00-0005	
CDKN1B	L-003472-00-0005	
DEPDC5	L-020708-00-0005	GGGGAUAUGUGGCGACUAA GAUCUGUGCGAGAGCGAGA UGUCUAUGUUAAUGUCGUA CAUGGGAGAGCAACCGUUA
FLCN	L-009998-02-0005	AAGAGACCUCCAUUAAAU CGGGAAUAUAUCAGCCAUGA ACACAGCCUUCACGCCAUU GAGGAUCCUUGGUCCAGA
LAMTOR 1	L-020916-02-0005	GUUUGUCACCCUCGAUAAA AAGUGAGGGUAGAACCUUU GGCUUAUACAGUACCCUAA UCUCCAGGAUAGCUGCUUA
LAMTOR 4	L-028918-02-0005	AGGCACACCUGUCGGUCUU UGUUUGUGGUGAAGAGGCA CAGCACAGCCUGCGGUUUC GUGCAGUGCUGGCGUCAUC
MCOLN1	L-006281-00-0005	GACCUUCGCCGUCGUCUCA UGAUCACGUUUGACAACAA CAACGACACAUUUGACAUU GAUCUCACCCUCUUGGAAA
MT1-MMP	L-004145-00-0005	GGAUGGACACGGAGAAUUU GAUCAAGGCCAAUGUUCGA GGUCUCAAAUGGCAACAUA GGAAACAAGUACUACCGUU
NPRL2	L-015645-00-0005	GCAAGACAGGCAUGAGCUA GACCCAAGAUCACCUAUCA GUACUACGGCGUUGUGACA GCAUCGAACACAAGAAGUA
RCTOR	L-016984-00-0005	
RHEB	L-009692-00-0005	

RPTOR	L-004107-00-0005	
RRAGA	L-016070-00-0005	
RRAGB	L-012189-01-0005	GAAGAAGAUUUGAGGCGUU GGGACAACAUCUUCCGAAA AGUGUAAAGAGCAGCGUGA CUGAGAAAACGACGGAGAA
RRAGC	L-017822-01-0005	GGUCGGAUGCCACGUGCUA GCAAUUAUCAAGCUGAAUA GGAUUCUGCUCAUGGGACU UCUAAAGCCUACAAAGUUA
RRAGD	L-016120-00-0005	
SLC38A9	L-007337-02-0005	
TFE3	L-009363-00-0005	
TFEB	L-009798-00-0005	GCAGAUGCCCAACACGCUA UGAAAGGAGACGAAGGUUC GCAGCCACCUGAAUGUGUA CAACAGUGCUGGGAAUAGC
TKS5	L-006657-00-0005	ACAAUAACCUCAAAGAUGU GGAUAAGUUUCCCAUUGAA CGACGGAACUCCUCCUUUA GGACGUAGCUGUGAAGAGA
VPS35	L-010894-00-0005	GAACAUAUUGCUACCAGUA GAAAAGAGCAUGAGUUGUUA GUUGUAAAACUGUAGGGAUG GAACAAAUUUGGUGCGCCU

Table S2: Antibodies used in this study

Antigen	Reference	Species	IF	WB (d, MW)
a-tubulin	*Sigma T-9026*	*Mouse (monoclonal)*	*X*	*1/10 000 55 kDa*
Actin	*Sigma A1978*	*Mouse (monoclonal)*	*X*	*1/10 000 42 kDa*
AKT	*Cell Signaling 9272*	*Rabbit (polyclonal)*	*X*	*1/1000 65 kDa*
ATG5	Novus Biologicals NB110-53818	Rabbit (polyclonal)	X	1/500 56 kDa
CD63 (LAMP3)	BD Pharmingen 556019	Mouse (monoclonal)	1/200	X
Collagen cleavage site	Immunoglobe 0217-050	Rabbit (polyclonal)	1/100 - 500	X
Cortactin	Merck 05-180-I	Mouse (monoclonal)	1-200	
EEA1	*BD Transd. Lab. 610457*	*Mouse (monoclonal)*	*1/200*	
FLCN	Cell Signaling 3697S	Rabbit (monoclonal)	X	1/1000 70 kDa
GAPDH	Santa Cruz 25788	Rabbit (polyclonal)	X	1/10 000 37 kDa
GFP	Abcam ab13970	Chicken (polyclonal)	1/500	X
GFP	Abcam ab6556	Rabbit (polyclonal)	X	1/500
LAMP1	*BD Pharmingen 555798*	*Mouse (monoclonal)*	*1/100*	
LAMTOR 1	Cell Signaling 8975	Rabbit (monoclonal)	1/100	1/1000 18 kDa
LAMTOR 4	Cell signaling 13140S	Rabbit (monoclonal)	1/250	1/10000 11 kDa
LC3	MBL M152-3	Mouse (monoclonal)	1/1000	X

MT1-MMP	Merk MAB3328	Mouse (monoclonal)	1/200	1/1000 66 kda
MT1-MMP (clone 2D7)	Homemade	Mouse (monoclonal)	1/100	X
mTOR	Cell Signaling 2983S	Rabbit (monoclonal)	1/400	X
NPRL2	Cell Signaling 37344	Rabbit (monoclonal)	X	1/1000 40 kDa
p27 Kip1/CDKN1B	Santa Cruz 1641	Mouse (monoclonal)	X	1/1000 20 kDa
p-4E-BP1	Cell Signaling 13443	Rabbit (monoclonal)		1/1000 20 kDa
p-AKT	Cell Signaling 4060S	Rabbit (monoclonal)	X	1/1000 65 kDa
p-p70 S6 kinase	Cell Signaling 9205	Rabbit (polyclonal)	X	1/1000 65 kDa
p70 S6 kinase	Cell Signaling 2708	Rabbit (monoclonal)	X	1/1000 65 kDa
Rab7	*Cell Signaling 9367*	*Rabbit (monoclonal)*	*1/100*	*1/1000 23 kDa*
RagA	Cell Signaling 4357	Rabbit (monoclonal)	1/100	1/1000 30 kDa
RagB	Cell Signaling 8150	Rabbit (monoclonal)		1/1000 40 kDa
RagC	Cell Signaling 9480S	Rabbit (monoclonal)	1/100	1/1000 50 kDa
Raptor	Santa Cruz 81537	Mouse (monoclonal)	X	1/100 130 kDa
TFE3	Cell Signaling	Rabbit (polyclonal)	Doesn't work	1/1000 60 kDa
TFEB	Cell Signaling 4240S	Rabbit (polyclonal)	Doesn't work	1/1000 65 kDa MILK
TKS5	Cell Signaling 16619	Rabbit (polyclonal)	1/100	1/200
Tubulin	Sigma T-9026	Mouse (monoclonal)	X	1/10 000 55 kDa

Vinculin	Merck MAB374-C	Mouse (monoclonal)	X	1/2000 130 kDa
Vps35 (clone B5)	Santa Cruz sc-374372	Mouse (monoclonal)	X	1/500 90 kDa
Secondary antibody	**Reference**	**IF**	**WB**	
Anti-Rabbit HRP	Sigma A0545	X	1/10 000	
Anti-Mouse HRP	Jackson IR 115-035-062	X	1/20 000	
Anti-Chicken AF488	Molecular Probes A11039	1/300	X	
Anti-Mouse AF488	Molecular Probes A21202	1/500	X	
Anti-Mouse Cy3	Jackson IR 715-165-151	1/500	X	
Anti-Mouse AF647	Invitrogen A31571	1/200	X	
Phalloidin AF488	Molecular Probes A12379	1/400	X	
Phalloidin AF546	Molecular Probes A22283	1/200	X	
Phalloidin AF633	Molecular Probes A22284	1/200	X	
Anti-Rabbit AF488	Molecular Probes A21206	1/200	X	
Anti-Rabbit Cy3	Jackson IR 711-165-152	1/800	X	

Table S3: Drugs used in this study

Reagent	Company	Reference	Vehicle	Working dilution
Apilimod	Euromedex	S6414	DMSO	1 µM
Everolimus	Novartis		Ultrapure water	100 nM
GM6001	Merck Millipore	CC1100	Ethanol	40 µM
Rapamycin	Tocris Biotechne	1292	Ethanol	20 nM
Torin-1	Tocris Biotechne	4247	DMSO	350 nM

Supplementary Movie 1. MT1-MMP^{pHLuorin} exocytosis at invadopodia in control cells. MDA-MB-231 expressing MT1-MMP^{pHLuorin} (green) and transfected with non-targeting siRNA for 72 hrs were seeded on a thin layer of fibrillar type I collagen (red) and analyzed by confocal spinning-disk microscopy. Inset shows higher magnification of boxed region for MT1-MMP^{pHLuorin} signal (represented in inverted Gray LUT). Images were taken every 20 sec for 15 minutes (time is in min:sec). Representative movie from three independent experiments.

Supplementary Movie 2. MT1-MMP^{pHLuorin} exocytosis at invadopodia in cells KD for RagC. MDA-MB-231 expressing MT1-MMP^{pHLuorin} (green) and transfected with RagC siRNA for 72 hrs were seeded on a thin layer of fibrillar type I collagen (red) and analyzed by confocal spinning-disk microscopy. Inset shows higher magnification of boxed region for MT1-MMP^{pHLuorin} signal (represented in inverted Gray LUT). Images were taken every 20 sec for 15 minutes (time is in min:sec). Representative movie from three independent experiments.

Supplementary Movie 3. PIV analysis of TKS5^{GFP}-invadopodia in control cells. MDA-MB-231 expressing TKS5^{GFP} (green) and transfected with non-targeting siRNA for 72 hrs were seeded on a thin layer of fibrillar type I collagen (red) and analyzed by confocal spinning-disk microscopy. The right panel shows TKS5^{GFP} (Gray LUT) analyzed by PIV. Velocimetry vectors are displayed. Orange vectors are interpolated vectors. Images were taken every min for 60 minutes (time is in min). Representative movie from three independent experiments.

Supplementary Movie 4. PIV analysis of TKS5^{GFP}-invadopodia in control cells. MDA-MB-231 expressing TKS5^{GFP} (green) and transfected with RagC siRNA for 72 hrs were seeded on a thin layer of fibrillar type I collagen (red) and analyzed by confocal spinning-disk microscopy. The right panel shows TKS5^{GFP} (Gray LUT) analyzed by PIV. Velocimetry vectors are displayed. Orange vectors are interpolated vectors. Images were taken every min for 60 minutes (time is in min). Representative movie from three independent experiments.

CONCLUSIONS AND DISCUSSION

1. Starved cancer cells engage an MT1-MMP-based matrix proteolysis program

Malignant cells require access to oxygen and nutrient to thrive and thus tumor progression is often accompanied by the formation of blood vessels through various molecular and cellular processes (Lugano et al., 2020). Tumoral vessels are very different from normal blood vessels and are characterized by endothelial gaps causing fluid leakage and interstitial pressure buildup, thin walls and an inconsistent basement membrane that makes vessels susceptible to collapse and a sluggish, inconstant blood flow which fails to deliver nutrients and oxygen optimally to tumor cells (Chaplin et al., 1987; Hashizume et al., 2000; Hida & Maishi, 2018). In certain solid tumors such as breast and pancreatic cancers, cells can adapt to nutrient depletion by internalizing extracellular seric proteins and ECM fragments as alternative sources of AA (Commisso et al., 2013; Gouirand et al., 2018, 2022; Kamphorst et al., 2015; Nazemi & Rainero, 2020; Nofal et al., 2017; Olivares et al., 2017; Pickup et al., 2014; Recouvreux et al., 2020). However, the mechanism underlying ECM breakdown under nutrient-depleted conditions was unknown and we hypothesized that the invadopodia TKS5/MT1-MMP axis could be involved in the production of ECM fragments under conditions of nutrient scarcity. Our results reveal that amino acid and growth factors starvation induced a potent ECM degradation response in breast cancer cells that was dependent on MT1-MMP and TKS5 expression. At the molecular and cellular levels, we showed that MT1-MMP was clustered in arrested CCPs at the plasma membrane of starved cells with TKS5 closely and stably associated with endocytosis-incompetent CCPs. (Colombero et al., 2021). The geometry of actin in clathrin-mediated endocytosis (CME) was recently studied using 3D super-resolution microscopy, revealing an asymmetry in N-WASP and Arp2/3 complex recruitment and in actin polymerization on one side of the CCP (Jin et al., 2021). Similarly, our immunofluorescence and TIRF microscopy experiments revealed a close and long-lasting association of TKS5 with arrested CCPs (Colombero et al., 2021). Further exploration will be necessary to unravel a potential function for TKS5 in arrested and possibly normal CCPs but these results could potentially implicate TKS5 in a novel role outside of classical invadopodia as a stabilizer of CCPs (**Figure 28**).

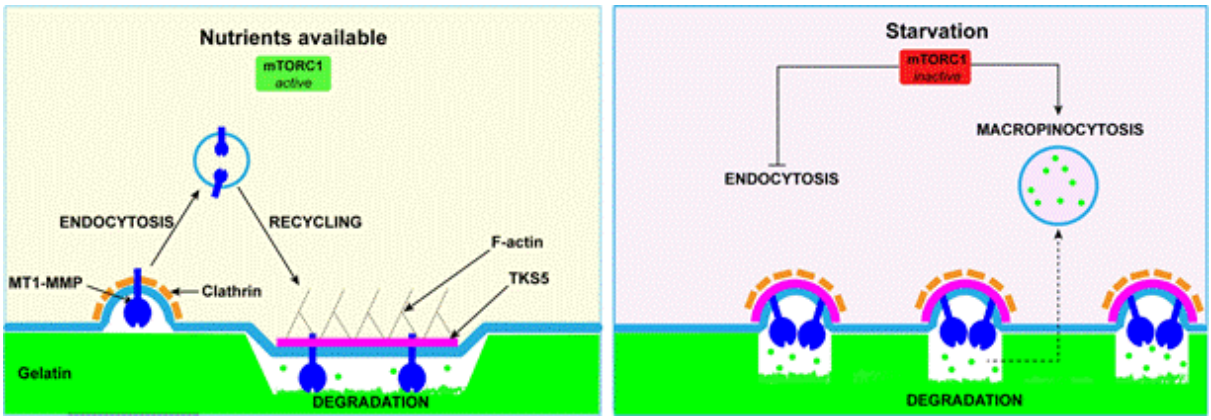

Figure 28: Schematic model of the promotion of an MT1-MMP/TKS5-based ECM degradation machinery in starved cancer cells. *In nutrient replete conditions, contact with the ECM promote TKS5-positive invadopodia formation wherein MT1-MMP is enriched from endolysosomal recycling. The invadopodia degrades the ECM. Starvation impedes the internalization of MT1-MMP from the plasma membrane by repressing clathrin-mediated endocytosis, leading to increased ECM degradation. The proteolytic fragments are internalized to fuel metabolism. In this model, TKS5 is associated with, and stabilizes the clathrin pits* (Colombero et al., 2021).

Our data revealed that reactivation of mTORC1 signaling in starved cells by supplementing the EBSS buffer with free AA or by silencing the TSC complex partially inhibited ECM degradation, which suggests that mTORC1 may modulate the dynamics of CME (Colombero et al., 2021). Similar to our observations, early studies in Drosophila *melanogaster* showed that inhibition of TORC1 signaling (by S6K knock-out, inactivation of the V-ATPase/TORC1 pathway, or overexpression of dominant negative Tor) reduced endocytosis (Gleixner et al., 2014; Hennig et al., 2006). Furthermore, analysis of the functions of human kinases in CME in HeLa cells also revealed that the silencing of FRAP1 (mTOR) and other components of the TOR signaling pathway blocked endocytosis of VSV virus, which is specifically internalized by CME (Pelkmans et al., 2005). In our study, starvation was achieved by cultivating our cells in EBSS buffer, which is commonly used to starve cells and study mTOR signaling, but the lack of AA and growth factors are harsh conditions that potentially impact many signaling pathways. As such, we noticed a significant (not total) inhibition of AKT phosphorylation after 1 h of starvation in EBSS, consistent with a decrease of mTORC2 activity. Using p-AKT inhibitor, MK2206, or RICTOR silencing, we observed a complete inhibition of p-AKT both in fed and starved cells. Although these conditions had no effect on ECM degradation by cells cultured in a complete medium, they partially repressed degradation induced by starvation (personal data not shown). These results suggest that while starvation-induced ECM degradation is dependent on mTORC1, it might also be regulated to some extent by mTORC2 (and growth factors) signaling. Interestingly, in Drosophila proximal tubular cells, depletion of Raptor

(mTORC1) alone or Raptor and Rictor (mTORC2) (but not Rictor alone) repressed receptor-mediated endocytosis of lactoglobulin (Grahammer et al., 2017). Although mechanistic insights are missing, these data are in line with our results showing that starvation and repression of both mTORC1 and mTORC2 repress CME and sequestrate MT1-MMP in arrested CCPs (Colombero et al., 2021). It would be interesting to further explore which of these pathways may be altered in starved cells and could contribute to the regulation of invadopodia activity.

Although collagen cleavage was increased by one order of magnitude by starved cancer cells, we have not studied if and how collagen could be internalized. The scavenging strategies of cancer cells are diverse and numerous internalization pathways of collagen have been described, mostly by binding to cellular receptors. Collagen has many known transmembrane cellular receptors such as integrins (α1β1, α2β1, α10β1, …), discoidin domain receptors (DDR), the urokinase plasminogen activator receptor-associated protein (uPARAP, also known as Endo180), and others (Elango et al., 2022). CME of uPARAP/Endo180 receptor bound to its collagen ligand is one of the most described endocytosis routes involved in physiological collagen turnover (Curino et al., 2005b). However, as CME is seemingly inhibited by starvation (Colombero et al., 2021), it is unlikely that collagen would be internalized through CME in starved cells. Furthermore, recent transmission electron microscopy studies revealed that fibroblasts of mice deficient for uPARAP/Endo180 could still uptake collagen *via* phagocytosis, which would suggest that this receptor does not play a (major) role in the uptake of collagen *in vivo* and that other alternative uptake routes of collagen might be at play (Sprangers et al., 2017). Phagocytosis of collagen may therefore be a potential candidate pathway for the uptake of collagen by starved breast cancer cells. Earlier work also revealed that MT1-MMP activity was required for collagen fragmentation prior to phagocytosis (H. Lee et al., 2007). α2β1 and α1β2 integrins have been implicated in collagen phagocytosis by fibroblasts during matrix turnover (Abraham et al., 2007; W. Lee et al., 1996; W. Lee & McCulloch, 1997; Moreno-Layseca et al., 2019; Staudinger et al., 2013), and integrin-mediated collagen phagocytosis may represent an exploitable pathway to uptake collagen fragments in starved cells. However, these studies were focused on phagocytosis by fibroblasts and macrophages and fairly little is known about phagocytosis by breast cancer cells or the role of starvation and mTOR signaling in phagocytosis. Although relatively less studied, integrins can also be internalized by caveolin-dependent endocytosis (Bass et al., 2011; F. Shi & Sottile, 2008), and interestingly, recent results in our lab show that integrin β1-bound collagen was found in lysosomes decorated with caveolin-1 in MDA-MB-231 and that his internalization required the cleavage of the collagen fiber (work of Pedro Monteiro). Furthermore, it was recently shown that treating MDA-MB-231 cells with the lipid raft-mediated endocytosis inhibitor Filipin repressed collagen internalization in AA-starved MDA-MB-231 cells (Nazemi et

al., 2021). As CME is impeded by starvation (Colombero et al., 2021), it is tempting to hypothesize that nutrient-depleted MDA-MB-231 cells could internalize collagen-bound integrins by caveolae-dependent endocytosis. Further experimental work is required to explore this hypothesis.

Nutrient depletion and mTORC1 repression in Ras-transformed cells induce internalization of extracellular proteins *via* macropinocytosis, a non-selective form of endocytosis through which cells assimilate both extracellular fluid and macromolecules by generating large, uncoated endocytic vesicles (macropinosomes) that range in diameter from 0.2 to 5.0 µm (Commisso et al., 2013; Davidson et al., 2017; Finicle et al., 2018; Kamphorst et al., 2015). Therefore, macropinocytosis is also an attractive putative pathway for collagen internalization by nutrient-challenged breast cancer cells. In that line, it was shown that collagen was scavenged by macropinocytosis in glucose-starved PDAC as starved cells treated with the macropinocytosis inhibitor EIPA could no longer internalize collagen (Olivares et al., 2017). Macropinocytosis is a process stimulated by growth factors which activate the Ras/PI3K/Rac1 pathway (Recouvreux & Commisso, 2017). In our experimental conditions, cells were deprived of growth factors. Activating mutations in Ras could circumvent the requirement for growth factors and constitutively activate macropinocytosis for ECM scavenging (Commisso et al., 2013).

Several studies have shown that internalized fragments of ECM are used as an alternative source of AAs to fuel cell metabolism and promote tumor survival and growth (Gouirand et al., 2022; Muranen et al., 2017; Olivares et al., 2017). The mechanisms underlying ECM degradation prior to internalization had not been studied yet. Although we showed that starvation increased collagen degradation by one order of magnitude, it remains unknown if this dramatic response generates ECM fragments that are small enough to be internalized, and if it could impact cell survival and metabolism. A recent study showed that Matrigel and collagen I matrices could be internalized by MDA-MB-231 cells, which were starved of AAs for three days (Nazemi et al., 2021). Collagen I is made mostly of three non-essential amino acids (proline, hydroxyproline, and glycine) but surprisingly, these authors reported that uptake of collagen I correlated with the enrichment of tyrosine and phenylalanine metabolism, two amino acids that can be transformed into fumarate and fuel the tricarboxylic acid cycle to promote cell proliferation (**Figure 29**). The metabolomic analysis performed by Nazemi and colleagues also revealed enrichment of proline and hydroxyproline in starved cells plated on collagen or Matrigel as compared to cells grown on plastic. Interestingly, in pancreatic ductal adenocarcinoma cells, proline derived from internalized collagen has been shown to promote cell survival in glucose- or glutamine-starved conditions (Olivares et al., 2017). Proline is a potent modulator of carcinogenesis and is converted to Glutamate by two

key enzymes, PRODH, which converts Proline to P5C, and P5CDH which reduces P5C to Glutamate. PRODH is upregulated upon inhibition of mTORC1 and nutrient stress (Pandhare et al., 2009). Moreover, elevated proline metabolism *via* PRODH activity has been shown to promote the formation of breast metastasis *in vivo* (Elia et al., 2017). Taken together, these data suggest a mechanism whereby AA starvation of carcinoma cells could unleash an MT1-MMP-based proteolysis response which would feed the cells with collagen fragments. These fragments would in turn be internalized (by an undefined route, see above) and used as an exogenous source of proline, a carcinogenic substrate that could promote cell survival, growth, and potentially invasion (**Figure 29**).

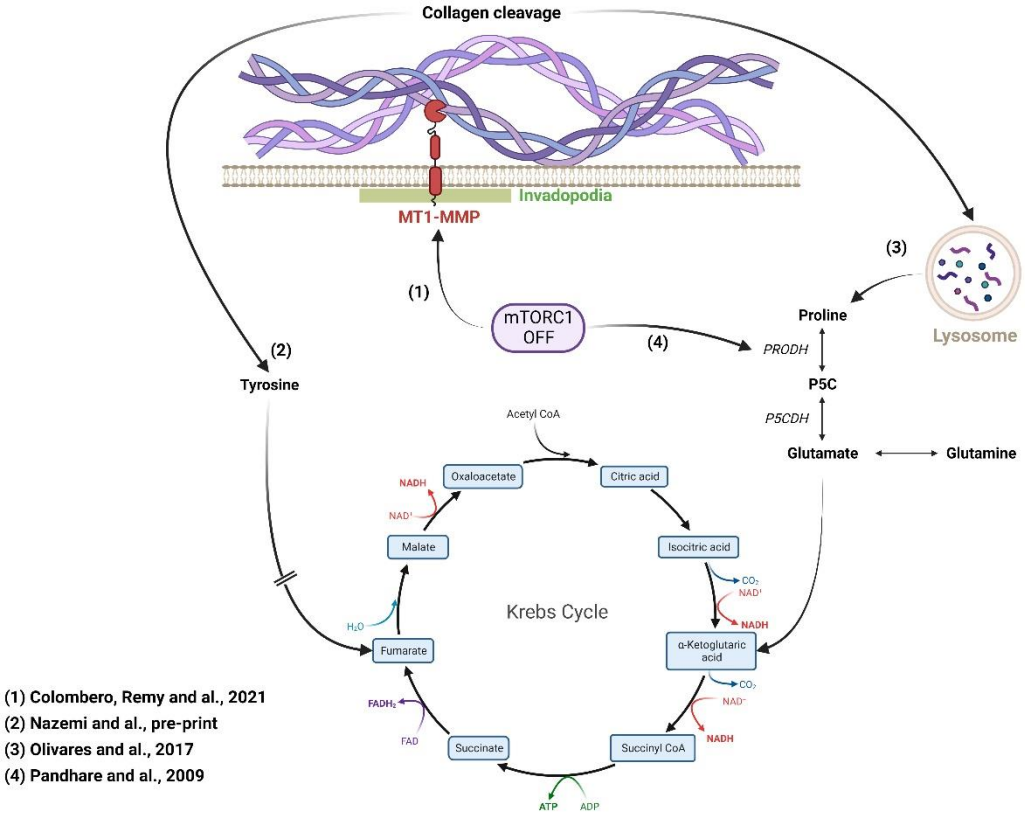

<u>Figure 29:</u> Scheme showing the potential role of the invadopodia in fueling starved cells with amino acids (Proline, Tyrosine, Phenylalanine) which can be transformed into TCA cycle intermediates and provide energy to the cell. In this model, starvation and mTORC1 repression would promote invadopodia-mediated collagen cleavage and catabolism of Proline, a carcinogenic substrate.

2. <u>The mTORC1/TFEB axis is a novel regulator of invadopodia.</u>

In order to minimize the contribution of mTORC2 and growth factors signaling, and in an effort to characterize the role of mTORC1 in the ECM degradation program of breast cancer cells, we used a siRNA-based approach to KD several key regulatory components of the

mTORC1 signaling pathway and assess their effect on matrix degradation in replete-nutrient conditions. We found a strong correlation between the repression of mTORC1 activity based on the phosphorylation of the classical S6K and 4E-BP1 substrates used as proxies, and induction of matrix degradation, in two different breast cancer cell lines and several triple-negative PDX models. Degradation was mediated by classical key invadopodia components, MT1-MMP and TKS5, and required the activation of transcription factor EB (TFEB). PIV analysis, used here for the first time to study the dynamics of linear invadopodia, revealed that TFEB activation stimulates the radial expansion and velocimetry of invadopodia, a process that was known to require MT1-MMP activity (Ferrari et al., 2019). Finally, we showed that mTORC1 repression in breast cancer spheroids or PDX organoids promoted a collagenolytic-dependent invasion program (**Figure 30**).

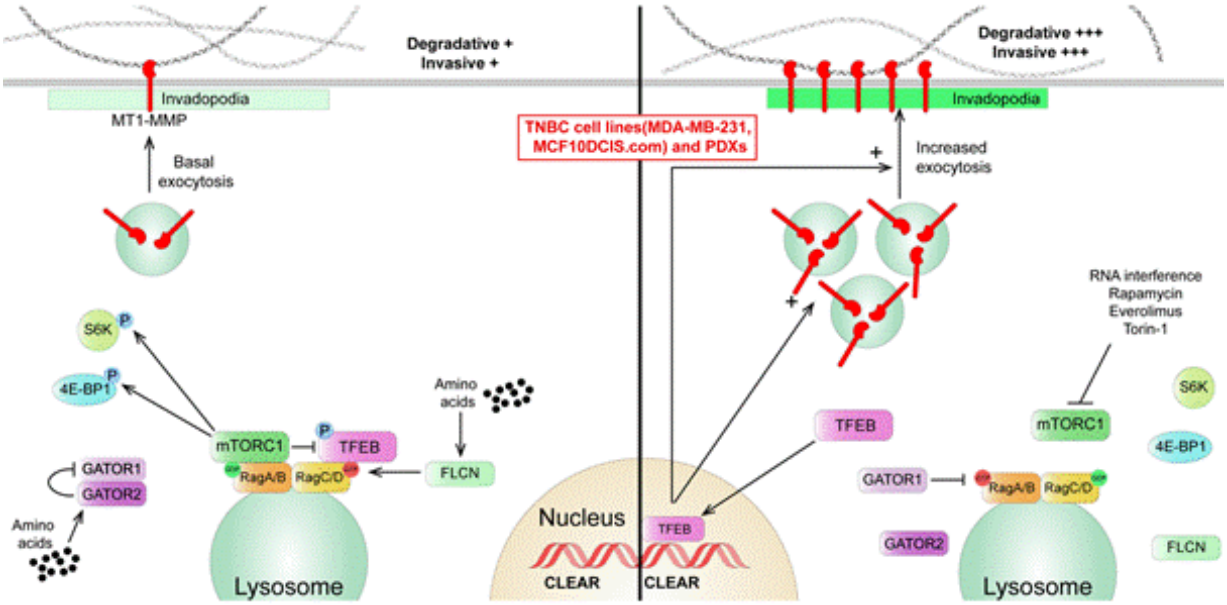

Figure 30: Regulation of the invadopodia by the mTORC1/TFEB signaling axis. *(Left) MT1-MMP is recycled to invadopodia from the endolysosomal compartment and cleaves the ECM fibers. The mTORC1 pathway is activated by nutrients such as amino acids and phosphorylates its substrates to promote anabolism and repress catabolic processes. (Right) Upon mTORC1 repression, TFEB translocates in the nucleus and activates the expression of genes from the CLEAR network, promoting lysosomal exocytosis of MT1-MMP at invadopodia. Increased surface exposure of MT1-MMP leads to enhanced ECM degradation and invasion by breast cancer cells.*

2.1. Beyond TFEB

TFEB recognizes and binds a consensus motif in the promoter region of its target genes to modulate their transcription. The genes belonging to this network (Coordinated Lysosomal

Expression and Regulation, CLEAR network of genes) are mostly associated with the lysosomal function (Palmieri et al., 2011). Interestingly, MT1-MMP protein levels were upregulated upon RagC KD and mTORC1 repression, and this effect was abolished by simultaneous TFEB knock-down, raising the possibility that MT1-MMP and possibly other invadopodia components could be part of the CLEAR network. Furthermore, we showed that mTORC1 repression and TFEB activation were required for the increase in ECM degradation which is supported by enhanced MT1-MMP exocytosis at the invadopodia. How TFEB can regulate MT1-MMP expression and exocytosis as well as the ECM degradation program remains an open question. We wish to compare the transcriptomes of MDA-MB-231 cells knocked down for RagC to assess the genes differentially expressed upon TFEB activation. Although these results are still pending, existing data from the CLEAR network suggest several possibilities to explain the phenotypes observed in our study.

TFEB has been shown to promote lysosomal exocytosis by upregulating the expression of several genes, such as mucolipin-1 (MCOLN1 or TRPML1). Increased Ca^{2+} efflux *via* MCOLN1 induces lysosomal exocytosis (Medina et al., 2011; Xu et al., 2021). Interestingly, KD of MCOLN1 could abolish the matrix degradation induced by RagC KD, suggesting that MT1-MMP exocytosis could require increased MCOLN1 activity downstream of mTORC1 repression and TFEB activation (**Figure 31**). However, calcineurin-mediated dephosphorylation of TFEB also requires Ca^{2+} released by MCOLN1 (Medina et al., 2015a). Activated nuclear TFEB then upregulates MCOLN1 expression in an auto-regulatory loop (Medina et al., 2011). Further work will thus be required to decipher the contribution of the TFEB/MCOLN1 axis in our cell models.

Autophagy is a multifaceted process with a complex and highly context-dependent role in tumorigenesis and has been proposed to have pleiotropic roles in the metastatic cascade (Mowers et al., 2016). As autophagy is regulated by mTORC1 and TFEB we sought to explore whether autophagy could influence ECM degradation upon mTORC1 repression. Upon RagC KD, the number of LC3-positive vesicles increased, which is characteristic of autophagy induction. KD of the autophagy initiator, Atg5, abolished the upregulation of LC3-positive vesicles, both in control and RagC KD cells. Interestingly, autophagy repression had no effect on the gelatin degradation response both in control and RagC KD cells, suggesting that autophagy is not involved in the upregulation of invadopodia activity in MDA-MB-231 cells (**Figure 31**).

A role for SNX-retromer proteins in the recycling of MT1-MMP from the endolysosomal compartment to the invadopodia has recently been described (P. Sharma et al., 2020). Retromer proteins Vps35 and Vps26 have also been recently described as being regulated by TFEB (Curnock et al., 2019). Knock-down of Vps35 abolished gelatin degradation by MDA-MB-231 cells, confirming earlier results (P. Sharma et al., 2020). Interestingly, Vps35 KD also

abolished siRagC-induced matrix degradation, suggesting that the recycling pathway of MT1-MMP at the invadopodia under mTORC1 repression shares similarities with the recycling pathway of control cells retaining mTORC1 activity (**Figure 31**).

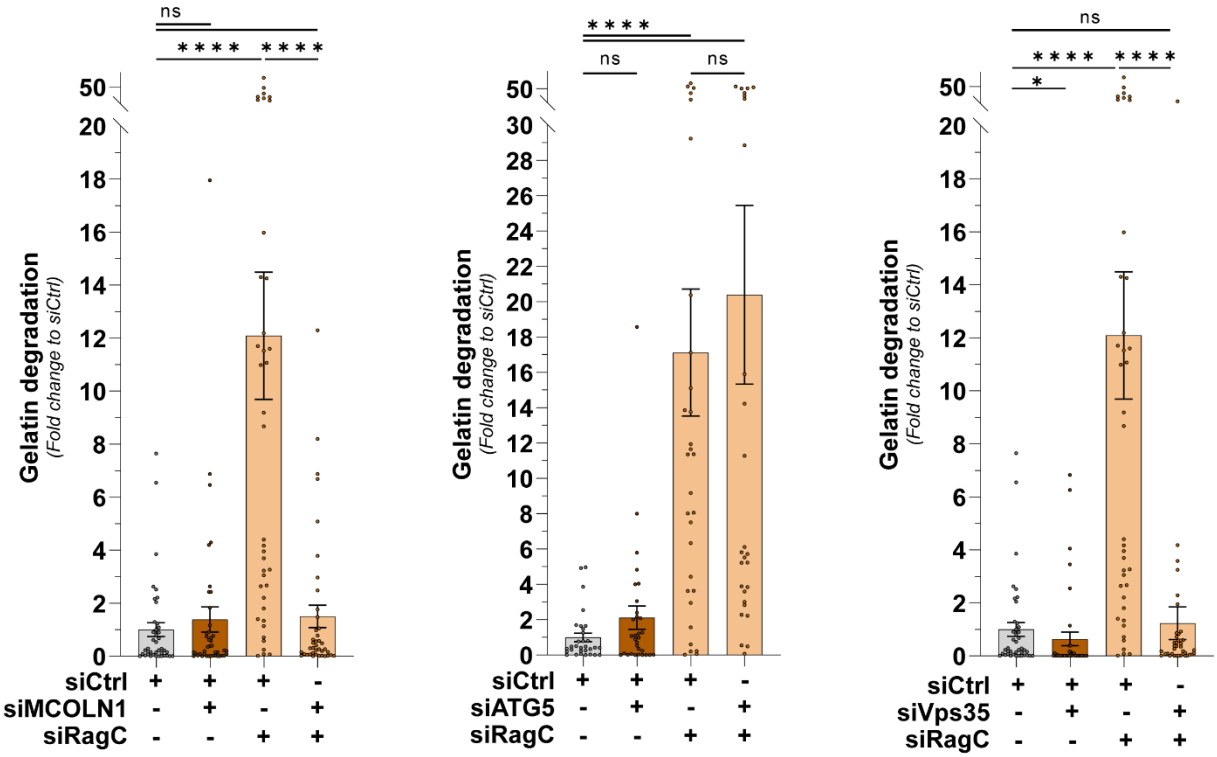

Figure 31: Exploring the CLEAR network. *MDA-MB-231 cells were transfected with indicated siRNAs for 72 h before assessing gelatin degradation as described in Material and Methods section.*

2.2. Decoupling mTORC1 signaling and TFEB activity

We show that mTORC1 repression is the leading cause for TFEB activation and for modification of invadopodia dynamics. The decoupling of TFEB and mTORC1 activity has been described in a handful of circumstances, including kidney, pancreatic and skin cancers and is generally (but not systemically) due to a perturbation of FLCN activity (Napolitano et al., 2022). FLCN is downregulated in basal-like breast cancers compared to adjacent healthy breast tissue and overexpression of FLCN in TNBC is sufficient to reduce angiogenesis and tumor growth (El-Houjeiri et al., 2021). It is tempting to postulate that active MiTF proteins (TFEB, TFE3) in TNBC cells lacking FLCN expression could stimulate an invadopodia-mediated invasion program.

2.3. Cell line-heterogeneity and diversity: adding a new layer of complexity to the Rag-ulation of the mTORC1 pathway

Knock-down of Lamtor 1 and Lamtor 4 (hereafter referred as Ragulator) in MDA-MB-231 cell lines was sufficient to down-modulate p-S6K and p-4E-BP1 and induce TFEB nuclearization, as previously described (Martina & Puertollano, 2013). However, it did not induce matrix degradation, which was surprising (see Figure 1 in Chapter 3). Further work is required to understand these disparate phenotypes but as Lamtor proteins have mTORC1-independent functions as direct regulators of MCOLN1-mediated release of calcium and of Arl8/BORC lysosomal trafficking and positioning, disrupting Lamtor proteins might promote TFEB activation but could also affect the trafficking of invadopodia components such as MT1-MMP and dysregulate TFEB-mediated ECM degradation. (Filipek et al., 2017; J. Sun et al., 2022). The majority of studies dissecting the mechanisms of mTORC1 regulation have been performed on the widely used cell lines HeLa, HEK293T, mouse embryonic fibroblasts, and their derivatives. As a central regulator of cell proliferation and growth, mTORC1 has different functions in different tissues which implies that the regulation of mTORC1 must not be identical depending on the tissue or cell type, especially when considering cancer cells. Our results hint at the existence of cell-to-cell heterogeneity in the regulation of mTORC1 signaling and although no molecular mechanism has been proposed to explain these disparities, the implications behind the existence of several programs of regulation of mTOR are intriguing and should be further explored. We illustrate these differences with our observations where Ragulator KD in MCF10DCIS.com cells induced collagen degradation, which was independent of TFEB (**Figure 32**). Furthermore, although p-S6K and p-4E-BP1 levels decreased upon Raptor KD in MCF10DCIS.com, there was no observable translocation of TFEB in the nucleus (**Figure 32**). TFEB is an atypical substrate compared to S6K and 4E-BP1 as it does not have a TOS motif and is recruited to the lysosome by the “active” GDP-bound form of RagC/RagD (Alesi et al., 2021; Gollwitzer et al., 2022; Martina & Puertollano, 2013; Napolitano et al., 2020; Roczniak-Ferguson et al., 2012; Settembre et al., 2012). However, recent structural data support the notion that Raptor and TFEB interact directly with no data to account for the function of this interaction yet (Cui et al., n.d.).

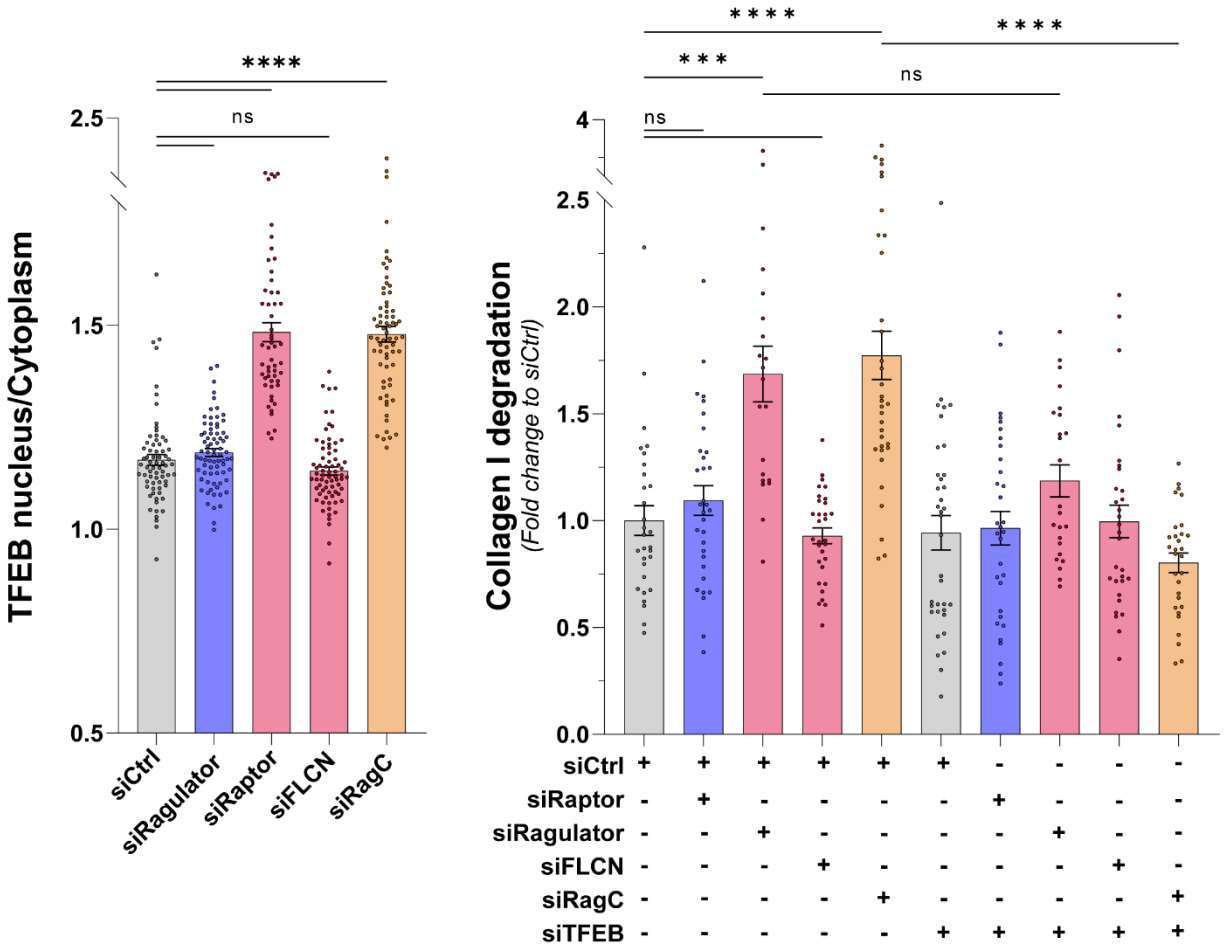

Figure 32: Cell line heterogeneity in mTORC1 regulation. *MCF10ADCIS.com cells were transfected with indicated siRNAs for 72 h before assessing endogenous TFEB localization (left graph) or collagen cleavage (right graph) as described in Material and Methods section.*

3. Inhibiting mTORC1 in breast tumors: a metastatic risk?

Our data demonstrate clearly that mTORC1 repression stimulates an invadopodia-mediated collagenolytic invasion program in breast cancer cells. RagC-silenced cells engineered as multicellular spheroids invade through the collagen 30 to 40% more than control spheroids. Furthermore, treatment with mTORC1 inhibitor Everolimus increases collagenolysis by one order of magnitude in TNBC PDX cells which is accompanied by an increase in the number of cells invading through the collagen matrix. Although mTORC1 pharmacological inhibition represses cell growth and proliferation *in vitro* and in *ex-vivo* PDX explants (Hatem et al., 2016), our results suggest that it could very well promote the expansion of a subpopulation of metastatic precursors by boosting invadopodia activity. Along this line, low expression of RAPTOR, FLCN and FRAP (mTOR) and high expression of TFEB at the mRNA level are associated with a lower probability of relapse-free survival and are considered

poor prognosis factors for patients diagnosed with TNBC (**Figure 33**) (Bertozzi et al., 2021; El-Houjeiri et al., 2021; Győrffy, 2021).

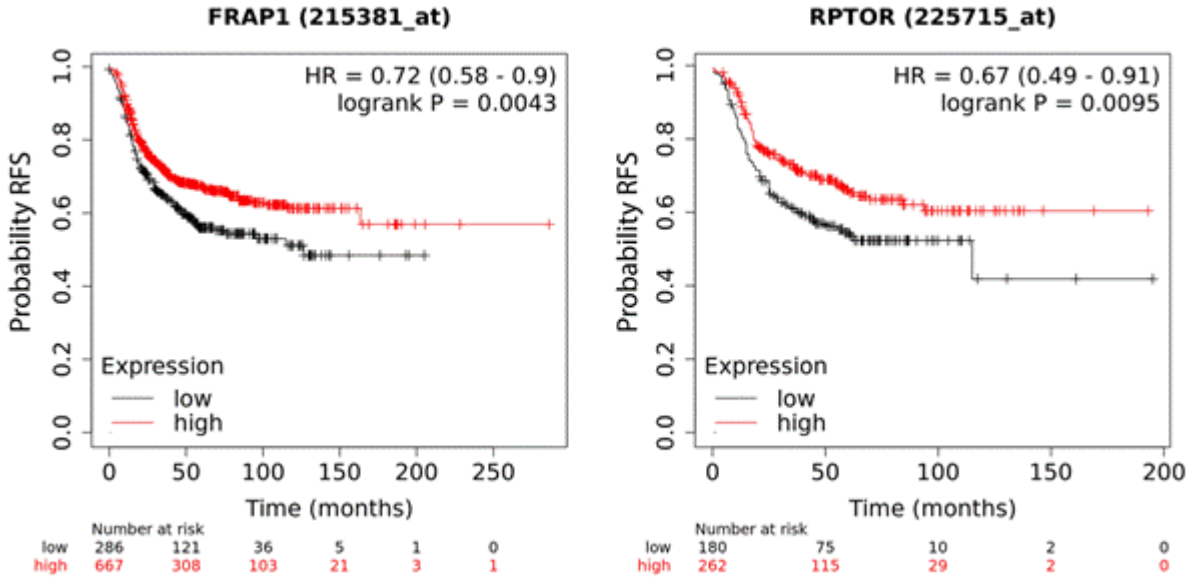

Figure 33: mTORC1 low expression as markers of poor prognosis in TNBC. *Kaplan-Meier survival analysis of relapse-free survival (RFS) probability in TNBC patients using gene chip data from GEO, EGA, and TCGA databases. Low expression of mTOR (FRAP1) and RPTOR are correlated to a worse prognosis.*

Everolimus may be offered as a second line of treatment to post-menopausal women with ER-positive, HER2-negative, locally advanced, or secondary breast cancer. Recently, a systematic review and meta-analysis of Everolimus in the treatment of advanced breast cancer from almost 3 000 patients revealed that Everolimus significantly increased the risk of developing grade III tumors, which are characterized by abnormal, poorly differentiated cells with a higher risk to spread and invade (Raphael et al., 2020). A growing body of literature based on cell proliferation and apoptosis assays shows that Everolimus treatment could be an effective course of treatment for TNBC (Costa et al., 2018; el Guerrab et al., 2020; J. Lee et al., 2021) but our results show that mTORC1 repression could potentiate tumor cell invasion. As proof of concept, we are currently analyzing the nuclear localization of TFEB and the expression of MT1-MMP in PDX cells implanted in the breast fat pad of mice treated with Everolimus or control. We expect to see nuclear translocation of TFEB in Everolimus-treated mice as well as a reduction in the levels of p-S6. PicroSirius Red staining to appraise collagen density will allow us to determine if the stroma of Everolimus-treated mice is reduced compared to control, which would suggest degradation of the extracellular matrix.

4. Concluding remarks

Tumor heterogeneity is the result of the interplay between genetic and environmental factors. Our work show that cancer cells respond to modifications in their immediate microenvironment, such as nutrient deprivation, by mounting a robust collagen proteolytic response based on MT1-MMP and the invadopodia scaffold protein TKS5. We propose a new mechanism of degradation by starved cancer cells where TKS5 associates and stabilizes CCPs to isolate and sequestrate a pool of MT1-MMP at the plasma membrane, supporting an enhanced propensity to degrade the ECM. The master regulator of nutrient mTORC1 plays a fundamental role in this process as its repression unleashes a dramatic invadopodia-mediated collagenolytic response which depends on TFEB activation. Genetic aberrations in TNBC and hyperactivation of the PI3K/AKT/mTOR pathway has fueled the need to use mTORC1 inhibitors. We show that inhibition of mTORC1 by neoplastic adjuvant chemotherapies (rapamycin, Everolimus) promotes the degradation and invasion of the collagen matrix by breast cancer cells, creating a potential for metastatic precursors.

REFERENCES

A long and winding sTORy. (2017). *Nature Cell Biology 2017 19:10*, *19*(10), 1131–1131. https://doi.org/10.1038/ncb3624

Abraham, L. C., Dice, J. F., Lee, K., & Kaplan, D. L. (2007). PHAGOCYTOSIS AND REMODELING OF COLLAGEN MATRICES. *Experimental Cell Research*, *313*(5), 1045. https://doi.org/10.1016/J.YEXCR.2006.12.019

Abram, C. L., Seals, D. F., Pass, I., Salinsky, D., Maurer, L., Roth, T. M., & Courtneidge, S. A. (2003). The adaptor protein fish associates with members of the ADAMs family and localizes to podosomes of Src-transformed cells. *The Journal of Biological Chemistry*, *278*(19), 16844–16851. https://doi.org/10.1074/JBC.M300267200

Aisenbrey, E. A., & Murphy, W. L. (2020). Synthetic alternatives to Matrigel. *Nature Reviews. Materials*, *5*(7), 539. https://doi.org/10.1038/S41578-020-0199-8

Alabi, A., Xia, X. D., Gu, H. M., Wang, F., Deng, S. J., Yang, N., Adijiang, A., Douglas, D. N., Kneteman, N. M., Xue, Y., Chen, L., Qin, S., Wang, G., & Zhang, D. W. (2021). Membrane type 1 matrix metalloproteinase promotes LDL receptor shedding and accelerates the development of atherosclerosis. *Nature Communications 2021 12:1*, *12*(1), 1–17. https://doi.org/10.1038/s41467-021-22167-3

Alesi, N., Akl, E. W., Khabibullin, D., Liu, H. J., Nidhiry, A. S., Garner, E. R., Filippakis, H., Lam, H. C., Shi, W., Viswanathan, S. R., Morroni, M., Ferguson, S. M., & Henske, E. P. (2021). TSC2 regulates lysosome biogenesis via a non-canonical RAGC and TFEB-dependent mechanism. *Nature Communications*, *12*(1). https://doi.org/10.1038/s41467-021-24499-6

Alfonso-Jaume, M. A., Mahimkar, R., & Lovett, D. H. (2004). Co-operative interactions between NFAT (nuclear factor of activated T cells) c1 and the zinc finger transcription factors Sp1/Sp3 and Egr-1 regulate MT1-MMP (membrane type 1 matrix metalloproteinase) transcription by glomerular mesangial cells. *The Biochemical Journal*, *380*(Pt 3), 735–747. https://doi.org/10.1042/BJ20031281

Annabi, B., Lachambre, M.-P., Bousquet-Gagnon, N., Pagé, M., Gingras, D., & Béliveau, R. (2001). Localization of membrane-type 1 matrix metalloproteinase in caveolae membrane domains. *Biochemical Journal*, *353*(3), 547–553. https://doi.org/10.1042/BJ3530547

Antonia, R. J., Castillo, J., Herring, L. E., Serafin, D. S., Liu, P., Graves, L. M., Baldwin, A. S., & Hagan, R. S. (2019). TBK1 Limits mTORC1 by Promoting Phosphorylation of Raptor Ser877. *Scientific Reports 2019 9:1*, *9*(1), 1–10. https://doi.org/10.1038/s41598-019-49707-8

Artym, V. v., Matsumoto, K., Mueller, S. C., & Yamada, K. M. (2011). Dynamic membrane remodeling at invadopodia differentiates invadopodia from podosomes. *European Journal of Cell Biology*, *90*(2–3), 172–180. https://doi.org/10.1016/J.EJCB.2010.06.006

Aspernig, H., Heimbucher, T., Qi, W., Gangurde, D., Curic, S., Yan, Y., Donner von Gromoff, E., Baumeister, R., & Thien, A. (2019). Mitochondrial Perturbations Couple mTORC2 to Autophagy in C. elegans. *Cell Reports*, *29*(6), 1399-1409.e5. https://doi.org/10.1016/J.CELREP.2019.09.072

Augoff, K., Hryniewicz-Jankowska, A., & Tabola, R. (2020). Invadopodia: clearing the way for cancer cell invasion. *Ann Transl Med*, *8*(14). https://doi.org/10.21037/atm.2020.02.157

Auvinen, P., Tammi, R., Parkkinen, J., Tammi, M., Ågren, U., Johansson, R., Hirvikoski, P., Eskelinen, M., & Kosma, V.-M. (2000). Hyaluronan in Peritumoral Stroma and Malignant Cells Associates with Breast Cancer Spreading and Predicts Survival. *The American Journal of Pathology*, *156*(2), 529–536. https://doi.org/10.1016/S0002-9440(10)64757-8

Aylett, C. H. S., Sauer, E., Imseng, S., Boehringer, D., Hall, M. N., Ban, N., & Maier, T. (2016). Architecture of human mTOR complex 1. *Science*, *351*(6268), 48–52. https://doi.org/10.1126/SCIENCE.AAA3870/SUPPL_FILE/AYLETT.SM.PDF

Ayuso, J. M., Gillette, A., Lugo-Cintrón, K., Acevedo-Acevedo, S., Gomez, I., Morgan, M., Heaster, T., Wisinski, K. B., Palecek, S. P., Skala, M. C., & Beebe, D. J. (2018).

Organotypic microfluidic breast cancer model reveals starvation-induced spatial-temporal metabolic adaptations. *EBioMedicine*, *37*, 144–157. https://doi.org/10.1016/J.EBIOM.2018.10.046

Bachelot, T., Bourgier, C., Cropet, C., Ray-Coquard, I., Ferrero, J. M., Freyer, G., Abadie-Lacourtoisie, S., Eymard, J. C., Debled, M., Spaëth, D., Legouffe, E., Allouache, D., el Kouri, C., & Pujade-Lauraine, E. (2012). Randomized phase II trial of everolimus in combination with tamoxifen in patients with hormone receptor-positive, human epidermal growth factor receptor 2-negative metastatic breast cancer with prior exposure to aromatase inhibitors: a GINECO study. *Journal of Clinical Oncology : Official Journal of the American Society of Clinical Oncology*, *30*(22), 2718–2724. https://doi.org/10.1200/JCO.2011.39.0708

Badowski, C., Pawlak, G., Grichine, A., Chabadel, A., Oddou, C., Jurdic, P., Pfaff, M., Albigès-Rizo, C., & Block, M. R. (2008). Paxillin phosphorylation controls invadopodia/podosomes spatiotemporal organization. *Molecular Biology of the Cell*, *19*(2), 633–645. https://doi.org/10.1091/MBC.E06-01-0088

Baffi, T. R., Lorden, G., Wozniak, J. M., Feichtner, A., Yeung, W., Kornev, A. P., King, C. C., Rio, J. C. D., Limaye, A. J., Bogomolovas, J., Gould, C. M., Chen, J., Kennedy, E. J., Kannan, N., Gonzalez, D. J., Stefan, E., Taylor, S. S., & Newton, A. C. (2021). mTORC2 controls the activity of PKC and Akt by phosphorylating a conserved TOR interaction motif. *Science Signaling*, *14*(678). https://doi.org/10.1126/SCISIGNAL.ABE4509

Ballabio, A. (2016). The awesome lysosome. *EMBO Molecular Medicine*, *8*(2), 73–76. https://doi.org/10.15252/EMMM.201505966

Barilari, M., Bonfils, G., Treins, C., Koka, V., Villeneuve, D. de, Fabrega, S., & Pende, M. (2017). ZRF1 is a novel S6 kinase substrate that drives the senescence programme. *The EMBO Journal*, *36*(6), 736–750. https://doi.org/10.15252/EMBJ.201694966

Bar-Peled, L., Chantranupong, L., Cherniack, A. D., Chen, W. W., Ottina, K. A., Grabiner, B. C., Spear, E. D., Carter, S. L., Meyerson, M., & Sabatini, D. M. (2013). A Tumor suppressor complex with GAP activity for the Rag GTPases that signal amino acid sufficiency to mTORC1. *Science (New York, N.Y.)*, *340*(6136), 1100–1106. https://doi.org/10.1126/SCIENCE.1232044

Barrio, A. v., & van Zee, K. J. (2017). Controversies in the Treatment of Ductal Carcinoma in Situ. *Annual Review of Medicine*, *68*, 197–211. https://doi.org/10.1146/ANNUREV-MED-050715-104920

Baselga, J., Campone, M., Piccart, M., Burris, H. A., Rugo, H. S., Sahmoud, T., Noguchi, S., Gnant, M., Pritchard, K. I., Lebrun, F., Beck, J. T., Ito, Y., Yardley, D., Deleu, I., Perez, A., Bachelot, T., Vittori, L., Xu, Z., Mukhopadhyay, P., … Hortobagyi, G. N. (2012). Everolimus in postmenopausal hormone-receptor-positive advanced breast cancer. *The New England Journal of Medicine*, *366*(6), 520–529. https://doi.org/10.1056/NEJMOA1109653

Bass, M. D., Williamson, R. C., Nunan, R. D., Humphries, J. D., Byron, A., Morgan, M. R., Martin, P., & Humphries, M. J. (2011). A syndecan-4 hair trigger initiates wound healing through caveolin- and RhoG-regulated integrin endocytosis. *Developmental Cell*, *21*(4), 681–693. https://doi.org/10.1016/J.DEVCEL.2011.08.007

Battaglioni, S., Benjamin, D., Wälchli, M., Maier, T., & Hall, M. N. (2022). mTOR substrate phosphorylation in growth control. *Cell*, *185*(11), 1814–1836. https://doi.org/10.1016/J.CELL.2022.04.013

Beaty, B. T., & Condeelis, J. (2014). Digging a little deeper: The stages of invadopodium formation and maturation. *European Journal of Cell Biology*, *93*(10–12), 438–444. https://doi.org/10.1016/J.EJCB.2014.07.003

Bella, J. (2016). Collagen structure: new tricks from a very old dog. *Biochemical Journal*, *473*(8), 1001–1025. https://doi.org/10.1042/BJ20151169

Ben-David, U., Beroukhim, R., & Golub, T. R. (2019). Genomic evolution of cancer models: perils and opportunities. *Nature Reviews. Cancer*, *19*(2), 97–109. https://doi.org/10.1038/S41568-018-0095-3

Bergers, G., & Benjamin, L. E. (2003). Tumorigenesis and the angiogenic switch. *Nature Reviews. Cancer*, *3*(6), 401–410. https://doi.org/10.1038/NRC1093

Bertozzi, S., Londero, A. P., Viola, L., Orsaria, M., Bulfoni, M., Marzinotto, S., Corradetti, B., Baccarani, U., Cesselli, D., Cedolini, C., & Mariuzzi, L. (2021). TFEB, SIRT1, CARM1, Beclin-1 expression and PITX2 methylation in breast cancer chemoresistance: a retrospective study. *BMC Cancer*, *21*(1). https://doi.org/10.1186/s12885-021-08844-y

Betz, C., & Hall, M. N. (2013). Where is mTOR and what is it doing there? *The Journal of Cell Biology*, *203*(4), 563–574. https://doi.org/10.1083/JCB.201306041

Böhm, R., Imseng, S., Jakob, R. P., Hall, M. N., Maier, T., & Hiller, S. (2021). The dynamic mechanism of 4E-BP1 recognition and phosphorylation by mTORC1. *Molecular Cell*, *81*(11), 2403-2416.e5. https://doi.org/10.1016/J.MOLCEL.2021.03.031

Boissan, M., Montagnac, G., Shen, Q., Griparic, L., Guitton, J., Romao, M., Sauvonnet, N., Lagache, T., Lascu, I., Raposo, G., Desbourdes, C., Schlattner, U., Lacombe, M. L., Polo, S., van der Bliek, A. M., Roux, A., & Chavrier, P. (2014). Membrane trafficking. Nucleoside diphosphate kinases fuel dynamin superfamily proteins with GTP for membrane remodeling. *Science (New York, N.Y.)*, *344*(6191), 1510–1515. https://doi.org/10.1126/SCIENCE.1253768

Bonnans, C., Chou, J., & Werb, Z. (2014). Remodelling the extracellular matrix in development and disease. *Nature Reviews. Molecular Cell Biology*, *15*(12), 786–801. https://doi.org/10.1038/NRM3904

Bonucci, M., Kuperwasser, N., Barbe, S., Koka, V., de Villeneuve, D., Zhang, C., Srivastava, N., Jia, X., Stokes, M. P., Bienaimé, F., Verkarre, V., Lopez, J. B., Jaulin, F., Pontoglio, M., Terzi, F., Delaval, B., Piel, M., & Pende, M. (2020). mTOR and S6K1 drive polycystic kidney by the control of Afadin-dependent oriented cell division. *Nature Communications 2020 11:1*, *11*(1), 1–17. https://doi.org/10.1038/S41467-020-16978-Z

Bowman, A. B., Kamal, A., Ritchings, B. W., Philp, A. V., McGrail, M., Gindhart, J. G., & Goldstein, L. S. B. (2000). Kinesin-dependent axonal transport is mediated by the sunday driver (SYD) protein. *Cell*, *103*(4), 583–594. https://doi.org/10.1016/S0092-8674(00)00162-8

Bretou, M., Sáez, P. J., Sanséau, D., Maurin, M., Lankar, D., Chabaud, M., Spampanato, C., Malbec, O., Barbier, L., Muallem, S., Maiuri, P., Ballabio, A., Helft, J., Piel, M., Vargas, P., & Lennon-Duménil, A. M. (2017). Lysosome signaling controls the migration of dendritic cells. *Science Immunology*, *2*(16). https://doi.org/10.1126/SCIIMMUNOL.AAK9573

Brugarolas, J., Lei, K., Hurley, R. L., Manning, B. D., Reiling, J. H., Hafen, E., Witters, L. A., Ellisen, L. W., & Kaelin, W. G. (2004). Regulation of mTOR function in response to hypoxia by REDD1 and the TSC1/TSC2 tumor suppressor complex. *Genes & Development*, *18*(23), 2893. https://doi.org/10.1101/GAD.1256804

Bruna, A., Rueda, O. M., Greenwood, W., Batra, A. S., Callari, M., Batra, R. N., Pogrebniak, K., Sandoval, J., Cassidy, J. W., Tufegdzic-Vidakovic, A., Sammut, S. J., Jones, L., Provenzano, E., Baird, R., Eirew, P., Hadfield, J., Eldridge, M., McLaren-Douglas, A., Barthorpe, A., … Caldas, C. (2016). A Biobank of Breast Cancer Explants with Preserved Intra-tumor Heterogeneity to Screen Anticancer Compounds. *Cell*, *167*(1), 260-274.e22. https://doi.org/10.1016/J.CELL.2016.08.041

Buyuk, B., Jin, S., & Ye, K. (2022). Epithelial-to-Mesenchymal Transition Signaling Pathways Responsible for Breast Cancer Metastasis. *Cellular and Molecular Bioengineering*, *15*(1), 1–13. https://doi.org/10.1007/s12195-021-00694-9

Cambi, A., & Chavrier, P. (2021). Tissue remodeling by invadosomes. *Faculty Reviews*, *10*. https://doi.org/10.12703/r/10-39

Carbognin, L., Miglietta, F., Paris, I., & Dieci, M. V. (2019). Prognostic and Predictive Implications of PTEN in Breast Cancer: Unfulfilled Promises but Intriguing Perspectives. *Cancers*, *11*(9). https://doi.org/10.3390/CANCERS11091401

Cardoso, C. M. P., Groth-Pedersen, L., Høyer-Hansen, M., Kirkegaard, T., Corcelle, E., Andersen, J. S., Jäättelä, M., & Nylandsted, J. (2009). Depletion of Kinesin 5B Affects Lysosomal Distribution and Stability and Induces Peri-Nuclear Accumulation of

Autophagosomes in Cancer Cells. *PLOS ONE*, *4*(2), e4424. https://doi.org/10.1371/JOURNAL.PONE.0004424
Case, L. B., & Waterman, C. M. (2015). Integration of actin dynamics and cell adhesion by a three-dimensional, mechanosensitive molecular clutch. *Nature Cell Biology 2015 17:8*, *17*(8), 955–963. https://doi.org/10.1038/ncb3191
Castagnino, A., Castro-Castro, A., Irondelle, M., Guichard, A., Lodillinsky, C., Fuhrmann, L., Vacher, S., Agüera-González, S., Zagryazhskaya-Masson, A., Romao, M., el Kesrouani, C., Noegel, A. A., Dubois, T., Raposo, G., Bear, J. E., Clemen, C. S., Vincent-Salomon, A., Bièche, I., & Chavrier, P. (2018). Coronin 1C promotes triple-negative breast cancer invasiveness through regulation of MT1-MMP traffic and invadopodia function. *Oncogene*, *37*(50), 6425–6441. https://doi.org/10.1038/s41388-018-0422-x
Castellano, B. M., Thelen, A. M., Moldavski, O., Feltes, M., van der Welle, R. E. N., Mydock-Mcgrane, L., Jiang, X., van Eijkeren, R. J., Davis, O. B., Louie, S. M., Perera, R. M., Covey, D., Nomura, D. K., Ory, D. S., & Zoncu, R. (2017). Lysosomal Cholesterol Activates mTORC1 via an SLC38A9-Niemann Pick C1 Signaling Complex HHS Public Access. *Science*, *355*(6331), 1306–1311. https://doi.org/10.1126/science.aag1417
Castro-Castro, A., Marchesin, V., Monteiro, P., Lodillinsky, C., Rossé, C., & Chavrier, P. (2016). Cellular and Molecular Mechanisms of MT1-MMP-Dependent Cancer Cell Invasion. In *Annual Review of Cell and Developmental Biology* (Vol. 32, pp. 555–576). Annual Reviews Inc. https://doi.org/10.1146/annurev-cellbio-111315-125227
Cathcart, J. M., Banach, A., Liu, A., Chen, J., Goligorsky, M., Cao, J., Cathcart, J. M., Banach, A., Liu, A., Chen, J., Goligorsky, M., & Cao, J. (2016). Interleukin-6 increases matrix metalloproteinase-14 (MMP-14) levels via down-regulation of p53 to drive cancer progression. *Oncotarget*, *7*(38), 61107–61120. https://doi.org/10.18632/ONCOTARGET.11243
Catteau, X., Simon, P., Jondet, M., Vanhaeverbeek, M., & Noël, J.-C. (2019). Quantification of stromal reaction in breast carcinoma and its correlation with tumor grade and free progression survival. *PLOS ONE*, *14*(3), e0210263. https://doi.org/10.1371/journal.pone.0210263
Chantranupong, L., Scaria, S. M., Saxton, R. A., Gygi, M. P., Shen, K., Wyant, G. A., Wang, T., Harper, J. W., Gygi, S. P., & Sabatini, D. M. (2016). The CASTOR Proteins Are Arginine Sensors for the mTORC1 Pathway. *Cell*, *165*(1), 153–164. https://doi.org/10.1016/J.CELL.2016.02.035/ATTACHMENT/FA90DFC7-F1D7-4904-AB97-2D0B9FA3D026/MMC1.PDF
Chao, L. H., & Avruch, J. (2019). Cryo-EM insight into the structure of MTOR complex 1 and its interactions with Rheb and substrates. *F1000Research*, *8*. https://doi.org/10.12688/F1000RESEARCH.16109.1/DOI
Chaplin, D. J., Olive, P. L., & Durand, R. E. (1987). Intermittent blood flow in a murine tumor: radiobiological effects. *Cancer Research*, *47*(2), 597–601.
Chen, J., Ou, Y., Luo, R., Wang, J., Wang, D., Guan, J., Li, Y., Xia, P., Chen, P. R., & Liu, Y. (2021). SAR1B senses leucine levels to regulate mTORC1 signalling. *Nature*, *596*(7871), 281–284. https://doi.org/10.1038/S41586-021-03768-W
Chen, Y., Lee, C. H., Tseng, B. Y., Tsai, Y. H., Tsai, H. W., Yao, C. L., & Tseng, S. H. (2018). AZD8055 Exerts Antitumor Effects on Colon Cancer Cells by Inhibiting mTOR and Cell-cycle Progression. *Anticancer Research*, *38*(3), 1445–1454. https://doi.org/10.21873/ANTICANRES.12369
Chetty, C., Lakka, S. S., Bhoopathi, P., & Rao, J. S. (2010). MMP-2 alters VEGF expression via αVβ3 integrin-mediated PI3K/AKT signaling in A549 lung cancer cells. *International Journal of Cancer*, *127*(5), 1081–1095. https://doi.org/10.1002/IJC.25134
Chevalier, C., Collin, G., Descamps, S., Touaitahuata, H., Simon, V., Reymond, N., Fernandez, L., Milhiet, P. E., Georget, V., Urbach, S., Lasorsa, L., Orsetti, B., Boissière-Michot, F., Lopez-Crapez, E., Theillet, C., Roche, S., & Benistant, C. (2016). TOM1L1 drives membrane delivery of MT1-MMP to promote ERBB2-induced breast cancer cell invasion. *Nature Communications 2016 7:1*, *7*(1), 1–16. https://doi.org/10.1038/ncomms10765

Clancy, J. W., Sedgwick, A., Rosse, C., Muralidharan-Chari, V., Raposo, G., Method, M., Chavrier, P., & D'Souza-Schorey, C. (2015). Regulated delivery of molecular cargo to invasive tumour-derived microvesicles. *Nature Communications 2015 6:1*, *6*(1), 1–11. https://doi.org/10.1038/ncomms7919

Colombero, C., Remy, D., Antoine-Bally, S., Macé, A. S., Monteiro, P., ElKhatib, N., Fournier, M., Dahmani, A., Montaudon, E., Montagnac, G., Marangoni, E., & Chavrier, P. (2021). mTOR Repression in Response to Amino Acid Starvation Promotes ECM Degradation Through MT1-MMP Endocytosis Arrest. *Advanced Science*, *8*(17). https://doi.org/10.1002/advs.202101614

Commisso, C., Davidson, S. M., Soydaner-Azeloglu, R. G., Parker, S. J., Kamphorst, J. J., Hackett, S., Grabocka, E., Nofal, M., Drebin, J. A., Thompson, C. B., Rabinowitz, J. D., Metallo, C. M., vander Heiden, M. G., & Bar-Sagi, D. (2013). Macropinocytosis of protein is an amino acid supply route in Ras-transformed cells. *Nature 2013 497:7451*, *497*(7451), 633–637. https://doi.org/10.1038/nature12138

Conant, K., Haughey, N., Nath, A., st. Hillaire, C., Gary, D. S., Pardo, C. A., Wahl, L. M., Bilak, M., Milward, E., & Mattson, M. P. (2002). Matrix metalloproteinase-1 activates a pertussis toxin-sensitive signaling pathway that stimulates the release of matrix metalloproteinase-9. *Journal of Neurochemistry*, *82*(4), 885–893. https://doi.org/10.1046/J.1471-4159.2002.01038.X

Conant, K., st. Hillaire, C., Nagase, H., Visse, R., Gary, D., Haughey, N., Anderson, C., Turchan, J., & Nath, A. (2004). Matrix Metalloproteinase 1 Interacts with Neuronal Integrins and Stimulates Dephosphorylation of Akt. *Journal of Biological Chemistry*, *279*(9), 8056–8062. https://doi.org/10.1074/JBC.M307051200

Condon, K. J., & Sabatini, D. M. (2019). Nutrient regulation of mTORC1 at a glance. *Journal of Cell Science*, *132*(21). https://doi.org/10.1242/JCS.222570

Conklin, M. W., Eickhoff, J. C., Riching, K. M., Pehlke, C. A., Eliceiri, K. W., Provenzano, P. P., Friedl, A., & Keely, P. J. (2011). Aligned Collagen Is a Prognostic Signature for Survival in Human Breast Carcinoma. *The American Journal of Pathology*, *178*(3), 1221–1232. https://doi.org/10.1016/j.ajpath.2010.11.076

Cooper, J., & Giancotti, F. G. (2019). Integrin Signaling in Cancer: Mechanotransduction, Stemness, Epithelial Plasticity, and Therapeutic Resistance. *Cancer Cell*, *35*(3), 347–367. https://doi.org/10.1016/J.CCELL.2019.01.007

Correia, A. L., Mori, H., Chen, E. I., Schmitt, F. C., & Bissell, M. J. (2013). The hemopexin domain of MMP3 is responsible for mammary epithelial invasion and morphogenesis through extracellular interaction with HSP90β. *Genes & Development*, *27*(7), 805–817. https://doi.org/10.1101/GAD.211383.112

Costa, R. L. B., Han, H. S., & Gradishar, W. J. (2018). Targeting the PI3K/AKT/mTOR pathway in triple-negative breast cancer: a review. *Breast Cancer Research and Treatment*, *169*(3), 397–406. https://doi.org/10.1007/S10549-018-4697-Y

Coussy, F., de Koning, L., Lavigne, M., Bernard, V., Ouine, B., Boulai, A., el Botty, R., Dahmani, A., Montaudon, E., Assayag, F., Morisset, L., Huguet, L., Sourd, L., Painsec, P., Callens, C., Chateau-Joubert, S., Servely, J. L., Larcher, T., Reyes, C., … Marangoni, E. (2019). A large collection of integrated genomically characterized patient-derived xenografts highlighting the heterogeneity of triple-negative breast cancer. *International Journal of Cancer*, *145*(7), 1902–1912. https://doi.org/10.1002/IJC.32266

Crino, P. B., Nathanson, K. L., & Henske, E. P. (2006). The tuberous sclerosis complex. *The New England Journal of Medicine*, *355*(13), 1345–1356. https://doi.org/10.1056/NEJMRA055323

Cserni, G., Chmielik, E., Cserni, B., & Tot, T. (2018). The new TNM-based staging of breast cancer. *Virchows Archiv : An International Journal of Pathology*, *472*(5), 697–703. https://doi.org/10.1007/S00428-018-2301-9

Cui, Z., Napolitano, G., G de Araujo, M. E., Esposito, A., Monfregola, J., Huber, L. A., Ballabio, A., Hurley, J. H., & Duncan, D. (n.d.). *Structural basis for mTORC1-dependent regulation of the lysosomal and autophagic transcription factor TFEB*. https://doi.org/10.1101/2022.09.12.507619

Curino, A. C., Engelholm, L. H., Yamada, S. S., Holmbeck, K., Lund, L. R., Molinolo, A. A., Behrendt, N., Nielsen, B. S., & Bugge, T. H. (2005a). Intracellular collagen degradation mediated by uPARAP/Endo180 is a major pathway of extracellular matrix turnover during malignancy. *The Journal of Cell Biology*, *169*(6), 977–985. https://doi.org/10.1083/JCB.200411153

Curino, A. C., Engelholm, L. H., Yamada, S. S., Holmbeck, K., Lund, L. R., Molinolo, A. A., Behrendt, N., Nielsen, B. S., & Bugge, T. H. (2005b). Intracellular collagen degradation mediated by uPARAP/Endo180 is a major pathway of extracellular matrix turnover during malignancy. *Journal of Cell Biology*, *169*(6), 977–985. https://doi.org/10.1083/jcb.200411153

Curnock, R., Calcagni, A., Ballabio, A., & Cullen, P. J. (2019). TFEB controls retromer expression in response to nutrient availability. *Journal of Cell Biology*, *218*(12), 3954–3966. https://doi.org/10.1083/JCB.201903006

Datta, A., Deng, S., Gopal, V., Yap, K. C.-H., Halim, C. E., Lye, M. L., Ong, M. S., Tan, T. Z., Sethi, G., Hooi, S. C., Kumar, A. P., & Yap, C. T. (2021). Cytoskeletal Dynamics in Epithelial-Mesenchymal Transition: Insights into Therapeutic Targets for Cancer Metastasis. *Cancers*, *13*(8), 1882. https://doi.org/10.3390/cancers13081882

Davidson, S. M., Jonas, O., Keibler, M. A., Hou, H. W., Luengo, A., Mayers, J. R., Wyckoff, J., del Rosario, A. M., Whitman, M., Chin, C. R., Condon, K. J., Lammers, A., Kellersberger, K. A., Stall, B. K., Stephanopoulos, G., Bar-Sagi, D., Han, J., Rabinowitz, J. D., Cima, M. J., … vander Heiden, M. G. (2017). Direct evidence for cancer-cell-autonomous extracellular protein catabolism in pancreatic tumors. *Nature Medicine*, *23*(2), 235–241. https://doi.org/10.1038/nm.4256

Davis, O. B., Shin, H. R., Lim, C. Y., Wu, E. Y., Kukurugya, M., Maher, C. F., Perera, R. M., Ordonez, M. P., & Zoncu, R. (2020). NPC1-mTORC1 Signaling Couples Cholesterol Sensing to Organelle Homeostasis and Is a Targetable Pathway in Niemann-Pick Type C. *Developmental Cell*, *56*(3), 260-276.e7. https://doi.org/10.1016/J.DEVCEL.2020.11.016

Dawson, J. E., Bah, A., Zhang, Z., Vernon, R. M., Lin, H., Chong, P. A., Vanama, M., Sonenberg, N., Gradinaru, C. C., & Forman-Kay, J. D. (2020). Non-cooperative 4E-BP2 folding with exchange between eIF4E-binding and binding-incompatible states tunes cap-dependent translation inhibition. *Nature Communications 2020 11:1*, *11*(1), 1–18. https://doi.org/10.1038/s41467-020-16783-8

de Araujo, M. E. G., Naschberger, A., Fürnrohr, B. G., Stasyk, T., Dunzendorfer-Matt, T., Lechner, S., Welti, S., Kremser, L., Shivalingaiah, G., Offterdinger, M., Lindner, H. H., Huber, L. A., & Scheffzek, K. (2017). Crystal structure of the human lysosomal mTORC1 scaffold complex and its impact on signaling. *Science (New York, N.Y.)*, *358*(6361), 377–381. https://doi.org/10.1126/SCIENCE.AAO1583

de Pasquale, V., & Pavone, L. M. (2020). Heparan Sulfate Proteoglycan Signaling in Tumor Microenvironment. *International Journal of Molecular Sciences 2020, Vol. 21, Page 6588*, *21*(18), 6588. https://doi.org/10.3390/IJMS21186588

Deleyto-Seldas, N., & Efeyan, A. (2021). The mTOR–Autophagy Axis and the Control of Metabolism. *Frontiers in Cell and Developmental Biology*, *9*, 1519. https://doi.org/10.3389/FCELL.2021.655731/BIBTEX

Demetriades, C., Doumpas, N., & Teleman, A. A. (2014). Regulation of TORC1 in response to amino acid starvation via lysosomal recruitment of TSC2. *Cell*, *156*(4), 786–799. https://doi.org/10.1016/j.cell.2014.01.024

Demetriades, C., Plescher, M., & Teleman, A. A. (2016). Lysosomal recruitment of TSC2 is a universal response to cellular stress. *Nature Communications 2016 7:1*, *7*(1), 1–14. https://doi.org/10.1038/ncomms10662

Derivery, E., Sousa, C., Gautier, J. J., Lombard, B., Loew, D., & Gautreau, A. (2009). The Arp2/3 activator WASH controls the fission of endosomes through a large multiprotein complex. *Developmental Cell*, *17*(5), 712–723. https://doi.org/10.1016/J.DEVCEL.2009.09.010

Derksen, P. W. B., Liu, X., Saridin, F., van der Gulden, H., Zevenhoven, J., Evers, B., van Beijnum, J. R., Griffioen, A. W., Vink, J., Krimpenfort, P., Peterse, J. L., Cardiff, R. D., Berns, A., & Jonkers, J. (2006). Somatic inactivation of E-cadherin and p53 in mice leads to metastatic lobular mammary carcinoma through induction of anoikis resistance and angiogenesis. *Cancer Cell*, *10*(5), 437–449. https://doi.org/10.1016/j.ccr.2006.09.013

Deugnier, M.-A., Faraldo, M. M., Janji, B., Rousselle, P., Thiery, J. P., & Glukhova, M. A. (2002). EGF controls the in vivo developmental potential of a mammary epithelial cell line possessing progenitor properties. *Journal of Cell Biology*, *159*(3), 453–463. https://doi.org/10.1083/jcb.200207138

Deville, S. S., & Cordes, N. (2019). The Extracellular, Cellular, and Nuclear Stiffness, a Trinity in the Cancer Resistome—A Review. *Frontiers in Oncology*, *9*, 1376. https://doi.org/10.3389/FONC.2019.01376/BIBTEX

di Martino, J., Paysan, L., Gest, C., Lagrée, V., Juin, A., Saltel, F., & Moreau, V. (2014). Cdc42 and Tks5: A minimal and universal molecular signature for functional invadosomes. *Cell Adhesion & Migration*, *8*(3), 280. https://doi.org/10.4161/CAM.28833

Díaz, B., Yuen, A., Iizuka, S., Higashiyama, S., & Courtneidge, S. A. (2013). Notch increases the shedding of HB-EGF by ADAM12 to potentiate invadopodia formation in hypoxia. *The Journal of Cell Biology*, *201*(2), 279–292. https://doi.org/10.1083/JCB.201209151

Dibble, C. C., Elis, W., Menon, S., Qin, W., Klekota, J., Asara, J. M., Finan, P. M., Kwiatkowski, D. J., Murphy, L. O., & Manning, B. D. (2012). TBC1D7 Is a Third Subunit of the TSC1-TSC2 Complex Upstream of mTORC1. *Molecular Cell*, *47*(4), 535–546. https://doi.org/10.1016/J.MOLCEL.2012.06.009

Djediai, S., Gonzalez Suarez, N., el Cheikh-Hussein, L., Rodriguez Torres, S., Gresseau, L., Dhayne, S., Joly-Lopez, Z., & Annabi, B. (2021). MT1-MMP Cooperates with TGF-β Receptor-Mediated Signaling to Trigger SNAIL and Induce Epithelial-to-Mesenchymal-like Transition in U87 Glioblastoma Cells. *International Journal of Molecular Sciences*, *22*(23), 13006. https://doi.org/10.3390/ijms222313006

Doyle, A. D., Nazari, S. S., & Yamada, K. M. (2022). Cell–extracellular matrix dynamics. *Physical Biology*, *19*(2), 021002. https://doi.org/10.1088/1478-3975/ac4390

Doyle, A. D., Sykora, D. J., Pacheco, G. G., Kutys, M. L., & Yamada, K. M. (2021). 3D mesenchymal cell migration is driven by anterior cellular contraction that generates an extracellular matrix prestrain. *Developmental Cell*, *56*(6), 826-841.e4. https://doi.org/10.1016/J.DEVCEL.2021.02.017

Du, L., Li, X., Zhen, L., Chen, W., Mu, L., Zhang, Y., & Song, A. (2018). Everolimus inhibits breast cancer cell growth through PI3K/AKT/mTOR signaling pathway. *Molecular Medicine Reports*, *17*(5), 7163–7169. https://doi.org/10.3892/MMR.2018.8769

East, L., McCarthy, A., Wienke, D., Sturge, J., Ashworth, A., & Isacke, C. M. (2003). A targeted deletion in the endocytic receptor gene Endo180 results in a defect in collagen uptake. *EMBO Reports*, *4*(7), 710–716. https://doi.org/10.1038/SJ.EMBOR.EMBOR882

Eckert, M. A., Lwin, T. M., Chang, A. T., Kim, J., Danis, E., Ohno-Machado, L., & Yang, J. (2011). Twist1-induced invadopodia formation promotes tumor metastasis. *Cancer Cell*, *19*(3), 372–386. https://doi.org/10.1016/J.CCR.2011.01.036

Eckert, M. A., Santiago-Medina, M., Lwin, T. M., Kim, J., Courtneidge, S. A., & Yang, J. (2017). ADAM12 induction by Twist1 promotes tumor invasion and metastasis via regulation of invadopodia and focal adhesions. *Journal of Cell Science*, *130*(12), 2036–2048. https://doi.org/10.1242/JCS.198200

Eddy, R. J., Weidmann, M. D., Sharma, V. P., & Condeelis, J. S. (2017). Tumor Cell Invadopodia: Invasive Protrusions that Orchestrate Metastasis. In *Trends in Cell Biology* (Vol. 27, Issue 8, pp. 595–607). Elsevier Ltd. https://doi.org/10.1016/j.tcb.2017.03.003

Egri, S. B., & Shen, K. (2021). An interdomain hydrogen bond in the Rag GTPases maintains stable mTORC1 signaling in sensing amino acids. *Journal of Biological Chemistry*, *297*(1), 100861. https://doi.org/10.1016/J.JBC.2021.100861

el Guerrab, A., Bamdad, M., Bignon, Y. J., Penault-Llorca, F., & Aubel, C. (2020). Co-targeting EGFR and mTOR with gefitinib and everolimus in triple-negative breast cancer cells. *Scientific Reports*, *10*(1). https://doi.org/10.1038/S41598-020-63310-2

Elango, J., Hou, C., Bao, B., Wang, S., Maté Sánchez de Val, J. E., & Wenhui, W. (2022). The Molecular Interaction of Collagen with Cell Receptors for Biological Function. *Polymers 2022, Vol. 14, Page 876*, *14*(5), 876. https://doi.org/10.3390/POLYM14050876

El-Houjeiri, L., Biondini, M., Paquette, M., Kuasne, H., Pacis, A., Park, M., Siegel, P. M., & Pause, A. (2021). Folliculin impairs breast tumor growth by repressing TFE3-dependent induction of the Warburg effect and angiogenesis. *The Journal of Clinical Investigation*, *131*(22). https://doi.org/10.1172/JCI144871

Elia, I., Broekaert, D., Christen, S., Boon, R., Radaelli, E., Orth, M. F., Verfaillie, C., Grünewald, T. G. P., & Fendt, S. M. (2017). Proline metabolism supports metastasis formation and could be inhibited to selectively target metastasizing cancer cells. *Nature Communications*, *8*. https://doi.org/10.1038/NCOMMS15267

Eliyatkın, N., Yalçın, E., Zengel, B., Aktaş, S., & Vardar, E. (2015). Molecular Classification of Breast Carcinoma: From Traditional, Old-Fashioned Way to A New Age, and A New Way. *The Journal of Breast Health*, *11*(2), 59. https://doi.org/10.5152/TJBH.2015.1669

Engelholm, L. H., List, K., Netzel-Arnett, S., Cukierman, E., Mitola, D. J., Aaronson, H., Kjøller, L., Larsen, J. K., Yamada, K. M., Strickland, D. K., Holmbeck, K., Danø, K., Birkedal-Hansen, H., Behrendt, N., & Bugge, T. H. (2003). uPARAP/Endo180 is essential for cellular uptake of collagen and promotes fibroblast collagen adhesion. *The Journal of Cell Biology*, *160*(7), 1009–1015. https://doi.org/10.1083/JCB.200211091

Espina, V., Mariani, B. D., Gallagher, R. I., Tran, K., Banks, S., Wiedemann, J., Huryk, H., Mueller, C., Adamo, L., Deng, J., Petricoin, E. F., Pastore, L., Zaman, S., Menezes, G., Mize, J., Johal, J., Edmiston, K., & Liotta, L. A. (2010). Malignant Precursor Cells Pre-Exist in Human Breast DCIS and Require Autophagy for Survival. *PLoS ONE*, *5*(4). https://doi.org/10.1371/journal.pone.0010240

Farías, G. G., Guardia, C. M., de Pace, R., Britt, D. J., & Bonifacino, J. S. (2017). BORC/kinesin-1 ensemble drives polarized transport of lysosomes into the axon. *Proceedings of the National Academy of Sciences of the United States of America*, *114*(14), E2955–E2964. https://doi.org/10.1073/PNAS.1616363114/-/DCSUPPLEMENTAL

Fendt, S. M., Frezza, C., & Erez, A. (2020). Targeting metabolic plasticity and flexibility dynamics for cancer therapy. *Cancer Discovery*, *10*(12), 1797. https://doi.org/10.1158/2159-8290.CD-20-0844

Ferrari, R., Martin, G., Tagit, O., Guichard, A., Cambi, A., Voituriez, R., Vassilopoulos, S., & Chavrier, P. (2019). MT1-MMP directs force-producing proteolytic contacts that drive tumor cell invasion. *Nature Communications*, *10*(1). https://doi.org/10.1038/s41467-019-12930-y

Ferré, P., & Foufelle, F. (2007). SREBP-1c transcription factor and lipid homeostasis: clinical perspective. *Hormone Research*, *68*(2), 72–82. https://doi.org/10.1159/000100426

Filipek, P. A., de Araujo, M. E. G., Vogel, G. F., de Smet, C. H., Eberharter, D., Rebsamen, M., Rudashevskaya, E. L., Kremser, L., Yordanov, T., Tschaikner, P., Fürnrohr, B. G., Lechner, S., Dunzendorfer-Matt, T., Scheffzek, K., Bennett, K. L., Superti-Furga, G., Lindner, H. H., Stasyk, T., & Huber, L. A. (2017). LAMTOR/Ragulator is a negative regulator of Arl8b- and BORC-dependent late endosomal positioning. *The Journal of Cell Biology*, *216*(12), 4199–4215. https://doi.org/10.1083/JCB.201703061

Finicle, B. T., Jayashankar, V., & Edinger, A. L. (2018). Nutrient scavenging in cancer. In *Nature Reviews Cancer* (Vol. 18, Issue 10, pp. 619–633). Nature Publishing Group. https://doi.org/10.1038/s41568-018-0048-x

Frantz, C., Stewart, K. M., & Weaver, V. M. (2010). The extracellular matrix at a glance. *Journal of Cell Science*, *123*(24), 4195–4200. https://doi.org/10.1242/jcs.023820

Fu, W., & Hall, M. N. (2020). Regulation of mTORC2 Signaling. *Genes 2020, Vol. 11, Page 1045*, *11*(9), 1045. https://doi.org/10.3390/GENES11091045

Gálvez, B. G., Matías-Román, S., Yáñez-Mó, M., Sánchez-Madrid, F., & Arroyo, A. G. (2002). ECM regulates MT1-MMP localization with β1 or αvβ3 integrins at distinct cell compartments modulating its internalization and activity on human endothelial cells. *Journal of Cell Biology*, *159*(3), 509–521. https://doi.org/10.1083/JCB.200205026/VIDEO-1

Gálvez, B. G., Matías-Román, S., Yáñez-Mó, M., Vicente-Manzanares, M., Sánchez-Madrid, F., & Arroyo, A. G. (2004). Caveolae Are a Novel Pathway for Membrane-Type 1 Matrix Metalloproteinase Traffic in Human Endothelial Cells. *Molecular Biology of the Cell*, *15*(2), 678. https://doi.org/10.1091/MBC.E03-07-0516

Gao, H., Chakraborty, G., Zhang, Z., Akalay, I., Gadiya, M., Gao, Y., Sinha, S., Hu, J., Jiang, C., Akram, M., Brogi, E., Leitinger, B., & Giancotti, F. G. (2016). Multi-organ Site Metastatic Reactivation Mediated by Non-canonical Discoidin Domain Receptor 1 Signaling. *Cell*, *166*(1), 47–62. https://doi.org/10.1016/J.CELL.2016.06.009

Garner, O. B., Bush, K. T., Nigam, K. B., Yamaguchi, Y., Xu, D., Esko, J. D., & Nigam, S. K. (2011). Stage-dependent regulation of mammary ductal branching by heparan sulfate and HGF-cMet signaling. *Developmental Biology*, *355*(2), 394–403. https://doi.org/10.1016/J.YDBIO.2011.04.035

Gerdes, M. J., Gökmen-Polar, Y., Sui, Y., Pang, A. S., Laplante, N., Harris, A. L., Tan, P. H., Ginty, F., & Badve, S. S. (2018). Single-cell heterogeneity in ductal carcinoma in situ of breast. *Modern Pathology : An Official Journal of the United States and Canadian Academy of Pathology, Inc*, *31*(3), 406–417. https://doi.org/10.1038/MODPATHOL.2017.143

Ghersi, G., Zhao, Q., Salamone, M., Yeh, Y., Zucker, S., & Chen, W. T. (2006). The protease complex consisting of dipeptidyl peptidase IV and seprase plays a role in the migration and invasion of human endothelial cells in collagenous matrices. *Cancer Research*, *66*(9), 4652–4661. https://doi.org/10.1158/0008-5472.CAN-05-1245

Gingras, A. C., Gygi, S. P., Raught, B., Polakiewicz, R. D., Abraham, R. T., Hoekstra, M. F., Aebersold, R., & Sonenberg, N. (1999). Regulation of 4E-BP1 phosphorylation: a novel two-step mechanism. *Genes & Development*, *13*(11), 1422–1437. https://doi.org/10.1101/GAD.13.11.1422

Gingras, A. C., Raught, B., Gygi, S. P., Niedzwiecka, A., Miron, M., Burley, S. K., Polakiewicz, R. D., Wyslouch-Cieszynska, A., Aebersold, R., & Sonenberg, N. (2001). Hierarchical phosphorylation of the translation inhibitor 4E-BP1. *Genes & Development*, *15*(21), 2852–2864. https://doi.org/10.1101/GAD.912401

Gleixner, E. M., Canaud, G., Hermle, T., Guida, M. C., Kretz, O., Helmstädter, M., Huber, T. B., Eimer, S., Terzi, F., & Simons, M. (2014). V-ATPase/mTOR signaling regulates megalin-mediated apical endocytosis. *Cell Reports*, *8*(1), 10–19. https://doi.org/10.1016/J.CELREP.2014.05.035

Godet, I., Shin, Y. J., Ju, J. A., Ye, I. C., Wang, G., & Gilkes, D. M. (2019). Fate-mapping post-hypoxic tumor cells reveals a ROS-resistant phenotype that promotes metastasis. *Nature Communications 2019 10:1*, *10*(1), 1–18. https://doi.org/10.1038/s41467-019-12412-1

Goicoechea, S. M., Zinn, A., Awadia, S. S., Snyder, K., & Garcia-Mata, R. (2017). A RhoG-mediated signaling pathway that modulates invadopodia dynamics in breast cancer cells. *Journal of Cell Science*, *130*(6), 1064–1077. https://doi.org/10.1242/JCS.195552/VIDEO-7

Gollwitzer, P., Grützmacher, N., Wilhelm, S., Kümmel, D., & Demetriades, C. (2022). A Rag GTPase dimer code defines the regulation of mTORC1 by amino acids. *Nature Cell Biology 2022 24:9*, *24*(9), 1394–1406. https://doi.org/10.1038/S41556-022-00976-Y

Gouirand, V., Gicquel, T., Lien, E. C., Jaune-Pons, E., Costa, Q. da, Finetti, P., Metay, E., Duluc, C., Mayers, J. R., Audebert, S., Camoin, L., Borge, L., Rubis, M., Leca, J., Nigri, J., Bertucci, F., Dusetti, N., Iovanna, J. L., Tomasini, R., … Vasseur, S. (2022). Ketogenic HMG-CoA lyase and its product β-hydroxybutyrate promote pancreatic cancer progression. *The EMBO Journal*, *41*(9), e110466. https://doi.org/10.15252/EMBJ.2021110466

Gouirand, V., Guillaumond, F., & Vasseur, S. (2018). Influence of the tumor microenvironment on cancer cells metabolic reprogramming. In *Frontiers in Oncology* (Vol. 8, Issue APR). Frontiers Media S.A. https://doi.org/10.3389/fonc.2018.00117

Grafinger, O. R., Gorshtein, G., Stirling, T., Geddes-McAlister, J., & Coppolino, M. G. (2021). Inhibition of β1 integrin induces its association with MT1-MMP and decreases MT1-MMP internalization and cellular invasiveness. *Cellular Signalling*, *83*, 109984. https://doi.org/10.1016/J.CELLSIG.2021.109984

Grahammer, F., Ramakrishnan, S. K., Rinschen, M. M., Larionov, A. A., Syed, M., Khatib, H., Roerden, M., Sass, J. O., Helmstaedter, M., Osenberg, D., Kühne, L., Kretz, O., Wanner, N., Jouret, F., Benzing, T., Artunc, F., Huber, T. B., & Theilig, F. (2017). mTOR Regulates Endocytosis and Nutrient Transport in Proximal Tubular Cells. *Journal of the American Society of Nephrology : JASN*, *28*(1), 230–241. https://doi.org/10.1681/ASN.2015111224

Gramolelli, S., Cheng, J., Martinez-Corral, I., Vähä-Koskela, M., Elbasani, E., Kaivanto, E., Rantanen, V., Tuohinto, K., Hautaniemi, S., Bower, M., Haglund, C., Alitalo, K., Mäkinen, T., Petrova, T. v., Lehti, K., & Ojala, P. M. (2018). PROX1 is a transcriptional regulator of MMP14. *Scientific Reports*, *8*(1). https://doi.org/10.1038/S41598-018-27739-W

Gregor, M. F., Misch, E. S., Yang, L., Hummasti, S., Inouye, K. E., Lee, A.-H., Bierie, B., & Hotamisligil, G. S. (2013). The Role of Adipocyte XBP1 in Metabolic Regulation during Lactation. *Cell Reports*, *3*(5), 1430–1439. https://doi.org/10.1016/j.celrep.2013.03.042

Gross, J., & Lapierre, C. M. (1962, June). *COLLAGENOLYTIC ACTIVITY IN AMPHIBIAN TISSUES: A TISSUE CULTURE ASSAY - PMC*. Proc Natl Acad Sci U S A. https://doi.org/10.1073/pnas.48.6.1014

Guardia, C. M., Farías, G. G., Jia, R., Pu, J., & Bonifacino, J. S. (2016). BORC Functions Upstream of Kinesins 1 and 3 to Coordinate Regional Movement of Lysosomes along Different Microtubule Tracks. *Cell Reports*, *17*(8), 1950–1961. https://doi.org/10.1016/J.CELREP.2016.10.062

Guerrero-Navarro, L., Jansen-Dürr, P., & Cavinato, M. (2022). Age-Related Lysosomal Dysfunctions. *Cells 2022, Vol. 11, Page 1977*, *11*(12), 1977. https://doi.org/10.3390/CELLS11121977

Guertin, D. A., Stevens, D. M., Thoreen, C. C., Burds, A. A., Kalaany, N. Y., Moffat, J., Brown, M., Fitzgerald, K. J., & Sabatini, D. M. (2006). Ablation in mice of the mTORC components raptor, rictor, or mLST8 reveals that mTORC2 is required for signaling to Akt-FOXO and PKCalpha, but not S6K1. *Developmental Cell*, *11*(6), 859–871. https://doi.org/10.1016/J.DEVCEL.2006.10.007

Guimbal, S., Morel, A., Guérit, D., Chardon, M., Blangy, A., & Vives, V. (2019). Dock5 is a new regulator of microtubule dynamic instability in osteoclasts. *Biology of the Cell*, *111*(11), 271–283. https://doi.org/10.1111/boc.201900014

Győrffy, B. (2021). Survival analysis across the entire transcriptome identifies biomarkers with the highest prognostic power in breast cancer. *Computational and Structural Biotechnology Journal*, *19*, 4101–4109. https://doi.org/10.1016/J.CSBJ.2021.07.014

Haas, T. L., Stitelman, D., Davis, S. J., Apte, S. S., & Madri, J. A. (1999). Egr-1 Mediates Extracellular Matrix-driven Transcription of Membrane Type 1 Matrix Metalloproteinase in Endothelium*. *Journal of Biological Chemistry*, *274*, 22679–22685. https://doi.org/10.1074/jbc.274.32.22679

Hahn-Dantona, E., Ruiz, J. F., Bornstein, P., & Strickland, D. K. (2001). The low density lipoprotein receptor-related protein modulates levels of matrix metalloproteinase 9 (MMP-9) by mediating its cellular catabolism. *The Journal of Biological Chemistry*, *276*(18), 15498–15503. https://doi.org/10.1074/JBC.M100121200

Hakulinen, J., Sankkila, L., Sugiyama, N., Lehti, K., & Keski-Oja, J. (2008). Secretion of active membrane type 1 matrix metalloproteinase (MMP-14) into extracellular space in microvesicular exosomes. *Journal of Cellular Biochemistry*, *105*(5), 1211–1218. https://doi.org/10.1002/JCB.21923

Hammond, E., Khurana, A., Shridhar, V., & Dredge, K. (2014). The role of heparanase and sulfatases in the modification of heparan sulfate proteoglycans within the tumour microenvironment and opportunities for novel cancer therapeutics. *Frontiers in Oncology*, *4 JUL*, 195. https://doi.org/10.3389/FONC.2014.00195/BIBTEX

Hamurcu, Z., Delibaşı, N., Geçene, S., Şener, E. F., Dönmez-Altuntaş, H., Özkul, Y., Canatan, H., & Ozpolat, B. (2018). Targeting LC3 and Beclin-1 autophagy genes suppresses proliferation, survival, migration and invasion by inhibition of Cyclin-D1 and uPAR/Integrin β1/ Src signaling in triple negative breast cancer cells. *Journal of Cancer Research and Clinical Oncology*, *144*(3), 415–430. https://doi.org/10.1007/S00432-017-2557-5

Han, J., Li, E., Chen, L., Zhang, Y., Wei, F., Liu, J., Deng, H., & Wang, Y. (2015). The CREB coactivator CRTC2 controls hepatic lipid metabolism by regulating SREBP1. *Nature*, *524*(7564), 243–246. https://doi.org/10.1038/NATURE14557

Han, J., & Wang, Y. (2018). mTORC1 signaling in hepatic lipid metabolism. *Protein and Cell*, *9*(2), 145–151. https://doi.org/10.1007/S13238-017-0409-3/FIGURES/1

Hanahan, D., & Weinberg, R. A. (2011). Hallmarks of Cancer: The Next Generation. *Cell*, *144*(5), 646–674. https://doi.org/10.1016/j.cell.2011.02.013

Harper, K., Arsenault, D., Boulay-Jean, S., Lauzier, A., Lucien, F., & Dubois, C. M. (2010). Autotaxin promotes cancer invasion via the lysophosphatidic acid receptor 4: participation of the cyclic AMP/EPAC/Rac1 signaling pathway in invadopodia formation. *Cancer Research*, *70*(11), 4634–4643. https://doi.org/10.1158/0008-5472.CAN-09-3813

Hasegawa, J., Tokuda, E., Yao, Y., Sasaki, T., Inoki, K., & Weisman, L. S. (2022). PP2A-dependent TFEB activation is blocked by PIKfyve-induced mTORC1 activity. *Molecular Biology of the Cell*, *33*(3), ar26. https://doi.org/10.1091/MBC.E21-06-0309

Hashizume, H., Baluk, P., Morikawa, S., McLean, J. W., Thurston, G., Roberge, S., Jain, R. K., & McDonald, D. M. (2000). Openings between Defective Endothelial Cells Explain Tumor Vessel Leakiness. *The American Journal of Pathology*, *156*(4), 1363. https://doi.org/10.1016/S0002-9440(10)65006-7

Hastings, J. F., Skhinas, J. N., Fey, D., Croucher, D. R., & Cox, T. R. (2019). The extracellular matrix as a key regulator of intracellular signalling networks. *British Journal of Pharmacology*, *176*(1), 82–92. https://doi.org/10.1111/bph.14195

Hatem, R., el Botty, R., Chateau-Joubert, S., Servely, J. L., Labiod, D., de Plater, L., Assayag, F., Coussy, F., Callens, C., Vacher, S., Reyal, F., Cosulich, S., Diéras, V., Bièche, I., & Marangoni, E. (2016). Targeting mTOR pathway inhibits tumor growth in different molecular subtypes of triple-negative breast cancers. *Oncotarget*, *7*(30), 48206–48219. https://doi.org/10.18632/ONCOTARGET.10195

Heimhalt, M., Berndt, A., Wagstaff, J., Anandapadamanaban, M., Perisic, O., Maslen, S., McLaughlin, S., Yu, C. W. H., Masson, G. R., Boland, A., Ni, X., Yamashita, K., Murshudov, G. N., Skehel, M., Freund, S. M., & Williams, R. L. (2021). Bipartite binding and partial inhibition links deptor and mtor in a mutually antagonistic embrace. *ELife*, *10*. https://doi.org/10.7554/ELIFE.68799

Helmlinger, G., Yuan, F., Dellian, M., & Jain, R. K. (1997). Interstitial pH and pO2 gradients in solid tumors in vivo: high-resolution measurements reveal a lack of correlation. *Nature Medicine*, *3*(2), 177–182. https://doi.org/10.1038/NM0297-177

Hennig, K. M., Colombani, J., & Neufeld, T. P. (2006). TOR coordinates bulk and targeted endocytosis in the Drosophila melanogaster fat body to regulate cell growth. *The Journal of Cell Biology*, *173*(6), 963. https://doi.org/10.1083/JCB.200511140

Hida, K., & Maishi, N. (2018). Abnormalities of tumor endothelial cells and cancer progression. *Oral Science International*, *15*(1), 1–6. https://doi.org/10.1016/S1348-8643(17)30041-1

Holmbeck, K., Bianco, P., Caterina, J., Yamada, S., Kromer, M., Kuznetsov, S. A., Mankani, M., Gehron Robey, P., Poole, A. R., Pidoux, I., Ward, J. M., & Birkedal-Hansen, H. (1999). MT1-MMP-deficient mice develop dwarfism, osteopenia, arthritis, and connective tissue disease due to inadequate collagen turnover. *Cell*, *99*(1), 81–92. https://doi.org/10.1016/S0092-8674(00)80064-1

Hong, Z., Pedersen, N. M., Wang, L., Torgersen, M. L., Stenmark, H., & Raiborg, C. (2017). PtdIns3P controls mTORC1 signaling through lysosomal positioning. *Journal of Cell Biology*, *216*(12), 4217–4233. https://doi.org/10.1083/JCB.201611073

Horton, J. D., Goldstein, J. L., & Brown, M. S. (2002). SREBPs: activators of the complete program of cholesterol and fatty acid synthesis in the liver. *The Journal of Clinical Investigation*, *109*(9), 1125–1131. https://doi.org/10.1172/JCI15593

Hosokawa, N., Hara, T., Kaizuka, T., Kishi, C., Takamura, A., Miura, Y., Iemura, S. I., Natsume, T., Takehana, K., Yamada, N., Guan, J. L., Oshiro, N., & Mizushima, N. (2009). Nutrient-dependent mTORC1 association with the ULK1-Atg13-FIP200 complex required for autophagy. *Molecular Biology of the Cell*, *20*(7), 1981–1991. https://doi.org/10.1091/MBC.E08-12-1248

Hotary, K., Allen, E., Punturieri, A., Yana, I., & Weiss, S. J. (2000). Regulation of cell invasion and morphogenesis in a three-dimensional type I collagen matrix by membrane-type matrix metalloproteinases 1, 2, and 3. *The Journal of Cell Biology*, *149*(6), 1309–1323. https://doi.org/10.1083/JCB.149.6.1309

Hovey, R. C., & Aimo, L. (2010a). Diverse and Active Roles for Adipocytes During Mammary Gland Growth and Function. *Journal of Mammary Gland Biology and Neoplasia*, *15*(3), 279–290. https://doi.org/10.1007/s10911-010-9187-8

Hovey, R. C., & Aimo, L. (2010b). Diverse and Active Roles for Adipocytes During Mammary Gland Growth and Function. *Journal of Mammary Gland Biology and Neoplasia*, *15*(3), 279–290. https://doi.org/10.1007/s10911-010-9187-8

Hynes, R. O. (2009). The Extracellular Matrix: Not Just Pretty Fibrils. *Science*, *326*(5957), 1216–1219. https://doi.org/10.1126/science.1176009

Iizuka, S., Leon, R. P., Gribbin, K. P., Zhang, Y., Navarro, J., Smith, R., Devlin, K., Wang, L. G., Gibbs, S. L., Korkola, J., Nan, X., & Courtneidge, S. A. (2020). Crosstalk between invadopodia and the extracellular matrix. *European Journal of Cell Biology*, *99*(7), 151122. https://doi.org/10.1016/J.EJCB.2020.151122

Ilha, J., do Espírito-Santo, C. C., & de Freitas, G. R. (2018). mTOR signaling pathway and protein synthesis: From training to aging and muscle autophagy. *Advances in Experimental Medicine and Biology*, *1088*, 139–151. https://doi.org/10.1007/978-981-13-1435-3_7

Infante, E., Castagnino, A., Ferrari, R., Monteiro, P., Agüera-González, S., Paul-Gilloteaux, P., Domingues, M. J., Maiuri, P., Raab, M., Shanahan, C. M., Baffet, A., Piel, M., Gomes, E. R., & Chavrier, P. (2018). LINC complex-Lis1 interplay controls MT1-MMP matrix digest-on-demand response for confined tumor cell migration. *Nature Communications*, *9*(1). https://doi.org/10.1038/s41467-018-04865-7

Inoki, K., Zhu, T., & Guan, K. L. (2003). TSC2 mediates cellular energy response to control cell growth and survival. *Cell*, *115*(5), 577–590. https://doi.org/10.1016/S0092-8674(03)00929-2

Itoh, Y. (2015). Membrane-type matrix metalloproteinases: Their functions and regulations. *Matrix Biology*, *44–46*, 207–223. https://doi.org/10.1016/J.MATBIO.2015.03.004

Itoh, Y., Takamura, A., Ito, N., Maru, Y., Sato, H., Suenaga, N., Aoki, T., & Seiki, M. (2001). Homophilic complex formation of MT1-MMP facilitates proMMP-2 activation on the cell surface and promotes tumor cell invasion. *The EMBO Journal*, *20*(17), 4782–4793. https://doi.org/10.1093/EMBOJ/20.17.4782

Jain, R. K., Martin, J. D., & Stylianopoulos, T. (2014a). The role of mechanical forces in tumor growth and therapy. *Annual Review of Biomedical Engineering*, *16*, 321. https://doi.org/10.1146/ANNUREV-BIOENG-071813-105259

Jain, R. K., Martin, J. D., & Stylianopoulos, T. (2014b). The Role of Mechanical Forces in Tumor Growth and Therapy. *Annual Review of Biomedical Engineering*, *16*(1), 321–346. https://doi.org/10.1146/annurev-bioeng-071813-105259

Javed, A., & Lteif, A. (2013). Development of the Human Breast. *Seminars in Plastic Surgery*, *27*(01), 005–012. https://doi.org/10.1055/s-0033-1343989

Jayadev, R., & Sherwood, D. R. (2017). Basement membranes. *Current Biology*, *27*(6), R207–R211. https://doi.org/10.1016/J.CUB.2017.02.006

Jeannot, P., Nowosad, A., Perchey, R., Callot, C., Bennana, E., Katsube, T., Mayeux, P., Guillonneau, F., Manenti, S., & Besson, A. (2017). P27kip1 promotes invadopodia turnover and invasion through the regulation of the PAK1/cortactin pathway. *ELife*, *6*. https://doi.org/10.7554/ELIFE.22207

Jeon, T. il, & Osborne, T. F. (2012). SREBPs: metabolic integrators in physiology and metabolism. *Trends in Endocrinology & Metabolism*, *23*(2), 65–72. https://doi.org/10.1016/J.TEM.2011.10.004

Jia, H., Janjanam, J., Wu, S. C., Wang, R., Pano, G., Celestine, M., Martinot, O., Breeze-Jones, H., Clayton, G., Garcin, C., Shirinifard, A., Zaske, A. M., Finkelstein, D., & Labelle, M. (2019). The tumor cell-secreted matricellular protein WISP1 drives pro-metastatic collagen linearization. *The EMBO Journal*, *38*(16), e101302. https://doi.org/10.15252/EMBJ.2018101302

Jiang, A., Lehti, K., Wang, X., Weiss, S. J., Keski-Oja, J., & Pei, D. (2001). Regulation of membrane-type matrix metalloproteinase 1 activity by dynamin-mediated endocytosis. *Proceedings of the National Academy of Sciences of the United States of America*, *98*(24), 13693. https://doi.org/10.1073/PNAS.241293698

Jiang, H., & Li, H. (2021). Prognostic values of tumoral MMP2 and MMP9 overexpression in breast cancer: a systematic review and meta-analysis. *BMC Cancer*, *21*(1), 1–13. https://doi.org/10.1186/S12885-021-07860-2/FIGURES/5

Jin, M., Shirazinejad, C., Wang, B., Yan, A., Schöneberg, J., Upadhyayula, S., Xu, K., & Drubin, D. G. (2021). Rescue of stalled clathrin-mediated endocytosis by asymmetric Arp2/3-mediated actin assembly. *BioRxiv*, 2021.07.16.452693. https://doi.org/10.1101/2021.07.16.452693

Jo, M., Lester, R. D., Montel, V., Eastman, B., Takimoto, S., & Gonias, S. L. (2009). Reversibility of Epithelial-Mesenchymal Transition (EMT) Induced in Breast Cancer Cells by Activation of Urokinase Receptor-dependent Cell Signaling. *Journal of Biological Chemistry*, *284*(34), 22825–22833. https://doi.org/10.1074/jbc.M109.023960

Johnson, M. C. (2010). Anatomy and Physiology of the Breast. In *Management of Breast Diseases* (pp. 1–36). Springer Berlin Heidelberg. https://doi.org/10.1007/978-3-540-69743-5_1

Joseph, C., Alsaleem, M., Orah, N., Narasimha, P. L., Miligy, I. M., Kurozumi, S., Ellis, I. O., Mongan, N. P., Green, A. R., & Rakha, E. A. (2020). Elevated MMP9 expression in breast cancer is a predictor of shorter patient survival. *Breast Cancer Research and Treatment*, *182*(2), 267. https://doi.org/10.1007/S10549-020-05670-X

Kajiho, H., Kajiho, Y., Frittoli, E., Confalonieri, S., Bertalot, G., Viale, G., Paolo, P., Fiore, D., Oldani, A., Garre, M., Beznoussenko, G. v, Palamidessi, A., Vecchi, M., Chavrier, P., Perez, F., & Scita, G. (2016). RAB2A controls MT1-MMP endocytic and E-cadherin polarized Golgi trafficking to promote invasive breast cancer programs. *EMBO Reports*, *17*(7), 1061–1080. https://doi.org/10.15252/EMBR.201642032

Kalluri, R., & Cosgrove, D. (2000). Assembly of Type IV Collagen: INSIGHTS FROM α3(IV) COLLAGEN-DEFICIENT MICE. *Journal of Biological Chemistry*, *275*(17), 12719–12724. https://doi.org/10.1074/JBC.275.17.12719

Kamat, A. A., Fletcher, M., Gruman, L. M., Mueller, P., Lopez, A., Landen, C. N., Han, L., Gershenson, D. M., & Sood, A. K. (2006). The Clinical Relevance of Stromal Matrix Metalloproteinase Expression in Ovarian Cancer. *Clinical Cancer Research : An Official Journal of the American Association for Cancer Research*, *12*(6), 1707. https://doi.org/10.1158/1078-0432.CCR-05-2338

Kamphorst, J. J., Nofal, M., Commisso, C., Hackett, S. R., Lu, W., Grabocka, E., vander Heiden, M. G., Miller, G., Drebin, J. A., Bar-Sagi, D., Thompson, C. B., & Rabinowitz, J. D. (2015). Human pancreatic cancer tumors are nutrient poor and tumor cells actively scavenge extracellular protein. *Cancer Research*, *75*(3), 544–553. https://doi.org/10.1158/0008-5472.CAN-14-2211

Kang, H., Hong, Z., Zhong, M., Klomp, J., Bayless, K. J., Mehta, D., Karginov, A. v., Hu, G., & Malik, A. B. (2019). Piezo1 mediates angiogenesis through activation of MT1-MMP signaling. *American Journal of Physiology - Cell Physiology*, *316*(1), C92–C103.

https://doi.org/10.1152/AJPCELL.00346.2018/ASSET/IMAGES/LARGE/ZH0001198361 0007.JPEG
Kauppila, S., Stenbäck, F., Risteli, J., Jukkola, A., & Risteli, L. (1998). Aberrant type I and type III collagen gene expression in human breast cancerin vivo. *The Journal of Pathology*, *186*(3), 262–268. https://doi.org/10.1002/(SICI)1096-9896(1998110)186:3<262::AID-PATH191>3.0.CO;2-3
Kay, E. J., Paterson, K., Riero-Domingo, C., Sumpton, D., Däbritz, J. H. M., Tardito, S., Boldrini, C., Hernandez-Fernaud, J. R., Athineos, D., Dhayade, S., Stepanova, E., Gjerga, E., Neilson, L. J., Lilla, S., Hedley, A., Koulouras, G., McGregor, G., Jamieson, C., Johnson, R. M., … Zanivan, S. (2022). Cancer-associated fibroblasts require proline synthesis by PYCR1 for the deposition of pro-tumorigenic extracellular matrix. *Nature Metabolism*, *4*(6), 693–710. https://doi.org/10.1038/s42255-022-00582-0
Kelm, J. M., Timmins, N. E., Brown, C. J., Fussenegger, M., & Nielsen, L. K. (2003). Method for generation of homogeneous multicellular tumor spheroids applicable to a wide variety of cell types. *Biotechnology and Bioengineering*, *83*(2), 173–180. https://doi.org/10.1002/BIT.10655
Keshwani, M. M., von Daake, S., Newton, A. C., Harris, T. K., & Taylor, S. S. (2011). Hydrophobic Motif Phosphorylation Is Not Required for Activation Loop Phosphorylation of p70 Ribosomal Protein S6 Kinase 1 (S6K1) *. *Journal of Biological Chemistry*, *286*(26), 23552–23558. https://doi.org/10.1074/JBC.M111.258004
Kim, J., & Guan, K. L. (2019). mTOR as a central hub of nutrient signalling and cell growth. In *Nature Cell Biology* (Vol. 21, Issue 1, pp. 63–71). Nature Publishing Group. https://doi.org/10.1038/s41556-018-0205-1
Kim, J., Kundu, M., Viollet, B., & Guan, K. L. (2011). AMPK and mTOR regulate autophagy through direct phosphorylation of Ulk1. *Nature Cell Biology 2011 13:2*, *13*(2), 132–141. https://doi.org/10.1038/ncb2152
Klymenko, Y., Kim, O., Loughran, E., Yang, J., Lombard, R., Alber, M., & Stack, M. S. (2017). Cadherin composition and multicellular aggregate invasion in organotypic models of epithelial ovarian cancer intraperitoneal metastasis. *Oncogene*, *36*(42), 5840–5851. https://doi.org/10.1038/ONC.2017.171
Knapinska, A. M., & Fields, G. B. (2019). The Expanding Role of MT1-MMP in Cancer Progression. *Pharmaceuticals*, *12*(2). https://doi.org/10.3390/PH12020077
Korolchuk, V. I., Saiki, S., Lichtenberg, M., Siddiqi, F. H., Roberts, E. A., Imarisio, S., Jahreiss, L., Sarkar, S., Futter, M., Menzies, F. M., O'Kane, C. J., Deretic, V., & Rubinsztein, D. C. (2011). Lysosomal positioning coordinates cellular nutrient responses. *Nature Cell Biology 2011 13:4*, *13*(4), 453–460. https://doi.org/10.1038/NCB2204
Kühn, K. (1995). Basement membrane (type IV) collagen. *Matrix Biology*, *14*(6), 439–445. https://doi.org/10.1016/0945-053X(95)90001-2
Kuriyama, S., Yoshida, M., Yano, S., Aiba, N., Kohno, T., Minamiya, Y., Goto, A., & Tanaka, M. (2016). LPP inhibits collective cell migration during lung cancer dissemination. *Oncogene*, *35*(8), 952–964. https://doi.org/10.1038/ONC.2015.155
Labrecque, L., Nyalendo, C., Langlois, S., Durocher, Y., Roghi, C., Murphy, G., Gingras, D., & Béliveau, R. (2004). Src-mediated tyrosine phosphorylation of caveolin-1 induces its association with membrane type 1 matrix metalloproteinase. *The Journal of Biological Chemistry*, *279*(50), 52132–52140. https://doi.org/10.1074/JBC.M409617200
Lai, J. P., Thompson, J. R., Sandhu, D. S., & Roberts, L. R. (2008). Heparin-degrading sulfatases in hepatocellular carcinoma: roles in pathogenesis and therapy targets. *Future Oncology (London, England)*, *4*(6), 803–814. https://doi.org/10.2217/14796694.4.6.803
Lamming, D. W., Ye, L., Katajisto, P., Goncalves, M. D., Saitoh, M., Stevens, D. M., Davis, J. G., Salmon, A. B., Richardson, A., Ahima, R. S., Guertin, D. A., Sabatini, D. M., & Baur, J. A. (2012). Rapamycin-induced insulin resistance is mediated by mTORC2 loss and uncoupled from longevity. *Science (New York, N.Y.)*, *335*(6076), 1638–1643. https://doi.org/10.1126/SCIENCE.1215135

Laplante, M., & Sabatini, D. M. (2012). MTOR signaling in growth control and disease. In *Cell* (Vol. 149, Issue 2, pp. 274–293). Elsevier B.V. https://doi.org/10.1016/j.cell.2012.03.017
Laronha, H., & Caldeira, J. (2020). Structure and Function of Human Matrix Metalloproteinases. *Cells*, *9*(5). https://doi.org/10.3390/CELLS9051076
Lawrence, R. E., Fromm, S. A., Fu, Y., Yokom, A. L., Kim, D. J., Thelen, A. M., Young, L. N., Lim, C. Y., Samelson, A. J., Hurley, J. H., & Zoncu, R. (2019). Structural mechanism of a Rag GTPase activation checkpoint by the lysosomal folliculin complex. *Science*, *366*(6468), 971–977. https://doi.org/10.1126/SCIENCE.AAX0364/SUPPL_FILE/AAX0364S1.MP4
Lee, B., Barretto, E. C., & Grewal, S. S. (2019). TORC1 modulation in adipose tissue is required for organismal adaptation to hypoxia in Drosophila. *Nature Communications 2019 10:1*, *10*(1), 1–14. https://doi.org/10.1038/s41467-019-09643-7
Lee, H., Sodek, K. L., Hwang, Q., Brown, T. J., Ringuette, M., & Sodek, J. (2007). Phagocytosis of collagen by fibroblasts and invasive cancer cells is mediated by MT1-MMP. *Biochemical Society Transactions*, *35*(4), 704–706. https://doi.org/10.1042/BST0350704
Lee, J., Liu, H., Pearson, T., Iwase, T., Fuson, J., Lalani, A. S., Eli, L. D., Diala, I., Tripathy, D., Lim, B., & Ueno, N. T. (2021). PI3K and MAPK Pathways as Targets for Combination with the Pan-HER Irreversible Inhibitor Neratinib in HER2-Positive Breast Cancer and TNBC by Kinome RNAi Screening. *Biomedicines*, *9*(7). https://doi.org/10.3390/BIOMEDICINES9070740
Lee, W., & McCulloch, C. A. G. (1997). Deregulation of collagen phagocytosis in aging human fibroblasts: Effects of integrin expression and cell cycle. *Experimental Cell Research*, *237*(2), 383–393. https://doi.org/10.1006/excr.1997.3802
Lee, W., Sodek, J., & McCulloch, C. A. (1996). Role of integrins in regulation of collagen phagocytosis by human fibroblasts. *Journal of Cellular Physiology*, *168*(3), 695–704. https://doi.org/10.1002/(SICI)1097-4652(199609)168:3<695::AID-JCP22>3.0.CO;2-X
Lee, Y.-H., Albig, A. R., Regner, M., Schiemann, B. J., & Schiemann, W. P. (2008). Fibulin-5 initiates epithelial-mesenchymal transition (EMT) and enhances EMT induced by TGF- in mammary epithelial cells via a MMP-dependent mechanism. *Carcinogenesis*, *29*(12), 2243–2251. https://doi.org/10.1093/carcin/bgn199
Levental, K. R., Yu, H., Kass, L., Lakins, J. N., Egeblad, M., Erler, J. T., Fong, S. F. T., Csiszar, K., Giaccia, A., Weninger, W., Yamauchi, M., Gasser, D. L., & Weaver, V. M. (2009). Matrix Crosslinking Forces Tumor Progression by Enhancing Integrin Signaling. *Cell*, *139*(5), 891–906. https://doi.org/10.1016/J.CELL.2009.10.027
Li, L., Friedrichsen, H. J., Andrews, S., Picaud, S., Volpon, L., Ngeow, K., Berridge, G., Fischer, R., Borden, K. L. B., Filippakopoulos, P., & Goding, C. R. (2018). A TFEB nuclear export signal integrates amino acid supply and glucose availability. *Nature Communications 2018 9:1*, *9*(1), 1–15. https://doi.org/10.1038/s41467-018-04849-7
Liang, N., Zhang, C., Dill, P., Panasyuk, G., Pion, D., Koka, V., Gallazzini, M., Olson, E. N., Lam, H., Henske, E. P., Dong, Z., Apte, U., Pallet, N., Johnson, R. L., Terzi, F., Kwiatkowski, D. J., Scoazec, J. Y., Martignoni, G., & Pende, M. (2014). Regulation of YAP by mTOR and autophagy reveals a therapeutic target of tuberous sclerosis complex. *Journal of Experimental Medicine*, *211*(11), 2249–2263. https://doi.org/10.1084/JEM.20140341
Lin, C. W., Sun, M. S., Liao, M. Y., Chung, C. H., Chi, Y. H., Chiou, L. T., Yu, J., Lou, K. L., & Wu, H. C. (2014). Podocalyxin-like 1 promotes invadopodia formation and metastasis through activation of Rac1/Cdc42/cortactin signaling in breast cancer cells. *Carcinogenesis*, *35*(11), 2425–2435. https://doi.org/10.1093/CARCIN/BGU139
Linder, S., & Kopp, P. (2005). Podosomes at a glance. *Journal of Cell Science*, *118*(10), 2079–2082. https://doi.org/10.1242/JCS.02390
Linder, S., & Scita, G. (2015). RABGTPases in MT1-MMP trafficking and cell invasion: Physiology versus pathology. *Small GTPases*, *6*(3), 145. https://doi.org/10.4161/21541248.2014.985484

Liu, G. Y., & Sabatini, D. M. (2020). mTOR at the nexus of nutrition, growth, ageing and disease. In *Nature Reviews Molecular Cell Biology* (Vol. 21, Issue 4, pp. 183–203). Nature Research. https://doi.org/10.1038/s41580-019-0199-y

Liu, L., Cash, T. P., Jones, R. G., Keith, B., Thompson, C. B., & Simon, M. C. (2006). Hypoxia-induced energy stress regulates mRNA translation and cell growth. *Molecular Cell*, *21*(4), 521–531. https://doi.org/10.1016/J.MOLCEL.2006.01.010

Liu, S., Dontu, G., & Wicha, M. S. (2005). Mammary stem cells, self-renewal pathways, and carcinogenesis. *Breast Cancer Research*, *7*(3), 86. https://doi.org/10.1186/bcr1021

Lodillinsky, C., Fuhrmann, L., Irondelle, M., Pylypenko, O., Li, X. Y., Bonsang-Kitzis, H., Reyal, F., Vacher, S., Calmel, C., de Wever, O., Bièche, I., Lacombe, M. L., Eiján, A. M., Houdusse, A., Vincent-Salomon, A., Weiss, S. J., Chavrier, P., & Boissan, M. (2021). Metastasis-suppressor NME1 controls the invasive switch of breast cancer by regulating MT1-MMP surface clearance. *Oncogene*, *40*(23), 4019–4032. https://doi.org/10.1038/S41388-021-01826-1

Lodillinsky, C., Infante, E., Guichard, A., Chaligné, R., Fuhrmann, L., Cyrta, J., Irondelle, M., Lagoutte, E., Vacher, S., Bonsang-Kitzis, H., Glukhova, M., Reyal, F., Bièche, I., Vincent-Salomon, A., & Chavrier, P. (2016). p63/MT1-MMP axis is required for in situ to invasive transition in basal-like breast cancer. *Oncogene*, *35*(3), 344–357. https://doi.org/10.1038/onc.2015.87

Lohi, J., Lehti, K., Valtanen, H., Parks, W. C., & Keski-Oja, J. (2000). Structural analysis and promoter characterization of the human membrane-type matrix metalloproteinase-1 (MT1-MMP) gene. *Gene*, *242*(1–2), 75–86. https://doi.org/10.1016/S0378-1119(99)00549-1

Lugano, R., Ramachandran, M., & Dimberg, A. (2020). Tumor angiogenesis: causes, consequences, challenges and opportunities. *Cellular and Molecular Life Sciences*, *77*(9), 1745–1770. https://doi.org/10.1007/S00018-019-03351-7/FIGURES/3

Macpherson, I. R., Rainero, E., Mitchell, L. E., van den Berghe, P. V. E., Speirs, C., Dozynkiewicz, M. A., Chaudhary, S., Kalna, G., Edwards, J., Timpson, P., & Norman, J. C. (2014). CLIC3 controls recycling of late endosomal MT1-MMP and dictates invasion and metastasis in breast cancer. *Journal of Cell Science*, *127*(18), 3893–3901. https://doi.org/10.1242/JCS.135947/VIDEO-5

Mantuano, E., Inoue, G., Li, X., Takahashi, K., Gaultier, A., Gonias, S. L., & Campana, W. M. (2008). The hemopexin domain of matrix metalloproteinase-9 activates cell signaling and promotes migration of schwann cells by binding to low-density lipoprotein receptor-related protein. *The Journal of Neuroscience : The Official Journal of the Society for Neuroscience*, *28*(45), 11571–11582. https://doi.org/10.1523/JNEUROSCI.3053-08.2008

Maquoi, E., Frankenne, F., Baramova, E., Munaut, C., Sounni, N. E., Remacle, A., Noël, A., Murphy, G., & Foidart, J. M. (2000). Membrane type 1 matrix metalloproteinase-associated degradation of tissue inhibitor of metalloproteinase 2 in human tumor cell lines. *The Journal of Biological Chemistry*, *275*(15), 11368–11378. https://doi.org/10.1074/JBC.275.15.11368

Marat, A. L., Wallroth, A., Lo, W. T., Müller, R., Norata, G. D., Falasca, M., Schultz, C., & Haucke, V. (2017). mTORC1 activity repression by late endosomal phosphatidylinositol 3,4-bisphosphate. *Science*, *356*(6341), 968–972. https://doi.org/10.1126/SCIENCE.AAF8310

Marchesin, V., Castro-Castro, A., Lodillinsky, C., Castagnino, A., Cyrta, J., Bonsang-Kitzis, H., Fuhrmann, L., Irondelle, M., Infante, E., Montagnac, G., Reyal, F., Vincent-Salomon, A., & Chavrier, P. (2015). ARF6-JIP3/4 regulate endosomal tubules for MT1-MMP exocytosis in cancer invasion. *Journal of Cell Biology*, *211*(2), 339–358. https://doi.org/10.1083/JCB.201506002/VIDEO-3

Marrero-Diaz, R., Bravo-Cordero, J. J., Megìas, D., Garcìa, M. A., Bartolomé, R. A., Teixido, J., & Montoya, M. C. (2009). Polarized MT1-MMP-CD44 interaction and CD44 cleavage during cell retraction reveal an essential role for MT1-MMP in CD44-mediated invasion. *Cell Motility and the Cytoskeleton*, *66*(1), 48–61. https://doi.org/10.1002/CM.20325

Marsh, T., Kenific, C. M., Suresh, D., Gonzalez, H., Shamir, E. R., Mei, W., Tankka, A., Leidal, A. M., Kalavacherla, S., Woo, K., Werb, Z., & Debnath, J. (2020). Autophagic Degradation of NBR1 Restricts Metastatic Outgrowth during Mammary Tumor Progression. *Developmental Cell*, *52*(5), 591-604.e6. https://doi.org/10.1016/J.DEVCEL.2020.01.025

Marsh, T., Tolani, B., & Debnath, J. (2021). *The pleiotropic functions of autophagy in metastasis*. https://doi.org/10.1242/jcs.247056

Martin, M. D., Carter, K. J., Jean-Philippe, S. R., Chang, M., Mobashery, S., Thiolloy, S., Lynch, C. C., Matrisian, L. M., & Fingleton, B. (2008). Effect of Ablation or Inhibition of Stromal Matrix Metalloproteinase-9 on Lung Metastasis in a Breast Cancer Model Is Dependent on Genetic Background. *Cancer Research*, *68*(15), 6251–6259. https://doi.org/10.1158/0008-5472.CAN-08-0537

Martina, J. A., Chen, Y., Gucek, M., & Puertollano, R. (2012). MTORC1 functions as a transcriptional regulator of autophagy by preventing nuclear transport of TFEB. *Autophagy*, *8*(6), 903–914. https://doi.org/10.4161/auto.19653

Martina, J. A., & Puertollano, R. (2013). Rag GTPases mediate amino acid-dependent recruitment of TFEB and MITF to lysosomes. *Journal of Cell Biology*, *200*(4), 475–491. https://doi.org/10.1083/jcb.201209135

Martinella-Catusse, C., Polette, M., Noel, A., Gilles, C., Dehan, P., Munaut, C., Colige, A., Volders, L., Monboisse, J. C., Foidart, J. M., & Birembaut, P. (2001). Down-Regulation of MT1-MMP Expression by the α3 Chain of Type IV Collagen Inhibits Bronchial Tumor Cell Line Invasion. *Laboratory Investigation 2001 81:2*, *81*(2), 167–175. https://doi.org/10.1038/labinvest.3780224

Masi, I., Caprara, V., Bagnato, A., & Rosanò, L. (2020). Tumor Cellular and Microenvironmental Cues Controlling Invadopodia Formation. *Frontiers in Cell and Developmental Biology*, *8*. https://doi.org/10.3389/FCELL.2020.584181

Medina, D. L., di Paola, S., Peluso, I., Armani, A., de Stefani, D., Venditti, R., Montefusco, S., Scotto-Rosato, A., Prezioso, C., Forrester, A., Settembre, C., Wang, W., Gao, Q., Xu, H., Sandri, M., Rizzuto, R., de Matteis, M. A., & Ballabio, A. (2015a). Lysosomal calcium signalling regulates autophagy through calcineurin and TFEB. *Nature Cell Biology 2014 17:3*, *17*(3), 288–299. https://doi.org/10.1038/ncb3114

Medina, D. L., di Paola, S., Peluso, I., Armani, A., de Stefani, D., Venditti, R., Montefusco, S., Scotto-Rosato, A., Prezioso, C., Forrester, A., Settembre, C., Wang, W., Gao, Q., Xu, H., Sandri, M., Rizzuto, R., de Matteis, M. A., & Ballabio, A. (2015b). Lysosomal calcium signalling regulates autophagy through calcineurin and TFEB. *Nature Cell Biology*, *17*(3), 288–299. https://doi.org/10.1038/ncb3114

Medina, D. L., Fraldi, A., Bouche, V., Annunziata, F., Mansueto, G., Spampanato, C., Puri, C., Pignata, A., Martina, J. A., Sardiello, M., Palmieri, M., Polishchuk, R., Puertollano, R., & Ballabio, A. (2011). Transcriptional activation of lysosomal exocytosis promotes cellular clearance. *Developmental Cell*, *21*(3), 421–430. https://doi.org/10.1016/j.devcel.2011.07.016

Mei, K., & Guo, W. (2018). The exocyst complex. *Current Biology*, *28*, R922–R925. https://doi.org/10.1016/j.cub.2018.06.042

Meng, J., & Ferguson, S. M. (2018). GATOR1-dependent recruitment of FLCN–FNIP to lysosomes coordinates Rag GTPase heterodimer nucleotide status in response to amino acids. *Journal of Cell Biology*, *217*(8), 2765–2776. https://doi.org/10.1083/JCB.201712177

Menon, S., Dibble, C. C., Talbott, G., Hoxhaj, G., Valvezan, A. J., Takahashi, H., Cantley, L. C., & Manning, B. D. (2014). Spatial control of the TSC complex integrates insulin and nutrient regulation of mTORC1 at the lysosome. *Cell*, *156*(4), 771–785. https://doi.org/10.1016/j.cell.2013.11.049

Mienaltowski, M. J., Gonzales, N. L., Beall, J. M., & Pechanec, M. Y. (2021). *Basic Structure, Physiology, and Biochemistry of Connective Tissues and Extracellular Matrix Collagens* (pp. 5–43). https://doi.org/10.1007/978-3-030-80614-9_2

Miller, F. R., Santner, S. J., Tait, L., & Dawson, P. J. (2000). MCF10DCIS.com Xenograft Model of Human Comedo Ductal Carcinoma In Situ. *JNCI: Journal of the National Cancer Institute*, *92*(14), 1185a–11186. https://doi.org/10.1093/JNCI/92.14.1185A

Miricescu, D., Totan, A., Stanescu-Spinu, I. I., Badoiu, S. C., Stefani, C., & Greabu, M. (2020). PI3K/AKT/mTOR Signaling Pathway in Breast Cancer: From Molecular Landscape to Clinical Aspects. *International Journal of Molecular Sciences*, *22*(1), 1–24. https://doi.org/10.3390/IJMS22010173

Miyagawa, T., Hasegawa, K., Aoki, Y., Watanabe, T., Otagiri, Y., Arasaki, K., Wakana, Y., Asano, K., Tanaka, M., Yamaguchi, H., Tagaya, M., & Inoue, H. (2019). MT1-MMP recruits the ER-Golgi SNARE Bet1 for efficientMT1-MMP transport to the plasmamembrane. *Journal of Cell Biology*, *218*(10), 3355–3371. https://doi.org/10.1083/JCB.201808149/VIDEO-5

Moavero, R., Mühlebner, A., Luinenburg, M. J., Craiu, D., Aronica, E., & Curatolo, P. (2022). Genetic pathogenesis of the epileptogenic lesions in Tuberous Sclerosis Complex: Therapeutic targeting of the mTOR pathway. *Epilepsy & Behavior*, *131*. https://doi.org/10.1016/J.YEBEH.2020.107713

Montagnac, G., Sibarita, J. B., Loubéry, S., Daviet, L., Romao, M., Raposo, G., & Chavrier, P. (2009). ARF6 Interacts with JIP4 to control a motor switch mechanism regulating endosome traffic in cytokinesis. *Current Biology : CB*, *19*(3), 184–195. https://doi.org/10.1016/J.CUB.2008.12.043

Monteiro, P., Rossé, C., Castro-Castro, A., Irondelle, M., Lagoutte, E., Paul-Gilloteaux, P., Desnos, C., Formstecher, E., Darchen, F., Perrais, D., Gautreau, A., Hertzog, M., & Chavrier, P. (2013). Endosomal WASH and exocyst complexes control exocytosis of MT1-MMP at invadopodia. *Journal of Cell Biology*, *203*(6), 1063–1079. https://doi.org/10.1083/jcb.201306162

Moreno-Layseca, P., Icha, J., Hamidi, H., & Ivaska, J. (2019). Integrin trafficking in cells and tissues. *Nature Cell Biology*, *21*(2), 122. https://doi.org/10.1038/S41556-018-0223-Z

Moshfegh, Y., Bravo-Cordero, J. J., Miskolci, V., Condeelis, J., & Hodgson, L. (2014). A Trio-Rac1-Pak1 signalling axis drives invadopodia disassembly. *Nature Cell Biology*, *16*(6), 571–583. https://doi.org/10.1038/NCB2972

Mowers, E. E., Sharifi, M. N., & Macleod, K. F. (2016). Autophagy in cancer metastasis. *Oncogene 2017 36:12*, *36*(12), 1619–1630. https://doi.org/10.1038/onc.2016.333

Mrozik, K. M., Blaschuk, O. W., Cheong, C. M., Zannettino, A. C. W., & Vandyke, K. (2018). N-cadherin in cancer metastasis, its emerging role in haematological malignancies and potential as a therapeutic target in cancer. *BMC Cancer*, *18*(1). https://doi.org/10.1186/S12885-018-4845-0

Mueller, M. M., & Fusenig, N. E. (2004). Friends or foes — bipolar effects of the tumour stroma in cancer. *Nature Reviews Cancer*, *4*(11), 839–849. https://doi.org/10.1038/nrc1477

Müller, S., Sindikubwabo, F., Cañeque, T., Lafon, A., Versini, A., Lombard, B., Loew, D., Wu, T. di, Ginestier, C., Charafe-Jauffret, E., Durand, A., Vallot, C., Baulande, S., Servant, N., & Rodriguez, R. (2020). CD44 regulates epigenetic plasticity by mediating iron endocytosis. *Nature Chemistry 2020 12:10*, *12*(10), 929–938. https://doi.org/10.1038/s41557-020-0513-5

Mundo, W., Wolfson, G., Moore, L. G., Houck, J. A., Park, D., & Julian, C. G. (2021). Hypoxia-induced inhibition of mTORC1 activity in the developing lung: A possible mechanism for the developmental programming of pulmonary hypertension. *American Journal of Physiology - Heart and Circulatory Physiology*, *320*(3), H980–H990. https://doi.org/10.1152/AJPHEART.00520.2020/ASSET/IMAGES/LARGE/AJ-AHRT210030F005.JPEG

Muñoz-Nájar, U. M., Neurath, K. M., Vumbaca, F., & Claffey, K. P. (2006). Hypoxia stimulates breast carcinoma cell invasion through MT1-MMP and MMP-2 activation. *Oncogene*, *25*(16), 2379–2392. https://doi.org/10.1038/sj.onc.1209273

Muranen, T., Iwanicki, M. P., Curry, N. L., Hwang, J., DuBois, C. D., Coloff, J. L., Hitchcock, D. S., Clish, C. B., Brugge, J. S., & Kalaany, N. Y. (2017). Starved epithelial cells uptake

extracellular matrix for survival. *Nature Communications*, *8*. https://doi.org/10.1038/ncomms13989

Murphy, D. A., & Courtneidge, S. A. (2011). The “ins” and “outs” of podosomes and invadopodia: characteristics, formation and function. *Nature Reviews Molecular Cell Biology 2011 12:7*, *12*(7), 413–426. https://doi.org/10.1038/nrm3141

Musa, J., Orth, M. F., Dallmayer, M., Baldauf, M., Pardo, C., Rotblat, B., Kirchner, T., Leprivier, G., & Grünewald, T. G. P. (2016). Eukaryotic initiation factor 4E-binding protein 1 (4E-BP1): a master regulator of mRNA translation involved in tumorigenesis. *Oncogene*, *35*(36), 4675–4688. https://doi.org/10.1038/ONC.2015.515

Mutvei, A. P., Nagiec, M. J., Hamann, J. C., Kim, S. G., Vincent, C. T., & Blenis, J. (2020). Rap1-GTPases control mTORC1 activity by coordinating lysosome organization with amino acid availability. *Nature Communications 2020 11:1*, *11*(1), 1–13. https://doi.org/10.1038/s41467-020-15156-5

Nakahara, H., Otani, T., Sasaki, T., Miura, Y., Takai, Y., & Kogo, M. (2003). Involvement of Cdc42 and Rac small G proteins in invadopodia formation of RPMI7951 cells. *Genes to Cells*, *8*(12), 1019–1027. https://doi.org/10.1111/J.1365-2443.2003.00695.X

Napolitano, G., di Malta, C., & Ballabio, A. (2022). Non-canonical mTORC1 signaling at the lysosome. *Trends in Cell Biology*. https://doi.org/10.1016/J.TCB.2022.04.012

Napolitano, G., di Malta, C., Esposito, A., de Araujo, M. E. G., Pece, S., Bertalot, G., Matarese, M., Benedetti, V., Zampelli, A., Stasyk, T., Siciliano, D., Venuta, A., Cesana, M., Vilardo, C., Nusco, E., Monfregola, J., Calcagnì, A., di Fiore, P. P., Huber, L. A., & Ballabio, A. (2020). A substrate-specific mTORC1 pathway underlies Birt–Hogg–Dubé syndrome. *Nature*, *585*(7826), 597–602. https://doi.org/10.1038/s41586-020-2444-0

Napolitano, G., Esposito, A., Choi, H., Matarese, M., Benedetti, V., di Malta, C., Monfregola, J., Medina, D. L., Lippincott-Schwartz, J., & Ballabio, A. (2018). mTOR-dependent phosphorylation controls TFEB nuclear export. *Nature Communications 2018 9:1*, *9*(1), 1–10. https://doi.org/10.1038/s41467-018-05862-6

Nascimento, R. G. do, & Otoni, K. M. (2020). Histological and molecular classification of breast cancer: what do we know? *Mastology*, *30*. https://doi.org/10.29289/25945394202020200024

Nazemi, M., & Rainero, E. (2020). Cross-Talk Between the Tumor Microenvironment, Extracellular Matrix, and Cell Metabolism in Cancer. *Frontiers in Oncology*, *10*. https://doi.org/10.3389/FONC.2020.00239

Nazemi, M., Yanes, B., Martinez, M. L., Walker, H., Bard, F., & Rainero, E. (2021). The extracellular matrix promotes breast cancer cell growth under amino acid starvation by promoting tyrosine catabolism. *BioRxiv*, 2021.06.09.447520. https://doi.org/10.1101/2021.06.09.447520

Nielsen, C. F., van Putten, S. M., Lund, I. K., Melander, M. C., Nørregaard, K. S., Jürgensen, H. J., Reckzeh, K., Christensen, K. R., Ingvarsen, S. Z., Gårdsvoll, H., Jensen, K. E., Hamerlik, P., Engelholm, L. H., & Behrendt, N. (2017). The collagen receptor uPARAP/Endo180 as a novel target for antibody-drug conjugate mediated treatment of mesenchymal and leukemic cancers. *Oncotarget*, *8*(27), 44605–44624. https://doi.org/10.18632/ONCOTARGET.17883

Nofal, M., Zhang, K., Han, S., & Rabinowitz, J. D. (2017). mTOR Inhibition Restores Amino Acid Balance in Cells Dependent on Catabolism of Extracellular Protein. *Molecular Cell*, *67*(6), 936-946.e5. https://doi.org/10.1016/j.molcel.2017.08.011

Northcott, J. M., Dean, I. S., Mouw, J. K., & Weaver, V. M. (2018). Feeling stress: The mechanics of cancer progression and aggression. *Frontiers in Cell and Developmental Biology*, *6*(FEB), 17. https://doi.org/10.3389/FCELL.2018.00017/BIBTEX

Nowosad, A., Jeannot, P., Callot, C., Creff, J., Perchey, R. T., Joffre, C., Codogno, P., Manenti, S., & Besson, A. (2020). p27 controls Ragulator and mTOR activity in amino acid-deprived cells to regulate the autophagy–lysosomal pathway and coordinate cell cycle and cell growth. *Nature Cell Biology 2020 22:9*, *22*(9), 1076–1090. https://doi.org/10.1038/s41556-020-0554-4

Nüchel, J., Tauber, M., Nolte, J. L., Mörgelin, M., Türk, C., Eckes, B., Demetriades, C., & Plomann, M. (2021). An mTORC1-GRASP55 signaling axis controls unconventional secretion to reshape the extracellular proteome upon stress. *Molecular Cell*, *81*(16), 3275-3293.e12. https://doi.org/10.1016/J.MOLCEL.2021.06.017

Ohanna, M., Sobering, A. K., Lapointe, T., Lorenzo, L., Praud, C., Petroulakis, E., Sonenberg, N., Kelly, P. A., Sotiropoulos, A., & Pende, M. (2005). Atrophy of S6K1(-/-) skeletal muscle cells reveals distinct mTOR effectors for cell cycle and size control. *Nature Cell Biology*, *7*(3), 286–294. https://doi.org/10.1038/NCB1231

Oikawa, T., Itoh, T., & Takenawa, T. (2008). Sequential signals toward podosome formation in NIH-src cells. *The Journal of Cell Biology*, *182*(1), 157–169. https://doi.org/10.1083/JCB.200801042

Olivares, O., Mayers, J. R., Gouirand, V., Torrence, M. E., Gicquel, T., Borge, L., Lac, S., Roques, J., Lavaut, M. N., Berthezène, P., Rubis, M., Secq, V., Garcia, S., Moutardier, V., Lombardo, D., Iovanna, J. L., Tomasini, R., Guillaumond, F., vander Heiden, M. G., & Vasseur, S. (2017). Collagen-derived proline promotes pancreatic ductal adenocarcinoma cell survival under nutrient limited conditions. *Nature Communications*, *8*. https://doi.org/10.1038/ncomms16031

O'Reilly, E. A., Gubbins, L., Sharma, S., Tully, R., Guang, M. H. Z., Weiner-Gorzel, K., McCaffrey, J., Harrison, M., Furlong, F., Kell, M., & McCann, A. (2015). The fate of chemoresistance in triple negative breast cancer (TNBC). *BBA Clinical*, *3*, 257–275. https://doi.org/10.1016/J.BBACLI.2015.03.003

Oser, M., Mader, C. C., Gil-Henn, H., Magalhaes, M., Bravo-Cordero, J. J., Koleske, A. J., & Condeelis, J. (2010). Specific tyrosine phosphorylation sites on cortactin regulate Nck1-dependent actin polymerization in invadopodia. *Journal of Cell Science*, *123*(21), 3662–3673. https://doi.org/10.1242/JCS.068163

Ostrowski, M., Carmo, N. B., Krumeich, S., Fanget, I., Raposo, G., Savina, A., Moita, C. F., Schauer, K., Hume, A. N., Freitas, R. P., Goud, B., Benaroch, P., Hacohen, N., Fukuda, M., Desnos, C., Seabra, M. C., Darchen, F., Amigorena, S., Moita, L. F., & Thery, C. (2009). Rab27a and Rab27b control different steps of the exosome secretion pathway. *Nature Cell Biology 2010 12:1*, *12*(1), 19–30. https://doi.org/10.1038/ncb2000

Ota, I., Li, X. Y., Hu, Y., & Weiss, S. J. (2009). Induction of a MT1-MMP and MT2-MMP-dependent basement membrane transmigration program in cancer cells by Snail1. *Proceedings of the National Academy of Sciences of the United States of America*, *106*(48), 20318–20323. https://doi.org/10.1073/PNAS.0910962106/SUPPL_FILE/0910962106SI.PDF

Ouyang, M., Lu, S., Kim, T., Chen, C. E., Seong, J., Leckband, D. E., Wang, F., Reynolds, A. B., Schwartz, M. A., & Wang, Y. (2013). N-cadherin regulates spatially polarized signals through distinct p120ctn and β-catenin-dependent signaling pathways. *Nature Communications*, *4*, 1589. https://doi.org/10.1038/NCOMMS2560

Overgaard, J., Yilmaz, M., Guldberg, P., Hansen, L. L., & Alsner, J. (2009). TP53 Mutation is an Independent Prognostic Marker for Poor Outcome in Both Node-negative and Node-positive Breast Cancer. *Https://Doi.Org/10.1080/028418600750013096*, *39*(3), 327–333. https://doi.org/10.1080/028418600750013096

Paine, I. S., & Lewis, M. T. (2017). The Terminal End Bud: the Little Engine that Could. *Journal of Mammary Gland Biology and Neoplasia*, *22*(2), 93–108. https://doi.org/10.1007/s10911-017-9372-0

Pal, R., Palmieri, M., Chaudhury, A., Klisch, T. J., di Ronza, A., Neilson, J. R., Rodney, G. G., & Sardiello, M. (2018). Src regulates amino acid-mediated mTORC1 activation by disrupting GATOR1-Rag GTPase interaction. *Nature Communications 2018 9:1*, *9*(1), 1–14. https://doi.org/10.1038/s41467-018-06844-4

Palm, W., Park, Y., Wright, K., Pavlova, N. N., Tuveson, D. A., & Thompson, C. B. (2015). The Utilization of Extracellular Proteins as Nutrients Is Suppressed by mTORC1. *Cell*, *162*(2), 259–270. https://doi.org/10.1016/j.cell.2015.06.017

Palm, W., & Thompson, C. B. (2017). Nutrient acquisition strategies of mammalian cells. In *Nature* (Vol. 546, Issue 7657, pp. 234–242). Nature Publishing Group. https://doi.org/10.1038/nature22379

Palmieri, M., Impey, S., Kang, H., di Ronza, A., Pelz, C., Sardiello, M., & Ballabio, A. (2011). Characterization of the CLEAR network reveals an integrated control of cellular clearance pathways. *Human Molecular Genetics*, *20*(19), 3852–3866. https://doi.org/10.1093/hmg/ddr306

Pandhare, J., Donald, S. P., Cooper, S. K., & Phang, J. M. (2009). Regulation and Function of Proline Oxidase under Nutrient Stress. *Journal of Cellular Biochemistry*, *107*(4), 759. https://doi.org/10.1002/JCB.22174

Pang, L., Li, Q., Li, S., He, J., Cao, W., Lan, J., Sun, B., Zou, H., Wang, C., Liu, R., Wei, C., Wei, Y., Qi, Y., Hu, J., Liang, W., Zhang, W. J., Wan, M., & Li, F. (2016). Membrane type 1-matrix metalloproteinase induces epithelial-to-mesenchymal transition in esophageal squamous cell carcinoma: Observations from clinical and in vitro analyses. *Scientific Reports*, *6*(1), 22179. https://doi.org/10.1038/srep22179

Parmar, H., & Cunha, G. R. (2004). Epithelial–stromal interactions in the mouse and human mammary gland in vivo. *Endocrine-Related Cancer*, *11*(3), 437–458. https://doi.org/10.1677/erc.1.00659

Pastushenko, I., Brisebarre, A., Sifrim, A., Fioramonti, M., Revenco, T., Boumahdi, S., van Keymeulen, A., Brown, D., Moers, V., Lemaire, S., de Clercq, S., Minguijón, E., Balsat, C., Sokolow, Y., Dubois, C., de Cock, F., Scozzaro, S., Sopena, F., Lanas, A., … Blanpain, C. (2018). Identification of the tumour transition states occurring during EMT. *Nature*, *556*(7702), 463–468. https://doi.org/10.1038/s41586-018-0040-3

Paterson, E. K., & Courtneidge, S. A. (2018). Invadosomes are coming: new insights into function and disease relevance. *The FEBS Journal*, *285*(1), 8–27. https://doi.org/10.1111/FEBS.14123

Paulsson, M. (1992). Basement membrane proteins: structure, assembly, and cellular interactions. *Critical Reviews in Biochemistry and Molecular Biology*, *27*(1–2), 93–127. https://doi.org/10.3109/10409239209082560

Pedchenko, V., Bauer, R., Pokidysheva, E. N., Al-Shaer, A., Forde, N. R., Fidler, A. L., Hudson, B. G., & Boudko, S. P. (2019). A chloride ring is an ancient evolutionary innovation mediating the assembly of the collagen IV scaffold of basement membranes. *Journal of Biological Chemistry*, *294*(20), 7968–7981. https://doi.org/10.1074/JBC.RA119.007426

Pedersen, N. M., Wenzel, E. M., Wang, L., Antoine, S., Chavrier, P., Stenmark, H., & Raiborg, C. (2020a). Protrudin-mediated ER–endosome contact sites promote MT1-MMP exocytosis and cell invasion. *Journal of Cell Biology*, *219*(8), e202003063. https://doi.org/10.1083/JCB.202003063

Pedersen, N. M., Wenzel, E. M., Wang, L., Antoine, S., Chavrier, P., Stenmark, H., & Raiborg, C. (2020b). Protrudin-mediated ER–endosome contact sites promote MT1-MMP exocytosis and cell invasion. *Journal of Cell Biology*, *219*(8). https://doi.org/10.1083/JCB.202003063/VIDEO-1

Pelkmans, L., Fava, E., Grabner, H., Hannus, M., Habermann, B., Krausz, E., & Zerial, M. (2005). Genome-wide analysis of human kinases in clathrin- and caveolae/raft-mediated endocytosis. *Nature 2005 436:7047*, *436*(7047), 78–86. https://doi.org/10.1038/nature03571

Pellikainen, J. M., Ropponen, K. M., Kataja, V. v., Kellokoski, J. K., Eskelinen, M. J., & Kosma, V. M. (2004). Expression of Matrix Metalloproteinase (MMP)-2 and MMP-9 in Breast Cancer with a Special Reference to Activator Protein-2, HER2, and Prognosis. *Clinical Cancer Research*, *10*(22), 7621–7628. https://doi.org/10.1158/1078-0432.CCR-04-1061

Pende, M., Kozma, S. C., Jaquet, M., Oorschot, V., Burcelin, R., le Marchand-Brustel, Y., Klumperman, J., Thorens, B., & Thomas, G. (2000). Hypoinsulinaemia, glucose intolerance and diminished beta-cell size in S6K1-deficient mice. *Nature*, *408*(6815), 994–997. https://doi.org/10.1038/35050135

Perou, C. M., Sørlie, T., Eisen, M. B., van de Rijn, M., Jeffrey, S. S., Rees, C. A., Pollack, J. R., Ross, D. T., Johnsen, H., Akslen, L. A., Fluge, Ø., Pergamenschikov, A., Williams, C., Zhu, S. X., Lønning, P. E., Børresen-Dale, A.-L., Brown, P. O., & Botstein, D. (2000). Molecular portraits of human breast tumours. *Nature*, *406*(6797), 747–752. https://doi.org/10.1038/35021093

Peterson, T. R., Sengupta, S. S., Harris, T. E., Carmack, A. E., Kang, S. A., Balderas, E., Guertin, D. A., Madden, K. L., Carpenter, A. E., Finck, B. N., & Sabatini, D. M. (2011). mTOR complex 1 regulates lipin 1 localization to control the SREBP pathway. *Cell*, *146*(3), 408–420. https://doi.org/10.1016/J.CELL.2011.06.034

Pickup, M. W., Mouw, J. K., & Weaver, V. M. (2014). The extracellular matrix modulates the hallmarks of cancer. *EMBO Reports*, *15*(12), 1243–1253. https://doi.org/10.15252/embr.201439246

Planchon, D., Morris, E. R., Genest, M., Comunale, F., Vacher, S., Bièche, I., Denisov, E. v., Tashireva, L. A., Perelmuter, V. M., Linder, S., Chavrier, P., Bodin, S., & Gauthier-Rouvière, C. (2018). MT1-MMP targeting to endolysosomes is mediated by upregulation of flotillins. *Journal of Cell Science*, *131*(17). https://doi.org/10.1242/JCS.218925

Poincloux, R., Lizárraga, F., & Chavrier, P. (2009a). Matrix invasion by tumour cells: A focus on MT1-MMP trafficking to invadopodia. *Journal of Cell Science*, *122*(17), 3015–3024. https://doi.org/10.1242/jcs.034561

Poincloux, R., Lizárraga, F., & Chavrier, P. (2009b). Matrix invasion by tumour cells: a focus on MT1-MMP trafficking to invadopodia. *Journal of Cell Science*, *122*(Pt 17), 3015–3024. https://doi.org/10.1242/JCS.034561

Porstmann, T., Santos, C. R., Griffiths, B., Cully, M., Wu, M., Leevers, S., Griffiths, J. R., Chung, Y. L., & Schulze, A. (2008). SREBP activity is regulated by mTORC1 and contributes to Akt-dependent cell growth. *Cell Metabolism*, *8*(3), 224–236. https://doi.org/10.1016/J.CMET.2008.07.007

Prvanović, M., Nedeljković, M., Tanić, N., Tomić, T., Terzić, T., Milovanović, Z., Maksimović, Z., & Tanić, N. (2021). Role of pten, pi3k, and mtor in triple-negative breast cancer. *Life*, *11*(11). https://doi.org/10.3390/LIFE11111247/S1

Pu, J., Keren-Kaplan, T., & Bonifacino, J. S. (2017). A Ragulator–BORC interaction controls lysosome positioning in response to amino acid availability. *The Journal of Cell Biology*, *216*(12), 4183. https://doi.org/10.1083/JCB.201703094

Pu, J., Schindler, C., Jia, R., Jarnik, M., Backlund, P., & Bonifacino, J. S. (2015). BORC, a Multisubunit Complex that Regulates Lysosome Positioning. *Developmental Cell*, *33*(2), 176. https://doi.org/10.1016/J.DEVCEL.2015.02.011

Puente, C., Hendrickson, R. C., & Jiang, X. (2016). Nutrient-regulated Phosphorylation of ATG13 Inhibits Starvation-induced Autophagy. *Journal of Biological Chemistry*, *291*(11), 6026–6035. https://doi.org/10.1074/JBC.M115.689646

Puertollano, R., Ferguson, S. M., Brugarolas, J., & Ballabio, A. (2018). The complex relationship between TFEB transcription factor phosphorylation and subcellular localization. *The EMBO Journal*, *37*(11). https://doi.org/10.15252/EMBJ.201798804

Qian, X., Anzovino, A., Kim, S., Suyama, K., Yao, J., Hulit, J., Agiostratidou, G., Chandiramani, N., McDaid, H. M., Nagi, C., Cohen, H. W., Phillips, G. R., Norton, L., & Hazan, R. B. (2014). N-cadherin/FGFR promotes metastasis through epithelial-to-mesenchymal transition and stem/progenitor cell-like properties. *Oncogene*, *33*(26), 3411. https://doi.org/10.1038/ONC.2013.310

Quintero-Fabián, S., Arreola, R., Becerril-Villanueva, E., Torres-Romero, J. C., Arana-Argáez, V., Lara-Riegos, J., Ramírez-Camacho, M. A., & Alvarez-Sánchez, M. E. (2019). Role of Matrix Metalloproteinases in Angiogenesis and Cancer. *Frontiers in Oncology*, *9*, 1370. https://doi.org/10.3389/FONC.2019.01370/BIBTEX

Raiborg, C., Wenzel, E. M., Pedersen, N. M., Olsvik, H., Schink, K. O., Schultz, S. W., Vietri, M., Nisi, V., Bucci, C., Brech, A., Johansen, T., & Stenmark, H. (2015). Repeated ER-endosome contacts promote endosome translocation and neurite outgrowth. *Nature*, *520*(7546), 234–238. https://doi.org/10.1038/NATURE14359

Rao, S. K., Huynh, C., Proux-Gillardeaux, V., Galli, T., & Andrews, N. W. (2004). Identification of SNAREs Involved in Synaptotagmin VII-regulated Lysosomal Exocytosis. *Journal of Biological Chemistry*, *279*(19), 20471–20479. https://doi.org/10.1074/JBC.M400798200

Raphael, J., Lefebvre, C., Allan, A., Helou, J., Boldt, G., Vandenberg, T., & Blanchette, P. S. (2020). Everolimus in Advanced Breast Cancer: A Systematic Review and Meta-analysis. *Targeted Oncology*, *15*(6), 723–732. https://doi.org/10.1007/S11523-020-00770-6

Rapti, M., Knäuper, V., Murphy, G., & Williamson, R. A. (2006). Characterization of the AB loop region of TIMP-2. Involvement in pro-MMP-2 activation. *The Journal of Biological Chemistry*, *281*(33), 23386–23394. https://doi.org/10.1074/JBC.M604423200

Rebbeck, C. A., Xian, J., Bornelöv, S., Geradts, J., Hobeika, A., Geiger, H., Alvarez, J. F., Rozhkova, E., Nicholls, A., Robine, N., Lyerly, H. K., & Hannon, G. J. (2022). Gene expression signatures of individual ductal carcinoma in situ lesions identify processes and biomarkers associated with progression towards invasive ductal carcinoma. *Nature Communications*, *13*(1), 3399. https://doi.org/10.1038/s41467-022-30573-4

Recouvreux, M. V., & Commisso, C. (2017). Macropinocytosis: A metabolic adaptation to nutrient stress in cancer. *Frontiers in Endocrinology*, *8*(SEP), 261. https://doi.org/10.3389/FENDO.2017.00261/BIBTEX

Recouvreux, M. V., Moldenhauer, M. R., Galenkamp, K. M. O., Jung, M., James, B., Zhang, Y., Lowy, A., Bagchi, A., & Commisso, C. (2020). Glutamine depletion regulates Slug to promote EMT and metastasis in pancreatic cancer. *Journal of Experimental Medicine*, *217*(9). https://doi.org/10.1084/JEM.20200388/151843

Remacle, A. G., Rozanov, D. v., Fugere, M., Day, R., & Strongin, A. Y. (2006). Furin regulates the intracellular activation and the uptake rate of cell surface-associated MT1-MMP. *Oncogene*, *25*(41), 5648–5655. https://doi.org/10.1038/SJ.ONC.1209572

Ridley, A. J., Schwartz, M. A., Burridge, K., Firtel, R. A., Ginsberg, M. H., Borisy, G., Parsons, J. T., & Horwitz, A. R. (2003). Cell Migration: Integrating Signals from Front to Back. *Science*, *302*(5651), 1704–1709. https://doi.org/10.1126/science.1092053

Ries, C., Egea, V., Karow, M., Kolb, H., Jochum, M., & Neth, P. (2007). MMP-2, MT1-MMP, and TIMP-2 are essential for the invasive capacity of human mesenchymal stem cells: differential regulation by inflammatory cytokines. *Blood*, *109*(9), 4055–4063. https://doi.org/10.1182/BLOOD-2006-10-051060

Risom, T., Glass, D. R., Averbukh, I., Liu, C. C., Baranski, A., Kagel, A., McCaffrey, E. F., Greenwald, N. F., Rivero-Gutiérrez, B., Strand, S. H., Varma, S., Kong, A., Keren, L., Srivastava, S., Zhu, C., Khair, Z., Veis, D. J., Deschryver, K., Vennam, S., … Angelo, M. (2022a). Transition to invasive breast cancer is associated with progressive changes in the structure and composition of tumor stroma. *Cell*, *185*(2), 299-310.e18. https://doi.org/10.1016/j.cell.2021.12.023

Risom, T., Glass, D. R., Averbukh, I., Liu, C. C., Baranski, A., Kagel, A., McCaffrey, E. F., Greenwald, N. F., Rivero-Gutiérrez, B., Strand, S. H., Varma, S., Kong, A., Keren, L., Srivastava, S., Zhu, C., Khair, Z., Veis, D. J., Deschryver, K., Vennam, S., … Angelo, M. (2022b). Transition to invasive breast cancer is associated with progressive changes in the structure and composition of tumor stroma. *Cell*, *185*(2), 299-310.e18. https://doi.org/10.1016/J.CELL.2021.12.023

Roczniak-Ferguson, A., Petit, C. S., Froehlich, F., Qian, S., Ky, J., Angarola, B., Walther, T. C., & Ferguson, S. M. (2012). *The Transcription Factor TFEB Links mTORC1 Signaling to Transcriptional Control of Lysosome Homeostasis*. www.SCIENCESIGNALING.org

Rossé, C., Lodillinsky, C., Fuhrmann, L., Nourieh, M., Monteiro, P., Irondelle, M., Lagoutte, E., Vacher, S., Waharte, F., Paul-Gilloteaux, P., Romao, M., Sengmanivong, L., Linch, M., van Lint, J., Raposo, G., Vincent-Salomon, A., Bièche, I., Parker, P. J., & Chavrier, P. (2014). Control of MT1-MMP transport by atypical PKC during breast-cancer progression. *Proceedings of the National Academy of Sciences of the United States of America*, *111*(18), E1872–E1879. https://doi.org/10.1073/PNAS.1400749111/SUPPL_FILE/PNAS.1400749111.SM03.AVI

Rowe, R. G., & Weiss, S. J. (2008a). Breaching the basement membrane: who, when and how? *Trends in Cell Biology*, *18*(11), 560–574. https://doi.org/10.1016/J.TCB.2008.08.007

Rowe, R. G., & Weiss, S. J. (2008b). Breaching the basement membrane: who, when and how? *Trends in Cell Biology*, *18*(11), 560–574. https://doi.org/10.1016/J.TCB.2008.08.007

Rowe, R. G., & Weiss, S. J. (2009). Navigating ECM Barriers at the Invasive Front: The Cancer Cell–Stroma Interface. *Http://Dx.Doi.Org.Insb.Bib.Cnrs.Fr/10.1146/Annurev.Cellbio.24.110707.175315*, *25*, 567–595. https://doi.org/10.1146/ANNUREV.CELLBIO.24.110707.175315

Sabeh, F., Ota, I., Holmbeck, K., Birkedal-Hansen, H., Soloway, P., Balbin, M., Lopez-Otin, C., Shapiro, S., Inada, M., Krane, S., Allen, E., Chung, D., & Weiss, S. J. (2004). Tumor cell traffic through the extracellular matrix is controlled by the membrane-anchored collagenase MT1-MMP. *The Journal of Cell Biology*, *167*(4), 769–781. https://doi.org/10.1083/JCB.200408028

Saini, H., Rahmani Eliato, K., Silva, C., Allam, M., Mouneimne, G., Ros, R., & Nikkhah, M. (2018). The Role of Desmoplasia and Stromal Fibroblasts on Anti-cancer Drug Resistance in a Microengineered Tumor Model. *Cellular and Molecular Bioengineering*, *11*(5), 419. https://doi.org/10.1007/S12195-018-0544-9

Salvatore, L., Gallo, N., Natali, M. L., Terzi, A., Sannino, A., & Madaghiele, M. (2021). Mimicking the Hierarchical Organization of Natural Collagen: Toward the Development of Ideal Scaffolding Material for Tissue Regeneration. *Frontiers in Bioengineering and Biotechnology*, *9*. https://doi.org/10.3389/fbioe.2021.644595

Sancak, Y., Bar-Peled, L., Zoncu, R., Markhard, A. L., Nada, S., & Sabatini, D. M. (2010). Ragulator-Rag complex targets mTORC1 to the lysosomal surface and is necessary for its activation by amino acids. *Cell*, *141*(2), 290–303. https://doi.org/10.1016/J.CELL.2010.02.024

Sancak, Y., Peterson, T. R., Shaul, Y. D., Lindquist, R. A., Thoreen, C. C., Bar-Peled, L., & Sabatini, D. M. (2008). The Rag GTPases bind raptor and mediate amino acid signaling to mTORC1. *Science (New York, N.Y.)*, *320*(5882), 1496–1501. https://doi.org/10.1126/SCIENCE.1157535

Sarbassov, D. D., Ali, S. M., & Sabatini, D. M. (2005). Growing roles for the mTOR pathway. *Current Opinion in Cell Biology*, *17*(6), 596–603. https://doi.org/10.1016/J.CEB.2005.09.009

Sarbassov, D. D., Ali, S. M., Sengupta, S., Sheen, J. H., Hsu, P. P., Bagley, A. F., Markhard, A. L., & Sabatini, D. M. (2006). Prolonged Rapamycin Treatment Inhibits mTORC2 Assembly and Akt/PKB. *Molecular Cell*, *22*(2), 159–168. https://doi.org/10.1016/J.MOLCEL.2006.03.029

Sardiello, M., Palmieri, M., di Ronza, A., Medina, D. L., Valenza, M., Gennarino, V. A., di Malta, C., Donaudy, F., Embrione, V., Polishchuk, R. S., Banfi, S., Parenti, G., Cattaneo, E., & Ballabio, A. (2009). A Gene Network Regulating Lysosomal Biogenesis and Function. *Science*, *325*(5939), 473–477. https://doi.org/10.1126/science.1174447

Saxton, R. A., Chantranupong, L., Knockenhauer, K. E., Schwartz, T. U., & Sabatini, D. M. (2016). Mechanism of arginine sensing by CASTOR1 upstream of mTORC1. *Nature*, *536*(7615), 229–233. https://doi.org/10.1038/NATURE19079

Saxton, R. A., Knockenhauer, K. E., Wolfson, R. L., Chantranupong, L., Pacold, M. E., Wang, T., Schwartz, T. U., & Sabatini, D. M. (2016). Structural basis for leucine sensing by the Sestrin2-mTORC1 pathway. *Science (New York, N.Y.)*, *351*(6268), 53–58. https://doi.org/10.1126/SCIENCE.AAD2087

Saxton, R. A., & Sabatini, D. M. (2017). mTOR Signaling in Growth, Metabolism, and Disease. In *Cell* (Vol. 168, Issue 6, pp. 960–976). Cell Press. https://doi.org/10.1016/j.cell.2017.02.004

Schalm, S. S., Fingar, D. C., Sabatini, D. M., & Blenis, J. (2003). TOS motif-mediated raptor binding regulates 4E-BP1 multisite phosphorylation and function. *Current Biology : CB*, *13*(10), 797–806. https://doi.org/10.1016/S0960-9822(03)00329-4

Scharfenberg, F., Helbig, A., Sammel, M., Benzel, J., Schlomann, U., Peters, F., Wichert, R., Bettendorff, M., Schmidt-Arras, D., Rose-John, S., Moali, C., Lichtenthaler, S. F., Pietrzik, C. U., Bartsch, J. W., Tholey, A., & Becker-Pauly, C. (2020). Degradome of soluble ADAM10 and ADAM17 metalloproteases. *Cellular and Molecular Life Sciences*, *77*(2), 331–350. https://doi.org/10.1007/s00018-019-03184-4

Schatzmann, F., Marlow, R., & Streuli, C. H. (2003). Integrin Signaling and Mammary Cell Function. *Journal of Mammary Gland Biology and Neoplasia*, *8*(4), 395–408. https://doi.org/10.1023/B:JOMG.0000017427.14751.8c

Schmidt, L. S., & Linehan, W. M. (2018). FLCN: The causative gene for Birt-Hogg-Dubé syndrome. *Gene*, *640*, 28–42. https://doi.org/10.1016/J.GENE.2017.09.044

Schröder, H. M., Hoffmann, S. C., Hecker, M., Korff, T., & Ludwig, T. (2013). The tetraspanin network modulates MT1-MMP cell surface trafficking. *The International Journal of Biochemistry & Cell Biology*, *45*(6), 1133–1144. https://doi.org/10.1016/J.BIOCEL.2013.02.020

Sekiguchi, R., & Yamada, K. M. (2018). *Basement Membranes in Development and Disease* (pp. 143–191). https://doi.org/10.1016/bs.ctdb.2018.02.005

Semenza, G. L. (2016). The hypoxic tumor microenvironment: A driving force for breast cancer progression. *Biochimica et Biophysica Acta (BBA) - Molecular Cell Research*, *1863*(3), 382–391. https://doi.org/10.1016/j.bbamcr.2015.05.036

Settembre, C., de Cegli, R., Mansueto, G., Saha, P. K., Vetrini, F., Visvikis, O., Huynh, T., Carissimo, A., Palmer, D., Jürgen Klisch, T., Wollenberg, A. C., di Bernardo, D., Chan, L., Irazoqui, J. E., & Ballabio, A. (2013). TFEB controls cellular lipid metabolism through a starvation-induced autoregulatory loop. *Nature Cell Biology*, *15*(6), 647–658. https://doi.org/10.1038/ncb2718

Settembre, C., di Malta, C., Polito, V. A., Arencibia, M. G., Vetrini, F., Erdin, S., Erdin, S. U., Huynh, T., Medina, D., Colella, P., Sardiello, M., Rubinsztein, D. C., & Ballabio, A. (2011). TFEB Links Autophagy to Lysosomal Biogenesis. *Science*, *332*(6036), 1429–1433. https://doi.org/10.1126/science.1204592

Settembre, C., Zoncu, R., Medina, D. L., Vetrini, F., Erdin, S., Erdin, S., Huynh, T., Ferron, M., Karsenty, G., Vellard, M. C., Facchinetti, V., Sabatini, D. M., & Ballabio, A. (2012). A lysosome-to-nucleus signalling mechanism senses and regulates the lysosome via mTOR and TFEB. *EMBO Journal*, *31*(5), 1095–1108. https://doi.org/10.1038/emboj.2012.32

Sha, Y., Rao, L., Settembre, C., Ballabio, A., & Eissa, N. T. (2017). STUB1 regulates TFEB-induced autophagy–lysosome pathway. *The EMBO Journal*, *36*(17), 2544–2552. https://doi.org/10.15252/EMBJ.201796699

Shackleton, M., Vaillant, F., Simpson, K. J., Stingl, J., Smyth, G. K., Asselin-Labat, M.-L., Wu, L., Lindeman, G. J., & Visvader, J. E. (2006). Generation of a functional mammary gland from a single stem cell. *Nature*, *439*(7072), 84–88. https://doi.org/10.1038/nature04372

Sharifi, M. N., Mowers, E. E., Drake, L. E., Collier, C., Chen, H., Zamora, M., Mui, S., & Macleod, K. F. (2016). Autophagy Promotes Focal Adhesion Disassembly and Cell Motility of Metastatic Tumor Cells through the Direct Interaction of Paxillin with LC3. *Cell Reports*, *15*(8), 1660–1672. https://doi.org/10.1016/J.CELREP.2016.04.065

Sharma, P., Parveen, S., Shah, L. v., Mukherjee, M., Kalaidzidis, Y., Kozielski, A. J., Rosato, R., Chang, J. C., & Datta, S. (2020). SNX27-retromer assembly recycles MT1-MMP to invadopodia and promotes breast cancer metastasis. *Journal of Cell Biology*, *219*(1). https://doi.org/10.1083/JCB.201812098/132732

Sharma, V. P., Eddy, R., Entenberg, D., Kai, M., Gertler, F. B., & Condeelis, J. (2013). Tks5 and SHIP2 regulate invadopodium maturation, but not initiation, in breast carcinoma cells. *Current Biology : CB*, *23*(21), 2079–2089. https://doi.org/10.1016/J.CUB.2013.08.044

Shen, K., Rogala, K. B., Chou, H. T., Huang, R. K., Yu, Z., & Sabatini, D. M. (2019). Cryo-EM Structure of the Human FLCN-FNIP2-Rag-Ragulator Complex. *Cell*, *179*(6), 1319-1329.e8. https://doi.org/10.1016/J.CELL.2019.10.036

Shen, K., & Sabatini, D. M. (2018). Ragulator and SLC38A9 activate the Rag GTPases through noncanonical GEF mechanisms. *Proceedings of the National Academy of Sciences of the United States of America*, *115*(38), 9545–9550. https://doi.org/10.1073/PNAS.1811727115/SUPPL_FILE/PNAS.1811727115.SAPP.PDF

Shi, F., & Sottile, J. (2008). Caveolin-1-dependent β1 integrin endocytosis is a critical regulator of fibronectin turnover. *Journal of Cell Science*, *121*(14), 2360–2371. https://doi.org/10.1242/JCS.014977

Shi, J. jie, Chen, S. meng, Guo, C. liang, Li, Y. xue, Ding, J., & Meng, L. hua. (2018). The mTOR inhibitor AZD8055 overcomes tamoxifen resistance in breast cancer cells by down-regulating HSPB8. *Acta Pharmacologica Sinica*, *39*(8), 1338–1346. https://doi.org/10.1038/APS.2017.181

Shoulders, M. D., & Raines, R. T. (2009a). Collagen Structure and Stability. *Annual Review of Biochemistry*, *78*(1), 929–958. https://doi.org/10.1146/annurev.biochem.77.032207.120833

Shoulders, M. D., & Raines, R. T. (2009b). Collagen Structure and Stability. *Annual Review of Biochemistry*, *78*(1), 929–958. https://doi.org/10.1146/annurev.biochem.77.032207.120833

Sobotič, B., Vizovišek, M., Vidmar, R., van Damme, P., Gocheva, V., Joyce, J. A., Gevaert, K., Turk, V., Turk, B., & Fonović, M. (2015). Proteomic identification of cysteine cathepsin substrates shed from the surface of cancer cells. *Molecular and Cellular Proteomics*, *14*(8), 2213–2228. https://doi.org/10.1074/MCP.M114.044628/ATTACHMENT/22635D98-0C10-4B71-A309-6947DABEDB73/MMC1.ZIP

Solin, L. J. (2019). Management of Ductal Carcinoma In Situ (DCIS) of the Breast: Present Approaches and Future Directions. *Current Oncology Reports*, *21*(4). https://doi.org/10.1007/S11912-019-0777-3

Sounni, N. E., Rozanov, D. v., Remacle, A. G., Golubkov, V. S., Noel, A., & Strongin, A. Y. (2010). Timp-2 binding with cellular MT1-MMP stimulates invasion-promoting MEK/ERK signaling in cancer cells. *International Journal of Cancer. Journal International Du Cancer*, *126*(5), 1067. https://doi.org/10.1002/IJC.24690

Sprangers, S., Behrendt, N., Engelholm, L., Cao, Y., & Everts, V. (2017). Phagocytosis of Collagen Fibrils by Fibroblasts In Vivo Is Independent of the uPARAP/Endo180 Receptor. *Journal of Cellular Biochemistry*, *118*(6), 1590–1595. https://doi.org/10.1002/JCB.25821

Stamatelos, S. K., Bhargava, A., Kim, E., Popel, A. S., & Pathak, A. P. (2019). Tumor Ensemble-Based Modeling and Visualization of Emergent Angiogenic Heterogeneity in Breast Cancer. *Scientific Reports 2019 9:1*, *9*(1), 1–14. https://doi.org/10.1038/s41598-019-40888-w

Staudinger, L. A., Spano, S. J., Lee, W., Coelho, N., Rajshankar, D., Bendeck, M. P., Moriarty, T., & McCulloch, C. A. (2013). Interactions between the discoidin domain receptor 1 and β1 integrin regulate attachment to collagen. *Biology Open*, *2*(11), 1148–1159. https://doi.org/10.1242/BIO.20135090

Steffen, A., le Dez, G., Poincloux, R., Recchi, C., Nassoy, P., Rottner, K., Galli, T., & Chavrier, P. (2008). MT1-MMP-dependent invasion is regulated by TI-VAMP/VAMP7. *Current Biology : CB*, *18*(12), 926–931. https://doi.org/10.1016/J.CUB.2008.05.044

Sternlicht, M. D. (2006). Key stages in mammary gland development: The cues that regulate ductal branching morphogenesis. *Breast Cancer Research*, *8*(1), 201. https://doi.org/10.1186/BCR1368

Strongin, A. Y., Collier, I., Bannikov, G., Marmer, B. L., Grant, G. A., & Goldberg, G. I. (1995). Mechanism of cell surface activation of 72-kDa type IV collagenase. Isolation of the activated form of the membrane metalloprotease. *The Journal of Biological Chemistry*, *270*(10), 5331–5338. https://doi.org/10.1074/JBC.270.10.5331

Stylli, S. S., Stacey, T. T. I., Verhagen, A. M., Xu, S. S., Pass, I., Courtneidge, S. A., & Lock, P. (2009). Nck adaptor proteins link Tks5 to invadopodia actin regulation and ECM

degradation. *Journal of Cell Science*, *122*(Pt 15), 2727–2740. https://doi.org/10.1242/JCS.046680

Suárez, H., López-Martín, S., Toribio, V., Zamai, M., Hernández-Riquer, M. V., Genís, L., Arroyo, A. G., & Yáñez-Mó, M. (2020a). Regulation of MT1-MMP Activity through Its Association with ERMs. *Cells 2020, Vol. 9, Page 348*, *9*(2), 348. https://doi.org/10.3390/CELLS9020348

Suárez, H., López-Martín, S., Toribio, V., Zamai, M., Hernández-Riquer, M. V., Genís, L., Arroyo, A. G., & Yáñez-Mó, M. (2020b). Regulation of MT1-MMP Activity through Its Association with ERMs. *Cells 2020, Vol. 9, Page 348*, *9*(2), 348. https://doi.org/10.3390/CELLS9020348

Sun, D., Wu, R., Zheng, J., Li, P., & Yu, L. (2018). Polyubiquitin chain-induced p62 phase separation drives autophagic cargo segregation. *Cell Research 2018 28:4*, *28*(4), 405–415. https://doi.org/10.1038/s41422-018-0017-7

Sun, J., Liu, Y., Hao, X., Lin, W., Su, W., Chiang, E., Baudry, M., & Bi, X. (2022). LAMTOR1 inhibition of TRPML1-dependent lysosomal calcium release regulates dendritic lysosome trafficking and hippocampal neuronal function. *The EMBO Journal*, *41*(5), e108119. https://doi.org/10.15252/EMBJ.2021108119

Sun, Z., Guo, S. S., & Fässler, R. (2016). Integrin-mediated mechanotransduction. *Journal of Cell Biology*, *215*(4), 445–456. https://doi.org/10.1083/jcb.201609037

Takahara, T., Amemiya, Y., Sugiyama, R., Maki, M., & Shibata, H. (2020). Amino acid-dependent control of mTORC1 signaling: a variety of regulatory modes. *Journal of Biomedical Science*, *27*(1). https://doi.org/10.1186/S12929-020-00679-2

Tallant, C., Marrero, A., & Gomis-Rüth, F. X. (2010). Matrix metalloproteinases: fold and function of their catalytic domains. *Biochimica et Biophysica Acta*, *1803*(1), 20–28. https://doi.org/10.1016/J.BBAMCR.2009.04.003

Tancini, B., Buratta, S., Delo, F., Sagini, K., Chiaradia, E., Pellegrino, R. M., Emiliani, C., & Urbanelli, L. (2020). Lysosomal Exocytosis: The Extracellular Role of an Intracellular Organelle. *Membranes 2020, Vol. 10, Page 406*, *10*(12), 406. https://doi.org/10.3390/MEMBRANES10120406

Taurin, S., & Alkhalifa, H. (2020). Breast cancers, mammary stem cells, and cancer stem cells, characteristics, and hypotheses. *Neoplasia*, *22*(12), 663–678. https://doi.org/10.1016/J.NEO.2020.09.009

Thakur, V., & Bedogni, B. (2016). The membrane tethered matrix metalloproteinase MT1-MMP at the forefront of melanoma cell invasion and metastasis. *Pharmacological Research*, *111*, 17–22. https://doi.org/10.1016/J.PHRS.2016.05.019

Thielicke, W., & Sonntag, R. (2021). Particle Image Velocimetry for MATLAB: Accuracy and enhanced algorithms in PIVlab. *Journal of Open Research Software*, *9*(1), 1–14. https://doi.org/10.5334/JORS.334/METRICS/

Tsai, P. Y., Lee, M. S., Jadhav, U., Naqvi, I., Madha, S., Adler, A., Mistry, M., Naumenko, S., Lewis, C. A., Hitchcock, D. S., Roberts, F. R., DelNero, P., Hank, T., Honselmann, K. C., Oyarvide, V. M., Mino-Kenudson, M., Clish, C. B., Shivdasani, R. A., & Kalaany, N. Y. (2021). Adaptation of pancreatic cancer cells to nutrient deprivation is reversible and requires glutamine synthetase stabilization by mTORC1. *Proceedings of the National Academy of Sciences of the United States of America*, *118*(10). https://doi.org/10.1073/PNAS.2003014118

Tsilibary, E. C., & Charonis, A. S. (1986). The role of the main noncollagenous domain (NC1) in type IV collagen self-assembly. *Journal of Cell Biology*, *103*(6), 2467–2473. https://doi.org/10.1083/jcb.103.6.2467

Tu, C., Ortega-Cava, C. F., Chen, G., Fernandes, N. D., Cavallo-Medved, D., Sloane, B. F., Band, V., & Band, H. (2008). Lysosomal cathepsin B participates in the podosome-mediated extracellular matrix degradation and invasion via secreted lysosomes in v-Src fibroblasts. *Cancer Research*, *68*(22), 9147–9156. https://doi.org/10.1158/0008-5472.CAN-07-5127

Turunen, S. P., Tatti-Bugaeva, O., & Lehti, K. (2017). Membrane-type matrix metalloproteases as diverse effectors of cancer progression. *Biochimica et Biophysica*

Acta (BBA) - Molecular Cell Research, *1864*(11), 1974–1988. https://doi.org/10.1016/J.BBAMCR.2017.04.002

Uekita, T., Itoh, Y., Yana, I., Ohno, H., & Seiki, M. (2001). Cytoplasmic tail–dependent internalization of membrane-type 1 matrix metalloproteinase is important for its invasion-promoting activity. *The Journal of Cell Biology*, *155*(7), 1345. https://doi.org/10.1083/JCB.200108112

Valacca, C., Tassone, E., & Mignatti, P. (2015). TIMP-2 Interaction with MT1-MMP Activates the AKT Pathway and Protects Tumor Cells from Apoptosis. *PLoS ONE*, *10*(9). https://doi.org/10.1371/JOURNAL.PONE.0136797

van den Dries, K., Linder, S., Maridonneau-Parini, I., & Poincloux, R. (2019). Probing the mechanical landscape – new insights into podosome architecture and mechanics. *Journal of Cell Science*, *132*(24). https://doi.org/10.1242/JCS.236828/223952

van Nostrand, J. L., Hellberg, K., Luo, E. C., van Nostrand, E. L., Dayn, A., Yu, J., Shokhirev, M. N., Dayn, Y., Yeo, G. W., & Shaw, R. J. (2020). AMPK regulation of Raptor and TSC2 mediate metformin effects on transcriptional control of anabolism and inflammation. *Genes & Development*, *34*(19–20), 1330–1344. https://doi.org/10.1101/GAD.339895.120

van Weering, J. R. T., Verkade, P., & Cullen, P. J. (2012). SNX-BAR-mediated endosome tubulation is co-ordinated with endosome maturation. *Traffic (Copenhagen, Denmark)*, *13*(1), 94–107. https://doi.org/10.1111/J.1600-0854.2011.01297.X

Vargo-Gogola, T., & Rosen, J. M. (2007). Modelling breast cancer: one size does not fit all. *Nature Reviews Cancer*, *7*(9), 659–672. https://doi.org/10.1038/nrc2193

Varone, A., Amoruso, C., Monti, M., Patheja, M., Greco, A., Auletta, L., Zannetti, A., & Corda, D. (2021). The phosphatase Shp1 interacts with and dephosphorylates cortactin to inhibit invadopodia function. *Cell Communication and Signaling*, *19*(1), 1–22. https://doi.org/10.1186/S12964-021-00747-6/FIGURES/9

Vaupel, P., Höckel, M., & Mayer, A. (2007). Detection and characterization of tumor hypoxia using pO2 histography. *Antioxidants & Redox Signaling*, *9*(8), 1221–1235. https://doi.org/10.1089/ARS.2007.1628

Venkitaraman, A. R. (2019). How do mutations affecting the breast cancer genes BRCA1 and BRCA2 cause cancer susceptibility? *DNA Repair*, *81*, 102668. https://doi.org/10.1016/J.DNAREP.2019.102668

Vera-Ramirez, L., Vodnala, S. K., Nini, R., Hunter, K. W., & Green, J. E. (2018). Autophagy promotes the survival of dormant breast cancer cells and metastatic tumour recurrence. *Nature Communications*, *9*(1). https://doi.org/10.1038/s41467-018-04070-6

Villadsen, R., Fridriksdottir, A. J., Rønnov-Jessen, L., Gudjonsson, T., Rank, F., LaBarge, M. A., Bissell, M. J., & Petersen, O. W. (2007). Evidence for a stem cell hierarchy in the adult human breast. *Journal of Cell Biology*, *177*(1), 87–101. https://doi.org/10.1083/jcb.200611114

Vinay, K., Abbas, A. K., Fauston, N., & Aster, J. C. (2005). Robbins and Cotran pathologic basis of disease. *New Delhi, India*, 628–636.

Vives, V., Cres, G., Richard, C., Busson, M., Ferrandez, Y., Planson, A. G., Zeghouf, M., Cherfils, J., Malaval, L., & Blangy, A. (2015). Pharmacological inhibition of Dock5 prevents osteolysis by affecting osteoclast podosome organization while preserving bone formation. *Nature Communications*, *6*. https://doi.org/10.1038/NCOMMS7218

Vu, H. N., Dilshat, R., Fock, V., & Steingrímsson, E. (2021). User guide to MiT-TFE isoforms and post-translational modifications. *Pigment Cell & Melanoma Research*, *34*(1), 13–27. https://doi.org/10.1111/PCMR.12922

Wada, S., Neinast, M., Jang, C., Ibrahim, Y. H., Lee, G., Babu, A., Li, J., Hoshino, A., Rowe, G. C., Rhee, J., Martina, J. A., Puertollano, R., Blenis, J., Morley, M., Baur, J. A., Seale, P., & Arany, Z. (2016). The tumor suppressor FLCN mediates an alternate mTOR pathway to regulate browning of adipose tissue. *Genes & Development*, *30*(22), 2551–2564. https://doi.org/10.1101/GAD.287953.116

Wälchli, M., Berneiser, K., Mangia, F., Imseng, S., Craigie, L. M., Stuttfeld, E., Hall, M. N., & Maier, T. (2021). Regulation of human mTOR complexes by DEPTOR. *ELife*, *10*. https://doi.org/10.7554/ELIFE.70871

Wang, H., Liu, Y., Ding, J., Huang, Y., Liu, J., Liu, N., Ao, Y., Hong, Y., Wang, L., Zhang, L., Wang, J., & Zhang, Y. (2020). Targeting mTOR suppressed colon cancer growth through 4EBP1/eIF4E/PUMA pathway. *Cancer Gene Therapy*, *27*(6), 448–460. https://doi.org/10.1038/S41417-019-0117-7

Wang, Q. M., Lv, L. I., Tang, Y., Zhang, L. I., & Wang, L. F. (2019). MMP-1 is overexpressed in triple-negative breast cancer tissues and the knockdown of MMP-1 expression inhibits tumor cell malignant behaviors in vitro. *Oncology Letters*, *17*(2), 1732. https://doi.org/10.3892/OL.2018.9779

Watt, D., Dixit, R., & Cavalli, V. (2015). JIP3 Activates Kinesin-1 Motility to Promote Axon Elongation. *The Journal of Biological Chemistry*, *290*(25), 15512–15525. https://doi.org/10.1074/JBC.M115.651885

What mechanisms drive invadopodia extension? | MBInfo. (n.d.). Retrieved August 1, 2022, from https://www.mechanobio.info/cytoskeleton-dynamics/what-are-invadopodia/what-mechanisms-drive-invadopodia-extension/

Wheelock, M. J., Shintani, Y., Maeda, M., Fukumoto, Y., & Johnson, K. R. (2008). Cadherin switching. *Journal of Cell Science*, *121*(6), 727–735. https://doi.org/10.1242/jcs.000455

Wieczorek-szukala, K., & Lewinski, A. (2021). The role of snail-1 in thyroid cancer—what we know so far. *Journal of Clinical Medicine*, *10*(11). https://doi.org/10.3390/JCM10112324

Williams, K. C., & Coppolino, M. G. (2011). Phosphorylation of Membrane Type 1-Matrix Metalloproteinase (MT1-MMP) and Its Vesicle-associated Membrane Protein 7 (VAMP7)-dependent Trafficking Facilitate Cell Invasion and Migration *. *Journal of Biological Chemistry*, *286*(50), 43405–43416. https://doi.org/10.1074/JBC.M111.297069

Williams, T. M., Medina, F., Badano, I., Hazan, R. B., Hutchinson, J., Muller, W. J., Chopra, N. G., Scherer, P. E., Pestell, R. G., & Lisanti, M. P. (2004). Caveolin-1 Gene Disruption Promotes Mammary Tumorigenesis and Dramatically Enhances Lung Metastasis in Vivo: ROLE OF CAV-1 IN CELL INVASIVENESS AND MATRIX METALLOPROTEINASE (MMP-2/9) SECRETION. *Journal of Biological Chemistry*, *279*(49), 51630–51646. https://doi.org/10.1074/JBC.M409214200

Winkler, J., Abisoye-Ogunniyan, A., Metcalf, K. J., & Werb, Z. (2020). Concepts of extracellular matrix remodelling in tumour progression and metastasis. *Nature Communications*, *11*(1), 5120. https://doi.org/10.1038/s41467-020-18794-x

Wolf, K., Mazo, I., Leung, H., Engelke, K., von Andrian, U. H., Deryugina, E. I., Strongin, A. Y., Bröcker, E. B., & Friedl, P. (2003). Compensation mechanism in tumor cell migration: mesenchymal-amoeboid transition after blocking of pericellular proteolysis. *The Journal of Cell Biology*, *160*(2), 267–277. https://doi.org/10.1083/JCB.200209006

Wolf, K., Wu, Y. I., Liu, Y., Geiger, J., Tam, E., Overall, C., Stack, M. S., & Friedl, P. (2007). Multi-step pericellular proteolysis controls the transition from individual to collective cancer cell invasion. *Nature Cell Biology*, *9*(8), 893–904. https://doi.org/10.1038/NCB1616

Wolfson, R. L., Chantranupong, L., Wyant, G. A., Gu, X., Orozco, J. M., Shen, K., Condon, K. J., Petri, S., Kedir, J., Scaria, S. M., Abu-Remaileh, M., Frankel, W. N., & Sabatini, D. M. (2017). KICSTOR recruits GATOR1 to the lysosome and is necessary for nutrients to regulate mTORC1. *Nature*, *543*(7645), 438–442. https://doi.org/10.1038/NATURE21423

Wu, X., Gan, B., Yoo, Y., & Guan, J. L. (2005). FAK-mediated src phosphorylation of endophilin A2 inhibits endocytosis of MT1-MMP and promotes ECM degradation. *Developmental Cell*, *9*(2), 185–196. https://doi.org/10.1016/J.DEVCEL.2005.06.006

Wu, X., Xu, Y., Liang, Q., Yang, X., Huang, J., Wang, J., Zhang, H., & Shi, J. (2022). Recent Advances in Dual PI3K/mTOR Inhibitors for Tumour Treatment. *Frontiers in Pharmacology*, *13*, 1597. https://doi.org/10.3389/FPHAR.2022.875372/BIBTEX

Wyant, G. A., Abu-Remaileh, M., Wolfson, R. L., Chen, W. W., Freinkman, E., Danai, L. v., vander Heiden, M. G., & Sabatini, D. M. (2017). mTORC1 Activator SLC38A9 Is

Required to Efflux Essential Amino Acids from Lysosomes and Use Protein as a Nutrient. *Cell*, *171*(3), 642-654.e12. https://doi.org/10.1016/J.CELL.2017.09.046
Xu, Y., Du, S., Marsh, J. A., Horie, K., Sato, C., Ballabio, A., Karch, C. M., Holtzman, D. M., & Zheng, H. (2021). TFEB regulates lysosomal exocytosis of tau and its loss of function exacerbates tau pathology and spreading. *Molecular Psychiatry*, *26*(10), 5925. https://doi.org/10.1038/S41380-020-0738-0
Yamada, K. M., & Sixt, M. (2019). Mechanisms of 3D cell migration. *Nature Reviews Molecular Cell Biology*, *20*(12), 738–752. https://doi.org/10.1038/s41580-019-0172-9
Yamaguchi, H., Takeo, Y., Yoshida, S., Kouchi, Z., Nakamura, Y., & Fukami, K. (2009a). Lipid rafts and caveolin-1 are required for invadopodia formation and extracellular matrix degradation by human breast cancer cells. *Cancer Research*, *69*(22), 8594–8602. https://doi.org/10.1158/0008-5472.CAN-09-2305/655618/P/LIPID-RAFTS-AND-CAVEOLIN-1-ARE-REQUIRED-FOR
Yamaguchi, H., Takeo, Y., Yoshida, S., Kouchi, Z., Nakamura, Y., & Fukami, K. (2009b). Lipid rafts and caveolin-1 are required for invadopodia formation and extracellular matrix degradation by human breast cancer cells. *Cancer Research*, *69*(22), 8594–8602. https://doi.org/10.1158/0008-5472.CAN-09-2305
Yana, I., Sagara, H., Takaki, S., Takatsu, K., Nakamura, K., Nakao, K., Katsuki, M., Taniguchi, S. I., Aoki, T., Sato, H., Weiss, S. J., & Seiki, M. (2007). Crosstalk between neovessels and mural cells directs the site-specific expression of MT1-MMP to endothelial tip cells. *Journal of Cell Science*, *120*(9), 1607–1614. https://doi.org/10.1242/JCS.000679
Yana, I., & Weiss, S. J. (2000). Regulation of membrane type-1 matrix metalloproteinase activity by proprotein convertases. *Molecular Biology of the Cell*, *11*(7), 2387–2401. https://doi.org/10.1091/MBC.11.7.2387/ASSET/IMAGES/LARGE/MK0701246009.JPEG
Yang, H., Rudge, D. G., Koos, J. D., Vaidialingam, B., Yang, H. J., & Pavletich, N. P. (2013). mTOR kinase structure, mechanism and regulation. *Nature 2013 497:7448*, *497*(7448), 217–223. https://doi.org/10.1038/NATURE12122
Yang, H., Yu, Z., Chen, X., Li, J., Li, N., Cheng, J., Gao, N., Yuan, H. X., Ye, D., Guan, K. L., & Xu, Y. (2021). Structural insights into TSC complex assembly and GAP activity on Rheb. *Nature Communications*, *12*(1). https://doi.org/10.1038/S41467-020-20522-4
Yap, A. S., & Kovacs, E. M. (2003). Direct cadherin-activated cell signaling: a view from the plasma membrane. *The Journal of Cell Biology*, *160*(1), 11. https://doi.org/10.1083/JCB.200208156
Yeo, S. K., & Guan, J.-L. (2017). Breast Cancer: Multiple Subtypes within a Tumor? *Trends in Cancer*, *3*(11), 753–760. https://doi.org/10.1016/j.trecan.2017.09.001
Yersal, O. (2014). Biological subtypes of breast cancer: Prognostic and therapeutic implications. *World Journal of Clinical Oncology*, *5*(3), 412. https://doi.org/10.5306/wjco.v5.i3.412
Young-Mi Kim, A., & Hwa Jung, C. (2015). mTORC1 Phosphorylates UVRAG to Negatively Regulate Autophagosome and Endosome Maturation. *Molecular Cell*, *57*, 207–218. https://doi.org/10.1016/j.molcel.2014.11.013
Yu, X., Zech, T., McDonald, L., Gonzalez, E. G., Li, A., Macpherson, I., Schwarz, J. P., Spence, H., Futó, K., Timpson, P., Nixon, C., Ma, Y., Anton, I. M., Visegrády, B., Insall, R. H., Oien, K., Blyth, K., Norman, J. C., & Machesky, L. M. (2012). N-WASP coordinates the delivery and F-actin-mediated capture of MT1-MMP at invasive pseudopods. *The Journal of Cell Biology*, *199*(3), 527–544. https://doi.org/10.1083/JCB.201203025
Yuzhalin, A. E., Lim, S. Y., Kutikhin, A. G., & Gordon-Weeks, A. N. (2018). Dynamic matrisome: ECM remodeling factors licensing cancer progression and metastasis. *Biochimica et Biophysica Acta (BBA) - Reviews on Cancer*, *1870*(2), 207–228. https://doi.org/10.1016/j.bbcan.2018.09.002
Zaffagnini, G., Savova, A., Danieli, A., Romanov, J., Tremel, S., Ebner, M., Peterbauer, T., Sztacho, M., Trapannone, R., Tarafder, A. K., Sachse, C., & Martens, S. (2018). p62

filaments capture and present ubiquitinated cargos for autophagy. *The EMBO Journal*, *37*(5), e98308. https://doi.org/10.15252/EMBJ.201798308

Zagryazhskaya-Masson, A., Monteiro, P., Macé, A. S., Castagnino, A., Ferrari, R., Infante, E., Duperray-Susini, A., Dingli, F., Lanyi, A., Loew, D., Génot, E., & Chavrier, P. (2020). Intersection of TKS5 and FGD1/CDC42 signaling cascades directs the formation of invadopodia. *Journal of Cell Biology*, *219*(9). https://doi.org/10.1083/jcb.201910132

Zhao, H., Yang, M., Zhao, J., Wang, J., Zhang, Y., & Zhang, Q. (2013). High expression of LC3B is associated with progression and poor outcome in triple-negative breast cancer. *Medical Oncology (Northwood, London, England)*, *30*(1). https://doi.org/10.1007/S12032-013-0475-1

Zhao, J., Brault, J. J., Schild, A., Cao, P., Sandri, M., Schiaffino, S., Lecker, S. H., & Goldberg, A. L. (2007). FoxO3 coordinately activates protein degradation by the autophagic/lysosomal and proteasomal pathways in atrophying muscle cells. *Cell Metabolism*, *6*(6), 472–483. https://doi.org/10.1016/J.CMET.2007.11.004

Zucker, S., Hymowitz, M., Conner, C., DeClerck, Y., & Cao, J. (2004). TIMP-2 is released as an intact molecule following binding to MT1-MMP on the cell surface. *Experimental Cell Research*, *293*(1), 164–174. https://doi.org/10.1016/J.YEXCR.2003.10.007

ANNEXE 1

Codependencies of mTORC1 signaling and endolysosomal actin structures.

Submitted (in review in Advanced Sciences)

Amulya Priya[1], Sandra Antoine-Bally[1], Anne-Sophie Macé[2], Pedro Monteiro[1], Valentin Sabatet[3], David Remy[1], Florent Dingli[3], Damarys Loew[3], Alexis M. Gautreau[4], and Philippe Chavrier[1,*]

[1] Institut Curie, CNRS UMR144, PSL Research University, Research Center, Actin and Membrane Dynamics Laboratory, 26 rue d'Ulm, Paris 75248 Cedex 05, France

[2] Institut Curie, PSL Research University, Cell and Tissue Imaging Facility (PICT-IBiSA), 26 rue d'Ulm, Paris 75248 Cedex 05, France

[3] Institut Curie, PSL Research University, CurieCoreTech Mass Spectrometry Proteomics, 26 rue d'Ulm, Paris 75248 Cedex 05, France

[4] Laboratoire de Biologie Structurale de la Cellule, CNRS, Ecole Polytechnique, IP Paris, Palaiseau, France

* Author for correspondence. E-mail : philippe.chavrier@curie.fr

ANNEXE 2

A mechanosensitive caveolae-invadopodia interplay drives matrix remodeling for cancer cell invasion.

Submitted (in review in Nature Cell Biology)

Pedro MONTEIRO [1,2,$], David REMY [1], Eline LEMERLE [3], Fiona ROUTET [1], Anne-Sophie MACE [4], Chloé GUEDJ [4], Benoit LADOUX [5], Stéphane VASSILOPOULOS [3], Christophe LAMAZE [2,*,$] and Philippe CHAVRIER [1,*,$]

1 Institut Curie – Research Center, CNRS UMR144, PSL Research University, Actin and Membrane Dynamics Laboratory, 26 rue d'Ulm, Paris 75248 Cedex 05, France

2 Institut Curie – Research Center, CNRS UMR3666, INSERM U1143, PSL Research University, Membrane Mechanics and Dynamics of Intracellular Signaling Laboratory, 26 rue d'Ulm, Paris 75248 Cedex 05, France

3 Sorbonne Université, INSERM UMRS 974, Institute of Myology, Paris, France

4 Institut Curie, PSL Research University, Cell and Tissue Imaging Facility (PICT-IBiSA), 26 rue d'Ulm, Paris 75248 Cedex 05, France

5 Institut Jacques Monod, Université de Paris, CNRS UMR 7592, 75013 Paris, France

* Co-last authors

$ Corresponding authors: pedro.monteiro@curie.fr, christophe.lamaze@curie.fr, philippe.chavrier@curie.fr

ANNEXE 3

Cell Migration in Three Dimensions, 1st ed. 2023; Methods in Molecular Bilogy Series, Vol. 2608

Coordinator: Margadant Coert

Invadopodia methods: detection of invadopodia formation and activity in cancer cells using reconstituted 2D and 3D collagen-based matrices

Accepted, to be published in January 2023.

David REMY, Anne-Sophie MACE, Philippe CHAVRIER, and Pedro MONTEIRO[,*]

[1] Institut Curie, CNRS UMR144, PSL Research University, Research Center, Actin and Membrane Dynamics Laboratory, 26 rue d'Ulm, Paris 75248 Cedex 05, France

[2] Institut Curie, PSL Research University, Cell and Tissue Imaging Facility (PICT-IBiSA), 26 rue d'Ulm, Paris 75248 Cedex 05, France

* Author for correspondence (pedro.monteiro@curie.fr)

Abstract

Tumor dissemination involves cancer cell migration through the extracellular matrix (ECM). ECM is mainly composed of collagen fibers that oppose cell invasion. To overcome hindrance in the matrix, cancer cells deploy a protease-dependent program in order to remodel the matrix fibers. Matrix remodeling requires the formation of actin-based matrix/plasma membrane contact sites called invadopodia, responsible for collagen cleavage through the accumulation and activity of the trans-membrane type-I matrix metalloproteinase (MT1-MMP). In this article, we describe experimental procedures designed to assay for invadopodia formation and for invadopodia activity using 2D and 3D models based on gelatin (denatured collagen) and fibrillar type-I collagen matrices.

Key words: collagen, gelatin, invadopodia, confocal spinning disk microscopy, indirect immunofluorescence, matrix degradation.

1. Introduction

Invadopodia were first reported in the early 80s as rosette-shaped actin-, vinculin-, and alpha-actinin-rich structures forming in chicken embryo fibroblasts transformed by the Rous sarcoma virus and associated with a robust matrix proteolytic activity (1,2). Invadopodia have since been shown to form specifically in cancer cells in contrast with podosomes that are found in noncancerous cells such as macrophages, osteoclasts, and dendritic cells (3-5). The generic term invadosome is a merge of the invadopodia and podosome appellations (6). Invadopodia have been extensively characterized at the structural and molecular level. In 2D culture systems, invadopodia form defined plasma membrane domains on the ventral surface of invasive cancer cells in contact with the extracellular matrix (ECM) and represent the major structures implicated in local degradation of the underlying ECM. Invadopodia distribution and morphology can vary according to cell models and biochemical and physical properties of the matrix (7,8). Cells plated on a thin layer of gelatin or denatured collagen develop discrete dot-like 0.5-1 μm diameter structures mainly located underneath the nucleus (9) (Figure 1). In contrast, when cultured on a thin layer of fibrillar type-I collagen fibers, invasive tumor cells form linear invadopodia, which are aligned along the collagen fibrils (10-15) (Figure 1). In a 3D collagen network, invadopodia were shown to form at plasma membrane-ECM fiber contact sites in a region anterior to the nucleus (relative to cell movement) (11,12,16,17) (Figure 1). This polarized distribution confers invadopodia a protective role for the nucleus by relaxing and weakening fibers that oppose cell and nuclear movement and that are responsible for nuclear deformation (11,12,18).

Invadopodia formation is a sequential process consisting of initiation, stabilization, and maturation steps (19-21). Invadopodia formation initiates with the local activation of actin polymerization machinery composed of the actin-nucleating ARP2/3 complex and its upstream activators and cofactors, N-WASP, cofilin, and cortactin (20; 22-24). The scaffolding protein, tyrosine kinase substrate 5 (TKS5; also known as SH3PXD2A) has emerged as a specific invadopodia component critically involved in the formation of podosomes and both dot-like and linear invadopodia (11, 23, 25, 26). Along with actin polymerization, invadopodia are sites of

active ECM proteolysis mostly due to the local accumulation of the membrane-tethered matrix metalloproteinase, MT1-MMP (aka MMP14). MT1-MMP has been described as the major invadopodia regulator of cancer cell invasion and metastasis programs in a wide range of malignancies (27). It is stored in intracellular endo/lysosomal compartments from which the protease can be recycled and trafficked back to invadopodia (10, 15, 28-32). Thus, F-actin polymerization and MT1-MMP-mediated matrix degradation are hallmarks of invadopodia formation and activity.

Since their discovery, invadopodia have mainly been studied owing to the relatively simple and widely used cross-linked gelatin assay, in which cells are seeded on top of a thin layer of fluorescently-labeled gelatin (19, 28). This experimental set-up allows easy and direct visualization of matrix degradation through the loss of gelatin fluorescence (Figure 1). Over the past years, new procedures have been developed to explore the mechanisms underlying invadopodia formation and activity in experimental conditions closer to the pathological situations. These include models based on reconstituted fibrillar type-I collagen, the main component of interstitial tissues in the body (10, 11, 13, 15, 26).

In this chapter, we present protocols for the experimental procedures currently available in our laboratory to study invadopodia formation and measure their proteolytic activity using 2D and 3D assays based on gelatin (denatured collagen) and fibrillar type-I collagen matrices. We use the human mesenchymal mammary adenocarcinoma cell line, MDA-MB-231, a widely used cell model for invadopodia and tumor cell invasion studies (10-12, 15, 30). We detail how to reconstitute gelatin and fibrillar type-I collagen matrices, and how to culture cells on top of these matrices and measure invadopodia formation and activity. Moreover, we discuss the strengths and weaknesses of each method.

Materials

a. Cell culture

1. T-75 flasks with filter cap.
2. Sterilized serological pipettes (5 – 25 mL).
3. Filtered pipette tips (0.01 – 1 mL).
4. Sterilized Eppendorf tubes.
5. 12-well culture plate (22.2 mm-diameter).
6. MDA-MB-231 breast adenocarcinoma cells (ATCC, HTB-26).
7. MDA-MB-231 stably expressing TKS5-GFP (available from the authors) (11).
8. Culture medium for MDA-MB-231 cells; Leibovitz-15 (L15) without L-Glutamine (Merck, Darmstadt, Germany), 2 mM L-Glutamine (ThermoFisher Scientific Inc.), 15% heat inactivated Fetal Bovine Serum (FBS) (Gibco).
9. Culture medium for live-cell imaging; Leibovitz-15 (L15) without L-Glutamine (Merck, Darmstadt, Germany), 2 mM L-Glutamine (ThermoFisher Scientific Inc.), 15% heat inactivated Fetal Bovine Serum (FBS) (Gibco), 20ng/mL hepatocyte growth factor (HGF) (ThermoFisher Scientific Inc.).
10. Phosphate-Buffered Saline 1X (PBS) suitable for cell culture pH 7.4; 137 mM NaCl, 2.7 mM KCl, 10 mM Na_2HPO_4, and 1.8 mM KH_2PO_4.
11. Trypsin TrypLE™ Express (1X) (Gibco).
12. Humidified cell culture incubator set at 37°C with 1% CO_2 for MDA-MB-231 cell line.
13. Cationic lipid and polyamine-based transfection reagent Lullaby (OZ Biosciences).
14. Opti-MEM™ 1X (Gibco).
15. Small interfering RNA (siRNA) (See Table 1)
16. Nucleofector™ 2B device (Lonza)
17. Cell Line Nucleofector™ Kit (Lonza).

b. Gelatin degradation assay

i. Resuspension of fluorescent gelatin

2. Sucrose solution (2% w/v in PBS).

3. Gelatin from pig skin, Oregon Green™ 488 conjugate, 5 mg (ThermoFisher Scientific Inc.) (see Notes 1 and 2).
4. 1.5 mL Eppendorf tubes.
5. 15 mL and 50 mL conical Falcon centrifuge tubes.
6. A centrifuge accepting Falcon tubes able to reach 3,800 xg centrifugal force.

i. Fluorescence labeling of gelatin

1. Gelatin from porcine skin, 100 g (ThermoFisher Scientific Inc.).
2. 0.1M Na_2CO_3 in sterile water.
3. 0.1M $NaHCO_3$ in sterile water, adjusted to pH 8.3 with Na_2CO_3 solution.
4. Dimethyl sulfoxide (DMSO) (Merck).
5. PBS.
6. Fluorophore of choice (we use Alexa Fluor™ 647 carboxylic acid, succimidyl ester, ThermoFischer Scientific Inc.). Of note, gelatin from pig skin conjugated with fluorescein or Oregon Green488 can be purchased (Invitrogen)
7. PD-10 filtration columns (GE Healthcare).
8. Calibrated pH meter.
9. A centrifuge accepting Falcon tubes able to reach 8,000 xg centrifugal force.
10. Pierce™ BCA Protein Assay Kit (ThermoFisher Scientific Inc.).
11. Spectrophotometer to detect absorbance at 280 nm and 562 nm.
12. A precision scale.

ii. Coverslip preparation for immunostaining

1. PBS.
2. Glutaraldehyde.
3. Sodium borohydride solution 133 mM in PBS.
4. Poly-L-lysine 0.005% in sterile water (see Note 4).
5. 12-well culture plate (22.2 mm-diameter).

6. Glass coverslips 18 mm-diameter, pre-sterilized (VWR).
7. Sharp precision tweezers.
8. Parafilm.
9. Ethanol 70%.

7.

i. MatTek preparation for live-cell imaging

1. PBS.
2. Glutaraldehyde 0.5% in PBS.
3. Sodium borohydride solution 133 mM in PBS.
4. Poly-L-lysine 0.005%in sterile water (see Note 4).
5. 35 mm Dish, No. 1.5 Coverslip, 10 mm Glass Diameter, Uncoated glass bottom microwell dishes (MatTek Corporation).

8.

a. Collagen degradation assay

i. Coverslip preparation and coating

1. Type-I Collagen, acid-extracted from rat tail, 100 mg (Corning®).
2. Type-I Collagen, acid-extracted from rat tail high concentration, 100 mg (Corning®).
3. Polymerization buffer; 100 µL of Minimum Essential Media (MEM) 10X (with Phenol red, without L-glutamine, HEPES and sodium bicarbonate), 50 µL of 0.34N NaOH and 30 µL of 1M HEPES.
4. pH strips (MQuant, Merck).
5. 12-well culture plate (22.2 mm-diameter well).
6. Glass coverslips 18 mm-diameter, pre-sterilized (VWR).
7. Sharp precision tweezers.

9.

i. Labeling of collagen

1. Neutralizing phosphate buffer; 20 mM NaH_2PO_4 in sterile water, 167 mM NaH_2PO_4 - H_2O in sterile water, 470 mM NaCl and 0.045 N NaOH.

2. 1M Na_2CO_3 pH11 in sterile water.
3. 1M $NaHCO_3$ pH8 in sterile water.
4. Carbonate buffer; 1M $NaHCO_3$ in sterile water adjusted to pH8.3 with Na_2CO_3 solution (see Note 12).
5. 0.22 µm polycarbonate filters.
6. PBS.
7. Sterile water.
8. Type-I Collagen, acid-extracted from rat tail, 100mg (Corning®).
9. Alexa Fluor™ 555 NHS Ester (Succinimidyl Ester) (Invitrogen); Alexa Fluor™ 488 NHS Ester (Succinimidyl Ester) (Invitrogen); Alexa Fluor™ 647 NHS Ester (Succinimidyl Ester) (Invitrogen).
10. A precision scale.
11. Heat-resistant glass bottle.

b. Fixation and immunolabeling

1. Paraformaldehyde (PFA) 16% (Electron Microscopy Sciences).
2. PFA 4% (diluted in PBS from 16% PFA).
3. TRITON® X-100 Detergent, Molecular Biology Grade (Merck).
4. TRITON® X-100 0.1% diluted in PFA 4% from stock TRITON X-100.
5. Blocking buffer (10% FBS diluted in PBS).
6. Primary and secondary antibodies (see Table 1).
7. Mounting medium Prolong™ Gold antifade reagent with DAPI (4',6-diamidino-2-phenylindole) (ThermoFischer Scientific Inc.).
8. PBS.
9. Sharp precision tweezers.
10. Microscope glass slides, precleaned.

Methods

c. Cell culture and cell plating

1. Aspirate culture medium from a confluent flask of MDA-MB-231 cells and gently add 5 mL of PBS.
2. Aspirate PBS and add 1 mL of Trypsin TrypLE^{TM} Express. Allow the Trypsin to cover the entire flask by tilting.
3. Quickly aspirate Trypsin and incubate the flask at 37°C, 1% CO_2 for 2 min.
4. After 2 min, remove flask from the incubator and resuspend cells in 10 mL of culture medium by pipetting vigorously to detach the cells from the surface and from each other.
5. Transfer the cell suspension to a 15 mL falcon and count cells manually or using an automated cell counting method.

10.

a. Invadopodia knockdown as negative control of invadopodia formation and matrix degradation

1. For one transfection reaction in one well of a 12-well plate, prepare the siRNA mix as follows: Tube 1 (96 µL of Opti-MEM + 4 µL of Lullaby) and Tube 2 (97.5 µL of Opti-MEM + 2.5 µL of siRNA stock 20 µM). siRNAs are usually used at 50 nM concentration in the final culture medium (see Table 2). Incubate at RT for 5 min.

~~11.~~ Add the content of tube 2 to tube 1 and incubate for 20 min at room temperature (RT).

2. While the siRNA/Lullaby transfection reagent mix is incubating, prepare 800 µL of a cell suspension containing 80,000 cells (100,000 cells/mL) for one well.
3. After 20 min of incubation, transfer the siRNA mix (200 µL) in the well and add 800 µL of cell suspension, dropwise.
4. Gently shake the plate and incubate at 37°C, 1% CO_2 for 72 h. If needed, medium can be changed 24 h after treatment.

a. Transient transfection of plasmids

1. Add 2 mL of complete medium to three wells of a 6-well plate. Incubate at 37°C to pre-heat medium.
2. Resuspend 1x10^6 MDA-MB-231 cells in 100 µL of the Nucleofector® Solution.
3. Transfer the cell suspension to a 1.5 mL Eppendorf tube.
4. Add 1 µg of purified DNA and mix well.
5. Transfer the content of the Eppendorf tube to an AMAXA cuvette.
6. Insert the cuvette into the Nucleofector® and launch the X-013 program (MDA-MB-231 program) by pressing the >>X<< button.
7. Using the furnished pipette, immediately remove the sample from the cuvette and add one drop of sample per well, in the pre-heated culture medium from step 1.
8. Incubate at 37°C for 4 h. Refresh medium and incubate for 48 h before analysis.

b. Gelatin degradation assay for immunofluorescence microscopy

i. Dissolution of commercial fluorescent-conjugated gelatin

1. Add 5 mL of 2% sucrose solution to the tube containing 5 mg of lyophilized gelatin-fluorescein (or Oregon Green 488) conjugate.
2. Mix well and transfer to a 50 mL conical Falcon tube.
3. Repeat steps 1 and 2 twice to efficiently extract all the powder from the commercial vial.
4. Adjust to 25 mL with 2% sucrose solution and dissolve for 60 min at RT on gentle agitation and protected from light.
5. Aliquot in 1.5 mL Eppendorf tubes and keep frozen at -18°C (in our hands, gelatin solution is stable for up to 3-5 years).

ii. Gelatin coupling to fluorophore

1. Adjust pH of $NaHCO_3$ solution to pH 8.3 using Na_2CO_3 solution (use a pH meter).
2. Dissolve 50 mg of gelatin in 4.5 mL of $NaHCO_3$ solution pH 8.3.
3. Centrifuge the gelatin solution at 8,000 xg for 30 min at RT (see Note 5).

4. Dissolve 1 mg of Alexa Fluor™ NHS Ester (Succinimidyl Ester) dye with the desired excitation/emission wavelengths in 100 µL of DMSO.
5. Add 100 µL of fluorophore solution to the gelatin solution, dropwise.
6. Gently rotate the gelatin-fluorophore mix on a spinning wheel for 60 min at RT, protected from light.
7. Remove the non-conjugated dye on two PD-10 gel filtration columns.
8. Equilibrate the column with 25 mL of PBS.
9. Add 2.5 mL of the gelatin solution on the equilibrated PD-10 column (use two columns for the 5 mL reaction).
10. Once all the gelatin solution has entered the column, elute with 3.5 mL of PBS.
11. Harvest eluate in 0.5 mL aliquots.
12. Measure absorbance at 280nm and pool peak fractions.
13. Measure protein concentration with method of choice (BCA kit for instance).
14. Adjust concentration to 0.2 mg/mL with 2% sucrose solution.
15. Prepare 1 mL aliquots and store at -20°C.

iii. Coverslips coating with gelatin

It is recommended to perform gelatin coating of the glass coverslips on the day of the experiment. The procedure described hereafter is for 18 mm-diameter coverslips in a 12-well plate.

1. Place one coverslip per well and add 1 mL of 0.5 µg/mL poly-L-lysine solution for 20 min at RT (see Note 4).
2. Aspirate poly-L-lysine solution from the well and rinse coverslip in 1 mL of PBS.
3. Aspirate PBS in the well and add 1 mL of 0.5% glutaraldehyde for 10 min at RT.
4. Aspirate the glutaraldehyde solution from the well and rinse the coverslip three times with 1 mL of PBS. Keep the coverslip in PBS until next step.

5. Place a parafilm on a sterile, flat surface (e.g., the lid of the 12-well plate) and sterilize the parafilm with 70% ethanol. Make sure the surface is flat to allow homogeneous coating of the coverslip with gelatin.
6. If using fluorescently-coated gelatin, it is preferable to perform all subsequent steps in the dark in order to avoid bleaching of the dye.
7. For each coverslip, place a drop of 80 µL of gelatin solution on the parafilm layer.
8. Retrieve the coverslip from the well using the sharp precision tweezers and place it on the gelatin drop, the top of the coverslip coated with poly-L-lysine facing down. Incubate in the dark for 10 min at RT.
9. Using the precision tweezers, transfer the coverslip back to the 12-well filled with PBS (see Note 6).
10. Aspirate the PBS and add 1 mL of 0.05 % sodium borohydride solution for 3 min at RT, in the dark (see Note 7 and 8).
11. Safely discard the sodium borohydride solution (see Note 7) and rinse the coverslip 3 times with 1 mL of PBS.
12. Aspirate PBS and add 1 mL of cell culture medium. Incubate the plate in a humidified 37°C, 1% CO_2 incubator while preparing the cell suspension.
13. Aspirate the culture medium and add 1 mL of MDA-MB-231 cell suspension (90,000 cells/mL) in the 12-well (see Note 9).
14. Incubate at 37°C, 1% CO_2 for 6 to 24 h (see Note 10 and 11).

12.

i. Gelatin coating of glass-bottom MatTek dish for live-cell imaging

1. Add 2 mL of 0.5 µg/mL poly-L-lysine solution in the MatTek dish for 20 min at RT (see Note 4).
2. Aspirate poly-L-lysine solution from the dish and wash with 2 mL of PBS.
3. Aspirate PBS and add 2 mL of 0.5% glutaraldehyde for 10 min at RT.
4. Aspirate 0.5% glutaraldehyde solution and wash the dish 3 times with 2 mL of PBS.

5. If using fluorescently-coated gelatin, all steps, from now on, should be performed in the dark in order to avoid bleaching of gelatin.
6. Remove PBS and add a drop of 80 µL of gelatin on the glass coverslip. Spread the drop around with the pipette tip to the borders of the glass coverslip. Incubate in the dark for 10 min at RT.
7. Rinse excess gelatin with 2 mL PBS and add 2 mL of 5 mg/mL sodium borohydride for 3 min at RT, in the dark (see Note 7).
8. Aspirate sodium borohydride (see Note 7) and rinse the dish 3 times with 2 mL of PBS.
9. Aspirate PBS and add 2 mL of cell culture medium. Transfer the plate to a humidified 37°C, 1% CO_2 incubator while preparing the cell suspension.
10. Prepare a 70,000 cell/mL suspension of MDA-MB-231 cells stably expressing TKS5-GFP (or MDA-MB-231 cells transfected with a construct encoding an invadopodia marker such as dsRed-Cortactin, available on demand). Aspirate the culture medium from the MatTek dish and add 2 mL of the cell suspension.
11. Incubate for 30 min in a 37°C, 1% CO_2 incubator to allow cells to adhere to the gelatin-coated glass bottom. Transfer the dish to the microscope stage and make proper set up for time lapse acquisition.

b. Collagen-based matrix for immunofluorescence microscopy

i. Collagen labeling

1. Filtrate neutralizing and carbonate buffers with a 0.22 µm polycarbonate filter.
2. Mix 2 mL of rat tail tendon type-I collagen stock solution (liquid in 0.02 N acetic acid, concentration range 3-4 mg/mL) with 0.5 mL of neutralizing buffer in a sterile 25 mL glass bottle and incubate 30 min at 37°C, 5% CO_2 for collagen polymerization (see Note 13).
3. Add 5 mL PBS to the collagen gel and leave for 10 min at RT. Repeat this step twice and make sure to carefully aspirate all the remaining PBS.

4. Mix 3 mL of sterile water with 1 mL of carbonate buffer (1M; pH8.3) and add this solution to the polymerized collagen gel. Final concentration is ~0.2 M taking into account the volume of the collagen gel (see Note 14).
5. Resuspend the Alexa Fluor™ NHS Ester (Succinimidyl Ester) dye with the desired excitation/emission wavelengths in 100 µL of DMSO. Add the dye solution to the bottle containing the collagen gel and the carbonate buffer. Incubate overnight at 4°C in the dark under constant agitation.
6. Remove the dye solution.
7. Wash 5-6 times with 5 mL PBS at RT under agitation for 30 min. Make sure to discard all the PBS after the final wash.
8. On ice, add 2 mL of cold 20 mM HCl to dissolve the labeled collagen.
9. Agitate in the cold room for at least 2-3 h until total dissolution of the labeled collagen (see Note 15).
10. Store solubilized fluorescently-labeled type-I collagen at 4°C. It can be stored for up to 6 months at 4°C in the dark.

ii. Preparation of fluorescently-labeled collagen solution

Collagen gelation is heat-sensitive. Thus, all steps of collagen preparation should be performed on ice using ice-cold reagents.

1. Reagents and solutions required for collagen polymerization are transferred to ice (*i.e.* type-I collagen solution, MEM 10X, HEPES 1M, NaOH 0.34N, sterile water).
2. Prepare the polymerization buffer.
3. Prepare 1 mL of collagen solution at 2.6 mg/mL by diluting stock collagen solution with sterile water (see Note 16).
4. Fluorescent collagen can be obtained by mixing fluorescently-labeled collagen (see section 3.5.1) with non-labeled collagen solution to a 1:20-1:40 ratio depending on required fluorescence.

5. Add 800 µL of collagen solution (2.6 mg/mL) to 180 µL of Polymerization Buffer. A 2.2 mg/mL type-I collagen polymerization solution is now ready. Keep it on ice until inducing polymerization (see Note 17).

iii. Polymerization of a type-I collagen layer for 2D assays

1. Add a 18 mm-diameter coverslip in a 12-well and transfer the plate on ice to let it cool down for 2-3 min.
2. Smear 200 µL of 2.2 mg/mL collagen Polymerization Solution on top of each coverslip. Try to cover the maximum surface of the coverslip. Be careful not to touch the edge to avoid collagen leaking out of the coverslip by capillarity.
3. Aspirate most of the ungelled collagen solution, leaving a thin layer of collagen solution on top of the coverslip.
4. Transfer the plate to a 37°C incubator, 1% CO_2 for 150 s to start collagen polymerization.
5. Remove the plate from the incubator and gently add 1 mL of PBS in order to hydrate the collagen gel and stop polymerization.
6. Remove the PBS and gently add 1 mL of culture medium. Incubate the plate with the collagen-coated coverslips in the incubator while preparing the cell suspension.
7. Prepare the MDA-MB-231 cell suspension (50,000 cells/mL). Aspirate the culture medium from the well containing the collagen-coated coverslip and gently add 1 mL of the cell suspension per well.
8. Incubate at 37°C, 1% CO_2 for the desired amount of time (typically 60 – 90 min).

13.

i. MatTek coating with collagen for 2D live-cell imaging

1. Prepare a 2.2 mg/mL collagen Polymerization Solution as described in section 3.5.2. (fluorescently-labeled or not).

1. Transfer a MatTek dish on ice and let it cool down for 2-3 min.

2. Spread 10 µL of 2.2 mg/mL collagen Polymerization Solution on the glass-bottom surface of the MatTek dish. Smear the collagen solution with the tip and make sure to touch the edge of the glass-bottom to allow the collagen gel to adhere better to the well.
3. Transfer the MatTek dish to the incubator at 37°C, 5% CO_2 for 150 s to start collagen polymerization.
4. Remove the dish from the incubator and gently add 1 mL of PBS.
5. Remove PBS and gently add 2 mL of culture medium. Place the MatTek dish in the incubator while preparing the cells.
6. Prepare MDA-MB-231 cells stably expressing TKS5-GFP (or MDA-MB-231 cells transfected with a construct encoding an invadopodia marker such as dsRed-Cortactin, available on demand) (50,000 cells/mL in culture medium). Aspirate the culture medium from the collagen-coated MatTek dish and add 2 mL of the cell suspension.
7. We recommend going straight to the microscope stage as cell adhesion to the collagen gel layer is very rapid.

ii. Coverslip coating with a 3D collagen drop

1. Add a 18 mm-diameter coverslip to a 12-wells plate.
2. Prepare a 2.2 mg/mL collagen Polymerization Solution as described in section 3.5.2 (fluorescently-labeled or not).
3. Centrifuge the cell suspension and resuspend 10,000 cells in 40 µL of the 2.2 mg/mL collagen Polymerization Solution. Add a 40 µL drop of collagen containing the cells on each coverslip.
4. Transfer the plate to a 37°C, 1% CO_2 incubator for 30 min to induce polymerization.
5. Add carefully 1 mL of culture medium in each well and incubate at 37°C, 1% CO_2 for 16 - 20 h (see Note 18).

iii. MatTek coating with bilayered collagen sandwich for 3D assay

1. Prepare a 5 mg/mL collagen Polymerization Solution following the procedure described in section 3.5.2 using fluorescently-labeled or unlabeled collagen.
2. Spread 10 µL of the 5 mg/mL collagen Polymerization Solution on the glass-bottom surface of a MatTek dish (as described in section 3.5.4) to prepare the collagen bottom layer. Let it polymerize for 150 s in a 37°C incubator (5% CO_2).
3. Then, gently add 2 mL of PBS to the well.
4. Aspirate the PBS and add 2 mL of culture medium. Transfer the dish to the incubator while preparing the cells.
5. Prepare MDA-MB-231 cells stably expressing TKS5-GFP (or MDA-MB-231 cells transfected with a construct encoding an invadopodia marker such as dsRed-Cortactin, available on demand) (50,000 cells/mL in culture medium). Allow cells to adhere to the collagen bottom layer for 30 min in a 37°C, 5% CO_2 incubator.
6. During this time, prepare a 2.2 mg/mL collagen Polymerization Solution as described in section 3.5.2.
7. After adhesion of the cells to the bottom collagen layer, remove the culture medium and add 50 µL of the 2.2 mg/mL collagen Polymerization Solution on top of the bottom collagen layer with the seeded cells on top of it and allow polymerization of the upper collagen layer for 90 min at 37°C, 1% CO_2 incubator. Cells will be sandwiched between a 5 mg/mL and a 2.2 mg/mL collagen layer.
8. Add 2 mL of culture medium for live-cell imaging to stimulate cell invasion. Incubate the plate for 60 min in the 37°C, 1% CO_2 incubator before acquisition.

b. Immunolabeling of invadopodia markers and collagen cleavage

i. Immunolabeling of invadopodia markers in fixed cells

All incubation periods should be performed in the dark to avoid bleaching of fluorescently-labeled matrices along with secondary antibodies.

1. Remove the plate(s) containing the coated coverslips from the incubator.

2. Aspirate the culture medium and wash cells once with 1 mL of PBS.
3. Aspirate PBS and pre-permeabilize cells for 90 sc at 37°C in a water bath with 1 mL of pre-heated 0.1% Triton X-100 (10 µL of Triton X-100 diluted in 1 mL of 4% PFA solution) (see Note 19).
4. Discard 0.1% Triton X-100/4% PFA pre-permeabilization solution and add 1 mL of pre-heated 4% PFA solution and incubate for 20 min in a 37°C water bath.
5. Aspirate the 4% PFA solution and wash three times with 1 mL of PBS at RT. At this stage, the plate can be stored at 4°C or the immunofluorescence labeling can be performed as described below.
6. Incubate coverslips in 1 mL of blocking buffer for 60 min at RT.
7. To probe invadopodia, cells can be stained for TKS5 or cortactin, both proteins being widely used as specific invadopodia markers (see introduction section). Antibody sources and dilution conditions are described in Table 1 (see Note 20).
8. Prepare the diluted primary antibodies in blocking buffer. Add 50 µL of diluted antibodies on a parafilm layer in a humidified chamber. Gently retrieve the coverslip from the well with precision tweezers and incubate on the antibody solution drop (cells facing down) for 60 min at RT in the dark (or overnight at 4°C; see Table 1).
9. Flip back and transfer the coverslip to the 12-well and wash three times in PBS (5 min each).
10. Prepare the diluted secondary antibodies (references and working dilutions in Table 1). As the gelatin or collagen matrices are fluorescently-labeled (commonly Oregon Green488 and Cy5, respectively), make sure to adapt the secondary antibody combination. Add a 50 µL drop of diluted antibodies on a parafilm layer in a humidified chamber and place the coverslip cell facing down on top the drop. Incubate for 60 min at RT in the dark.
11. Flip the coverslip back and transfer to the 12-well plate and wash three times in PBS (5 min each).
12. After a quick wash in distilled water, mount the coverslip (cells facing down) on a precleaned microscope glass slide using mounting medium. Keep the mounted glass

coverslips in the dark overnight at RT to let the mounting medium dry, before storing at 4°C.

13. Acquire images on a fluorescence microscope with the appropriate filters and imaging software (Figure 1).

ii. Immunolabeling of MMP-cleaved collagen

Proceed with step 1-6 from section 3.6.1.

7. Prepare the diluted antibodies (usually Col1-$^{3/4}$C and anti-cortactin for visualization of cleaved collagen and invadopodia, respectively) in blocking buffer (the reference and dilution factor used for rabbit polyclonal Col1-$^{3/4}$C antibody are described in Table 1). Transfer a 50 µL drop of diluted antibodies to a parafilm layer in a humidified chamber. Place the coverslip on top of the antibody solution (cells facing down) for 2 h on ice.
8. Flip the coverslip back and transfer to the 12-well plate and wash three times with cold PBS on ice for 10 min.
9. Prepare the diluted anti-rabbit IgG Cy^{TM}3 and anti-mouse IgG Alexa Fluor^{TM}488 secondary antibodies (references and working dilutions in Table 1).
10. Add a 50 µL drop of diluted antibodies to a parafilm layer in a humidified chamber. Place the coverslip on top of the antibody solution (cells facing down) for 1 h on ice.
11. Flip the coverslip back and transfer to the 12-well plate and wash three times with cold PBS on ice for 10 min.
12. After a quick wash in distilled water, mount the coverslip (cells facing down) on a precleaned microscope glass slide using mounting medium. Keep the mounted glass coverslips in the dark overnight at RT to let the mounting medium dry, before storing at 4°C.
13. Acquire images on a fluorescence microscope with the appropriate filters and imaging software.

c. Image acquisition and analysis

i. Image acquisition and analysis of gelatin degradation and invadopodia parameters

1. To determine the percentage of degrading cells, image acquisitions should be done using a 63X objective. To determine the area of degradation per cell, imaging can be performed with a 63X or 100X objective. Use the same acquisition setups for image comparison. Acquire a z-stack.
2. Gelatin degradation fields should be acquired in a non-biased way by scanning the coverslip based on TKS5 or cortactin staining. Select individual cells that are nicely spread and with good staining (Figure 1). Acquire a z-stack from the bottom to the top of the cell. To be unbiased, do not check the gelatin channel. To have statistical power, it is advised to acquire at least 15 images and/or 20 cells for each condition. Repeat the experiment at least three independent times.
3. For analysis in ImageJ, open the GFP z-stack (corresponding to the gelatin channel) and select the gelatin and degradation plane. Apply an “Unsharp mask” with a radius of 5 pixels and a mask of 0.8 (“Process” → “Filters” → “Unsharp Mask”) and a “Mean” filter with a radius of 1 pixel (“Process” → “Filters” → “Mean…”).
4. Use the threshold command of ImageJ (“Image” → “Adjust” → “Threshold…”) to highlight the degradation zones (black pixels). Then run Analyze Particles (“Analyze” → “Analyze Particles”). Be sure to check the “Summarize” checkbox.
5. Calculate the degradation index by dividing the total area of degradation (found in the “Total Area” column of the “Summary” windows generated by the “Analyze Particles” command) by the number of nuclei present in the field. Plot the degradation index for the different conditions.
6. For quantification of gelatin degradation and analysis of invadopodia number, size and distance to nucleus, semi-automated macros are available (see Supplemental files 3-5).

14. Precise and unbiased delimitation of the gelatin degradation can be automatically performed using the NIS.AI tool from NIS Elements software, more precisely the Convert.AI module. The software training phase requires at least 50 annotated images and should be

conducted as follows: in ImageJ, manually create and save the degradation regions of interest (ROIs) as explained in steps 1-5. Then process z-stacks with the Extended Depth of Field (EDF) plug-in to obtain one picture focused on the gelatin plane (plugin available on ImageJ, direct method) (33). Train NIS.AI with the EDF pictures and the associated degradation ROIs. For the analysis phase, simply process the stacks with the EDF plug-in. NIS.AI automatically detects degradation area and provides a 16-bits picture of the degraded gelatin. Back to ImageJ, get the area of the degraded zones using the AutoThreshold (Method: MaxEntropy dark) and Analyze Particle commands and measure the degradation index as previously described (degradation area/number of nuclei) (see Note 21).

i. Live-cell imaging of invadopodia dynamics in cells plated on gelatin

1. To monitor the dynamics of TKS5-positive invadopodia, it is recommended to use a confocal spinning disk microscope with a 63X or 100X oil-objective. If available, TIRF microscopy could be used to have a better definition of events occurring at the ventral plasma membrane.
2. For acquisition settings, since gelatin is highly sensitive to light, and depending on the total time of the acquisition, we recommend acquiring the samples with a 1:10 ratio (*i.e.* one excitation of the gelatin channel for 10 illuminations of the TKS5 channel).
3. Acquire 10 to 15 fields and one to two focal planes (if gelatin layer is not absolutely flat).
4. The dynamics of gelatin degradation can be quantified by measuring the area of degradation per cell over time.
5. Invadopodia dynamics can be quantified using the TrackMate ImageJ plugin. It is necessary to adjust the parameters of the plugin according to your objective, laser intensity and exposure time.

15.

i. Image acquisition and analysis of invadopodia formation and collagen cleavage on a 2D collagen layer

1. As mentioned in section 3.7.1 concerning gelatin degradation, for determination of the percentage of cells forming invadopodia and degrading collagen, image acquisition should be done using a 100X oil-objective (Figure 1).
2. Images should be acquired in a non-biased way by scanning the coverslip using the cortactin channel. Select individual cells that are spread on collagen fibers and have a good staining. Acquire a z-stack from the bottom of the cell to the top. To have statistical power, it is advised to acquire at least 15 images and/or 20 cells for each condition. Repeat the experiment at least three independent times.
3. For analysis and quantification in ImageJ, semi-automated macros are available (Supplemental file 2). Briefly, open the Cy^{TM}5 channel picture (corresponding to the collagen fibers) and select the plane of collagen fibers. Apply an “Unsharp mask” with a radius of 7 pixels and a mask of 0.8 (“Process” → “Filters” → “Unsharp Mask”) and a “Mean” filter with a radius of 1 pixel (“Process” → “Filters” → “Mean…”). This will create a mask of the collagen fibers. Then draw the cell contour. Using commands on ROIs toolbox, combine “collagen mask” with “cell contour” in order to create a mask of collagen fibers associated to each cell area. Open the TKS5 image and use the threshold command of ImageJ (“Image” → “Adjust” → “Threshold…”) to highlight TKS5-positive invadopodia. Run Analyze Particles (“Analyze” → “Analyze Particles”). Be sure to check the “Summarize” checkbox. The percentage of cell-associated collagen fibers positive for invadopodia is found in the “Summary” table.
4. To determine the capacity of cells to cleave collagen fibers, image processing can be performed as described above (steps 1 and 2). Then, quantify the total degradation by cell. Briefly, segment the Col1-$^{3/4}$C signal using a threshold command of ImageJ (“Image” → “Adjust” → “Threshold…”) to highlight Col1-$^{3/4}$C-positive cleaved collagen. Then run Analyze Particles (“Analyze” → “Analyze Particles”). A collagen cleavage index per cell is then used to measured collagenolytic activity of cells. Semi-automated macros are available for quantification (Supplemental File 1).

ii. Image acquisition and analysis of cell invasion and collagen cleavage into a 3D collagen gel

1. To determine the capacity of cells to form invadopodia and degrade collagen fibers in a 3D environment, we recommend using confocal microscopy or confocal spinning disk microscopy with a 63X oil-objective. A 40X oil-objective can be used for collagen cleavage, but the resolution will decrease.
2. Image processing can be performed as described in section 3.6.3 (for 2D collagen-coated coverslips). However, when using a 40X and to some extent also a 63X objective, collagen mask is difficult to perform. Thus, we quantify the total degradation in the field and normalize to the number of nuclei present in that field. Briefly, segment the Col1-$^{3/4}$C signal using a threshold command of ImageJ ("Image" → "Adjust" → "Threshold…") to highlight Col1-$^{3/4}$C-positive cleaved collagen. Then run Analyze Particles ("Analyze" → "Analyze Particles"). A collagen cleavage index per cell is then used to measure collagenolytic activity of cells.

iii. Live-cell imaging of cells plated into 3D collagen gel and bilayered type-I collagen sandwich (3D assays)

1. To measure TKS5-positive invadopodia dynamics into a bilayered type-I collagen sandwich, we recommend using confocal spinning disk microscopy with a long working distance (0.59 – 0.61 mm) 40X water immersion-objective (40X Nikon CFI Apo LWD Lambda S 40XC WI) (Figure 1). For the acquisition settings, as invadopodia formation and collagen remodeling are relatively dynamic processes occurring in 30 to 60 min following cell-matrix contact, we recommend using a time interval of 1 min between 2 successive time points.
2. Since collagen coupled to a fluorophore is highly sensitive to light, and depending on the total time of the acquisition, we recommend acquiring the samples with a 1:3 ratio (*i.e.* 1 picture of the collagen channel for 3 pictures of the TKS5 channel) and to not go beyond this 1:3 ratio.

3. Acquire 10 to 15 fields. We recommend acquiring a z-stack of at least three frames around collagen fibers where TKS5-positive invadopodia are found.
4. Invadopodia dynamics (such as elongation rate measurement) can be quantified as described in Ferrari et al., 2019 (11).

Notes

1. Gelatin from pig skin, fluorescein conjugate, 5 mg (Ref. G13187 ThermoFisher Scientific Inc.) can also be used as an alternative, albeit that fluorescein is more sensitive to photobleaching and has a relatively broad fluorescence emission spectrum.
2. Alternatively, non-labeled gelatin can be labeled with any other fluorophore of choice by following the procedure described in section 2.2.2. and 3.4.2.
3. Diluted glutaraldehyde can be prepared in advance and stored at -20°C.
4. Cell lines overexpressing invadopodia components (TKS5, MT1-MMP) are highly degradative. Thus, it is recommended to use 50 µg/mL of poly-L-lysine.
5. The centrifugation should spin down non-dissolved gelatin chunks. If dissolution is complete, then the pellet should be invisible.
6. Be careful during coverslip handling not to drop them or flip upside down. The gelatin-coated side of the coverslip is not easy to distinguish from the non-coated side.
7. Sodium borohydride is a carcinogenic, mutagenic and reprotoxic (CMR) substance that must be handled with extreme caution.
8. As sodium borohydride is an effervescent solution, it will create air bubbles which could make coverslips float to the surface. Make sure to submerge the coverslips again using a yellow tip of a pipette.
9. Cell number is calculated for MDA-MB-231 cells. If using other cell types with different cell size, adjust the number of cells if required.
10. Seeding time on gelatin may be cell line dependent and should be adjusted accordingly.
11. The thickness of the crosslinked gelatin coat obtained using this procedure is typically 50–100 nm, as estimated by electron microscopy analysis (9,16,19). Therefore, this assay is

suitable for measurement of gelatin degradation but does not provide any information regarding the cell/membrane protrusive activity.

12. It is recommended to prepare neutralizing and carbonate buffers on the day when labeling is performed.
13. Rat tail tendon type-I collagen concentration is batch-dependent and can vary. In case of consequent variation, adapt the quantity of buffer used.
14. The carbonate buffer is kept at 4°C and pre-warmed at room temperature before use to dissolve precipitates.
15. If the collagen is difficult to dissolve, add a drop of 1 M HCl. Make sure pH is always ~2. Keep the collagen solution in a glass bottle at 4°C. The solution can be shelved for up to 6 months.
16. As 800 µL of collagen solution will be mixed with 180 µL of Polymerization Buffer, this will change the desired final concentration (in our case, 2.2 mg/mL). Thus, we recommend preparing an intermediate solution of collagen (in our case, at 2.6 mg/mL) by diluting stock collagen solution with sterile water in order to reach this 2.6 mg/mL concentration.
17. If necessary, at this step, add drugs to the collagen polymerization solution (*i.e.* protease inhibitor GM6001) or vehicle at working concentration (see Table 1).
18. Make sure to add the culture medium gently to avoid detaching the polymerized collagen drop.
19. Since pre-permeabilization step is short, it is better to use pre-heated permeabilization solution.
20. Novus anti-TKS5 antibodies work well for Western Blot and immunofluorescence analysis (gelatin and collagen) but the quality of staining is batch-dependent. CST antibodies work well for Western Blot analysis. For immunofluorescence staining using a collagen matrix, we advise to perform overnight incubation at 4°C. Note that this antibody gives a strong nuclear background signal.
21. A macro which automatizes this process is available on demand to the authors.

Acknowledgements

The authors thank all past and present members of PC's lab who contributed to the invadopodia methods described in this article and provided insightful comments during the preparation of this manuscript. DR was supported by a grant from Paris Sciences et Lettres (PSL) University. PM was supported by a grant from INCa (2019-1-PL BIO-07-ICR-1) to PC. This work was supported by Fondation ARC pour la Recherche contre le Cancer (ARCPGA12019120000973_1574), INCa grant (2019-1-PL BIO-07-ICR-1), and by institutional support from Institut Curie and the Centre National pour la Recherche Scientifique to PC.

References

1. David-Pfeuty T, Singer SJ (1980) Altered distributions of the cytoskeletal proteins vinculin and α-actinin in cultured fibroblasts transformed by Rous sarcoma virus. Proc. Natl. Acad. Sci. U. S. A. 77:6687–6691

2. Chen W-T (1989) Proteolytic activity of specialized surface protrusions formed at rosette contact sites of transformed cells. J Experimental Zoology 251:167–185

3. Calle Y, Burns S, Thrasher AJ, Jones GE (2006) The leukocyte podosome. Eur J Cell Biol 85:151–157

4. Hartwig JH, Davies WA, Stossel TP (1977) Evidence for contractile protein translocation in macrophage spreading, phagocytosis, and phagolysosome formation. J Cell Biol 75:956–967

5. Destaing O et al (2003) Podosomes display actin turnover and dynamic self-organization in osteoclasts expressing actin-green fluorescent protein. Mol Biol Cell 14(2):407-16

6. Linder S, Wiesner C, Himmel M (2011) Degrading devices: invadosomes in proteolytic cell invasion. Annu Rev Cell Dev Biol 27:185–211

7. Artym VV et al (2015) Dense fibrillar collagen is a potent inducer of invadopodia via a specific signaling network. J Cell Biol 208:331–350

8. Parekh A et al (2011) Sensing and modulation of invadopodia across a wide range of rigidities. Biophys J 100:573–582

9. Revach OY et al (2015) Mechanical interplay between invadopodia and the nucleus in cultured cancer cells. Sci Rep 5:1–13

10. Castagnino A et al (2018) Coronin 1C promotes triple-negative breast cancer invasiveness through regulation of MT1-MMP traffic and invadopodia function. Oncogene 37:6425–6441

11. Ferrari R et al (2019) MT1-MMP directs force-producing proteolytic contacts that drive tumor cell invasion. Nat Commun 10:1–15

12. Infante E et al (2018) LINC complex-Lis1 interplay controls MT1-MMP matrix digest-on-demand response for confined tumor cell migration. Nat Commun 9(1):2443

13. Juin A et al (2012) Physiological type I collagen organization induces the formation of a novel class of linear invadosomes. Mol Biol Cell 23:297–309

14. Juin A et al (2014) Discoidin domain receptor 1 controls linear invadosome formation via a Cdc42-Tuba pathway. J Cell Biol 207:517–533

15. Monteiro P et al (2013) Endosomal WASH and exocyst complexes control exocytosis of MT1-MMP at invadopodia. J Cell Biol 203:1063–1079

16. Cambi A, Chavrier P (2021) Tissue remodeling by invadosomes. Faculty Reviews 10(39)

17. Tolde O, Rösel D, Veselý P, Folk P, Brábek J (2010) The structure of invadopodia in a complex 3D environment. Eur J Cell Biol 89:674–680

18. Ferrari R, Infante E, Chavrier P (2019) Nucleus–Invadopodia Duo During Cancer Invasion. Trends Cell Biol 29:93–96

19. Artym VV et al (2006) Dynamic interactions of cortactin and membrane type 1 matrix metalloproteinase at invadopodia: Defining the stages of invadopodia formation and function. Cancer Res. 66:3034–3043

20. Beaty BT, Condeelis J (2014) Digging a little deeper: The stages of invadopodium formation and maturation. Eur J Cell Biol 93:438–444

21. Sharma VP et al (2013) Tks5 and SHIP2 regulate invadopodium maturation, but not initiation, in breast carcinoma cells. Curr Biol 23:2079–2089

22. Yamaguchi H et al (2005) Molecular mechanisms of invadopodium formation: The role of the N-WASP-Arp2/3 complex pathway and cofilin. J Cell Biol 168:441–452

23. Seals DF et al (2005) The adaptor protein Tks5/Fish is required for podosome formation and function, and for the protease-driven invasion of cancer cells. Cancer Cell 7:155–165

24. Oser M et al (2009) Cortactin regulates cofilin and N-WASp activities to control the stages of invadopodium assembly and maturation. J Cell Biol 186:571–587

25. Saini P, Courtneidge SA (2018) Tks adaptor proteins at a glance. J Cell Sci 131:0–1

26. Zagryazhskaya-Masson A et al (2020) Intersection of TKS5 and FGD1/CDC42 signaling cascades directs the formation of invadopodia. J Cell Biol 219:9

27. Castro-Castro A, Marchesin V, Monteiro P, Lodillinsky C, Rossé C, Chavrier P (2016) Cellular and Molecular Mechanisms of MT1-MMP-Dependent Cancer Cell Invasion. Annu Rev Cell Dev Biol 32:555–576

28. Steffen A et al (2008) MT1-MMP-Dependent Invasion Is Regulated by TI-VAMP/VAMP7. Curr Biol 18:926–931

29. Jacob A et al (2016) The role and regulation of Rab40b-Tks5 complex during invadopodia formation and cancer cell invasion. J Cell Sci 129:4341–4353

30. Marchesin V et al (2015) ARF6-JIP3/4 regulate endosomal tubules for MT1-MMP exocytosis in cancer invasion. J. Cell Biol 211:339–358

31. Poincloux R, Lizárraga F, Chavrier P (2009) Matrix invasion by tumour cells: A focus on MT1-MMP trafficking to invadopodia. J Cell Sci 122(17):3015–3024

32. Rossé C et al (2014) Control of MT1-MMP transport by atypical PKC during breast-cancer progression. Proc. Natl. Acad. Sci. U. S. A. 111(18)

33. Forster B, Van De Ville D, Berent J, Sage D, Unser M (2004) Complex Wavelets for Extended Depth-of-Field: A New Method for the Fusion of Multichannel Microscopy Images. Microsc Res Tech 65(1-2):33-42

Figure 1. Invadopodia formation on different collagen matrices by breast cancer cells

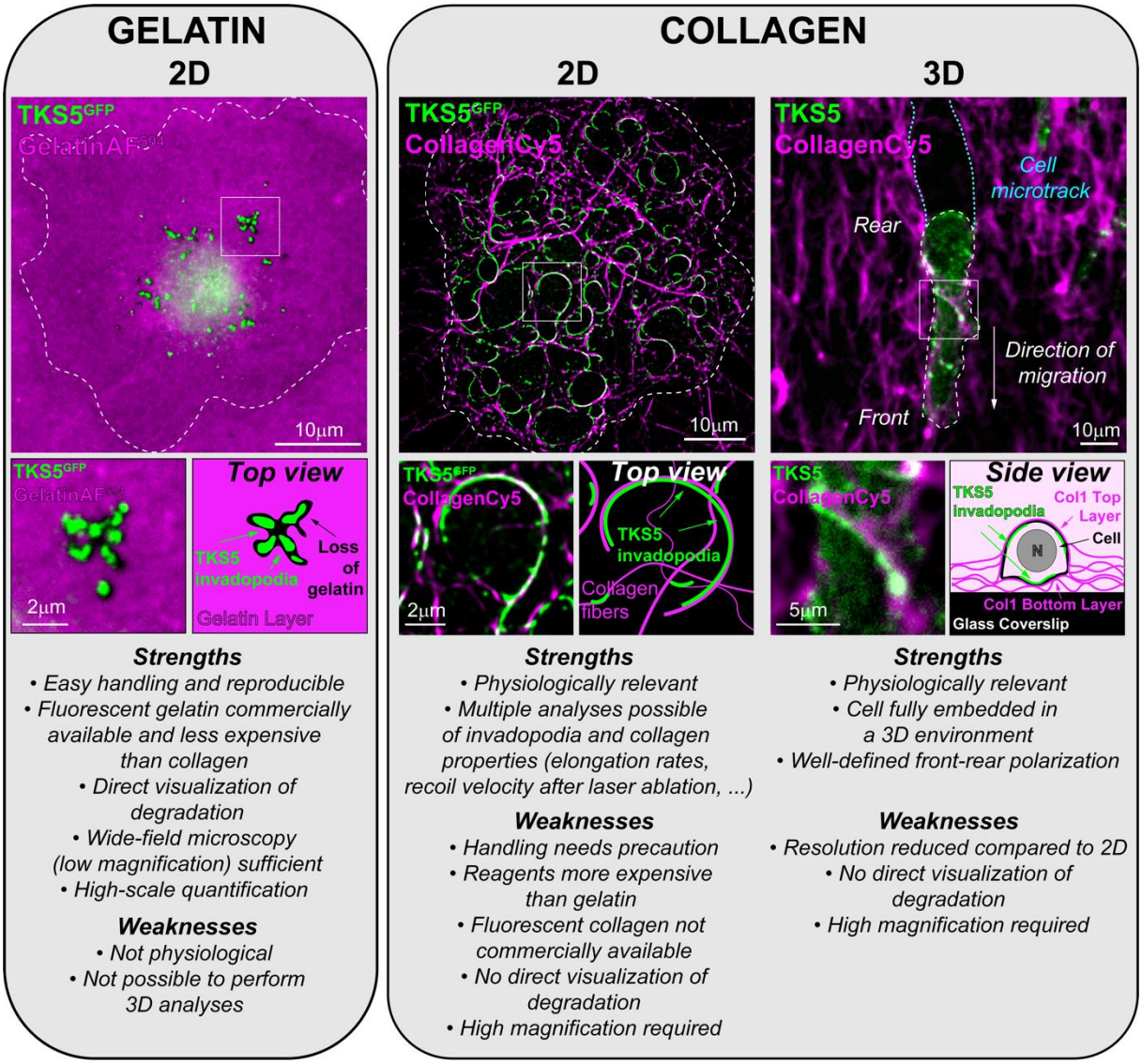

Figure Legend: MDA-MB-231 cells expressing TKS5^{GFP} (green) plated on fluorescently-labeled matrix (magenta). Matrix is gelatin in the left panel and 2D or 3D fibrillar type I collagen in the right panel. Higher magnification of the boxed region and schematic representation is shown in the insets. Dotted line, cell contour. The strengths and weaknesses of each matrix are listed.

Table 1. Antibodies used to probe invadopodia formation and collagen cleavage.

Antigen/Antibody ID	Company (Reference)	Species	Dilution	Comments
TKS5	Novus Biologicals (NBP1-90454)	Rabbit	1/100	Efficiency is batch dependent. Works by immunostaining (60 min incubation, RT)
TKS5	Cell Signaling (16619)	Rabbit	1/100	Requires overnight incubation at 4°C. Produces unspecific nuclear background. Does not work in gelatin assay.
Cortactin	Merck (05-180-I)	Mouse	1/100	Does not work if cells are not pre-permeabilized
Col1-$^{3/4}$C	Immunoglobe GmbH (0217-050)	Rabbit	1/100	May generate unspecific nuclear background
GFP	Abcam (ab13970)	Chicken	1/500	Works well
Anti-Chicken Secondary Ab	Molecular Probes (A11039)	Goat	1/300	Works well

Table 2. siRNAs and drugs used to probe invadopodia formation and collagen cleavage.

siRNA ID	Company
Non-targeting (NT)	Dharmacon (D-001810-01-20)
MMP14 (MT1-MMP)	Dharmacon (L-004145-00-0005)
SH3PXD2A (TKS5)	Dharmacon (L-006657-00-0005)

Pharmacological inhibitor	Company
GM6001 (MMP Inhibitor)	Merck (CC1100)

RÉSUMÉ

Les métastases sont la principale cause de décès liés aux cancers. La formation de métastases implique une dissémination des cellules cancéreuses à travers les matrices extracellulaires (MEC). Cette migration cellulaire requiert la protéolyse de la MEC par la métalloprotéase transmembranaire MT1-MMP qui est concentrée dans des structures d'actine, les invadopodes. Toutefois, les mécanismes de régulation des invadopodes par le microenvironnement tumoral sont mal connus. Dans certains cancers, l'apport en nutriments est limité, ce qui influence la voie de signalisation mTORC1 qui contrôle le métabolisme cellulaire. Les cellules carencées en acides aminés (AA) survivent et prolifèrent en utilisant des fragments de la MEC comme source nutritive alternative. Néanmoins, les mécanismes de production de ces fragments restent inconnus. Pendant ma thèse, j'ai montré que la répression de mTORC1 par la carence en AA ou par inhibition pharmacologique stimule fortement la dégradation de la MEC. Je me suis intéressé aux mécanismes moléculaires du contrôle des invadopodes par mTORC1 et j'ai montré que la répression de mTORC1 active son substrat Transcription Factor EB (EB) qui stimule de façon transcriptionnelle l'exocytose de MT1-MMP au niveau des invadopodes. L'enrichissement de MT1-MMP au niveau des invadopodes stimule la dégradation de la MEC et l'invasion des cellules de xénogreffes dérivées de cancer du sein de patientes. Nos résultats mettent en lumière les potentielles retombées de l'utilisation des inhibiteurs de mTOR en thérapie antitumorale, car cette inhibition pourrait favoriser la formation de métastases dans les cancers du sein.

MOTS CLÉS

Invadopode, MT1-MMP, mTOR, TFEB, Carcinome mammaire, Invasion

ABSTRACT

Metastases are the leading cause of cancer-related death. The formation of metastases involves the dissemination of cancer cells through the extracellular matrices (ECM). This cell migration requires the proteolysis of the ECM by the transmembrane metalloprotease MT1-MMP which is concentrated in actin structures: the invadopodia. However, the mechanisms of regulation of invadopodia by the tumor microenvironment are poorly understood. In some cancers, nutrient supply is limited, which influences the mTORC1 signaling pathway that controls cellular metabolism. Cells starved of amino acids (AA) survive and proliferate by using ECM fragments as an alternative nutrient source. However, the mechanisms underlying the production of these fragments remain unknown. During my Ph.D., I showed that the repression of mTORC1 by AA deficiency or by pharmacological inhibition strongly stimulates the degradation of ECM. Furthermore, I sought to elucidate the molecular mechanisms by which mTORC1 signaling controls invadopodia and I showed that the repression of mTORC1 activates its substrate Transcription Factor EB (EB) which transcriptionally stimulates the exocytosis of MT1-MMP at invadopodia. Subsequently, ECM degradation is increased and promotes invasion of breast cancer patient-derived xenografts. Our results highlight the potential downfalls of inhibitors of mTORC1 used in breast cancer therapies as they could unleash a powerful invadopodia-based dissemination program.

KEYWORDS

Invadopodia, MT1-MMP, mTOR, TFEB, Breast cancer, Invasion